

## **ALCONPAT Internacional**

### **Founders members:**

Liana Arrieta de Bustillos – **Venezuela**  
Antonio Carmona Filho - **Brazil**  
Dante Domene – **Argentina**  
Manuel Fernández Cánovas – **Spain**  
José Calavera Ruiz – **Spain**  
Paulo Helene, **Brazil**

### **Board of Directors International:**

#### **President of Honor**

Carmen Andrade Perdrix, **Spain**

#### **President**

Enio Pazini Figueiredo, **Brazil**

#### **General Director**

Pedro Castro Borges, **Mexico**

#### **Executive Secretary**

César Juárez Alvarado, **Mexico**

#### **Technical Vice President**

Pedro Garcés Terradillos, **Spain**

#### **Administrative Vice President**

Luis Álvarez Valencia, **Guatemala**

#### **Treasurer**

Jose Manuel Mendoza Rangel, **Mexico**

#### **Manager**

Enrique Cervera Aguilar, **Mexico**  
Paulo Helene, **Brazil**

## **Revista ALCONPAT**

### **Editor in Chief:**

Dr. Pedro Castro Borges  
Centro de Investigación y de Estudios Avanzados del  
Instituto Politécnico Nacional, Unidad Mérida  
(CINVESTAV IPN – Mérida)  
Merida, Yucatan, **Mexico**

### **Co-Editor in Chief (2022-2023):**

Dra. Edna Possan  
Universidade Tecnológica Federal do  
Paraná, Curitiba, **Brazil**

### **Executive Editor:**

Dr. José Manuel Mendoza Rangel  
Universidad Autónoma de Nuevo León,  
Facultad de Ingeniería Civil  
Monterrey, Nuevo León, **Mexico**

### **Associate Editors:**

Dr. Manuel Fernández Cánovas  
Universidad Politécnica de Madrid.  
Madrid, **Spain**

Ing. Raúl Husni

Facultad de Ingeniería - Universidad de Buenos Aires.  
Buenos Aires, **Argentina**

Dr. Paulo Roberto do Lago Helene

Universidade de São Paulo.

São Paulo, **Brazil**

Dr. José Iván Escalante García

Centro de Investigación y de Estudios Avanzados del  
Instituto Politécnico Nacional (Unidad Saltillo)  
Saltillo, Coahuila, **Mexico**.

Dra. Oladis Troconis de Rincón

Centro de Estudios de Corrosión

Universidad de Zulia

Maracaibo, **Venezuela**

Dr. Fernando Branco

Universidade Técnica de Lisboa

Lisboa, **Portugal**

Dr. Pedro Garcés Terradillos

Universidad de Alicante

San Vicente, **Spain**

Dr. Andrés Antonio Torres Acosta

Instituto Tecnológico y de Estudios Superiores de  
Monterrey, Querétaro

Querétaro, **Mexico**

Dr. Filippo Ubertini

Universidad de Perugia,

Perugia, **Italy**

Dr. Ravindra Gettu

Instituto Indio de Tecnología de Madrás,

Chennai, **India**

RAV13N2, May – August 2023

*Message from the Editor in Chief*

**JOURNAL OF THE LATIN AMERICAN  
ASSOCIATION OF QUALITY CONTROL,  
PATHOLOGY AND RECOVERY OF  
CONSTRUCTION**

<http://www.revistaalconpat.org>

With great satisfaction, we present the second issue of the thirteenth year of the ALCONPAT Journal.

The objective of the Journal is the publication of contributions on basic or applied research directly related to solving problems about quality control, pathology and recovery of constructions, with related case studies being welcome in these areas.

This V13N2 edition begins with a work from **Mexico**, where Alejandro Meza and colleagues evaluate the effect of experimental variables in the study of chloride degradation of steel fiber reinforced concrete (SFRCs). The information was collected from different literary sources to later be treated through Taguchi's experimental design and regression analysis. The results show that the most influential factors in the degradation of SFRCs degraded by chloride are the load during degradation and the crack width, factors that statistically impact on residual resistance and maximum flexural load. However, others such as the water/cement ratio, fiber volume, chloride concentration and degradation time showed little influence on the mechanical response of the SFRCs.

In the second work, from **Mexico**, Marco Antonio Navarrete-Seras and colleagues analyze the influence of the proportion of sand in Type II mortars according to standard N-CMT-2-01-004/02 using three types of aggregates from the region of Morelia, Michoacán, determining its influence on its physical-mechanical properties, contemplating the use of different cementing materials (MC): Portland cement plus lime (B1) and Portland cement plus masonry cement (B2). Mixtures for B1 and B2 were prepared with sand/MC volume ratios, from 2.25 to 4, determining fluidity, uniaxial compression resistance (UCS) and wet electrical resistivity (WER). The relationship between fluidity and the amount of water/MC was studied, concluding that the type of aggregate and proportions modify the fluidity and demand for fresh water, impacting on UCS and WER.

The third work in this issue is from **Brazil**, where Rafael P. Gurkewicz and colleagues study the water absorption capacity of concrete panels and their self-healing process by adding an additive to the concrete or applying it on the surface. Through permeability, water absorption by immersion and capillarity tests, after wet curing, the panels with crystallizing additive applied on the surface showed lower absorption capacity, followed by those without additive and those with incorporated additive, which showed higher absorption. Through microscopy, it was possible to observe that the crystallization of the panels with surface additive was more advanced compared to those with incorporated additive.

The induced cracks did not reach the complete filling of the pores after curing in both types of application.

In the fourth article from **Mexico**, Arnulfo Luévanos Rojas shows a new model for the complete design of isolated rectangular footings under uniaxial and biaxial bending, considering that the area of the footing in contact with the ground works partially in compression. The methodology is presented by integration to obtain moments, bending shears and penetration. Numerical examples are presented for the design of isolated rectangular footings under uniaxial and biaxial flexure and are compared to the current model (total area works in compression) in terms of volumes of concrete and steel. The current model shows higher volumes of concrete and steel. Therefore, the new model is the most appropriate, since it presents better quality control in the resources used.

The fifth article, by Marian Diniz and R. Melo, comes from **Brazil** and analyzes the correlation between the pavement condition index and the condition of two surface drainage elements: storm drains and gutters. The study was carried out from the analysis of 19 sections, distributed throughout the Tambaú neighborhood, in João Pessoa-PB. The calculation of the state of the pavements was carried out by the PCI method and the state of the drainage elements was verified through subjective analysis. The results of the investigation showed when the elements fit or not in the ideal conditions, and although the drainage elements are considered in the performance of the pavement, the statistical evaluation showed a weak correlation between the condition of the pavement and the drainage elements evaluated.

The sixth work of this issue was written by Michel Donadio and colleagues from **Switzerland and Mexico**, in which they make a documentary analysis of the different corrosion mitigation techniques currently available, such as repair mortars, active and passive corrosion inhibitors, corrosion, protective coatings and induced current or galvanic cathodic protection. These structures, built to last a long time, are subject to aging due to influences from their environment, such as water, atmospheric carbon dioxide and other harmful elements such as chlorides and pollution. The most common deterioration process in reinforced concrete structures is corrosion and the consequent expansion of the steel reinforcement, which causes cracking and spalling of the concrete.

The article that closes the issue is by Patricia Angulo and Carlos Ochoa from **Mexico**, who identify and discuss the most eco-efficient sustainable strategies to take advantage of or reduce NO<sub>x</sub>, SO<sub>x</sub> and SiO<sub>2</sub> dust emissions in cement manufacturing, with the aim of improving competitiveness in the Mexican cement industry. The research design was qualitative, observational and deductive. The results showed that SO<sub>x</sub> waste bioreactors have higher eco-efficiency; followed by the domes to capture and take advantage of the SiO<sub>2</sub> and the bag filters. These strategies are effective for specific pollutants from cement production. This study investigates a topic that is rarely addressed in Mexico, the sustainability of cement. By applying these strategies, the Mexican cement sector would boost its business competitiveness.

We are sure that the articles in this issue will constitute an important reference for those readers involved with questions of evaluation and characterization of materials, elements and structures. We thank the authors participating in this issue for their willingness and effort to present quality articles and meet the established deadlines.

We invite you to collaborate by submitting articles for our next special issue (RA V13 N3): “Combined binders for sustainable and durable concrete”, where Dr. Ravindra Gettu (India) and Dr. Yuvaraj Dhandapani (England) will be the Guest Editors.

At the close of the last V13 N1 2023 issue, 12 years after having started operations, our performance as Alconpat Journal was finally rewarded with our inclusion in one of the two best indexes for journals such as Elsevier's Scopus. Our Scopus membership has its historic beginning on December 29, 2022, the date on which we received approval from Elsevier. This is one more reason of celebration for our community that has made a scientific investment in our journal waiting for moments like this. Congratulations to all.

On behalf of the Editorial Board

A handwritten signature in black ink, appearing to read 'Pedro Castro Borges', written over a circular stamp or seal.

Pedro Castro Borges

Editor in Chief



## Influence of experimental variables on the mechanical properties of steel fiber reinforced concrete (SFRC) in chloride degradation experiments: bibliographic review and statistical analysis

O. Becerra<sup>1</sup> , A. Meza<sup>1\*</sup> , R. Salinas<sup>2</sup> 

\*Contact author: [alejandro.ml@aguascalientes.tecnm.mx](mailto:alejandro.ml@aguascalientes.tecnm.mx)

DOI: <https://doi.org/10.21041/ra.v13i2.641>

Received: 04/10/2022 | Received in revised form: 15/04/2023 | Accepted: 23/04/2023 | Published: 01/05/2023

### ABSTRACT

This research aims to evaluate the effect of experimental variables in the study of chloride degradation of steel fiber reinforced concretes (SFRCs). The information was collected from different literary sources to be treated through Taguchi's experimental design and regression analysis. The results show that the most influential factors in the degradation of SFRCs by chloride are the load during degradation and the crack width, residual resistance, and maximum flexural load. However, others, such as the water/cement ratio, fiber volume, chloride concentration, and degradation time, showed little influence on the mechanical response of the SFRCs.

**Keywords:** steel fiber reinforced concrete; degradation; chlorides; experimental variables; mechanical properties.

**Cite as:** Becerra, O., Meza, A., Salinas, R. (2023), "Influence of experimental variables on the mechanical properties of steel fiber reinforced concrete (SFRC) in chloride degradation experiments: bibliographic review and statistical analysis", Revista ALCONPAT, 13 (2), pp. 143 – 157, DOI: <https://doi.org/10.21041/ra.v13i2.641>

<sup>1</sup> Departamento de Ingeniería Metal-Mecánica, Facultad de Ingeniería, Tecnológico Nacional de México/IT de Aguascalientes, Aguascalientes, México.

<sup>2</sup> Departamento de Estadística, Centro de Ciencias Básicas, Universidad Autónoma de Aguascalientes, Aguascalientes, México.

### Contribution of each author

In this work, the author Oslerly Becerra Pérez contributed to the search and compilation of information, with the statistical analysis of said information in around 50%, the discussion of the results in 40%, and the preparation of the draft of the article. The author Alejandro Meza de Luna contributed to the direction and management of the investigation, the discussion of the results 40%, the revision and adjustments of the article 80%, and the functions of the corresponding author. The author Rogelio Salinas contributed to the statistical analysis of all the information found by 50%, the discussion of the results by 20%, and the review and adjustments of the article by 20%.

### Creative Commons License

Copyright 2023 by the authors. This work is an Open-Access article published under the terms and conditions of an International Creative Commons Attribution 4.0 International License ([CC BY 4.0](https://creativecommons.org/licenses/by/4.0/)).

### Discussions and subsequent corrections to the publication

Any dispute, including the replies of the authors, will be published in the first issue of 2024 provided that the information is received before the closing of the third issue of 2023.

## Influencia de variables experimentales en las propiedades mecánicas de los concretos reforzados con fibras de acero (SFRC) en experimentos de degradación por cloruros: revisión bibliográfica y análisis estadístico

### RESUMEN

La presente investigación tiene como objetivo evaluar el efecto de variables experimentales en el estudio de la degradación por cloruros de concretos reforzados con fibras de acero (SFRCs). La información fue recopilada de diferentes fuentes literarias para después ser tratada mediante el diseño experimental de Taguchi y análisis de regresión. Los resultados muestran que los factores más influyentes en la degradación de SFRCs degradados por cloruro son la carga durante la degradación y el ancho de fisura, factores que impactan estadísticamente sobre resistencia residual y la carga máxima a flexión. Sin embargo, otros como la relación agua/cemento, el volumen de fibras, la concentración de cloruros y el tiempo de degradación demostraron poca influencia sobre la respuesta mecánica de los SFRCs.

**Palabras clave:** concretos reforzados con fibra de acero; degradación; cloruros; variables experimentales; propiedades mecánicas.

## Influência de variáveis experimentais nas propriedades mecânicas do concreto reforçado com fibras de aço (SFRC) em experimentos de degradação de cloretos: revisão bibliográfica e análise estatística

### RESUMO

O objetivo desta pesquisa é avaliar o efeito de variáveis experimentais no estudo da degradação de cloretos de concretos reforçados com fibras de aço (SFRCs). As informações foram coletadas de diferentes fontes literárias e tratadas por meio do ábaco experimental de Taguchi e da análise de regressão. Os resultados mostram que os fatores mais influentes na degradação dos SFRCs degradados por cloreto são a carga durante a degradação e a abertura da fissura, fatores que impactam estatisticamente na resistência residual e na carga máxima de flexão. No entanto, outros como relação água/cimento, volume de fibras, concentração de cloretos e tempo de degradação mostraram pouca influência na resposta mecânica dos SFRCs.

**Palavras-chave:** concreto reforçado com fibras de aço; degradação; cloretos; variáveis experimentais; propriedades mecânicas.

#### Nomenclature:

Vrr: Variation of residual resistance (%)

Vcm: Maximum load variation (%)

Rac: Water/cement ratio

Vf: Fiber volume (%)

Td: Degradation time (days)

C: Chloride concentration (% w/w)

Cd: Load exerted during degradation (kN)

Ca: Accelerated corrosion ( $\mu\text{A}/\text{cm}^2$ )

Ag: Width of controlled cracks (mm)

Te: Type of experiment

#### Legal Information

Revista ALCONPAT is a quarterly publication by the Asociación Latinoamericana de Control de Calidad, Patología y Recuperación de la Construcción, Internacional, A.C., Km. 6 antigua carretera a Progreso, Mérida, Yucatán, 97310, Tel.5219997385893, [alconpat.int@gmail.com](mailto:alconpat.int@gmail.com), Website: [www.alconpat.org](http://www.alconpat.org)

Reservation of rights for exclusive use No.04-2013-011717330300-203, and ISSN 2007-6835, both granted by the Instituto Nacional de Derecho de Autor. Responsible editor: Pedro Castro Borges, Ph.D. Responsible for the last update of this issue, Informatics Unit ALCONPAT, Elizabeth Sabido Maldonado.

The views of the authors do not necessarily reflect the position of the editor.

The total or partial reproduction of the contents and images of the publication is carried out in accordance with the COPE code and the CC BY 4.0 license of the Revista ALCONPAT.

## 1. INTRODUCTION

Concrete is the most used construction material worldwide, mainly due to the availability of the materials that constitute it (Chen et al., 2021). Concrete has properties that have made it the construction material par excellence since it has a high resistance to compression, being able to go decades without requiring practically any maintenance or replacement (Paul et al., 2020). Despite these qualities, concrete has a relatively low flexural resistance due to the tensile stresses. It has become necessary to use reinforcing materials to prepare concrete, which allows for improving its characteristics. (Chen et al., 2021). From the 19th century to the present, steel in the form of bars has been used to reinforce concrete structures. Although reinforcing bars are still the most widely used for this purpose, the use of fibers has had a significant boom in recent decades, generating what is known as steel fiber reinforced concrete (SFRC). , the fibers improve the tensile properties of concrete, fatigue resistance, impact resistance, and toughness and help control cracking (Behbahani & Nematollahi, 2011; Kaur et al., (2012), Ferreira et al., 2018; Zhang et al., 2020). SFRC is used, for example, in tunnel lining, highway construction, and buildings prone to earthquake damage (Berrocal, 2015; Marcos-Meson et al., 2019; Zhang et al., 2020). In addition, the SFRC is applied in infrastructures with aggressive environments, such as industrial floors, buildings to store nuclear waste, and hydraulic and marine structures, such as docks, oil platforms, and gas pipelines (Doo-Yeol et al., 2021; Hou et al., 2021). Among the most commonly used materials for this purpose are steel, polymeric materials, and carbon fibers, although the use of glass, coconut, jute, and asbestos has also been reported (Meza & Siddique, 2019; Paul et al., 2020; Meza & Shaikh, 2020; Meza et al., 2021), as well as agave vegetable fiber (Juárez-Alvarado et al., 2017). Steel fibers have been widely used and studied as concrete reinforcement (Horszczaruk, 2009; Hou et al., 2021). As previously seen, SFRCs are used in infrastructures subjected to aggressive environments; therefore, the scientific community has been in charge of investigating the different degradation processes to which structures made with SFRCs may be subjected. Various investigations indicate that corrosion is the primary mechanism of the degradation of reinforced concrete structures (Paul et al., 2020; Berrocal et al., 2015; Berrocal et al., 2017). Corrosion causes a decrease in the cross-section of the steel reinforcement (Berrocal, 2015), which negatively influences the mechanical characteristics of the concrete reinforced with steel bars and the SFRC. Besides, it is essential to say that the corrosion process affects not only the reinforcement but also the concrete that surrounds them; this is due to the formation of corrosion products, which accumulate at the steel-concrete interface, and as the volume increases, internal pressures originate that cause cracking of the concrete, a process known as spalling (Simões & Santo, 2019), which in turn increases the corrosion rate and thereby causes changes in its mechanical properties, including maximum load and residual resistance (Berrocal et al., 2017; Paul et al., 2020). According to Abbas et al. (2014), the penetration of chlorides in tunnel walls causes the corrosion of the reinforcement, thus reducing its load capacity. Also, other researchers, such as Granju and Balouch (2005) and Carrillo et al. (2017), affirm that corrosive environments can affect the flexural performance of the SFRCs if the steel fibers are corroded since these cause reductions in the maximum peak load accompanied by brittle and brittle post-peak behavior. In addition, studies such as that of Hou et al. (2021) indicate that the decrease in residual resistance in SFRCs is closely linked with the loss of reinforcement mass, pitting corrosion, and deterioration of the adhesion between the reinforcement-concrete-corrosion rate.

On the other hand, several factors influence the corrosion process since this depends on the corroded metal's characteristics and the surrounding environment in which it is found. One of these factors is the presence of external agents, such as salts containing the chloride ion, such as aluminum chloride, iron chloride, ammonium chloride, and sodium chloride. Upon entering the concrete, these salts lower their pH and accelerate the corrosion process of the steel reinforcement

(Salazar-Jiménez, 2015). Specifically, chloride degradation causes the so-called pitting corrosion effect; this occurs when enough chlorides accumulate on the reinforcement surface, thus favoring the corrosive process in a specific area of the material (Berrocal et al., 2015).

The degradation of fiber-reinforced concrete by the action of chlorides has been widely studied due to the exposure of infrastructures to aggressive environments with high concentrations of this anion (Berrocal et al., 2015). For this reason, research has been carried out focused on the effect of degradation on the fibers, concrete, and fiber-concrete set, obtaining that their mechanical properties vary so much after being subjected to degradable processes by chlorides. Dissimilar types of fibers and concrete under different experimental conditions have been put to the test, this has given rise to the results obtained in said investigations being very varied and not always correlated with each other, so it is still not completely clear what they are the experimental variables that most affect the mechanical characteristics of concrete and to what extent they do so which could be solved by carrying out comparative analyzes and research.

For the reasons mentioned above, this study compiles experimental data obtained under laboratory conditions related to the degradation of SFRC under the action of chlorides. The data from different investigations were subjected to a statistical analysis where the experimental variables that most influence the corrosion of the fibers, the general deterioration of the concrete, and the extent to which they affect their properties when subjected to flexural stress were identified. For this, the analysis of experimental data obtained from the bibliography was carried out using Taguchi's robust experimental design, an analysis method focused on maximizing a specific signal-to-noise ratio (S/N) for each variable studied (Kuehl, 2000). The objective of the present investigation is to know the experimental variables that affect the responses, which are the decrease in the maximum load and the decrease in the residual resistance after the degradation process. A regression analysis was also used to represent the results obtained through the experimental analysis. It is hoped that the results achieved serve as a basis for researchers who begin the study of concrete reinforced with steel fibers and their degradation by the action of chlorides since a review and bibliographic analysis of the most relevant published regarding this subject is made theme in recent years.

## 2. PROCEDURE

As part of the procedure followed in this research, firstly, the experimental variables studied over time were identified by performing flexural tests of SFRCs that have been previously exposed to degradation by chlorides and whose variation directly influences the mechanical properties of maximum load and residual resistance. For the data analysis, the Taguchi experimental design was used with the help of the Minitab Software (Minitab 17.0); a regression analysis was carried out where the influence of the experimental variables on the response variable was corroborated (see Figure 1).

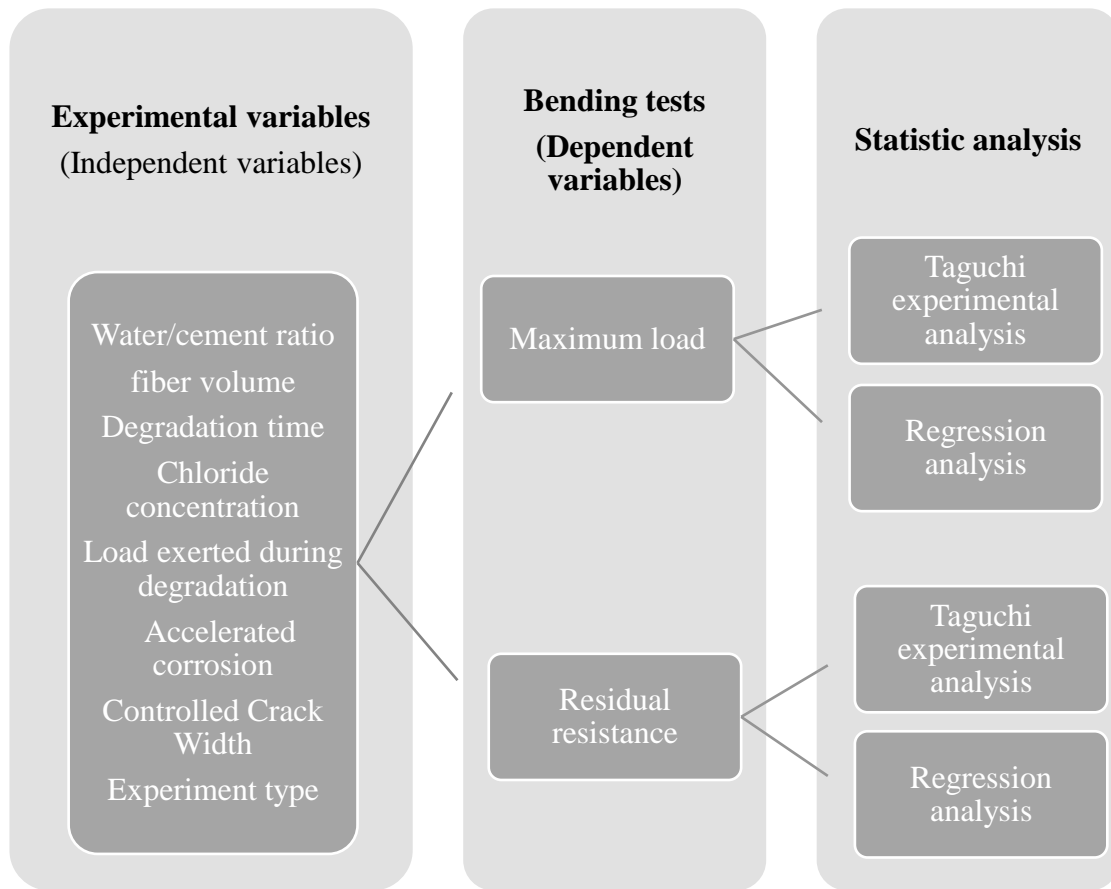


**Figure 1.** Representative scheme of the procedure followed in the investigation.

The water/cement ratio ( $R_{ac}$ ) is one of the most studied variables. The proportions of water and cement that are used when preparing the concrete influence the corrosive processes that the structure can suffer; this is because the greater the amount of water, the greater the density of micropores there will be in the concrete matrix, which facilitates the entry of corrosive agents such as chlorides. Furthermore, the greater the amount of water, the greater the moisture in the structure, which is the electrolyte that facilitates the oxidation reaction of the steel fibers. According to Balouch et al. (2010), when there are high water/cement ratios ( $R_{ac}$ ) ( $R_{ac} = 0.78$ ), the fibers that are close to the surface of the concrete ( $< 1$  mm), show signs of corrosion, and the more this proportion was reduced, the smaller necessary thickness was so that there was no corrosion in the fibers. Another determinant variable in the degradation of the SFRC is the volume of fibers ( $V_f$ ) to be used in the preparation of the samples; several authors have directed their studies to determine its influence on the mechanical properties of these concretes. For example, in their study, Chen et al. (2021) concluded that after the degradation process with sodium chloride, using a higher fiber content increases dynamic resistance and hence increases the strain. Also, the concentration of chlorides ( $C$ ) of the aqueous solution with which the piece of concrete under study is degraded significantly influences the corrosion of the fibers and, therefore, the properties of the concrete studied. It has been shown that the maximum chloride content in conventional concrete structures should not exceed 0.4 to 1.0% by weight of cement, this figure being higher for SFRCs, reaching permissible values of up to 1.7% (Berrocal et al., 2013). On the other hand, in various studies, it has been decided to crack the concrete to obtain higher corrosion rates in shorter periods. For this reason, the width of controlled cracks ( $A_g$ ) is a variable to be considered in this research; the results show that cracks allow the transport of aggressive agents into the structures (Berrocal et al., 2015; Blagojevic, 2016), demonstrating that if this exceeds a certain crack width threshold, they could be seen. affect the properties of concrete. Investigations have revealed that the chloride diffusion

coefficient is similar in uncracked and cracked SFRC with crack widths less than 0.2 mm (Hou et al., 2021), which gives a certain measure of crack width to use in experiments of this type. Another variable to consider is the degradation time ( $T_d$ ) to which the studied sample is subjected; the degradation process of reinforced concrete can be divided into two fundamental stages: initiation and propagation. The first stage is considered the time external agents require to enter the concrete structures and cause the de-passivation of the steel. In the second stage, the propagation of the steel corrosion occurs, and changes begin to occur in the structure that reduces its safety, which indicates that the longer the time spent in degraded conditions, it is to be expected that the damage to the structure is greater (Berrocal et al., 2015). On the other hand, it is important to mention that SFRC structures subjected to degradative environments and under-bending loads could suffer effects on their mechanical properties due to the double influence of corrosion and the application of an external force. For this reason, the charge during degradation ( $C_d$ ) is a variable investigated in various studies dedicated to this topic. Although the influence of loads during the corrosion process of fiber-reinforced concrete is still not completely clear, it has been shown that the action of forces on experimental beams of SFRCs has increased the width of controlled cracks formed, which could cause an increase in the corrosion rate of the fibers (Li et al., 2018). It is important to note that many researchers use alternative methods to carry out degradation experiments on concrete reinforced with steel fibers; this is because the corrosion process of the fibers is slow, and in some cases, it could take years for there to be appreciable damage effects. in concrete naturally (Taqi et al., 2021). Therefore, accelerated corrosion ( $C_a$ ) emerges as an appropriate experimental alternative in these cases, which consists of making an electric current flow in the SFRC specimens while they are under the action of chlorides. This combined effect causes the chloride threshold that must be exceeded for the de-passivation of the steel to decrease and, therefore, the corrosion of the fibers to occur more quickly (Tang & Wilkinson, 2020). Finally, another experimental variable to consider in degradation studies is the type of experiment ( $T_e$ ) since there are two ways to perform these tests. One consists of continuous wetting of the concrete piece with sodium chloride (NaCl) solution for a determined time (continuous). The other is based on wetting and drying cycles, submerging the concrete specimens in sodium chloride solutions. NaCl for a certain time and then left to dry for another defined period, so the cycle is repeated several times (wet-dry). It has been shown that this type of experiment is the most unfavorable environmental condition for SFRC structures subjected to degradation conditions caused by the action of chlorides (Balouch et al., 2010). Through the bibliographic review carried out, experimental data was obtained from different works related to the degradation of concrete reinforced with steel fibers (see Table 1). As mentioned, this work focused on the influence of the aforementioned experimental variables on the reduction of the maximum load and the residual resistance after the degradation process in bending tests. In general, the authors relied on the standard EN 14651: 2007 for three-point bending tests (Marcos-Meson et al., 2021), as well as the standards EN 1015-3:1999, EN 413-2 : 2016 and EN 14889-1: 2006 for the use of superplasticizer, the air content and the type of fiber to be used respectively in the preparation of concrete specimens (Marcos-Meson et al., 2020).

**Table 1.** List of works consulted to obtain the data studied.

Author	Rac	Vf (%)	Td (días)	C (%w/w)	Cd (kN)	Ca ( $\mu\text{A}/\text{cm}^2$ )	Ag (mm)	Vcm (%)	Vrr (%)
Nguyen, 2018	0.54	1.30	812	3.5	0.0	0	0.00	-	28.79
Nguyen, 2018	0.54	1.30	812	3.5	54.0	0	0.00	-	42.28
Nguyen, 2018	0.54	1.30	812	3.5	89.0	0	0.14	-	66.62
Marcos-Meson, 2021	0.44	1.20	365	3.5	0.0	0	0.15	5.45	9.41
Marcos-Meson, 2021	0.44	1.20	365	3.5	0.0	0	0.30	-22.14	-18.87
Marcos-Meson, 2021	0.44	1.20	365	7.0	0.0	0	0.15	-1.92	2.35
Marcos-Meson, 2021	0.44	1.20	365	7.0	0.0	0	0.30	-32.82	-33.96
Marcos-Meson, 2021	0.44	1.20	730	3.5	0.0	0	0.15	3.25	-11.30
Marcos-Meson, 2021	0.44	1.20	730	3.5	0.0	0	0.30	16.01	1.64
Marcos-Meson, 2021	0.44	1.20	730	7.0	0.0	0	0.15	-21.75	-7.83
Marcos-Meson, 2021	0.44	1.20	730	7.0	0.0	0	0.30	17.20	12.30
Michel, 2013	0.43	0.50	24	3.0	0.0	150	0.07	-	26.44
Michel, 2013	0.43	1.00	24	3.0	0.0	150	0.07	-	20.39
Berrocal, 2017	0.47	0.50	27	3.5	0.0	100	0.00	1.29	17.98
Berrocal, 2017	0.47	0.50	97	3.5	0.0	100	0.00	-23.56	19.10
Bui, 2021	0.50	1.00	28	3.0	0.0	150	0.00	2.66	29.59
Bui, 2021	0.50	1.50	28	3.0	0.0	150	0.00	1.30	19.39
Bui, 2021	0.50	2.00	28	3.0	0.0	150	0.00	0.86	16.33
Doo-Yeol, 2020	0.20	2.00	28	3.5	0.0	0	0.00	-1.90	1.43
Doo-Yeol, 2020	0.20	2.00	70	3.5	0.0	0	0.00	1.24	-10.00
Doo-Yeol, 2020	0.20	2.00	140	3.5	0.0	0	0.00	3.86	22.86
Bernard, 2019	0.50	1.50	176	3.5	0.0	0	0.15	15.31	37.50
Hou, 2021	0.47	0.75	72	3.5	13.6	200	0.06	23.35	1.98
Hou, 2021	0.47	0.75	72	3.5	20.4	200	0.09	13.55	2.97
Hou, 2021	0.47	0.75	72	3.5	27.2	200	0.12	30.51	4.95
Hou, 2021	0.47	0.75	72	3.5	34.0	200	0.14	14.23	5.94

### 3. RESULTS AND DISCUSSION

#### 3.1. Effect of experimental variables on the variation of the maximum load

The values of maximum load decrease that were repeated the most in flexural tests of SFRCs after being subjected to degradation processes by chlorides were selected to determine the effect of the experimental variables on the variation of the maximum load ( $V_{cm}$ ). For this, a histogram was made with these values, obtaining that the most significant number of variations are from -6 to 5% (see Figure 2); however, in this work, it was decided not to work with negative values, since this means that there is an increase in the maximum load in the concretes studied after being exposed to chlorides. The study of this behavior is not the objective of the present investigation; therefore, positive values from 0 to 31% were taken, and these data were used.

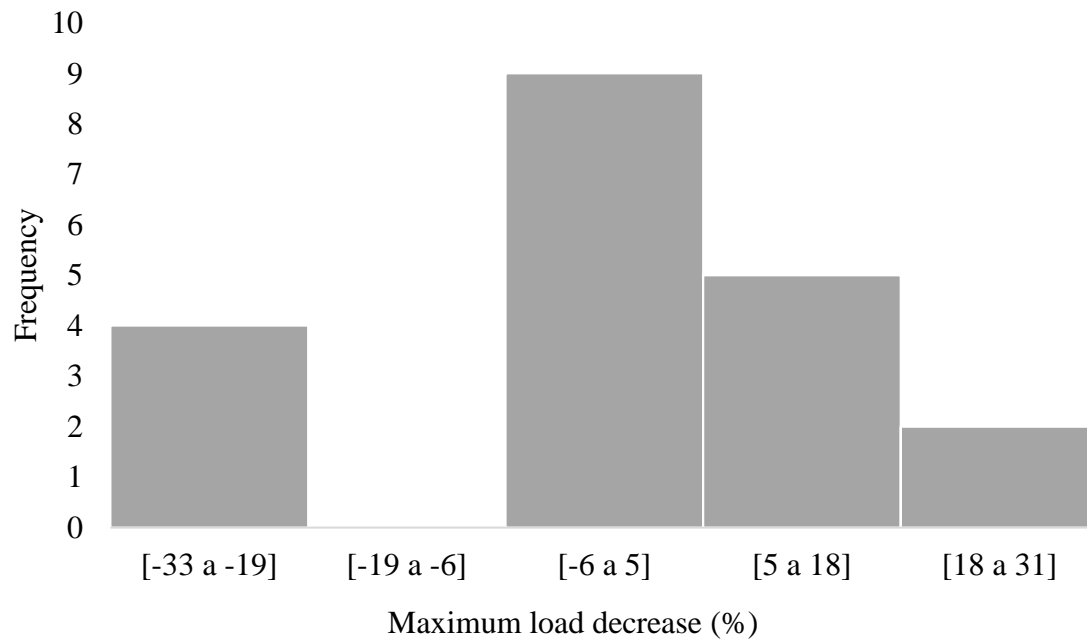


**Figure 2.** Histogram of maximum load variation.

##### 3.1.1. Signal-Noise Plot Analysis

It is possible to determine which control factors have the most significant incidence on the response variable (the variation of the maximum load) by analyzing Figure 3; this is done by observing the lines in each variable. There is no present effect when the lines are horizontal, and each level affects the response similarly. In contrast, when the lines are not horizontal, if there is a main effect and each level influences the response differently, the greater the distance in the vertical position between the points plotted, the greater the magnitude of the effect (Antony et al., 2006). Therefore, it is possible to affirm that width of controlled cracks ( $A_g$ ) is the variable with the greatest effect on the maximum flexural load capacity of SFRCs specimens degraded by chlorides. This variable is followed by fiber volume ( $V_f$ ), degradation time ( $T_d$ ), chloride concentration ( $C$ ), and accelerated corrosion ( $C_a$ ) in order of incidence in the response variable, which is those with the greatest separation between their levels. Finally, the water/cement ratio ( $R_{ac}$ ), the load during degradation ( $C_d$ ), and the type of experiment ( $T_e$ ) are the factors with the least effect on the variation of the maximum load. However, this work aims to find the values of the experimental variables that cause a significant decrease in the maximum load. These values can be determined by the maximum value of each factor in the signal-noise plot in Figure 3 (indicated by a red circle). Therefore, a recommended experiment design to obtain the most remarkable experimental effects of maximum flexural load variation in SFRCs specimens is the following:  $R_{ac}$  (0.47),  $V_f$  (0.75%),

Td (72 days), C (7% ), Cd (27.2 kN), Ca (200 uA/cm2), Ag (0.12) and Te (wet-dry).

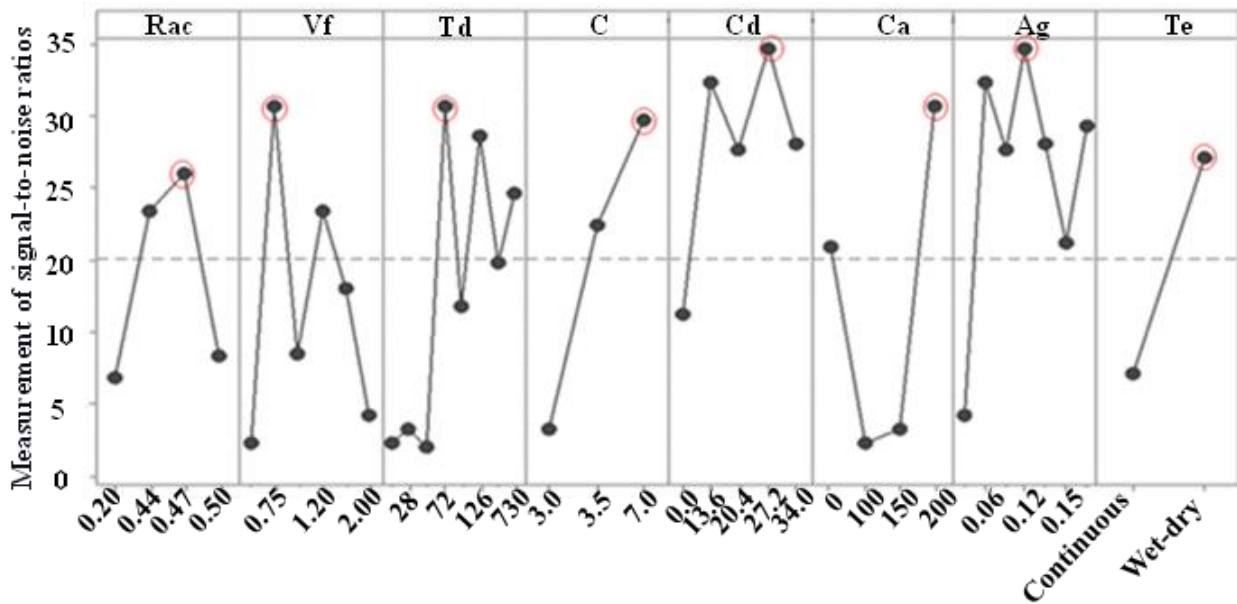


Figure 3. Main effects plot for signal-to-noise ratios for maximum load experiments.

### 3.1.2. Regression analysis

Analyzing Table 2, which is the result of the analysis of variance for the variables studied, it can be determined that, for none of the variables studied, the p-value is less than 0.05, which means that do not have a statistical impact on the results of variation of the maximum load in flexure. The variable with the greatest statistical impact in the previous figure, the width of controlled cracks, had a p-value of 0.081 in this analysis. In this case, it shows that the analysis of variance is not a useful tool to determine the influence of the explanatory variables on the response variable.

Table 2. Analysis of variance of the variables studied for maximum load variation.

Variables	p-value
Water/cement ratio	0.544
Fiber percentage	0.841
Degradation time	0.305
NaCl concentration	0.963
Charge during degradation	0.812
Accelerated corrosion	0.557
Width of controlled cracks	0.081
Experiment type	0.677

By analyzing the regression equations for the qualitative variable, which in this study is the type of experiment, it is possible to determine which experimental variables have explanatory power over the response variable (see equations 1 and 2). This explanatory capacity can be determined by the variables with a positive coefficient, which are the controlled crack width, NaCl concentration, and accelerated corrosion. These equations were obtained with the data used in this study using Minitab.

The regression equation for the type of continuous experiment variable:

$$V_{cm} = 13.0 - 28.4 R_{ac} - 1.35 V_f - 0.027 T_d + 0.14C - 0.126 C_d + 0.045 C_a + 112.0 A_g \quad (1)$$

The regression equation for the wet-dry type of experiment variable:

$$V_{cm} = 17.6 - 28.4 R_{ac} - 1.35 V_f - 0.027 T_d + 0.14C - 0.126 C_d + 0.045 C_a + 112.0 A_g \quad (2)$$

Therefore, the studies carried out to determine the influence of the experimental variables on the variation of the maximum load, which were the graph of main effects for signal-noise relationships, the analysis of variance, and the regression equations, allow us to conclude that the width of controlled cracks is the experimental variable that has the greatest effect on the maximum load in concrete reinforced with steel fibers that suffer degradation by chlorides. However, no works are explicitly dedicated to studying this variable's influence on the maximum load. In investigations such as that of Hou et al. (2021), contradictory results are shown since when using  $A_g = 0.06$  mm, the decrease in the maximum load is 23.35%, while for crack widths of 0.09 mm, it is 13.55%. For values of 0.12 mm, the variation is 30.51%, which shows that this property's variation does not depend only on this variable. On the other hand, another of the variables with influence on the variation of the maximum load according to the results obtained here is the concentration of chlorides. However, this information has yet to be corroborated due to a lack of bibliographic information; studies such as that of Marcos-Meson et al. (2021) show how this variable negatively influences the properties of the SFRCs studied.

### 3.2. Effect of experimental variables on the variation of the residual resistance

It was done similarly to the maximum flexural load data to analyze the residual resistance variation data ( $V_{rr}$ ) obtained. A histogram of the variation of the residual resistance was made. As observed in Figure 4, the highest frequency of variations is from 0 to 17% and from 17 to 34%; therefore, these are the data taken for continuing this study. It is also observed that there are values below zero and data greater than 34% since these rare results were not used for the abovementioned reasons.

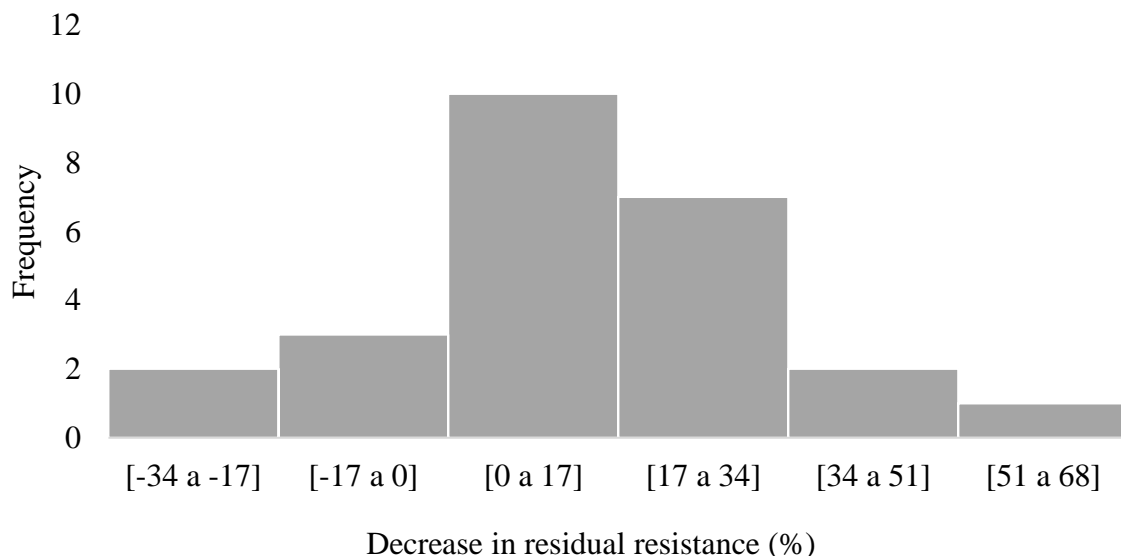
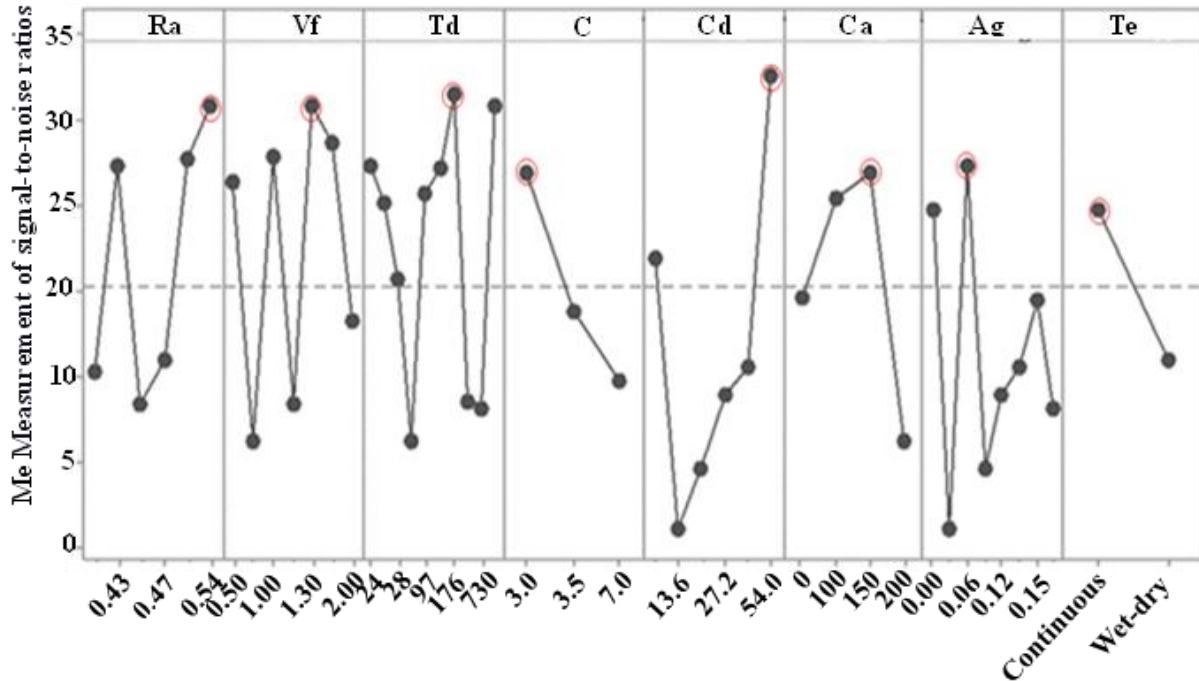


Figure 4. Histogram of residual resistance variation.

### 3.2.1. Signal-Noise Plot Analysis

It is possible to determine the control factors that reduce variability by analyzing Figure 5; This shows that, first of all, the response variable is affected by the bending load during degradation since it is the one that presents a greater vertical trend in the signal-noise graph.



**Figure 5.** Main effects plot for signal-noise relationships for residual resistance experiments.

The other variables with explanatory power over the dependent variable are the water/cement ratio, the volume of fibers, the degradation time, and the width of controlled cracks, the following levels being recommended in each case to obtain more significant effects in reducing the residual resistance: Cd (54 kN), Rac (0.54), Vf (1.3%), Td (176 days) and Ag (0.07 mm), respectively. These values were obtained by taking the value of the highest level in each factor from Figure 5, marked with a red circle. On the other hand, the other variables are closer to the mean and have less effect on the signal-noise ratio; however, an experimental design must be carried out also to obtain the highest levels of variation of the residual resistance must be taken into account. Therefore, in the case of chloride concentration, accelerated corrosion, and the type of experiment, the recommended values are 3%, 150 uA/cm<sup>2</sup>, and continuous, respectively.

### 3.2.2. Regression analysis

A regression analysis was also carried out where the analysis of variance was studied (Table 3), obtaining that the p-value was less than 0.05 in the variables: load during degradation (0.000) and type of experiment (0.002), which means that these variables have a greater influence on the variation of the residual resistance to flexion than the others. Said result is not coincident with those obtained in the Signal/Noise graph since, in said figure, the type of experiment variable has little influence on the response variable, which is an element to be analyzed in future studies.

**Table 3.** Analysis of variance of the variables studied for residual resistance variation.

Variables	Valor p
Water/cement ratio	0.401
Fiber percentage	0.452
Degradation time	0.196
NaCl concentration	0.085
Charge during degradation	0.000
Accelerated corrosion	0.907
Width of controlled cracks	0.081
Experiment type	0.002

On the other hand, by analyzing the coefficients of each factor in the regression equations (see equations 3 and 4), it is possible to determine the variables with the greatest influence on the response: the load during degradation, the water/cement ratio and the time of degradation, which agrees with the results obtained in Figure 5 and in part with Table 3.

The regression equation for the type of continuous experiment variable

$$V_{rr} = 19.5 + 23.4 R_{ac} - 4.93 V_f + 0.019 T_d - 2.81C + 0.555 C_d - 0.006 C_a - 46.8 A_g \quad (3)$$

The regression equation for the wet-dry type of experiment variable

$$V_{rr} = 3.1 + 23.4 R_{ac} - 4.93 V_f + 0.019 T_d - 2.81C + 0.555 C_d - 0.006 C_a - 46.8 A_g \quad (4)$$

In the studies of SFRCs degradation by the action of chlorides, the experimental variable with the greatest incidence of the variation of the residual resistance is the load to which the concrete specimens are subjected during the degradation. Similar results were found by Nguyen et al. (2018), which obtained a decrease in the load capacity of the concrete studied once cracked by having been subjected to a sustained load while exposed to chlorides; found that steel fibers corroded when the applied load was 50% of the yield load. Similarly, Hou et al. 2021 found that by increasing the levels of sustained load to the concrete and under severe corrosion conditions, the load capacity of these was affected. In the same way, the water/cement ratio has a marked influence on the variation of the residual resistance, according to the results found here. However, no studies in the literature are dedicated to comparing how this variable influences said property. Finally, as has been seen, the degradation time also influences this characteristic, which is contradictory to that obtained by Marcos-Meson et al., 2021, since they got few changes in the mechanical performance of the degraded SFRCs. by chlorides and carbon dioxide for 1 and 2 years. It means that the results obtained in this type of study remain contradictory and future research is required.

## 4. CONCLUSIONS

Through the analysis of the studies carried out regarding the degradation of concrete reinforced with steel fibers by the action of chlorides, and taking into account the main experimental variables that affect the properties of residual resistance and maximum load of said concretes, it is possible to arrive at the following conclusions:

1. The results found in the bibliography show that the degradation processes by chlorides not only negatively affect the mechanical properties of the SFRCs but that, in some cases, said properties could have an improvement after the degradation; this is attributed to an increased

- bond strength between concrete and fiber due to increased surface roughness due to corrosion.
2. Analyzing the results obtained for the experiments where the variation of the maximum flexural load was evaluated, it is found that the variable whose variation affects this property the most is the width of controlled cracks, with the value of 0.12 mm being the most relevant. In the same way, when ordering the variables according to their influence on the variation of the maximum load supported by the CRFAs after degradation processes due to chlorides, it would be as follows: Ag (0.12 mm), Vf (0.75%), Td (72 days), C (7%), Ca (200 uA/cm<sup>2</sup>), type of experiment (wet-dry) and Rac (0.47).
  3. In the case of residual flexural strength, the experimental variable that has the greatest effect on this property is the load during degradation, and it was shown that the higher the load, it is to be expected that the residual strength after the degradation process will be more affected. In the same way, an order of variables was obtained in terms of their influence on the residual resistance, so it is possible to recommend the following values of each variable to be used to obtain the greatest decreases in this property in chloride degradation experiments: Cd (54 kN), Rac (0.54), Vf (1.3%), Td (176 days), Ag (0.07 mm), C (3%), Ca (150 uA/cm<sup>2</sup>) and type of experiment (continuous). These variables were arranged from highest to lowest influence on residual resistance.
  4. Due to the results obtained, it is recommended to continue with the study of the influence of experimental variables such as the material of the fibers, the size and shape of the concrete specimens, and the type of raw material used for the elaboration of these in mechanical characteristics such as durability, toughness, and ductility.

## 5. REFERENCES

- Abbas, S., Soliman, A. M., Nehdi, M. L. (2014), *Mechanical Performance of reinforced Concrete and Steel Fiber-Reinforced Concrete Precast Tunnel Lining Segments: A Case Study*, *Aci Materials Journal*, 501-510.
- Antony, F., Perry, D., Wang, C., Kumar, M. (2006), *An application of Taguchi method of experimental design for new product design and development process*, Operations and Quality Management Unit, Caledonian Business School, Glasgow Caledonian University, Glasgow, UK, <http://dx.doi.org/10.1108/01445150610645611>.
- Balouch, S. U., Forth, J. P., Granju, J. L. (2010), *Surface corrosion of steel fibre reinforced concrete*, *Cement and Concrete Research*, 40, 410–414, <http://dx.doi.org/10.1016/j.cemconres.2009.10.001>.
- Behbahani, H., Nematollahi, B. (2011), *Steel Fiber Reinforced Concrete: A Review*, ICSECM, Kandy-SriLanka.
- Bernard, E. S. (2019), *Durability of fibre-reinforced shotcrete*, TSE P/L, Penrith, Australia, <http://dx.doi.org/10.1201/9780203023389.ch6>.
- Berrocal, C. G., Fernandez, I., Lundgren, K., Löfgren, I. (2017), *Corrosion-induced cracking and bond behaviour of corroded reinforcement bars in SFRC*, *Composites Part B*, <http://dx.doi.org/10.1016/j.compositesb.2017.01.020>.
- Berrocal, C. G., Lundgren, K., Löfgren, I. (2015), *Corrosion of Steel bars embedded in fibre reinforced concrete under chloride attack: State of the art*, *Cement and Concrete Research*, <http://dx.doi.org/10.1016/j.cemconres.2015.10.006>.
- Berrocal, C. G., Lundgren, K., Löfgren, I. (2013), *Influence of steel fibres on corrosion of reinforcement in concrete in chloride environments: a review*, *Fibre concrete*, Prague, Czech Republic.

- Blagojevic, A. (2016), *The Influence of Cracks on the Durability and Service Life of Reinforced Concrete Structures in relation to Chloride-Induced Corrosion: A Look from a Different Perspective*, Doctoral Thesis, Delft University of Technology: Delft, The Netherlands.
- Bui, L. V. H., Jongvivatsakul, P., Limpaninlachat, P., Stitmannathum, B., Nguyen, T. T., Nguyen, T. P. (2021), *Simulation of shear behavior of corroded reinforced concrete beams flexurally repaired with steel fiber-reinforced concrete*, *Structures*, 34, 1545–1559. <http://dx.doi.org/10.1016/j.istruc.2021.08.087>.
- Carrillo, J., Cárdenas, Pulido, J., Aperador, W. (2017), *Propiedades mecánicas a flexión del concreto reforzado con fibras de acero bajo ambientes corrosivos*, *Revista Ingeniería de Construcción*, 32, 59-72.
- Chen, H., Zhou, X., Li, Q., He, R., Huang, X. (2021), *Dynamic Compressive Strength Tests of Corroded SFRC Exposed to Drying–Wetting Cycles with a 37 mm Diameter SHPB*, *Materials*, 14, 2267, <http://dx.doi.org/10.3390/ma14092267>.
- Doo-Yeol, Y., Shin, W., Chun, B., Banthia, N. (2021), *Assessment of steel fiber corrosion in self-healed ultra-high-performance fiber-reinforced concrete and its effect on tensile performance*, *Cement and Concrete Research*, 133, 106091, <http://dx.doi.org/10.1016/j.cemconres.2020.106091>.
- Ferreira, M. P., Oliveira, M. H., Lima, Neto A. F., Tapajós, L. S., Nascimento, A. J. C., Freire, M. C. (2018), *Influencia del anclaje en la resistencia a la flexión de vigas reforzadas con mantas de PRFC*, *Revista ALCONPAT*, 9 (1), 30 – 47, <http://dx.doi.org/10.21041/ra.v9i1.269>.
- Granju, J. L., Balouch, S. U. (2005), *Corrosion of steel fibre reinforced concrete from the cracks*, *Cement and Concrete Research*, 572– 577, <http://dx.doi.org/10.1016/j.cemconres.2004.06.032>.
- Horszczaruk, E. K. (2009), *Hydro-abrasive erosion of high performance fiber-reinforced concrete*, *Wear*, 267, 110–115, <http://dx.doi.org/10.1016/j.wear.2008.11.010>.
- Hou, L., Peng, Y., Xu, R., Zhang, X., Huang, T., Chen, D. (2021), *Corrosion behavior and flexural performance of reinforced SFRC beams under sustained loading and chloride attack*, 242, 112553. <http://dx.doi.org/10.1016/j.engstruct.2021.112553>.
- Juárez-Alvarado, C. A., González López, J. R., Mendoza-Rangel, J. M., Zaldivar Cadena, A. A. (2017), *Compuestos cementantes fibroreforzados de bajo impacto ambiental comportamiento mecánico*, *Revista ALCONPAT*, 7 (2), 135-147, <http://dx.doi.org/10.21041/ra.v7i2.189>.
- Kaur, G., Pal Singh, S. (2012), *Flexural performance of fibrous concrete with cement additions*, *Construction Materials*, 167, 14-25, <http://dx.doi.org/10.1680/coma.12.00008>.
- Kuehl, R. O. (2000), *Diseño de experimentos. Principios estadísticos de diseño y análisis de investigación*, Arizona.
- Li, H., Li B., Jin, R., Li, S., Yu, J. G. (2018), *Effects of sustained loading and corrosion on the performance of reinforced concrete beams*, *Construction and Building Materials*, 169, 179–187.
- Marcos-Meson, V., Fischer, G., Edvardsen, C., Skovhus, T. L., Michel, A. (2019), *Durability of Steel Fibre Reinforced Concrete (SFRC) exposed to acid attack – A literature review*, *Construction and Building Materials*, 200, 490–501, <https://doi.org/10.1016/j.conbuildmat.2018.12.051>.
- Marcos-Meson, V., Fischer, G., Solgaard, A., Edvardsen, C., Michel, A. (2021), *Mechanical Performance of Steel Fibre Reinforced Concrete Exposed to Wet–Dry Cycles of Chlorides and Carbon Dioxide*, *Materials*, 14, 2642, <http://dx.doi.org/10.3390/ma14102642>.
- Marcos-Meson, V., Geiker, M., Fischer, G., Solgaard, A., Jakobsen, U. H., Edvardsen, C., Skovhus, T. L., Michel, A., Danner, T. (2020), *Durability of cracked SFRC exposed to wet-dry cycles of chlorides and carbon dioxide – Multiscale deterioration phenomena*, *Cement and Concrete Research*, 135, 106120, <https://doi.org/10.1016/j.cemconres.2020.106120>.
- Meza, A., Shaikh, F. U. A. (2020), *Anisotropy and bond behaviour of recycled Polyethylene terephthalate (PET) fibre as concrete reinforcement*, *Constr. Build. Mater*, 265, 120331, <http://dx.doi.org/10.1016/j.conbuildmat.2020.120331>.

- Meza, A., Pujadas, P., Meza, L. M., Pardo-Bosch, F., López-Carreño, R. D. (2021), *Mechanical Optimization of Concrete with Recycled PET Fibres Based on a Statistical-Experimental Study*, *Materials*, 14-240, <http://dx.doi.org/10.3390/ma14020240>.
- Meza, A., Siddique, S. (2019), *Effect of aspect ratio and dosage on the flexural response of FRC with recycled fiber*, *Construction and Building Materials*, 213, 286–291, <http://dx.doi.org/10.1016/j.conbuildmat.2019.04.081>.
- Michel, A., Solgaard, A. O. S., Pease, B. J., Geiker, M. R., Stang, H., Olesen, J. F. (2013), *Experimental investigation of the relation between damage at the concrete-steel interface and initiation of reinforcement corrosion in plain and fibre reinforced concrete*, *Corrosion Science*, 77, 308–321, <http://dx.doi.org/10.1016/j.corsci.2013.08.019>.
- Nguyen, W., Duncan, J. F., Jen, G., Ostertag, C. P. (2018), *Influence of matrix cracking and hybrid fiber reinforcement on the corrosion initiation and propagation behaviors of reinforced concrete*, *Corrosion Science*, <http://dx.doi.org/10.1016/j.corsci.2018.06.004>.
- Paul, S. C., Van Zijl, G. P., Branko Šavija, B. (2020), *Efect of Fibers on Durability of Concrete: A Practical Review*, *Materials*, 13, 4562, <http://dx.doi.org/10.3390/ma13204562www>.
- Salazar-Jiménez, J. A. (2015), *Introducción al fenómeno de corrosión: tipos, factores que influyen y control para la protección de materiales (Nota técnica)*, *Tecnología en Marcha*, 28, 127-136.
- Simões, Y. S., Santo, C. F. R. (2019), *Contribución de las vigas de concreto armado degradadas por la acción del fuego: Análisis comparativo entre el refuerzo estructural con fibras de carbono y láminas metálicas*, *Revista ALCONPAT*, 9 (1), 48 – 64, <http://dx.doi.org/10.21041/ra.v9i1.259>.
- Tang, K., Wilkinson, S. (2020), *Corrosion resistance of electrified railway tunnels made of steel fiber reinforced concrete*, *Construction and Building Materials*, 230, 117006, <http://dx.doi.org/10.1016/j.conbuildmat.2019.117006>.
- Taqi, F. Y., Mashrei, M. A., Oleiwi, H. M. (2021), *Experimental study on the effect of corrosion on shear strength of fibre-reinforced concrete beams*, *Structures*, 33, 2317-2333, <http://dx.doi.org/10.1016/j.istruc.2021.06.006>.
- Zhang, P., Kang, L., Wang, J., Guo, J., Hu, S., Ling, Y. (2020), *Mechanical Properties and Explosive Spalling Behavior of Steel-Fiber-Reinforced Concrete Exposed to High Temperature—A Review*, *Applied Sciences*, 10, 2324, <http://dx.doi.org/10.3390/app10072324>.

## Influence of sand proportion in the physical and mechanical properties of construction and building mortars

M. Navarrete-Seras<sup>1\*</sup> , W. Martinez-Molina<sup>1</sup> , H. L. Chavez-Garcia<sup>1</sup> ,  
A. Sanchez-Calvillo<sup>2,1</sup> , M. Arreola-Sanchez<sup>1,4</sup> , J. A. Borrego-Perez<sup>1,4</sup> ,  
N. A. Perez-Castellanos<sup>5,4</sup> , R. P. Ruiz-Torres<sup>6</sup> , A. M. Duran-Ramos<sup>1</sup>,  
E. M. Alonso-Guzman<sup>1,3\*</sup> 

\*Contact author: [mnavarrete@umich.mx](mailto:mnavarrete@umich.mx)

DOI: <https://doi.org/10.21041/ra.v13i2.684>

Received: 01/04/2023 | Received in revised form: 16/04/2023 | Accepted: 19/04/2023 | Published: 01/05/2023

### ABSTRACT

The influence of the sand proportion in mortars Type II was studied, according to the standard N-CMT-2-01-004/02, using three fine aggregates from the region of Morelia, in Michoacan, and determining their influence in the physico-mechanical properties, while considering the use of different cementitious materials (CM): Portland cement plus lime (B1), and Portland cement plus construction cement (B2). Mortar mixtures were designed for B1 and B2 with volume ratios of aggregates/CM, from 2.25 to 4, determining the fluency, the uniaxial compressive strength (UCS) and the wet electrical resistivity (WER). The relation between the fluency and the ratio water/CM were studied, concluding that the aggregate type and the proportions employed modify the fluency and the water demand in the fresh state of the mortar, and consequently impact the UCS and WER.

**Keywords:** construction mortars; electrical resistivity; fine aggregates; mechanical resistance; sieve analysis.

**Cite as:** Navarrete-Seras, M., Martinez-Molina, W., Chavez-Garcia, H. L., Sanchez-Calvillo, A., Arreola-Sanchez, M., Borrego-Perez, J. A., Perez-Castellanos, N. A., Ruiz-Torres, R. P., Duran-Ramos, A. M., Alonso-Guzman, E. M. (2023), "Influence of sand proportion in the physical and mechanical properties of construction and building mortars", Revista ALCONPAT, 13 (2), pp. 158 – 174, DOI: <https://doi.org/10.21041/ra.v13i2.684>

<sup>1</sup> Materials Department, Faculty of Civil Engineering, Universidad Michoacana de San Nicolás de Hidalgo, Morelia, Michoacán, México, 58040.

<sup>2</sup> Sustainable Energy, Machinery and Buildings (SEMB), Universitat de Lleida, Lleida, Spain, 25002.

<sup>3</sup> PIDA, Faculty of Architecture, Universidad Michoacana de San Nicolás de Hidalgo, Morelia, Michoacán, México 58040.

<sup>4</sup> Consejo Nacional de Ciencia y Tecnología, CONACYT.

<sup>5</sup> Instituto de Investigaciones Estéticas, UNAM, Coyoacán, CDMX, México, 04510.

<sup>6</sup> Faculty of Architecture, UNACH, Tuxtla Gutiérrez, Chiapas, México, 29050.

### Contribution of each author

En este trabajo la experimentación fue llevada a cabo por M. Navarrete-Seras (50%), A.M. Duran-Ramos (50%); la actividad de búsqueda bibliográfica M. Navarrete-Seras (25%), A.M. Duran-Ramos (25%), A. Sanchez-Calvillo (25%) y E.M. Alonso-Guzman (25%); la actividad de extracción de información por W. Martinez-Molina (20%), J.A. Borrego-Perez (20%), H.L. Chavez Garcia (20%), E.M. Alonso-Guzman (20%) y M. Arreola-Sanchez (20%); análisis y discusión de resultados por M. Navarrete (20%), W. Martinez-Molina (20%), M. Arreola-Sanchez (20%), J. A. Borrego-Perez (20%) y H.L. Chavez García (20%); la redacción del documento por A. Sanchez-Calvillo (20%), N.A. Perez-Castellanos (20%), R.P. Ruiz-Torres (20%), W. Martinez-Molina (20%) y M. Arreola-Sanchez (20%); la revisión del texto por A.M. Duran-Ramos (20%), N.A. Perez-Castellanos (20%), R.P. Ruiz-Torres (20%), M. Navarrete-Seras (20%) y E. M. Alonso-Guzman (20%); el diseño de figuras y la adaptación al formato por W. Martinez-Molina (25%), H. L. Chavez-Garcia (25%), M. Arreola-Sanchez (25%) y J.A. Borrego-Perez (25%); traducción al Inglés por A. Sanchez-Calvillo (60%), N.A. Perez-Castellanos (20%) y R. P. Ruiz-Torres (20%).

## Influencia de la proporción de arena en las propiedades físicas y mecánicas de morteros para la edificación

### RESUMEN

Se analizó la influencia de la proporción de arena en morteros Tipo II según norma N-CMT-2-01-004/02 empleando tres tipos de áridos de la región de Morelia, Michoacán determinando su influencia en sus propiedades físico-mecánicas, contemplando el uso de diferentes materiales cementantes (MC): el cemento Portland más cal (B1), cemento Portland más cemento de albañilería (B2). Se elaboraron mezclas para B1 y B2 con relaciones en volumen arena/MC, desde 2.25 hasta 4, determinando la fluidez, resistencia a compresión uniaxial (UCS) y resistividad eléctrica húmeda (WER). Se estudió la relación entre la fluidez y la cantidad de agua/MC, concluyendo que el tipo de árido y proporciones modifican la fluidez y demanda de agua en estado fresco impactando en UCS y WER.

**Palabras clave:** morteros de construcción; resistividad eléctrica; agregados finos; resistencia mecánica, granulometría.

## Influência da proporção de areia nas propriedades físicas e mecânicas de argamassas para construção

### RESUMO

As proporções de areia nas argamassas de tipo II foram analisadas de acordo com a norma N-CMT-2-01-004/02. Foram utilizados três tipos de agregados da região de Morelia, Michoacán para determinar a sua influência nas suas propriedades físico-mecânicas. Considerando a utilização de diferentes materiais cimentícios (CM): cimento Portland mais cimento de alvenaria (B2) e cimento Portland mais cal (B1). Foram preparadas misturas para B1 e B2 com relações areia/MC de 2,25 para 4. Foram determinadas a fluidez, resistência uniaxial à compressão (UCS) e resistividade elétrica úmida (WER). Estudando a relação entre a fluidez e a quantidade de água/MC, concluindo que o tipo de agregado e as proporções modificam a fluidez e a demanda de água no estado fresco com impacto no UCS e no WER.

**Palavras-chave:** argamassas de construção; resistividade elétrica; agregados finos; resistência mecânica, dimensão das partículas.

#### Creative Commons License

Copyright 2023 by the authors. This work is an Open-Access article published under the terms and conditions of an International Creative Commons Attribution 4.0 International License ([CC BY 4.0](https://creativecommons.org/licenses/by/4.0/)).

#### Discussions and subsequent corrections to the publication

Any dispute, including the replies of the authors, will be published in the first issue of 2024 provided that the information is received before the closing of the third issue of 2023.

#### Legal Information

Revista ALCONPAT is a quarterly publication by the Asociación Latinoamericana de Control de Calidad, Patología y Recuperación de la Construcción, Internacional, A.C., Km. 6 antigua carretera a Progreso, Mérida, Yucatán, 97310, Tel.5219997385893, [alconpat.int@gmail.com](mailto:alconpat.int@gmail.com), Website: [www.alconpat.org](http://www.alconpat.org)

Reservation of rights for exclusive use No.04-2013-011717330300-203, and ISSN 2007-6835, both granted by the Instituto Nacional de Derecho de Autor. Responsible editor: Pedro Castro Borges, Ph.D. Responsible for the last update of this issue, Informatics Unit ALCONPAT, Elizabeth Sabido Maldonado.

The views of the authors do not necessarily reflect the position of the editor.

The total or partial reproduction of the contents and images of the publication is carried out in accordance with the COPE code and the CC BY 4.0 license of the Revista ALCONPAT.

## 1. INTRODUCTION

Traditionally, the residential buildings have been built with different construction materials like the regular and irregular stones, ceramic bricks, wood, or earthen blocks among many others. These walls and floors often have joining mortars to bind the masonries, or to act as the coatings or refurbishments (which are called “plasters” or plastering” by archaeologists) that cover the wall systems (Álvarez Galindo et al., 1995). Mortars are mixtures of inorganic conglomerates, aggregates, water, and other elements used as additives. Their main purpose is joining the construction elements, filling the void spaces as binding agents, and protecting the surfaces and systems from external agents (Sánchez Tizapa et al., 2017; Wu et al., 2021).

In the ancient Rome the containers where the mixtures of lime paste and sand were transported were called “mortarius”; and over time this term has derived to the one utilized to designate the actual mixture. As a matter of fact, the first records of lime mortars can be found in the Vitruvius works, where the selection and manufacturing process of limestone are described to be used for building purposes (Navarro-Mendoza et al., 2023). These traditional systems were utilized for centuries in the construction of foundations, walls, pavements and coatings; until the appearance and popularization of Portland cement (Álvarez Galindo et al., 1995; Navarro-Mendoza et al., 2020).

The mortars have had multiple uses in the construction industry over time; for instance, in residential buildings, they were utilized to provide thermal and acoustic insulation properties, to avoid the proliferation of harmful or problematic fauna and flora, or to obtain certain aesthetic features. Regarding the joining purposes of the mortars, they need to achieve adequate mechanical resistances to allow the masonries of the structural elements to withstand the required loadings of the constructions.

Before the emergence of the contemporary construction cement, in Mexico, the artisans and builders used to add lime for increasing the setting times of the mortars. Lime had the function of retaining the water and allow the internal curing and hydration of the mortar. This mixture, resulting from the experience at works, receives the name of tertiary mortar, on account of the three employed elements: Portland cement, lime and fine aggregates.

This mortar is easy to purchase, as the basic elements required (water, adhesives and sand) to make the mixture are affordable, and the application of the product is simple. Nevertheless, the users have neglected the importance of the proper proportions of the components, and this situation has brought problems such as the decrease of the adherence and the mechanical resistance, structural deterioration, or shrinkage resulting into cracks that reduce the lifetime of the mortar (Jacques et al., 2023; Li et al., 2023). Additionally, in most cases, the physical and mechanical properties of the FA extracted from quarries are unknown, and the selection of the materials is determined by the cheap prices and proximity.

The type and proportions of the constituent materials of a mortar will influence the properties in the fresh state (Giordani & Masuero, 2019), and consequently, their performance in the hardened state (Haach et al., 2011). One of the most desired features during the fresh state is the workability, which must be adequate for the execution of the coating or render, to guarantee its performance in terms of adhesion to the substrate (Ribeiro & Oliveira Rey, 2019; Tena et al., 2017). Some elements which affect directly the mortar properties are the raw materials and their quality, especially the FA. Therefore, an adequate rheology analysis must be performed to determine if they comply with the established standards, and that the FA are not affecting the mortar viscosity and workability (Danish & Ozbakkaloglu, 2023; Li et al., 2022; Westerholm et al., 2008).

Typically, the FA represent more than 35% of the total volume of the mortar, being one of the most important components of the mixture. Consequently, using different FA with irregular shapes and an ineffective distribution will result in a deterioration of fluency properties, decreasing the density

and increasing the specific surface area while reducing the paste thickness (Hafid et al., 2016; Stolz & Masuero, 2018). The morphology of these FA also plays an important role in the physical properties, due to impact on mortar rheology (Durán Ramos, 2021; Ren et al., 2021).

Different studies have been carried out to understand the importance of the FA and their feasible substitution in mortar mixtures. It was reported how the single use of FA increased by 30% the plastic viscosity of the mortar designs (Hu, 2005); another research compared the difference in the performance of Portland cement mortars and geopolymers with residual fine glass aggregate (Gao et al., 2022); the carbonation behavior of mortars was also analyzed by adding different waste materials with cementitious and/or pozzolanic properties as replacements of the Portland cement, determining if the additions could limit or improve the carbonation of the mixtures when they harden (Martinez-Molina et al., 2021).

Other works investigated the suitability of waste plastic aggregates instead of FA, reporting that proportions from 10 to 20% may decrease the compressive strength and splitting tensile strength (Ullah et al., 2021). The influence of fiber additions was also analyzed on the fresh properties, as well as the deformability and the mechanical behavior (Brazão Farinha et al., 2021); also, the effects of additions like silica fume, superplasticizer and the water/binder ratio have been studied (Senff et al., 2009). The partial substitution of cement by limestone powder (0, 9, 16, 23 and 30 %) has proven an affectation in the rheological, mechanical and durability properties (Souza et al., 2020), as well as fine eggshell powder (Beng Wei et al., 2021), or natural pozzolans (HAMMAT et al., 2021).

The issues described about the importance of the FA properties within the mortars, as well as the ambiguity of the Mexican standards (NMX-C-486-ONNCCE-2014 and N-CMT-2-01-004/02) regarding the water and CM proportions led to this research. It is important to note that the analyses were performed with sand quarries from a particular region of Mexico (in Morelia). The relevance of the research relies on the visualization of the differences in the workability and the hardened state of the mortars in function of the different FA quarries of the same region; furthermore, it allows to assess the reliability and quality of the mortars used as structural coatings.

The present research work focuses on the analysis of the relation FA/CM to comply with the existing regulations, while determining the maximum amount of sand utilized to design a mortar with structural purposes. Additionally, three different natural sands (FA) were studied, with different combinations of hydraulic cement (Portland cement), construction cement, and lime; analyzing the influence of sand proportion in the physico-mechanical properties of the mortars. These mixtures were characterized with non-destructive techniques and mechanical tests to assess the better combinations in function of the regulation requirements. All of this, with the objective of increasing the scientific and technical knowledge of the common construction and building mortars, impacting positively on their quality and durability.

## 2. MATERIALS AND PROCEDURE METHODS

The mortars were designed to be used outside and inside the buildings, but they were particularly conceived for self-construction purposes in residential housing. In the standard N-CMT-2-01-004/02, the masonry mortars are classified into three classes: I, II, and III, depending on the components and the minimum mechanical resistance value. The mixtures were based on the mortars Type II (ONNCCEE, 2002), consisting in a combination of cement, lime, and different proportions of sand to determine the better behaviors. The sand proportion should not be less than 2.25 nor more than 4 times the sum of the CM in volume.

In this research, all the mortar mixtures were designed and tested in the materials laboratory, starting from the characterization and quality control of the prime materials. The cement employed, CPC 30R RS, is classified as Type II according to the standard ASTM C150-C150M-22 (ASTM

International, 2022c). Conversely, the lime complies with the standard ASTM E1266-20 (ASTM International, 2020b). The sands were sampled from quarries in the State of Michoacan, in Mexico, and tested in the laboratory, with each data being the average of three tests. The physical characterization of the sands was performed as indicated in American Society and Testing and Materials (ASTM) international standards, and the Organismo Nacional de Normalización y Certificación de la Construcción y Edificación (ONNCCE) of Mexico.

The mixtures were elaborated and then the fluency in fresh state was determined, later they were tested to obtain mechanical properties like the Uniaxial Compressive Strength (UCS), considering the minimum resistance of 75 kgf/cm<sup>2</sup> requested by the standard NMX-C-486-ONNCCE-2014 (ONNCCE, 2014); or other characteristics by means of non-destructive techniques (NDT), like the Wet Electrical Resistivity (WER) at 7 and 28 days of age.

## 2.1 Design of the mixtures

The mortar specimens, all being type II according to the standards, were prepared in laboratory conditions with different proportions of cement, lime, aggregates and water, as it is shown in Table 1. Half of the mortars (B1) were prepared with hydraulic cement, lime and sand; while the other half (B2) were prepared mixing hydraulic cement, construction cement and sand. For both kind of mortars, different proportions of sand (from 2.25 to 4) were used, obtaining a great quantity of samples; for all of them the standard fluidity, which must range between 105% and 130% (ONNCCE, 2015b), was calculated. Later, the samples were cured in water as it is indicated in the standard ASTM C31-C31M-22 (ASTM International, 2022a), and the water employed was obtained from the public water network of the UMSNH university campus. 6 cubes were made for each mixture, resulting in 96 cubes for each type of sand due to the multiple combinations and proportions.

Table 1. Mixture design and proportions.

Code	Hydraulic cement (Portland cement)	Construction cement	Lime	Sand
B1	1	-	½	2.25, 2.5, 2.75, 3, 3.25, 3.5, 3.75, 4
B2	1	1	-	2.25, 2.5, 2.75, 3, 3.25, 3.5, 3.75, 4

## 2.2 Characterization and properties of the fine aggregates

The FA were extracted from surrounding quarry stones in the state of Michoacan, in Mexico. The State of Michoacan is located in the Trans-Mexican Volcanic Belt, where the extrusive igneous rocks and the siliceous materials are abundant, like the river aggregates or the quartz sands. The three FA utilized in this research are all natural sands, not being submitted to any grinding or artificial procedures. First, we find the “El Coro” quarry (CH) in the municipality of Zinapécuaro, near the Cuitzeo Lake, in Latitude 19.893889, Longitude -100.875833; secondly, the “El Cuervo” quarry (R), near the Huajumbaro river in the Balsas basin region, in Latitude 19.626110, Longitude -100.636667; last, the “Joyitas” quarry (J), in Morelia, Latitude 19.727222, Longitude -101.385278. The three sands are displayed in figure 1.



Figure 1. Sand aggregates: a) Joyitas volcanic sand; b) El Coro volcanic silty sand; (c) El Cuervo river sand. Image sources: (Durán, 2021; Durán, 2021; Mondragón, 2021).

The sands were sampled from the mentioned quarries and transported to the materials laboratory to be analyzed. They were dried and prepared as representative sampling quantities (100 kg) to undertake the mortars design process. The geomaterials don't have the same strict quality control as the cement, because of their natural origin; instead, commonly, the mortars are based on the previous experience of users, artisans and builders. The table 2 presents the set of characterization methods applied for the three different FA utilized in the research work before the manufacturing of the mortars (ASTM International, 2017, 2018, 2019b, 2022b; ONNCCE, 2004, 2006, 2020).

Table 2. Test methods performed on the aggregates.

Test method	Standard	CH	R	J
Standard Practice for Sampling Aggregates (kg)	ASTM D75/D75M-19	100	100	100
Standard Test Method for Relative Density (Specific Gravity) and Absorption of Fine Aggregate (g/cm <sup>3</sup> ) Aggregates – Determination of the relative density and water absorption of fine aggregate – Test method (g/cm <sup>3</sup> )	ASTM C128-22 NMX-C-165-ONNCCE	2.22	2.13	2.40
Standard Test Method for Relative Density (Specific Gravity) and Absorption of Fine Aggregate (%) Aggregates – Determination of the relative density and water absorption of fine aggregate – Test method (g/cm <sup>3</sup> )	ASTM C128-22 NMX-C-165-ONNCCE	7.02	5.92	4.75
Standard Test Method for Bulk Density and Voids in Aggregate (g/cm <sup>3</sup> ) Aggregate for Concrete - Volumetric Mass - Test Method (g/cm <sup>3</sup> )	ASTM C29/C29M-17a NMX-C-073-ONNCCE	1.18	1.23	1.36
Standard Test Method for Bulk Density and Voids in Aggregate (g/cm <sup>3</sup> ) Aggregates Particles Finer Than 0.075 mm (No. 200) Sieve by Washing – Test Method (g/cm <sup>3</sup> )	ASTM C29/C29M-17a NMX-C-084-ONNCCE	1.28	1.36	1.42
Standard Specification for Concrete Aggregates (fineness modulus)	ASTM C33-C33M-18	3.51	2.98	3.87

\* The density and absorption values are detached in the table but they correspond to the same standards.

The bulk density was calculated for all the sands, obtaining similar results for each specimen (ASTM International, 2017); on the other hand, the CH material had an absorption coefficient higher than 7%, while J had a lower value of 4.75%, being a prominent feature. This condition can have a direct affectation on the mortar's properties, as it could increase the water demand and consequently decrease the compression strength.

The figure 2 displays the sieve analysis and particle size of the different FA used in the research. The upper and lower limits of the standard are represented (ASTM International, 2018), showing how R adapts perfectly to the granulometric curve; on the other hand, CH presents an excess of

fine material from the 0.1 to 0.4 mm range approximately, while R slightly oversteps the lower limit. These conditions can have consequences on some properties of the mortar mixtures like the fluency and the water demand in the fresh state of the mortars, as it will be displayed later in figures 6 and 7.

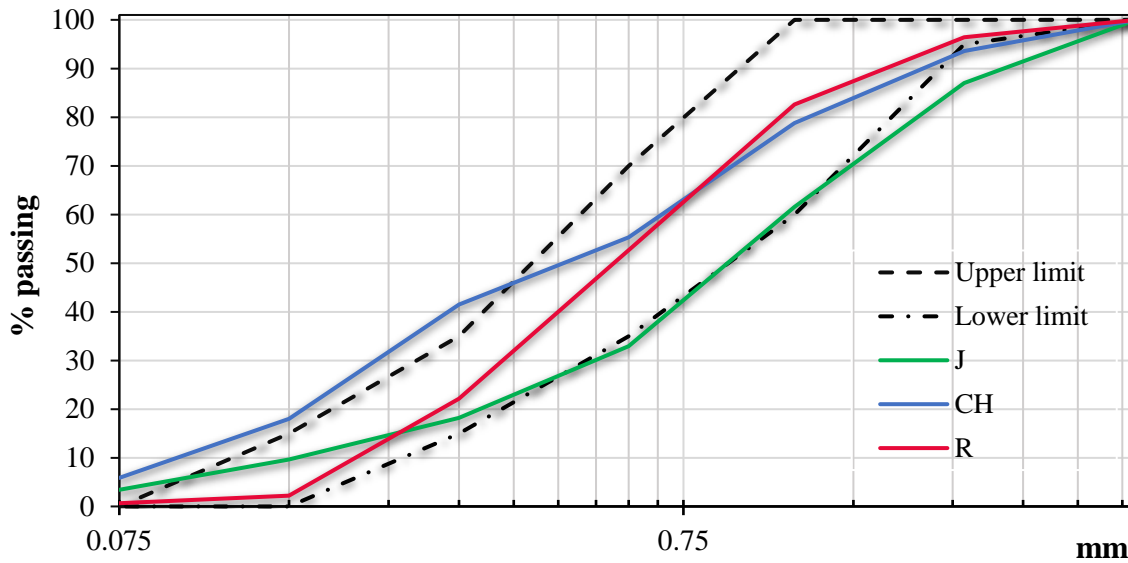


Figure 2. Sieve analysis of the sand aggregates.

### 2.3 Test methods performed on the mortars

The Table 3 displays the set of test methods used for the characterization of the mortar mixtures in both fresh and hardened state. The international and Mexican standards (ASTM and ONNCCE) were followed to analyze the different combinations. Additionally, the three trials and their procedure are detailed in the following section (ASTM International, 2019a, 2020a, 2021; ONNCCE, 2014, 2015a, 2019).

Table 3. Test methods performed on the mortars.

Test methods	Standard	Conditions
Uniaxial Compression Strength (UCS)	ASTM C109/C109M-21 NMX-C-486-ONNCCE-2014	Solid cubes 5x5x5 cm <sup>3</sup>
Wet Electrical Resistivity (WER)	ASTM C1876-19 NMX-C-514-ONNCCE-2016	Solid cubes 5x5x5 cm <sup>3</sup>
Mechanical Mixing of Hydraulic Cement Pastes and Mortars of Plastic Consistency	ASTM C305-20 NMX-C-061-ONNCCE-2015	Fresh state mixture

#### 2.3.1. Fluency

The fluency test (see figure 3) allows to determine the flow or workability of the mortar mixture in fresh state, according to the water content utilized. The trial denotes the consistency of the mixture as well as its suitability for each specific technique and application, according equation 1. The limits required for this the test rely in a range between 105 and 130 %

$$Fluency (\%) = \frac{Extended\ diameter - 25\ cm}{25\ cm} \times 100 \tag{1}$$



Figure 3. Trials on the mortar mixtures: a) Mixture in mold; b) Consistency; c) Adherence. Image source: (Duran, 2021).

### 2.3.2. Wet Electrical Resistivity (WER)

The WER is an alternative test to evaluate the homogeneity in concrete matrices, allowing us to obtain relevant information about the performance of the material, without physically compromising the structure, being a NDT. The test was performed according to standards NMX-C-514-ONNCCE and ASTM C1876-19 (see figure 4). The procedure is based on the Ohm's Law, that indicates that the electrical resistivity is a reciprocal property of the conductivity, as it is considered a volumetric property of materials that indicates their resistance to the passage of electric charges. The WER is represented by the following equation 2, where R is the electrical resistivity in  $k\Omega\text{-cm}$ , l is the specimen length in cm and A is the specimen cross-sectional area in  $\text{cm}^2$ .

$$R = \frac{V}{I} = \rho \frac{l}{A} \quad (2)$$



Figure 4. Nilsson resistivity apparatus.

### 2.3.3. Uniaxial compressive strength (UCS)

The objective of this test is determining the uniaxial compressive strength (UCS) of 50 mm cubic specimens (see figure 5), standardized by the standards NMX-C-486-ONNCCE and ASTM C109/C109M-21. The UCS is obtained with equation 3, where UCS is the uniaxial compressive strength in  $\text{kgf/cm}^2$ , W is the maximum load of the specimen in kgf, and A is the specimen contact area, in  $\text{cm}^2$ .

$$UCS = \frac{W}{A} \quad (3)$$



Figure 5. Uniaxial compressive strength (UCS) testing machine for mortars.

### 3. RESULTS

The research work analyzed the properties of the three FA in the mortar mixtures and their different dosages. The figure 6 displays the comparison between the fluency of the three FA and the volumetric relation of the water content and the CM of each B1 specimen; in this case the aggregates CH and J required the same amount of water (the curves overlap), while R needed less content, similar than the research performed by Hu et al. (2005). On the other hand, the figure 7 shows the results of the B2 mortars; in this case, each sand required different quantity of water, and until the 3.25 proportion, the water demand for R was the lower of all the FA, like other authors reported before (Durán Ramos, 2021; Ren et al., 2021). As it was mentioned before, the fluency limits must range between 105 and 130 %, and all the samples fulfilled this condition. For both classes of mortars, it was corroborated that with a higher sand proportion the water/CM ratio also increases, according to Giordani and Masuero (2019).

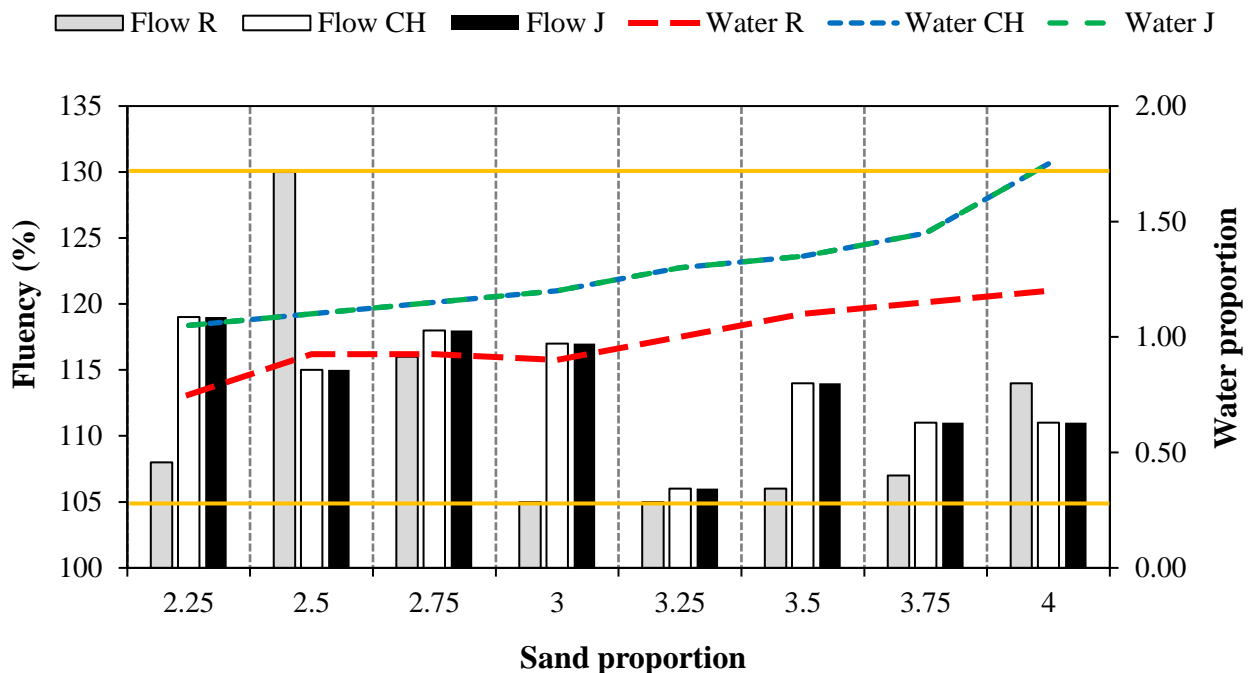


Figure 6. Fluency and volumetric relation of water/CM of B1 mortars.

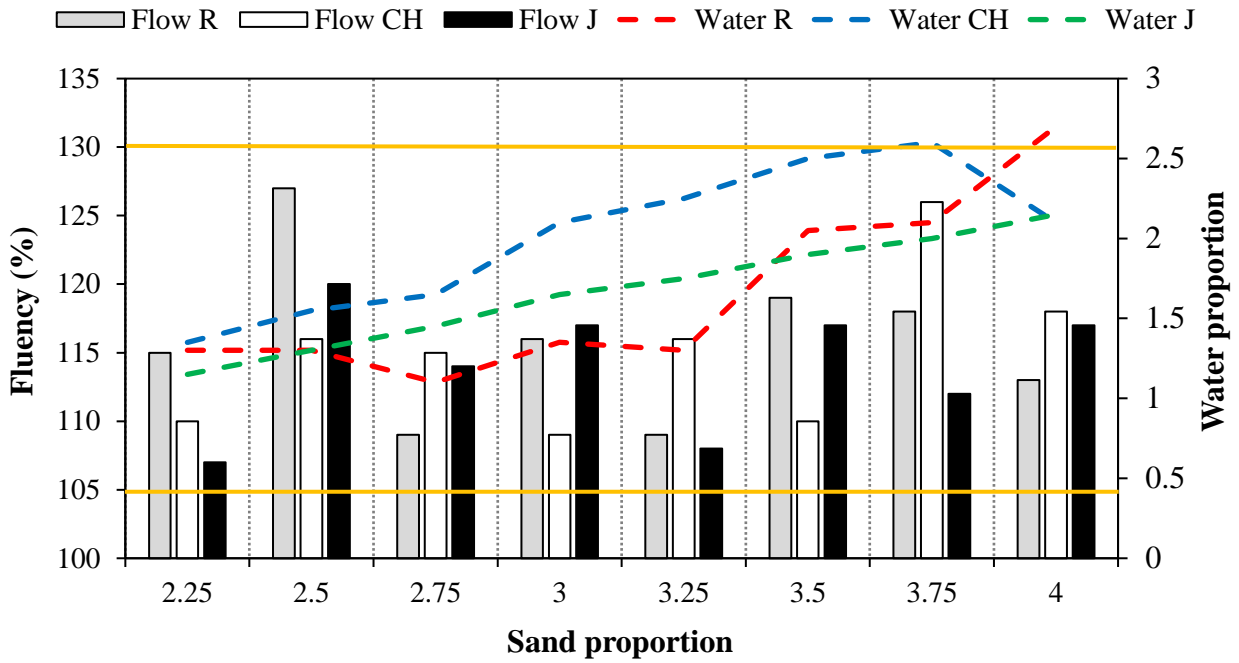


Figure 7. Fluency and volumetric relation of water/CM of B2 mortars.

Figures 8 and 9 display the results of the WER test at 7 and 28 days for B1 and B2 mortars. We can also find the behavior of the three different FA employed and how they work with the different cementitious materials. The minimum limit suggested by the standard NMX-C-514-ONNCCE-2019 is 10 kΩ-cm; a higher value might suggest an excessive porosity of the mortars. All the samples complied with the standard, being able to be utilized as Type II mortars for building construction; nevertheless, we can find higher results for the B2 mortars, which are closer to the minimum limit. For both B1 and B2, the CH sand was the one that presented higher electrical resistivity values, which could be related with the higher content of coarse material and the lower density obtained.

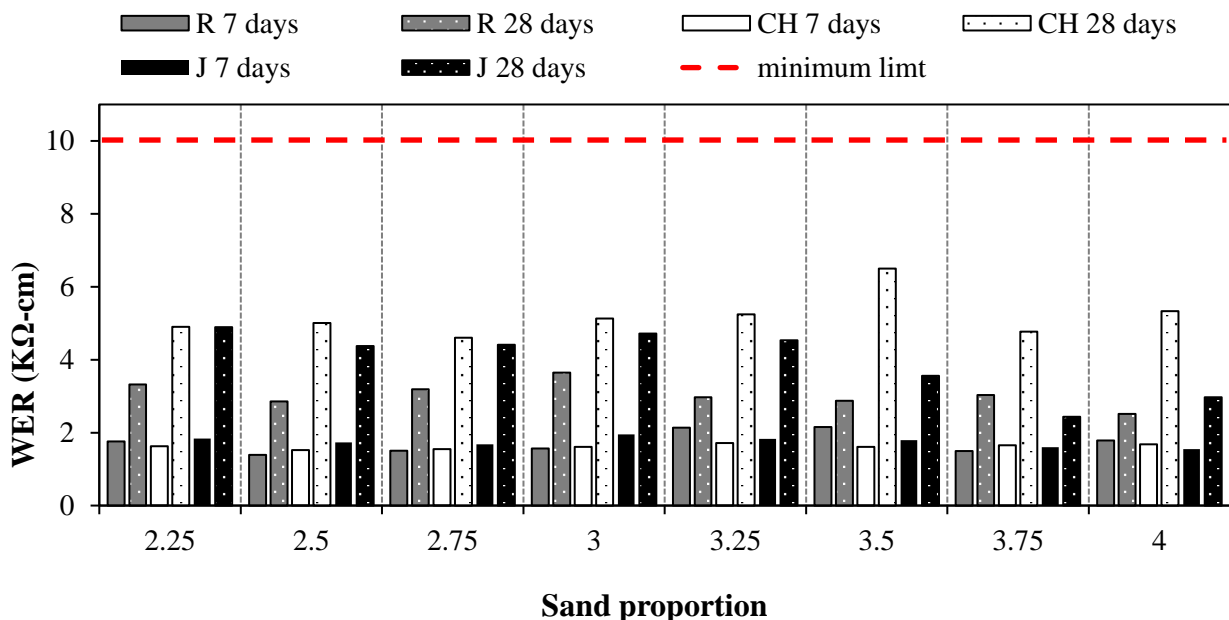


Figure 8. Wet electrical resistivity of B1 mortars as a function of the sand proportion.

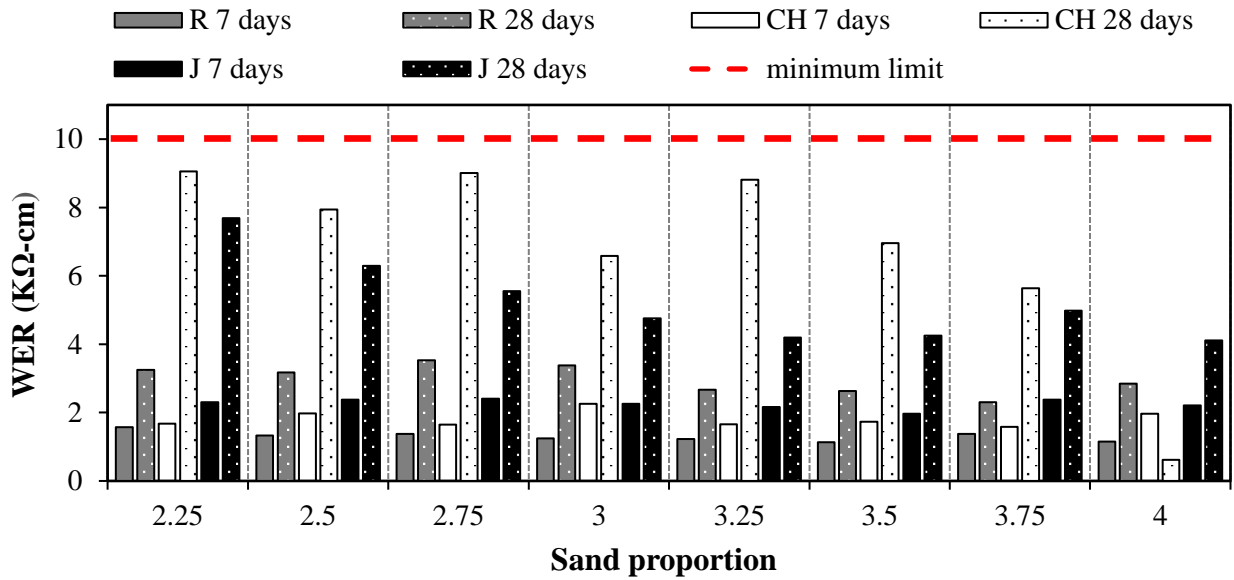


Figure 9. Wet electrical resistivity of B2 mortars as a function of the sand proportion.

Figures 10 and 11 show the UCS of B1 and B2 mortars in function of the sand proportions utilized (from 2.25 to 4), at 7 and 28 days respectively. The minimum individual compressive strength required is  $f_j = 75 \text{ kg/cm}^2$  (7.5 MPa), according to the standard N-CMT-2-01-004/02, considering the utilization and application of these mortars.

Logically, the mortars increased their resistance over time, as the samples at 28 days reported higher values. In general, the sand proportions from 2.25 to 3 worked better, since from the 3.25 value, the mixtures did not comply with the standard. We can see how the B1 lime mortars functioned better, with more specimens reaching the minimum strength required of  $75 \text{ kgf/cm}^2$ , according to the results reported by other authors (Beng Wei et al., 2021; HAMMAT et al., 2021; Souza et al., 2020). For B1 mortars the best aggregate was R; while for the B2 mortars, the best one was J.

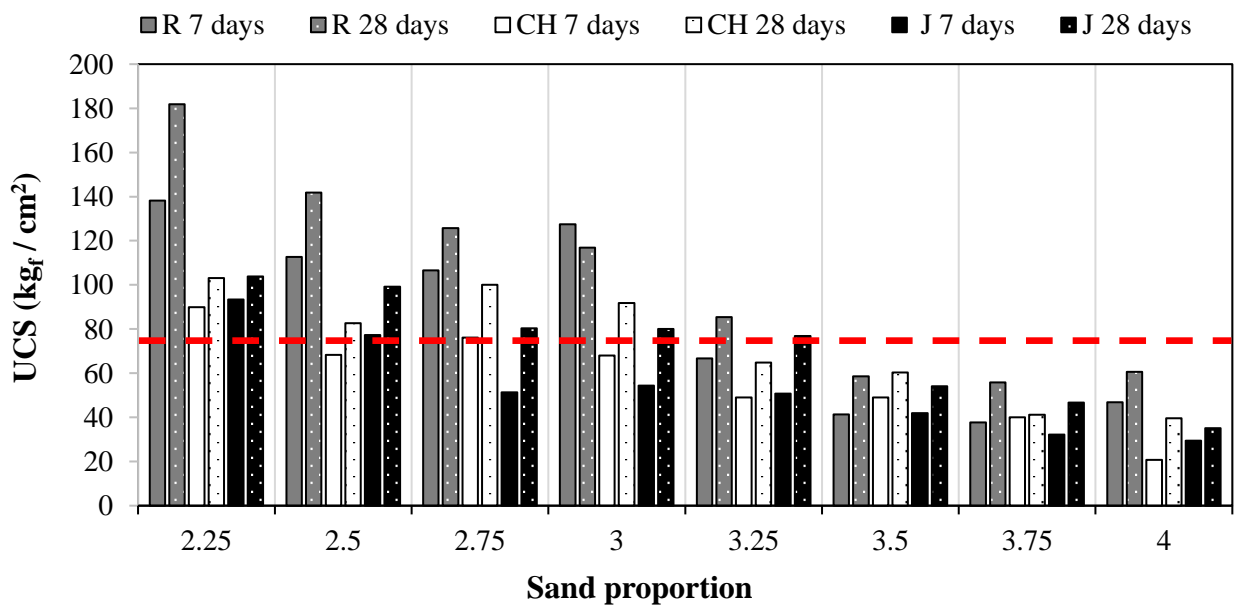


Figure 10. Compressive strength of B1 mortars as a function of the sand proportion.

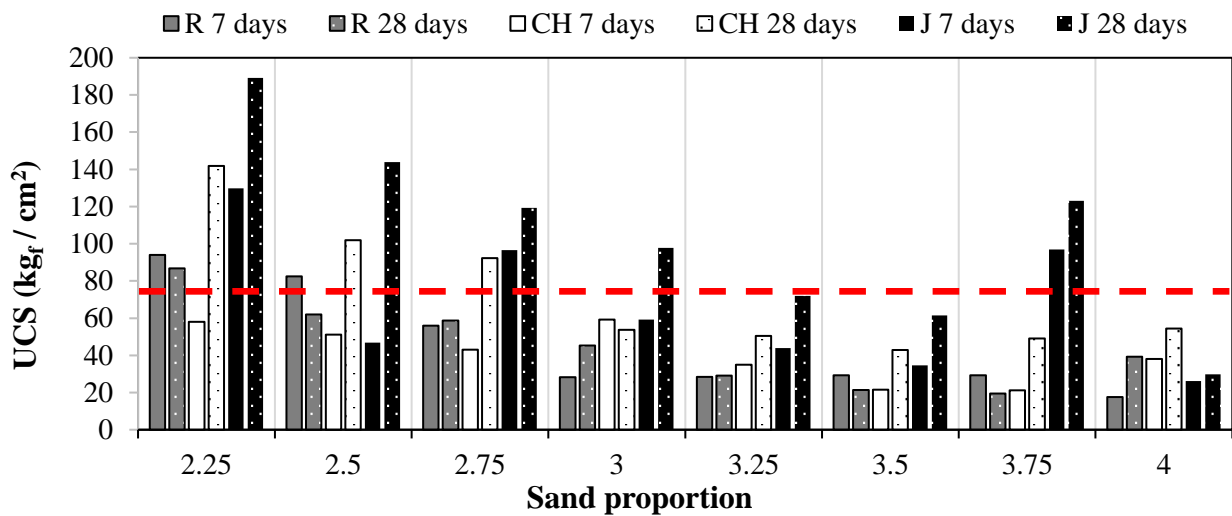


Figure 11. Compressive strength of B2 mortars as a function of the sand proportion.

The figure 12 shows the correlation of the designed mortars between the UCS and the WER results at 28 days. The aggregate J presented the best trend line with a correlation coefficient of  $R^2 = 0.87$  for the B2 type mortars and  $R^2 = 0.87$  for the B1 mixtures. This great correlation of the two method tests could be related to the low absorption and high density of the material, in addition to its granulometric curve with a good distribution according to the standard ASTM C-91. On the other hand, the R and CH sands evidenced a worst correlation, especially the last. These mortars presented higher water absorption and more fine material during the sieve analysis, which increased the water demand and consequently the water/CM ratio, as it was reported before by Haach et al. (2011).

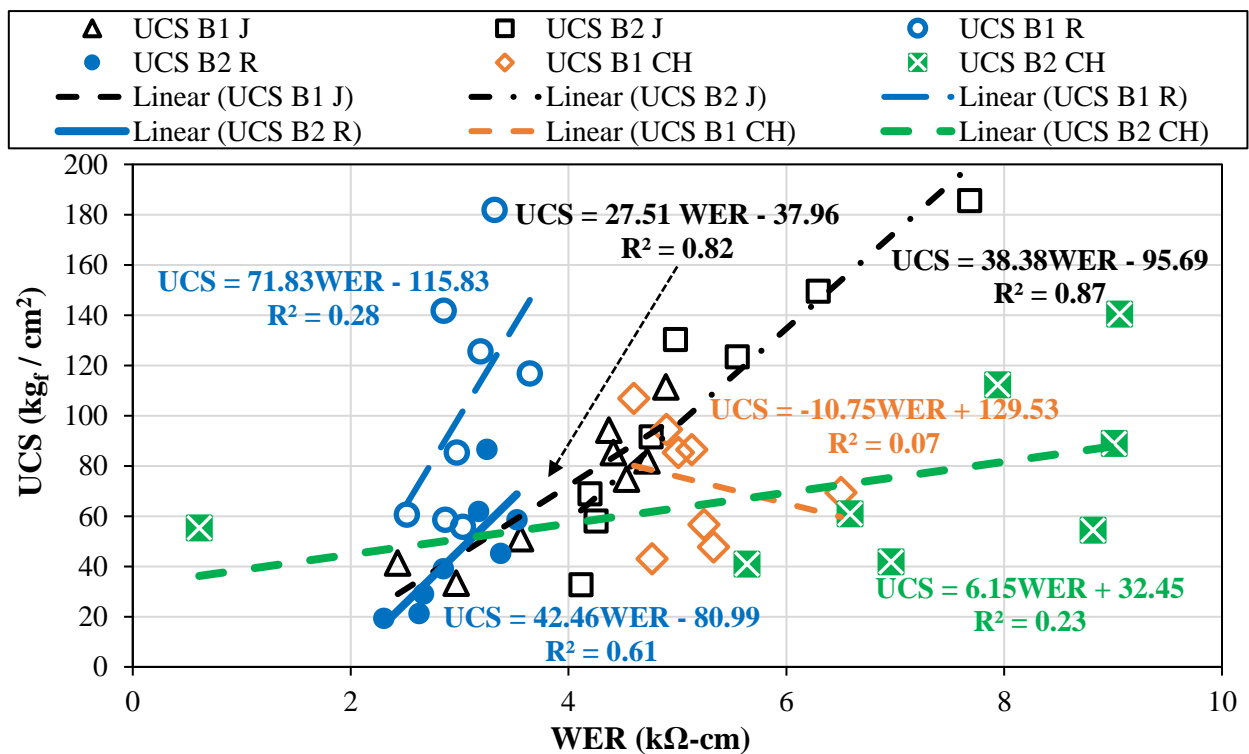


Figure 12. Correlation between UCS and WER of the mortars at 28 days.

## 4. DISCUSSION

The Joyitas sand (J) historically has been the most employed material by the builders and artisans in the region near Morelia, in Michoacan. This dark volcanic sand, according to the sieve analysis presented fewer fine materials and a slightly excess of coarse grains, which were retained in the meshes n° 16 and 30, providing a greater mechanical behavior compared to the two other quarries. Furthermore, J presented greater density values and the lowest water absorption, justifying the choice of the local users in the region.

The characterization process allowed to assess the three FA and determine how they work with each type of mortar (B1 and B2) and which proportions obtain the best results. It is important to understand that other than the compliance with the minimum requirements, each mixture could be useful under specific conditions. The WER test is a great NDT to assess the durability of concretes and mortars, and infer the porosity, while all this data can be related to the sieve analysis and particle size of the studied sands. To this effect, the CH sand presented the higher electrical resistivity values, while it contained great amounts of fine material retained in the meshes #100 and #200, and they act as fillers, sealing the porosity of the mixtures and impeding the permeability of depassivating ions, which could reduce the durability of reinforced concrete and mortar structures, as some researchers reported (Durán Ramos, 2021; Giordani & Masuero, 2019; Haach et al., 2011; Ren et al., 2021).

The lower sand proportions achieved the better mechanical behavior, at the same time that they complied with the fluency required values for mortar design. Regarding the WER, all the specimens remained under the limit of 10 kΩ-cm imposed by the standard NMX-C- 514-2019. Even though this parameter is associated to concrete mixtures, the mortars were designed with high ratios of water/CM, as it is displayed in the figures 8 and 9. Due to the desired fluency requirements to achieve a good workability, the mortars need good adherence either for its use as joining elements or coatings.

Additionally, it was corroborated how the sand proportion has a direct correlation with the water demand, resulting in an increase of the water/CM ratio. Therefore, the better and more adequate mortars are the ones with lower sand proportions without taking account of their typology or cementitious products employed, like other authors have stated (Hafid et al., 2016; Stolz & Masuero, 2018). It is interesting to prove how the B1 mortars achieved a satisfactory performance for all the test methods, considering that they were elaborated with lime, a material which is known for its low strength (Souza et al., 2020), and commonly substituted by Portland cement (Navarro-Mendoza et al., 2023). Notwithstanding the lower mechanical behavior of the B1 mixtures, they had a considerably lower water demand than B2, while they achieved the same fluency requirements, being this a great attribute to consider.

The WER technique has demonstrated to be really useful to characterize materials and components while assessing their durability. The higher correlation values of  $R^2$  for J sands indicate how the density, the electrical resistivity and the mechanical resistance are related. The correlation coefficient between UCS and WER is strongly related with the absorption and density of the FA. When these two variables increase, the coefficient will considerably alter, with a dispersion of the data. For this reason, it is important to combine the NDT with the mechanical test methods to have a better understanding of the construction and building materials.

According to the regulations, the fineness modulus (FN) of the FA employed in mortars for construction and building processes must range between 1.6 and 2.5. The three sands analyzed met this parameter: CH presented the lower FM value, with 2.06; also presenting a slight excess of fine material, as it was shown in figure 2. These particles can act as fillers, shuttering the porosity and consequently increasing the electrical resistivity of mortars B1 and especially B2, compromising the durability of the mortars at 28 days.

## 5. CONCLUSIONS

The results showed how the water demand of the studied mortars increases at the same time than the relation FA/CM. For both mixtures, B1 and B2, the reduction of the volumetric proportion of FA/CM, increased the UCS, while the fluency remained in the expected range of 105 to 130 %. Regarding the water/CM relation, it increased with the sand proportion from 1.10 to 1.80 for the B1 mixtures, and from 1.10 to 2.60 for the B2 mixtures; noting that the incorporation of lime improves this relation, especially for the higher sand proportions.

Regarding the WER, at early ages of 7 days both mixtures B1 and B2 presented a similar behavior, with slight advantage of J over CH and R; however, at 28 days CH stood out for B2 mixtures, with a closer value to 10 k $\Omega$ -cm for the FA/CM ratio of 2.25 (the minimum WER required for the elaboration of hydraulic concrete mixtures considering the corrosion velocity).

With the results obtained in this research, it is confirmed that is necessary to study and characterize properly the construction materials, especially the compound ones like the construction and building mortars. An inadequate utilization of the FA and the CM could affect hugely their mechanical resistance. These research works enhance the technical and scientific knowledge of construction mortars, allowing the builders and workers to make better decisions based in these formal studies.

## 6. ACKNOWLEDGEMENTS

Authors want to acknowledge the sponsor by CIC Projects of the Universidad Michoacana de San Nicolas de Hidalgo (UMSNH); and also the funding by Consejo Nacional de Ciencia y Tecnología (CONACYT), through the Project PRONACE 321260: Desarrollo de un modelo de producción social replicable de vivienda y habitat, and the Project CF-2023-G-985, Concretos y morteros auto degradantes de biota y compuestos contaminantes presentes en la atmósfera, para su aplicación en vivienda digna de interés social, en ciudades medias mexicanas; the SEP-Prodep program; and the technical support of the Laboratory “Ing. Luis Silva Ruelas”, in the Faculty of Civil Engineering of UMSNH. Finally, the authors thank the civil engineering students Ana Miriam Duran Ramos and Saul Mondragon-Martinez for their support during the laboratory tests.

## 7. REFERENCES

- Álvarez Galindo, J. I., Martín Pérez, A., García Casado, P. J. (1995). *Historia de los morteros*. Revista PH, 13, 52. <https://doi.org/10.33349/1995.13.263>
- ASTM International. (2017). *ASTM C29/C29M 17a. Standard Test Method for Bulk Density (“Unit Weight”) and Voids in Aggregate*. ASTM International.
- ASTM International. (2018). *ASTM C33-C33M-18. Standard Specification for Concrete Aggregates*. ASTM International. [https://doi.org/10.1520/C0033\\_C0033M-18](https://doi.org/10.1520/C0033_C0033M-18)
- ASTM International. (2019a). *ASTM C1876-19. Standard Test Method for Bulk Electrical Resistivity or Bulk Conductivity of Concrete*. ASTM International. <https://doi.org/10.1520/C1876-19>
- ASTM International. (2019b). *ASTM D75/D75M-19. Standard Practice for Sampling Aggregates*. ASTM International.
- ASTM International. (2020a). *ASTM C305-20. Standard Practice for Mechanical Mixing of Hydraulic Cement Pastes and Mortars of Plastic Consistency*. ASTM International. <https://doi.org/10.1520/C0305-20>

- ASTM International. (2020b). *ASTM E1266-20. Standard Practice for Processing Mixtures of Lime, Fly Ash, and Heavy Metal Wastes in Structural Fills and Other Construction Applications*. ASTM International. <https://doi.org/10.1520/E1266-20>
- ASTM International. (2021). *ASTM C109/C109M-21. Standard Test Method for Compressive Strength of Hydraulic Cement Mortars (Using 2-in. or [50 mm] Cube Specimens)*. ASTM International. [https://doi.org/10.1520/C0109\\_C0109M-21](https://doi.org/10.1520/C0109_C0109M-21)
- ASTM International. (2022a). *ASTM C31/C31M-22. Standard Practice for Making and Curing Concrete Test Specimens in the Field*. ASTM International. [https://doi.org/10.1520/C0031\\_C0031M-22](https://doi.org/10.1520/C0031_C0031M-22)
- ASTM International. (2022b). *ASTM C128-22. Standard Test Method for Relative Density (Specific Gravity) and Absorption of Fine Aggregate*. ASTM International.
- ASTM International. (2022c). *ASTM C150-C150M-22. Standard Specification for Portland Cement*. ASTM International. <https://doi.org/10.1520/C0150-07>
- Beng Wei, C., Othman, R., Yee Ying, C., Putra Jaya, R., Shu Ing, D., Ali Mangi, S. (2021). *Properties of mortar with fine eggshell powder as partial cement replacement*. *Materials Today: Proceedings*, 46, 1574–1581. <https://doi.org/10.1016/j.matpr.2020.07.240>
- Brazão Farinha, C., de Brito, J., Veiga, R. (2021). *Incorporation of high contents of textile, acrylic and glass waste fibres in cement-based mortars. Influence on mortars' fresh, mechanical and deformability behaviour*. *Construction and Building Materials*, 303, 124424. <https://doi.org/10.1016/j.conbuildmat.2021.124424>
- Danish, A., Ozbakkaloglu, T. (2023). *Impact of nano-silica on the mechanical properties of mortar containing e-waste plastic as fine aggregates*. *Materials Today: Proceedings*. <https://doi.org/10.1016/j.matpr.2023.03.182>
- Durán Ramos, A. M. (2021). *Diseño de mezclas plásticas aglomerantes y su consideración de proporcionamiento por medio del ensayo de fluidez (Bachelor's Degree Thesis)*. Universidad Michoacana de San Nicolás de Hidalgo.
- Gao, X., Yao, X., Xie, R., Li, X., Cheng, J., Yang, T. (2022). *Performance of fly ash-based geopolymer mortars with waste cathode ray tubes glass fine aggregate: A comparative study with cement mortars*. *Construction and Building Materials*, 344, 128243. <https://doi.org/10.1016/j.conbuildmat.2022.128243>
- Giordani, C., Masuero, A. B. (2019). *Blended mortars: Influence of the constituents and proportioning in the fresh state*. *Construction and Building Materials*, 210, 574–587. <https://doi.org/10.1016/j.conbuildmat.2019.02.077>
- Haach, V. G., Vasconcelos, G., Lourenço, P. B. (2011). *Influence of aggregates grading and water/cement ratio in workability and hardened properties of mortars*. *Construction and Building Materials*, 25(6), 2980–2987. <https://doi.org/10.1016/j.conbuildmat.2010.11.011>
- Hafid, H., Ovarlez, G., Toussaint, F., Jezequel, P. H., Roussel, N. (2016). *Effect of particle morphological parameters on sand grains packing properties and rheology of model mortars*. *Cement and Concrete Research*, 80, 44–51. <https://doi.org/10.1016/j.cemconres.2015.11.002>
- Hammat, S., Menadi, B., Kenai, S., Thomas, C., Kirgiz, M. S., Sousa Galdino, A. G. de. (2021). *The effect of content and fineness of natural pozzolana on the rheological, mechanical, and durability properties of self-compacting mortar*. *Journal of Building Engineering*, 44, 103276. <https://doi.org/10.1016/j.jobbe.2021.103276>
- Hu, J. (2005). *A study of effects of aggregate on concrete rheology* [Iowa State University, Digital Repository]. <https://doi.org/10.31274/rtd-180813-15380>
- Jacques, K. T. J., Zengyao, W., Shoude, W., Shifeng, H., Xin, C. (2023). *The influence of different fine aggregate and cooling regimes on the engineering properties of sulphoaluminate cement mortar after heating*. *Case Studies in Construction Materials*, 18, e01866. <https://doi.org/10.1016/j.cscm.2023.e01866>

- Li, T., Nogueira, R., de Brito, J., & Liu, J. (2023). *Underlying mechanisms of the influence of fine aggregates' content and properties on mortar's plastic viscosity*. Journal of Building Engineering, 67, 106016. <https://doi.org/10.1016/j.jobe.2023.106016>
- Li, T., Zhou, Y., Zhu, J., Liu, J. (2022). *Effect of fine aggregate gradation on the rheology of mortar*. Construction and Building Materials, 332, 127362. <https://doi.org/10.1016/j.conbuildmat.2022.127362>
- Martinez-Molina, W., Chavez-Garcia, H. L., Perez-Lopez, T., Alonso-Guzman, E. M., Arreola-Sanchez, M., Navarrete-Seras, M. A., Borrego-Perez, J. A., Sanchez-Calvillo, A., Guzman-Torres, J. A., Perez-Quiroz, J. T. (2021). *Effect of the Addition of Agribusiness and Industrial Wastes as a Partial Substitution of Portland Cement for the Carbonation of Mortars*. Materials, 14(23), 7276. <https://doi.org/10.3390/ma14237276>
- Navarro-Mendoza, E. G., Alonso-Guzman, E. M., Ruvalcaba-Sil, J. L., Sánchez-Calvillo, A., Martínez-Molina, W., García, H. L. C., Bedolla-Arroyo, J. A., Becerra-Santacruz, H., Borrego-Pérez, J. A. (2020). *Compressive strength and ultrasonic pulse velocity of mortars and pastes, elaborated with slaked lime and high purity hydrated lime, for restoration works in Mexico*. In Key Engineering Materials: Vol. 862 KEM. <https://doi.org/10.4028/www.scientific.net/KEM.862.51>
- Navarro-Mendoza, E. G., Alonso-Guzman, E. M., Sanchez-Calvillo, A., Bedolla-Arroyo, J. A., Becerra-Santacruz, H., Navarro-Ezquerria, A., Gonzalez-Sanchez, B., Martinez-Molina, W. (2023). *Physical and Mechanical Characterization of Lime Pastes and Mortars for Use in Restoration*. Heritage, 6(3), 2582–2600. <https://doi.org/10.3390/heritage6030136>
- ONNCCE. (2004). *NMX-C-073-ONNCCE-2004. Industria de la construcción - Agregados - Masa volumétrica. Método de prueba*. Organismo Nacional de Normalización y Certificación de la Construcción y Edificación.
- ONNCCE. (2006). *NMX-C-084-ONNCCE-2006. Industria de la construcción - Agregados para Concreto - Partículas más Finas que la Criba 0,075 mm (No. 200) por Medio de Lavado – Método de Prueba*. Organismo Nacional de Normalización y Certificación de la Construcción y Edificación.
- ONNCCE. (2014). *NMX-C-486-ONNCCE-2014. Industria de la construcción-Mampostería - Mortero para uso estructural- especificaciones y métodos de ensayo*. Organismo Nacional de Normalización y Certificación de la Construcción y la Edificación.
- ONNCCE. (2015a). *NMX-C-061-ONNCCE-2015. Building Industry – Hydraulic Cements – Determination of Compressive Strength of Hydraulic Cements*. Organismo Nacional de Normalización y Certificación de la Construcción y Edificación.
- ONNCCE. (2015b). *NMX-C-144-ONNCCE-2015. Building Industry - Hydraulic Cement - Specifications for the Apparatus used in the Flow Test for Mortars made of Hydraulic Cements*. Organismo Nacional de Normalización y Certificación de la Construcción y Edificación.
- ONNCCE. (2019). *NMX-C-514-ONNCCE-2019. Building Industry – Electrical Resistivity of Hydraulic Concrete - Specifications and Testing Methods*. Organismo Nacional de Normalización y Certificación de la Construcción y Edificación.
- ONNCCE. (2020). *NMX-C-165-ONNCCE-2020. Industria de la construcción - Agregados para concreto - Determinación de la reactividad potencial*. Organismo Nacional de Normalización y Certificación de la Construcción y Edificación.
- ONNCCE. (2002). *N-CMT-2-01-004/02. Characteristics of Materials. Materials For Structures. Materials For Hydraulic Concrete*. Organismo Nacional de Normalización y Certificación de la Construcción y Edificación.
- Ren, Q., Tao, Y., Jiao, D., Jiang, Z., Ye, G., De Schutter, G. (2021). *Plastic viscosity of cement mortar with manufactured sand as influenced by geometric features and particle size*. Cement and Concrete Composites, 122, 104163. <https://doi.org/10.1016/j.cemconcomp.2021.104163>

- Ribeiro, D. V., Oliveira Rey, R. (2019). *Avaliação dos agregados utilizados na região metropolitana de Salvador quanto à ocorrência de Reatividade Alcalis-Agregado (RAA)*. Revista ALCONPAT, 9(2), 185–199. <https://doi.org/10.21041/ra.v9i2.326>
- Sánchez Tizapa, S., Villaseñor Franco, A., Guinto Herrera, E., Barragán Trinidad, R., Mebarki, A. (2017). *Propuesta de valores de referencia para la resistencia de diseño a compresión diagonal y compresión de la mampostería en el estado de Guerrero, México*. Revista ALCONPAT, 7(3), 231–246. <https://doi.org/10.21041/ra.v7i3.159>
- Senff, L., Barbeta, P. A., Repette, W. L., Hotza, D., Paiva, H., Ferreira, V. M., Labrincha, J. A. (2009). *Mortar composition defined according to rheometer and flow table tests using factorial designed experiments*. Construction and Building Materials, 23(10), 3107–3111. <https://doi.org/10.1016/j.conbuildmat.2009.06.028>
- Souza, A. T., Barbosa, T. F., Riccio, L. A., Santos, W. J. dos. (2020). *Effect of limestone powder substitution on mechanical properties and durability of slender precast components of structural mortar*. Journal of Materials Research and Technology, 9(1), 847–856. <https://doi.org/10.1016/j.jmrt.2019.11.024>
- Stolz, C. M., Masuero, A. B. (2018). *Influence of grain distribution on the rheological behavior of mortars*. Construction and Building Materials, 177, 261–271. <https://doi.org/10.1016/j.conbuildmat.2018.05.131>
- Tena, A., Liga, A., Pérez, A., González, F. (2017). *Proposal for improved mixes to produce concrete masonry units with commonly used aggregates available in the Valley of Mexico*. Revista ALCONPAT, 7(1), 36–56. <https://doi.org/10.21041/ra.v7i1.170>
- Ullah, Z., Qureshi, M. I., Ahmad, A., Khan, S. U., Javaid, M. F. (2021). *An experimental study on the mechanical and durability properties assessment of E-waste concrete*. Journal of Building Engineering, 38, 102177. <https://doi.org/10.1016/j.jobbe.2021.102177>
- Westerholm, M., Lagerblad, B., Silfwerbrand, J., Forssberg, E. (2008). *Influence of fine aggregate characteristics on the rheological properties of mortars*. Cement and Concrete Composites, 30(4), 274–282. <https://doi.org/10.1016/j.cemconcomp.2007.08.008>
- Wu, M., Zhao, Q., Shen, W., Zhao, J., Xu, G., Zhao, D., Xiong, X. (2021). *Mix design of self-leveling mortar prepared by crushed sand with high flowability and early strengthening*. Construction and Building Materials, 283, 122679. <https://doi.org/10.1016/j.conbuildmat.2021.122679>

## Study of waterproofed concrete panels with silicate-based permeability reducing admixtures

F. E. Z. Alves<sup>1</sup> , R. P. Gurkewicz<sup>1,2,3\*</sup> , E. C. Zancan<sup>1,2</sup> ,  
L. J. J. Nieves<sup>1,2</sup> , E. G. P. Antunes<sup>1,2</sup> 

\*Contact author: [rafaelpgurkewicz@unesc.net](mailto:rafaelpgurkewicz@unesc.net)

DOI: <https://doi.org/10.21041/ra.v13i2.643>

Received: 28/02/2022 | Received in revised form: 09/04/2023 | Accepted: 11/04/2023 | Published: 01/05/2023

### ABSTRACT

This research studies the water absorption capacity of concrete panels and its self-healing process, using the incorporation of admixtures to the concrete or its application on the surface. Through permeability tests, water absorption by immersion and by capillarity, after the wet curing, the panels with crystalline admixtures applied superficially showed lower absorption capacity, followed by those without admixtures and those with the admixtures incorporated into the concrete, which showed greater absorption. Microscopy characterization was performed on the panels split in half, it was observed that the crystallization of the panels with superficial admixtures was more advanced compared to those with the incorporated admixtures. The induced fissures did not reach full pore filling after curing in both types of application.

**Keywords:** crystalline admixtures; fissure; self-healing; waterproofing; concrete.

**Cite as:** Alves, F. E. Z., Gurkewicz, R. P., Zancan, E. C., Nieves, L. J. J., Antunes, E. G. P. (2023), "Study of waterproofed concrete panels with silicate-based permeability reducing admixtures", Revista ALCONPAT, 13 (2), pp. 175 – 191, DOI: <https://doi.org/10.21041/ra.v13i2.643>

<sup>1</sup> Departamento de Engenharia Civil, UNESC, Criciúma, Santa Catarina, Brasil.

<sup>2</sup> GPDECC, Grupo de Pesquisa em Desempenho de Estruturas e Construção Civil, UNESC, Criciúma, Santa Catarina, Brasil.

<sup>3</sup> Programa de Pós-Graduação em Ciências e Engenharia de Materiais, UNESC, Criciúma, Santa Catarina, Brasil

### Contribution of each author

In this work, the author F. E. Z. Alves contributed with the conceptualization activity in 80%, experimentation in 75%, data analysis in 75% and writing in 70%, the author R. D. P. Gurkewicz contributed with the conceptualization activity in 20%, writing in 30%, 33% proofreading and 50% translation, author E. C. Zancan contributed experimentation activity 25%, data analysis 25%, and supervision 50%, author L. J. J. Nieves contributed proofreading activity in 33% and translation in 50%, the author E. G. P. Antunes contributed with the review activity in 34% and supervision in 50%..

### Creative Commons License

Copyright 2023 by the authors. This work is an Open-Access article published under the terms and conditions of an International Creative Commons Attribution 4.0 International License ([CC BY 4.0](https://creativecommons.org/licenses/by/4.0/)).

### Discussions and subsequent corrections to the publication

Any dispute, including the replies of the authors, will be published in the first issue of 2024 provided that the information is received before the closing of the third issue of 2023.

## **Estudio de paneles de hormigón impermeabilizado con aditivo reductor de permeabilidad a base de silicatos**

### **RESUMEN**

Esta investigación estudia la capacidad de absorción de agua de los paneles de hormigón y su proceso de autorreparación, mediante la incorporación de aditivo al hormigón o aplicación sobre la superficie. Mediante ensayos de permeabilidad, absorción de agua por inmersión y capilaridad, después del curado en húmedo, los paneles con aditivo cristalizante aplicado superficialmente mostraron menor capacidad de absorción, seguidos de los sin aditivo y los con aditivo incorporado, que mostraron mayor absorción. A través de la microscopía, se pudo observar que la cristalización de los paneles con aditivo superficial fue más avanzada en comparación con aquellos con aditivo incorporado. Las fisuras inducidas no alcanzaron el llenado completo de los poros después del curado, en ambos tipos de aplicación.

**Palabras clave:** aditivo cristalizante; fisura; autorreparación; impermeabilización; hormigón.

## **Estudo de painéis de concreto impermeabilizados com aditivo redutor de permeabilidade a base de silicato**

### **RESUMO**

Esta pesquisa estuda a capacidade de absorção de água em painéis de concreto e seu processo de autocicatrização, através da incorporação de aditivo ao concreto ou aplicação na superfície. Através de ensaios de permeabilidade, absorção de água por imersão e por capilaridade, após a cura úmida dos painéis, os painéis com aditivo cristalizante aplicado superficialmente apresentaram menor capacidade de absorção, seguido pelos sem aditivo e as com o aditivo incorporado ao concreto. Através da microscopia realizada nos painéis partidos ao meio, pôde-se observar que a cristalização dos painéis com aditivo superficial estavam mais avançadas em comparação aos com o aditivo incorporado. As fissuras induzidas não atingiram o total preenchimento de poros após a cura, em ambos os tipos de aplicação.

**Palavras-chave:** aditivo cristalizante; fissura; auto cicatrização; impermeabilização; concreto.

### **Legal Information**

Revista ALCONPAT is a quarterly publication by the Asociación Latinoamericana de Control de Calidad, Patología y Recuperación de la Construcción, Internacional, A.C., Km. 6 antigua carretera a Progreso, Mérida, Yucatán, 97310, Tel.5219997385893, [alconpat.int@gmail.com](mailto:alconpat.int@gmail.com), Website: [www.alconpat.org](http://www.alconpat.org)

Reservation of rights for exclusive use No.04-2013-011717330300-203, and ISSN 2007-6835, both granted by the Instituto Nacional de Derecho de Autor. Responsible editor: Pedro Castro Borges, Ph.D. Responsible for the last update of this issue, Informatics Unit ALCONPAT, Elizabeth Sabido Maldonado.

The views of the authors do not necessarily reflect the position of the editor.

The total or partial reproduction of the contents and images of the publication is carried out in accordance with the COPE code and the CC BY 4.0 license of the Revista ALCONPAT.

## 1. INTRODUCTION

In recent years, with the decrease in demand and the increase in competitiveness in the civil construction market, companies have begun to pay more attention to the materials used in their buildings, to minimize costs, rework and, in this way, remain competitive in the market. In addition to economic factors, the performance standard, as NBR 15575:2013 is known, with an emphasis on meeting user requirements, provides opportunities for the search and use of new materials and construction methods in buildings.

Among the many materials used in a building, those used for waterproofing deserve special attention, given that their cost is 1% to 3% of the value of the building (VEDACIT, 2019).

Currently, the products used in the waterproofing process are divided into 2 groups according to NBR 9574:2008, rigid and flexible materials. Thus, they must be applied in locations consistent with their technical characteristics to ensure the efficiency of the system. Within the rigid group, there are the crystallizing additives. Composed of silicates, which when mixed with water and in contact with the alkalinity of the concrete, become hydrosilicates, an insoluble crystal. Crystals can fill pores and fissures in concrete, making it waterproof.

The ability to fill fissures, also called self-healing, is a great advantage of the system, especially in structures that need to be impermeable to negative pressures, according to the process described by the NBR 9574:2008 standard. Through the self-healing capacity of concrete, these fissures, if they do not exceed the limit of 0.6 mm of opening, can be automatically filled.

According to Takagi, Almeida Júnior and Oliveira (2007), the crystallization treatment is a physical-chemical process where the active ingredients of the crystallizer trigger catalytic reactions, compatible with the cement hydration reactions, in which the formation of non-soluble crystals occurs and non-toxic in the concrete structure. In this way, ensuring that there is no penetration of water by capillarity, supporting both positive and negative hydrostatic pressures of up to 0.7 MPa.

As they are added to fresh concrete, after hardening, the crystallizers prevent the passage of water in the liquid phase, but do not completely prevent the passage when in the gaseous phase. This behavior can be validated by the authors Pazderka and Hájková (2016), who, after testing with two different crystallizers, obtained percentages of only 16% and 20% of reduction in the absorption of water steam.

Recently studies conducted by Huang et al. (2016), with the aid of magnetic resonance, pointed out that in concrete with permeability-reducing additives, after a few hours, the non-chemically bound water content decreased in areas adjacent to the fissures, proving that the water that had penetrated the fissure was used in hydration processes, making these areas denser.

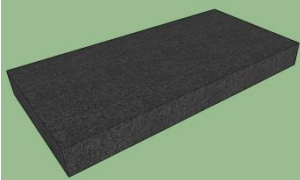
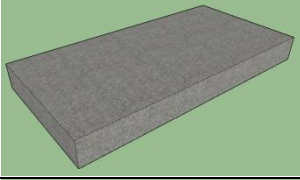
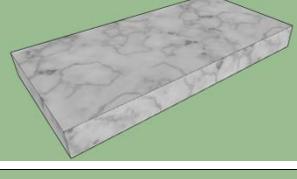
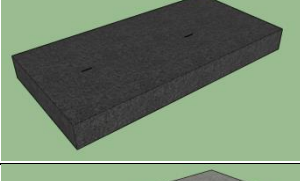
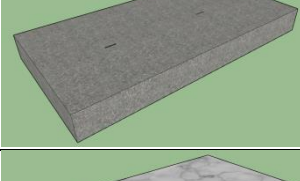
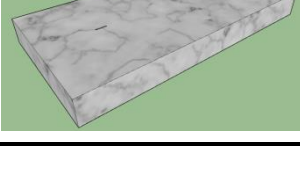
According to the company that manufactures the product used in the present work, concrete with additives can fill fissures of up to 0.6 mm, this value being 0.2 mm higher than the maximum allowed by the NBR 6118:2014 standard, for reinforced concrete inserted in the class of environmental aggressiveness I.

This research studies and evaluates the water absorption capacity of concrete panels and their self-healing process, through two methods of application of permeability-reducing additives.

## 2. PROCEDURE

In order to verify the impermeability and the self-healing effect in concrete panels, an experimental procedure was elaborated that consists in the execution of 2 groups of panels with 3 subgroups each. The distinction between the first and second groups refers to the presence of induced fissures, that is, one group had two induced fissures across the entire thickness of the panel, while the second group did not. The subgroups are distinguished according to the waterproofing treatment used, with the first subgroup not having any type of waterproofing treatment, while the second and third subgroups were waterproofed, but in a different way between them. The second subgroup was waterproofed by incorporating the crystallizing additive into the concrete and in the third subgroup the crystallizing additive was applied on one of the panel faces. For this, 18 panels were produced (9 for each group, 3 for each subgroup). Table 1 presents the groups and subgroups developed, in addition to the nomenclature adopted for each subgroup of panels.

Tabela 1. Modelos de painéis.

GROUP	SUBGROUP		NOMENCLATURE
NO FISSURE		Control Panel Without Crystallizing Additive	S CRI
		Panel With Crystallizing Additive Mixed To Concrete Still Fresh	C CRI
		Panel With Crystallizing Additive Applied Superficially After Curing Time	C CRI SOB
WITH FISSURE		Control Panel Without Crystallizing Additive	S CRI+F
		Panel With Crystallizing Additive Mixed To Concrete Still Fresh	C CRI+F
		Panel With Crystallizing Additive Applied Superficially After Curing Time	C CRI SOB+F

The panels produced measure 50 x 25 x 5 cm (length x width x thickness) and 2 cm thick wooden molds were used for their execution. The concrete used was dosed in a machined plant with an average strength of 10 MPa, with a slump of  $10 \pm 2$  cm, in accordance with NBR 16889:2020. The filling of the molds was done manually.

The application of the crystallizing additive on the panels of the subgroups “C CRI SOB” and “C CRI SOB+F” occurred after 28 days of curing the panels. Figure 1(a) illustrates the casting of concrete into the molds and Figure 1(b) the mold filled with concrete.

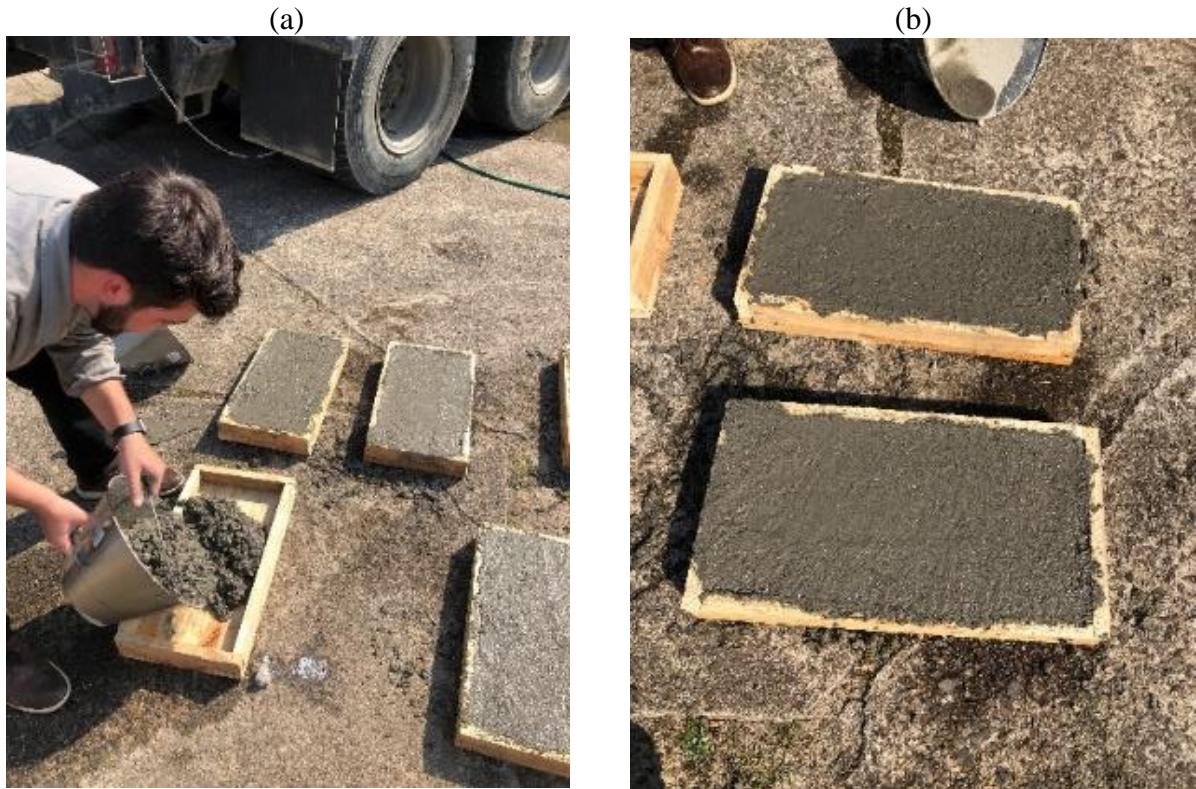


Figure 1. Molds: (a) concreting of a panel, (b) mold filled with concrete

The fissures were induced in the panels by inserting two 0.4 mm thick aluminum sheets, which were introduced into each panel shortly after concreting and removed after 48 hours of concreting, when its fluidity was not able to cause closure from the fissure. The thickness of the sheets was determined following NBR 6118:2014, which limits the value of 0.4 mm as the largest permissible dimension of fissures in structural elements of reinforced concrete and the manufacturer's recommendation on the maximum dimension of clogging of the product.

Figure 2(a) shows the aluminum sheets inserted in a panel and Figure 2(b) the fissure induced by the aluminum sheet, both 48 hours after concreting, that is, when it was already possible to remove the sheets of concrete panels.

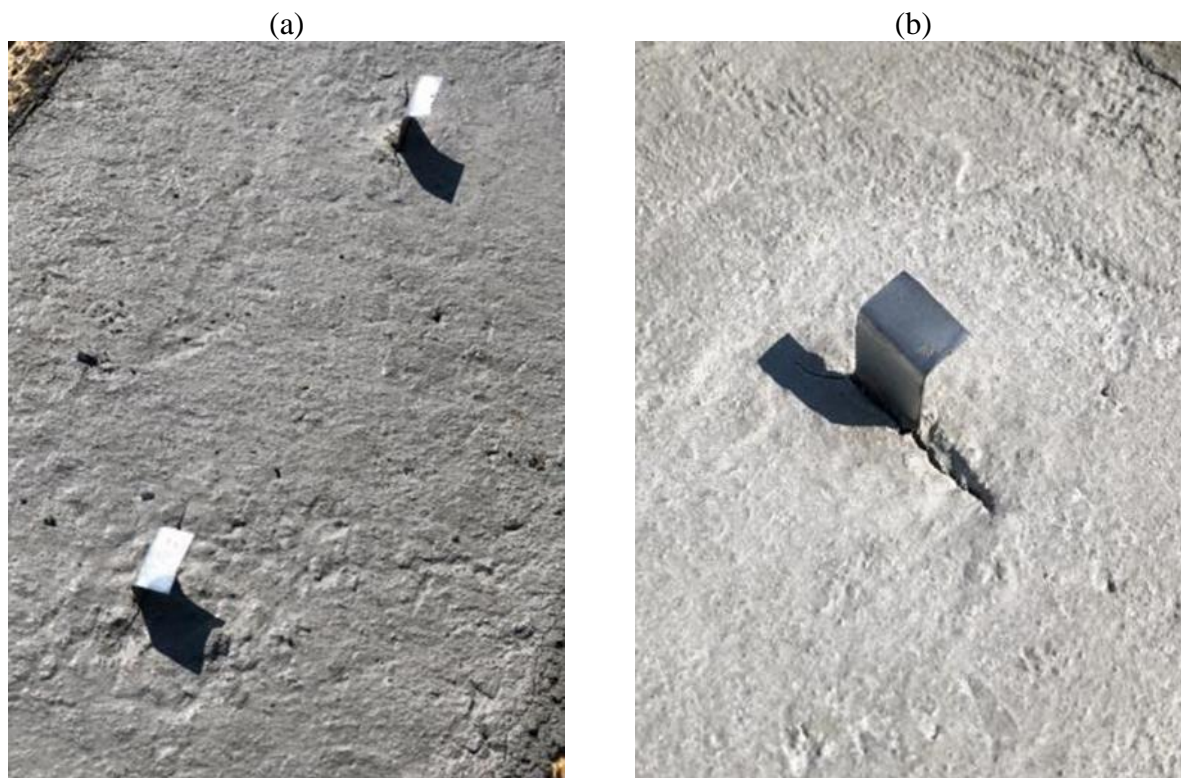


Figure 2. Sheets for fissure induction: (a) panel with two sheets, (b) sheet in detail.

Table 2 presents the characteristics of the crystallizing additive used in the research.

Table 2. characteristics of the crystallizing additive

<b>Density</b>	1.200 Kg/m <sup>3</sup>
<b>Base</b>	Silicate
<b>Dosage</b>	200 ml for every 50 kg of cement or 1.2 l for every m <sup>3</sup> of concrete
<b>Appearance</b>	Yellow liquid
<b>pH</b>	11
<b>Viscosity (Ford 4 at 25°C)</b>	12 seconds
<b>Validity</b>	24 months from fabrication date

To mix the additive to the concrete, a concrete mixer was used. It should be noted that such action was necessary in order not to contaminate the concrete of the panels without the use of the additive. Figure 3(a) shows the amount of product used for concreting and Figure 3(b) the process of incorporating the additive into the concrete.

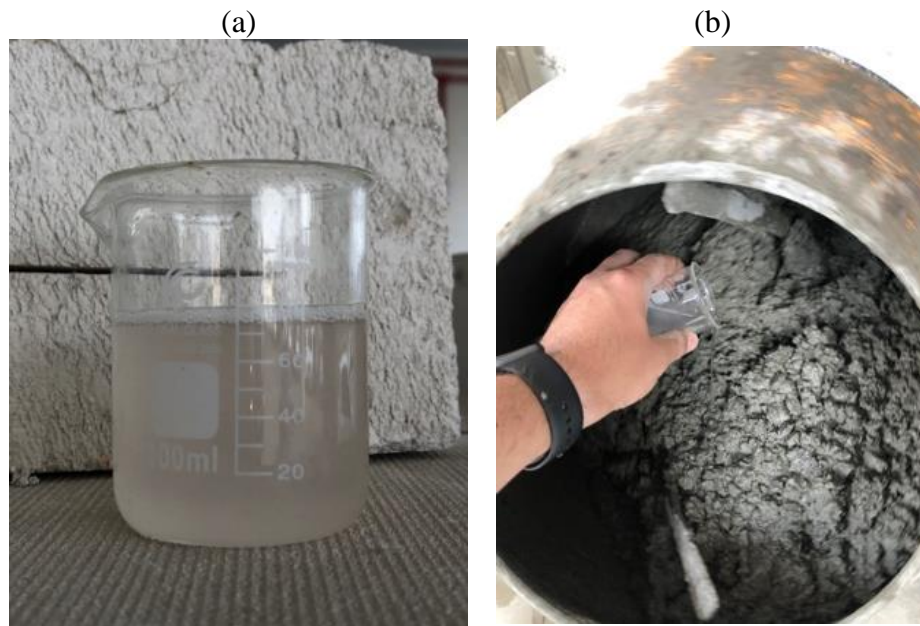


Figure 3. Crystallizer mixing process: (a) required amount of crystallizer, (b) mixing process in the concrete mixer.

After the execution and deforming of the panels, which took place on the third day, the panels were submitted to submerged curing for a period of 28 days. To avoid contamination of the samples not yet waterproofed, the panels with waterproofing incorporated into the concrete were separated into different tanks. After 28 days of curing, the panels were oven-dried for 72 hours at a temperature of  $40 \pm 5$  °C. Figure 4(a) shows the panels during submerged curing and Figure 4(b) the panels after the curing and drying process.

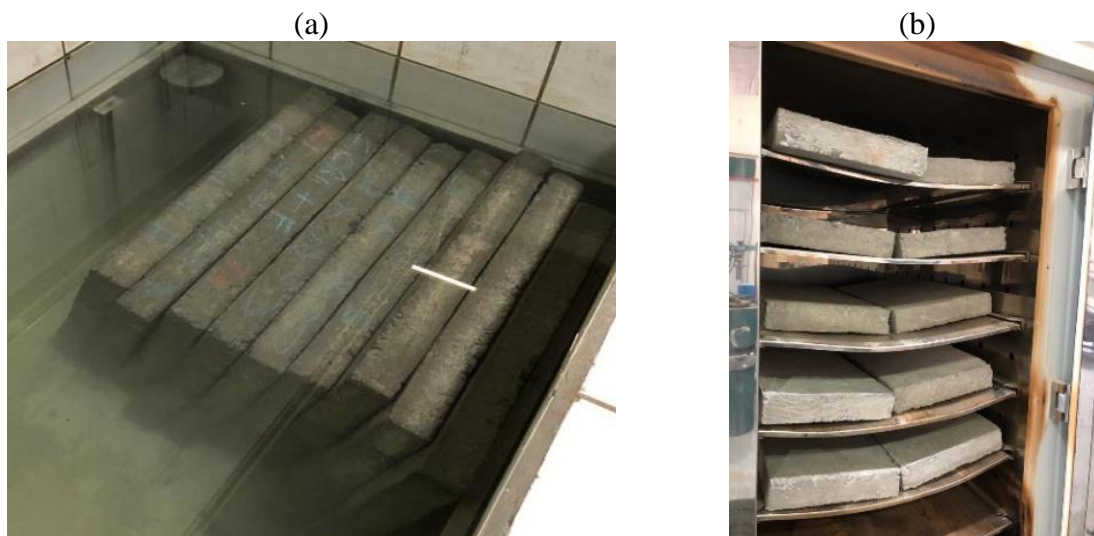


Figure 4. Panels during submerged curing and drying: (a) panels in tank, (b) panels in oven.

Once the panels were dry, the crystallizing additive was applied to the panels of the subgroups “C CRI SOB” and “C CRI SOB+F”. The application was performed through 2 coats of the product with the aid of a brush. The surface of these panels was completely saturated with the crystallizing additive and it took approximately 3 hours for the additive to be completely absorbed by the panels. Subsequently, these panels were stored outdoors for 3 days, and during these days they were exposed to rain, which aids in the hydration of the crystallizing additive. Figure 5(a) shows the

surface application of the additive on one side of the plates, Figure 5(b) the plates during the product absorption process and Figure 5(c) the curing process of the panels with surface application.

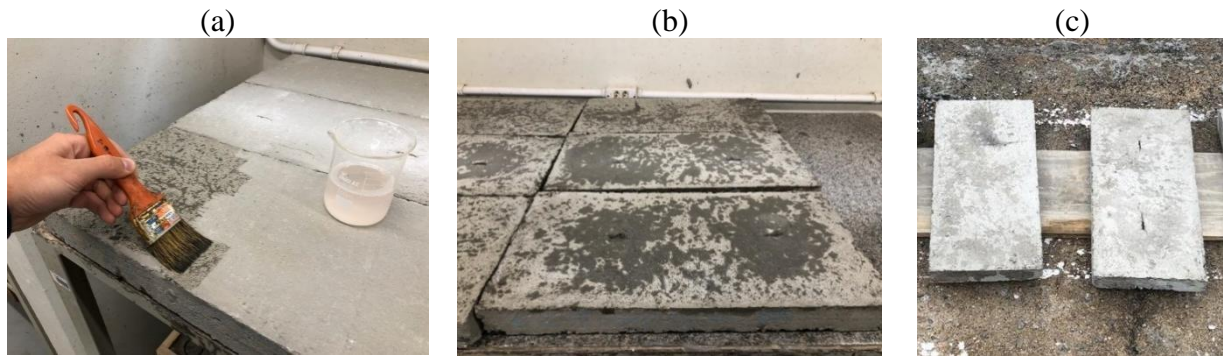


Figure 5. Crystallizer application process: (a) application with a brush, (b) waterproofed panels, (c) panels during the curing process.

The “C CRI SOB” and “C CRI SOB+F” panels received a total of 14.4 mm of rain, as shown in Figure 6, taken from the meteorological station close to the test site.

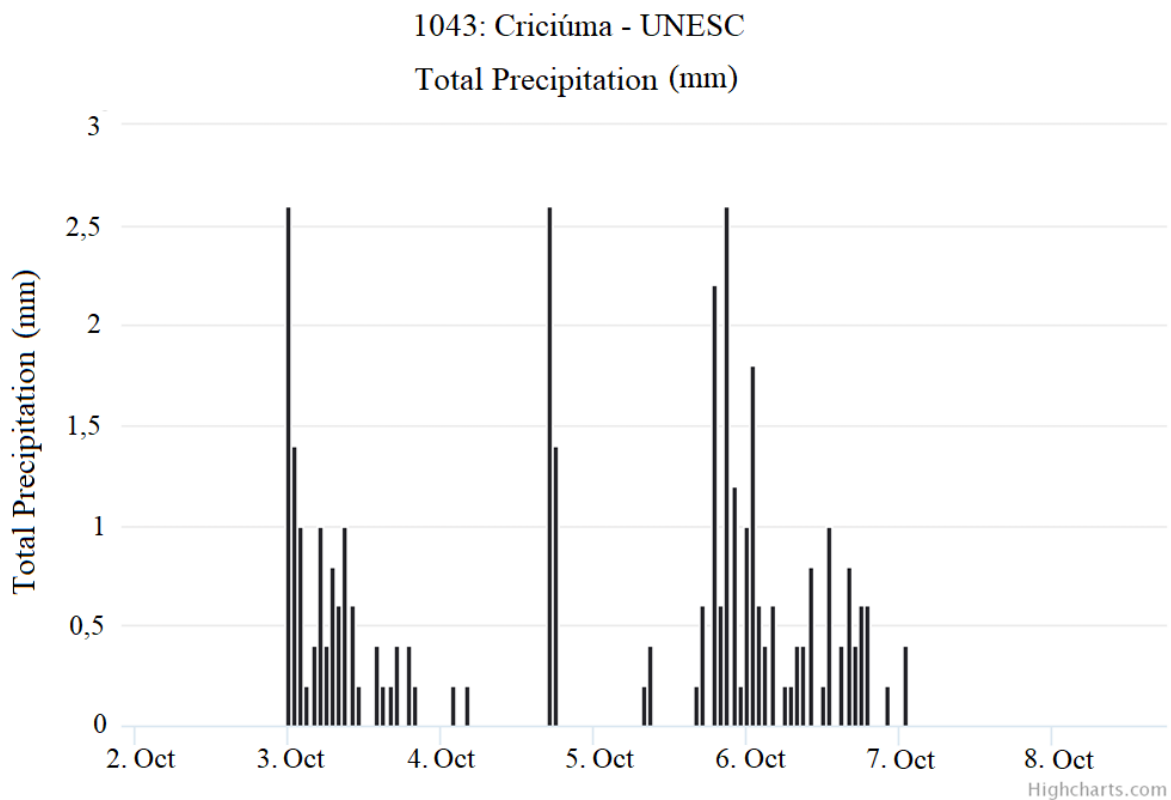


Figure 6. Pluviometric index graph (Source: EPAGRI).

Once the stage of execution, waterproofing and curing of the panels was over, tests were started to verify the permeability of the panels. The tests carried out were: determination of water absorption by immersion, water absorption by capillarity with calculation of the void ratio and water absorption by the Karsten Tube.

The first test performed was the test to determine permeability using the Karsten tube. This test was carried out in accordance with NBR 14992:2003, which specifies such verification for Portland cement-based mortars for grouting ceramic tiles. The Karsten tubes were placed on the concrete panels, and their lateral bases, which were in contact with the face of the panels, were sealed with polyurethane. Each tube was fixed 10 cm away from the edges and 30 cm spacing between the tubes, thus, two tubes per panel. The Karsten tubes were filled with water up to the predefined volume of 3.5 ml and later the level measurements were performed after 60, 120, 180 and 240 minutes. Each panel had two points of permeability measurement.

Figure 7(a) shows the test being performed on the panel with crystallizer and Figure 7(b) the Karsten tube over the fissure of a plate with crystallizer applied on the concrete.



Figure 7. Karsten tubes fixed on the panels: (a) Panel tube without fissure, (b) Panel tube with fissure.

The second test carried out was the determination of the panel's water absorption and the calculation of the void ratio, as described by NBR 9778:2005, using three panels per condition. The panels were initially dried in an oven at  $105 \pm 5$  °C for 72 hours and the dry mass was measured, then immersed in water for another 72 hours, for complete saturation. After removing the saturated panels, the saturated sample was weighed and another weighing was carried out using a hydrostatic balance, as shown in Figure 8. From these values, it was possible to determine the water absorption, the voids ratio, dry specific mass and saturated specific mass.



Figure 8. Hydrostatic weighing.

The percentage of water absorption can be calculated with Equation 1.

$$A = \frac{m_{sat} - m_s}{m_s} \times 100 \quad (1)$$

Wherein

$A$  is the absorption rate, expressed in percentage;  
 $m_{sat}$  is the mass of the sample saturated in water after immersion and boiling;  
 $m_s$  is the mass of the sample dried in the oven.

The last test carried out was the determination of water absorption by capillarity, described by the NBR 9779:1995 standard. To carry out this test, the panels were placed in a water depth of 0.5 cm for a period of 72 hours, in order to verify the absorption of water by capillarity. In order to be able to observe variations in absorption between the panels, the waterproofed upper faces were submerged. Mass measurements were taken after 3, 6, 24, 48 and 72 hours.

Figure 9(a) shows the verification of the water depth of 0.5 cm, Figure 9(b) the panels arranged in the tank during the absorption process and Figure 9(c) the weighing of one of the panels.

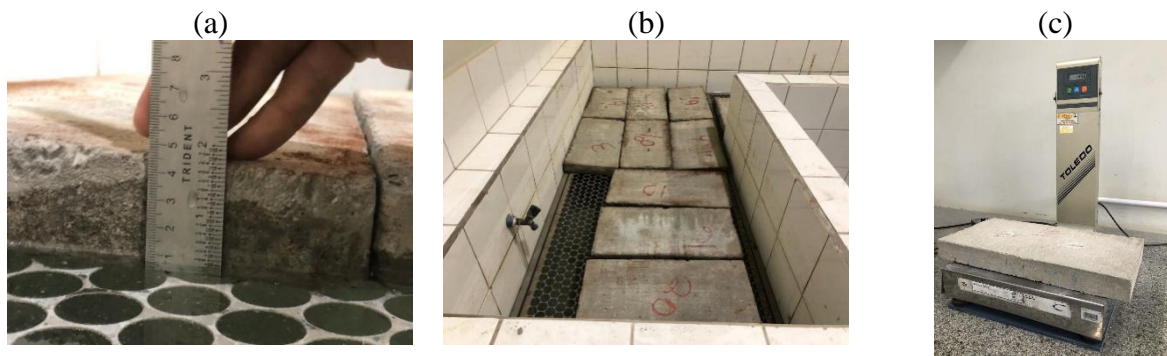


Figure 9. Capillarity absorption test: (a) Submerged panel 0.5 cm deep, (b) Panels in the tank, (c) Panel being weighted.

The water absorption by capillarity can be calculated with Equation 2.

$$C = \frac{m_{sat} - m_s}{S} \quad (2)$$

Wherein

$C$  is the water absorption by capillarity, expressed in grams per square centimeter;  
 $m_{sat}$  is the saturated mass of the specimen that remains with one side in contact with the water during a specified period, expressed in grams;  
 $m_s$  is the mass of the dry specimen, as soon as it reaches a temperature of  $23 \pm 2$  °C, expressed in grams.  
 $S$  is the cross-sectional area, expressed in square centimeters.

The data from the results were analyzed using analysis of variance (ANOVA) and the Tukey test, when necessary, with a significance of 95%.

After finishing the tests, a microscopy of the plates was performed for a better observation of the state of crystallization of the pores. For this purpose, 3 plates were broken, “S CRI”, “COM CRI” and “C CRI SOB”, and a digital microscope with 1600x magnification capacity.

### 3. RESULTS AND DISCUSSION

The results of the permeability test with a Karsten Tube, represented by Figure 10, indicate the permeability values obtained over time (60, 120, 180 and 240 min). As can be seen, the panels with the highest permeability at 240 minutes, the final measurement time, were the panels with crystallizer additive incorporated into the concrete, followed by panels without crystallizer and, finally, by the panel with crystallizer applied on its surface.

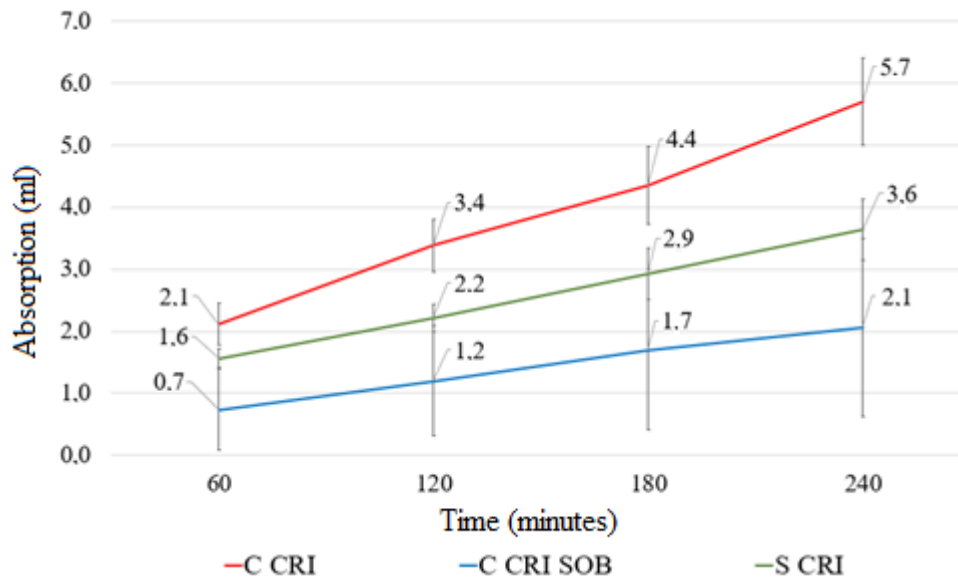


Figure 10. Average absorption over time.

Through the analysis of the permeability values presented graphically, it was possible to observe that both the initial absorption and the absorption speed of the panels with the incorporation of the crystallizing additive were superior to those of the other panels. The highest permeability, since the first measurement of the “C CRI” panels in relation to the other panels reached 171.43% more absorption in comparison to the “C CRI SOB” and 58.33% more in relation to the “S CRI” panel. The higher water absorption speed of the “C CRI” panels can be visualized by their steeper inclination in relation to the other panels, as well as by the greater difference between the initial and final absorption, which was 171.34%, being that for the “C CRI SOB” panels it was 200% and for the “S CRI” panels it was 125%.

After statistical analysis, through analysis of variance (ANOVA), it was possible to conclude that the panels present a significant difference between them in the permeability test through the Karsten tube, that is, the type of waterproofing treatment influenced the results of this verification. Through the Tukey Test ( $p = 4.13477E-05$ ) it can be stated that the “C CRI” panels were the most permeable, followed by the “S CRI” panels and, finally, by the “C CRI SOB” panel.

It is important to mention that it was not possible to analyze the permeability by the Karsten tube method of the “C CRI + F”, “S CRI + F” and “C CRI SOB + F” panels, with induced fissures, due to the final dimension of the fissure opening, approximately 1.3 mm. Even so, it should be noted that an attempt was made to carry out the test, however, given the thickness of the opening, the water from the Karsten tube, which was inserted exactly over the fissure, completely drained through it in seconds. Figure 11(a) shows the sheet after 48 hours of concreting the panels and Figure 11(b) the fissure after the panels curing process.



Figura 11. Fissuras: (a) Fissura ainda com a lâmina, (b) Fissura após a retirada da lâmina

The induced fissure, which had been planned for 0.4 mm, exceeded its opening by 0.9 mm, as it ended at 1.3 mm (Figure 11), extrapolating the 0.6 mm presented by the company as the maximum dimension for clogging fissures.

During the hardening process of concrete, reactions occur that cause plastic shrinkage. According to Marin, Brasil (2016) plastic shrinkage occurs by evaporation of water on the surface of freshly compacted concrete and is influenced by climatic conditions to which the concrete is exposed. Therefore, it was not possible to evaluate the clogging of the induced fissures through the permeability test using the Karsten tube method, considering that the induced fissures had a final opening thickness of approximately 1.3 mm. In addition, the clogging process by the “self-healing” effect is slow, since, as presented by Venquiaruto (2017), after 91 days of wet curing, there was a partial recovery of the micro fissures, in relation to the analyzes after 3 and 28 days. After 3 days of healing, the fissures ranged from 2,294  $\mu\text{m}$  to 5,410  $\mu\text{m}$ , and at 91 days they had dimensions from 1,204  $\mu\text{m}$  to 3,077  $\mu\text{m}$ .

Through the results of the water absorption test by immersion, presented from Figures 12 and 13, it can be concluded that again the panels with crystallizer incorporated into fresh concrete showed a higher void rate and, consequently, a greater absorption after 72 hours submerged. Panels with superficially applied crystallizer had the lowest void ratio and an average of 1.29% lower than panels with crystallizer mixed with concrete.

The results were condensed into “C CRI and C CRI+F” (with crystallizer and with crystallizer + induced fissure), “C CRI SOB and C CRI SOB+F” (with crystallizer superficially and with crystallizer superficially + induced fissure), “S CRI and S CRI + F” (without crystallizer and without crystallizer + induced fissure).

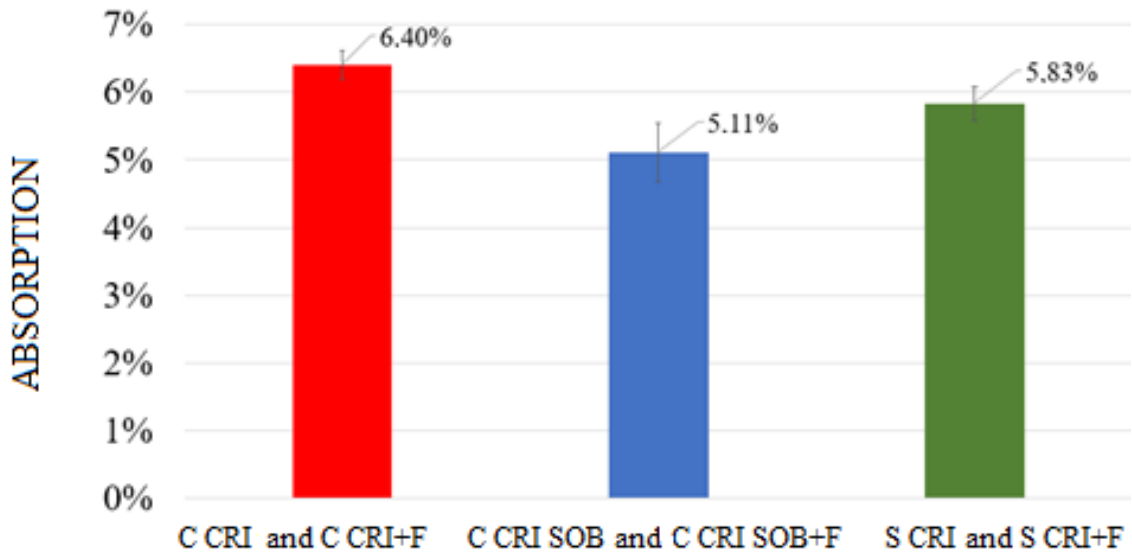


Figure 12. Absorption after 72 hours.

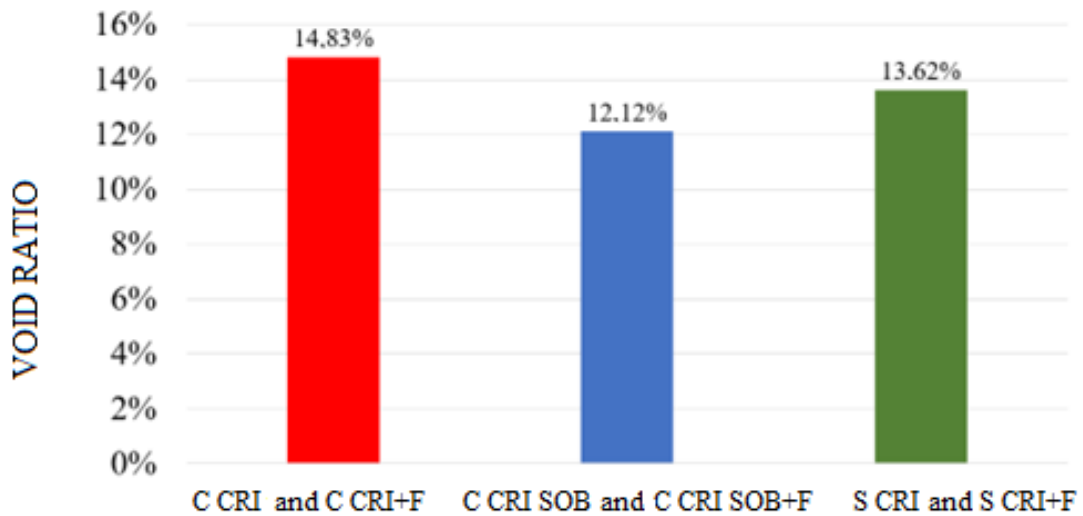


Figure 13. Void ratio.

The results of the water absorption by capillarity test can be seen in Figure 14. Again, it was found that the “C CRI” and “C CRI + F” panels showed values that demonstrated greater permeability of these panels in relation to the others.

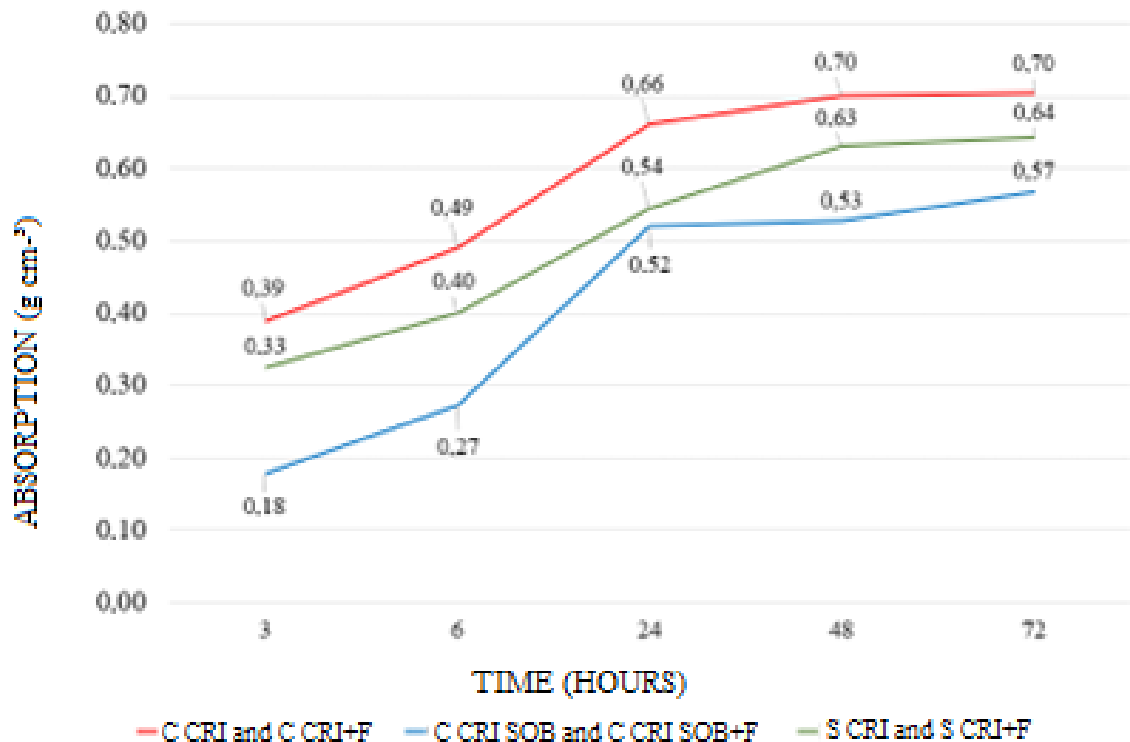


Figure 14. Absorption by capillarity.

In this test, the “C CRI” and “C CRI+F” panels had an absorption of 9.38% higher than the reference panels, while the “C CRI SOB” and “C CRI SOB+F” panels showed a decrease of 10.94%. It is also possible to observe that during the periods of 3 and 24 hours there was the highest absorption by the panels, after these periods the plates had low absorptions.

After statistical analysis using analysis of variance (ANOVA) and Tukey test, with a significance of 95% ( $p=0.000142449$ ), it was possible to conclude that the panels present a significant difference in their absorption by capillarity results in 72 hours.

Based on the results obtained in the three tests (Karsten tube, absorption by immersion and absorption by capillarity) it can be concluded that the incorporation of the permeability-reducing additive caused a significant increase in permeability and water absorption in relation to the other types of treatments. Meanwhile, the “C CRI SOB” and “C CRI SOB + F” panels had a significant decrease in their permeability compared to untreated panels (“S CRI” and “S CRI + F”). This behavior can be explained by the process of crystallization of the permeability-reducing additive. For the reaction of the silicate additive to occur, it is necessary to hydrate it, similarly to the hydration reactions of cement grains. Therefore, the water initially made available in the mixture ends up being necessary for both actives in the first days, causing a slower formation of concrete crystals and the crystals that fill the pores.

The presence of the additive mixed with the concrete during the curing process can cause internal reactions that divide the crystallization power, since both use water for the process. Thus, the crystallization of the product combined with the crystallization of calcium hydroxide may be responsible for the greater initial absorption. The slow formation of crystals, when the additive is incorporated into the concrete, is due to the gradual formation of crystals in the cement, created during the curing process, since the product reacts both with the cement and with the water for its crystallization. In this way, the crystals of the additive and the concrete begin to hydrate more slowly than with the panels without the crystallizer.

This behavior was also observed by Araújo, Saviatto (2018), who, after an absorption and compression test, observed an increase in permeability and a decrease in resistance in the plates with the additive mixed with the concrete, after 28 days of submerged curing.

The surface application on the panels after the curing process presents a better initial performance due to the higher surface concentration of the product and the calcium hydroxide crystals in the concrete being mostly hydrated at the time of application of the permeability-reducing additive.

For a better visualization of the crystalline processes in the 3 types of panels, microscopies were performed with a digital microscope that has a 1600x magnification capacity. These images are represented in Figure 15(a) which illustrates the panel after the cutting process, Figure 15(b) microscopy of the “C CRI” panel, Figure 15(c) panel “C CRI SOB” and Figure 15(d) “S CRI” panel. The cut on the panel was performed with a diamond saw and water cooling at the cutting site, minimizing vibrations, in accordance with NBR 7680: 2015.

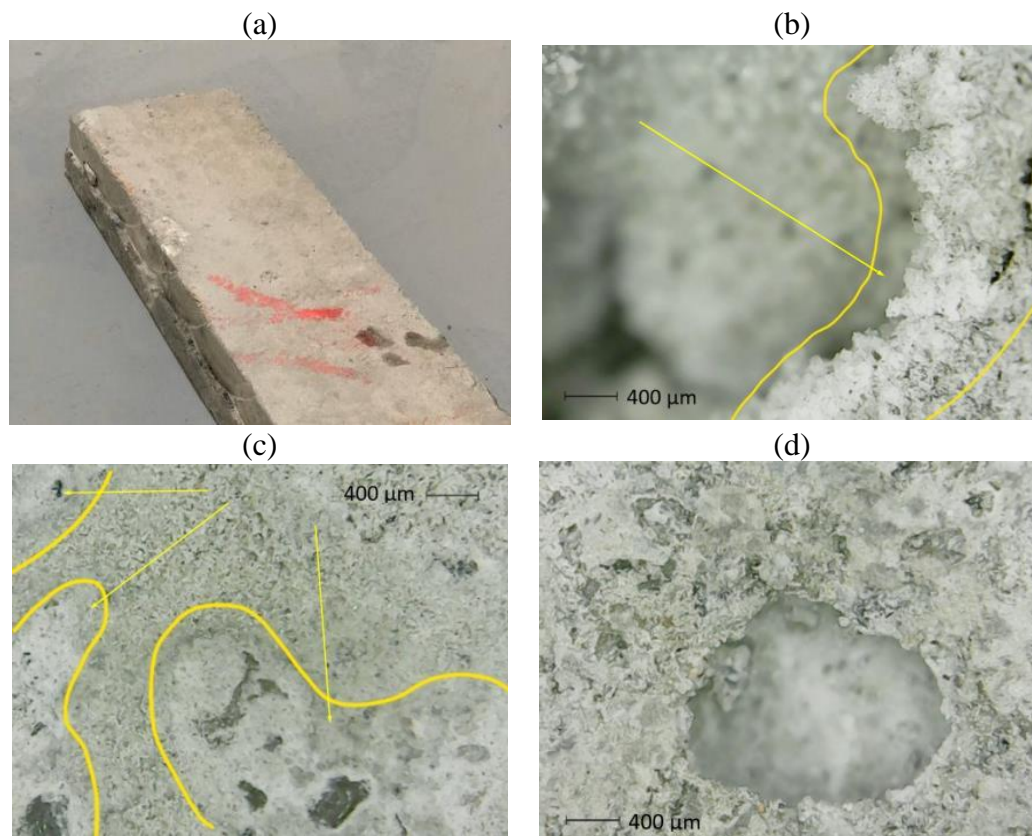


Figure 15. Microscopy: (a) Panel cut in half, (b) Panel with crystallizer mixed with concrete, (c) Panel with crystallizer applied over it, (d) Reference panel.

In the panels with the application of the additive incorporated into the concrete (C CRI), it was possible to observe few crystals on the pore surfaces, which may indicate an initiating crystallization process. In the panels with superficial application of the crystallizer (C CRI SOB), it was possible to observe a greater clogging, with many being completely obstructed by the crystals.

## 4. CONCLUSIONS

Through the analysis of the results, a similarity can be portrayed in the data obtained from the tests, which present the same behavior regarding the absorption capacity and permeability of the panels. Pointing out the samples with the crystallizing additive applied superficially, with the lowest water permeability, and the samples with the additive mixed with the concrete, with the highest voids and water absorption ratios.

The superior performance of panels with surface application can be explained by the high concentration of the additive on the face, obtaining a greater crystallization capacity since the crystals from the concrete curing are completely hydrated, in this way the additive manages to have a more effective initial performance.

Panels with additive mixed with concrete showed higher absorption in all tests and higher void ratio after submerged time. This happens because its crystallization process has not ended, as it uses water and crystals from cement hydration, which are being formed simultaneously with the additive crystals, making the process slower, and it is not possible to observe improvements after 28 days of submerged curing.

Despite not having presented clogging of the fissure after the curing time, the crystallization process was present in the fissures, requiring more time in contact for the clogging to possibly end. For future works, it is recommended to use more resistant concrete, with at least 20 Mpa. Carry out the same tests, but verifying the results after 1, 20, 40, 60 and 90 days after the submerged curing process, in order to verify the evolution of the process and monitor the clogging of the pores over time.

## 5. REFERENCES

- Araújo, M. D., Saviatoo, M. S. C. (2018), *Estudo da influência de aditivo impermeabilizante em concreto*. 83 f. Monografia (Especialização) - Curso de Engenharia Civil, Universidade do Sul de Santa Catarina, Palhoça. Disponível em: <https://repositorio.animaeducacao.com.br/handle/ANIMA/4666>
- ASSOCIAÇÃO BRASILEIRA DE NORMAS TÉCNICAS. *NBR 14.992: Argamassa à base de cimento Portland para rejuntamento de placas cerâmicas – Requisitos e métodos de ensaio*. Rio de Janeiro, 2003.
- ASSOCIAÇÃO BRASILEIRA DE NORMAS TÉCNICAS. *NBR 16889: Concreto – Determinação da consistência pelo abatimento do tronco de cone*. Rio de Janeiro, 2020.
- ASSOCIAÇÃO BRASILEIRA DE NORMAS TÉCNICAS. *NBR 9778: Argamassa e concreto endurecido – Determinação de absorção de água por imersão – Índice de vazios e massa específica*. Rio de Janeiro, 1987.
- ASSOCIAÇÃO BRASILEIRA DE NORMAS TÉCNICAS. *NBR 15.575: Edificações habitacionais- Desempenho*. Rio de Janeiro, 2013.
- ASSOCIAÇÃO BRASILEIRA DE NORMAS TÉCNICAS. *NBR 9574: Execução de impermeabilização*. Rio de Janeiro, 2008.
- ASSOCIAÇÃO BRASILEIRA DE NORMAS TÉCNICAS. *NBR 9779: Argamassas e concreto endurecidos – Determinação da absorção de água por capilaridade*. Rio de Janeiro, 1995.
- ASSOCIAÇÃO BRASILEIRA DE NORMAS TÉCNICAS. *NBR 6118: Projeto de estruturas de concreto – Procedimento*. Rio de Janeiro, 2014.
- ASSOCIAÇÃO BRASILEIRA DE NORMAS TÉCNICAS. *NBR 7610: Concreto — Extração, preparo, ensaio e análise de testemunhos de estruturas de concreto*. Rio de Janeiro, 2015.

- Huang, H., Ye, G., Pel, L. (2016), *New insights into autogenous self-healing in cement paste based on nuclear magnetic resonance (NMR) tests*. Materials and Structures 49, no. 7, p. 2509-2524. DOI: <https://doi.org/10.1617/s11527-015-0664-9>
- Marin, J. S., Brasil, K. F. (2016), *Controle da retração plástica em lajes de cobertura de concreto armado*. 67f. Trabalho de Conclusão de Curso (Bacharelado em Engenharia Civil) Universidade Tecnológica Federal do Paraná. Pato Branco, 2016. Disponível em: <http://repositorio.utfpr.edu.br/jspui/handle/1/14309>
- Neville, A. M. (2016), *Propriedades do concreto*. 5 ed. Porto Alegre: Bookman.
- Pazderka, J., Hajková, E. (2016), *Crystalline admixtures and their effect on selected properties of concrete*. Journal of Advanced Engineering. Praga, República Checa. DOI: <https://doi.org/10.14311/AP.2016.56.0306>
- Takagi, E. M., Almeida, W. J., Oliveira, F. S. (2007), *Tratamento químico cristalizante para impermeabilização e proteção de estrutura de concreto armado*. In: CONGRESSO BRASILEIRO DO CONCRETO, 45, Florianópolis.
- VEDACIT (2013), *Manual técnico de impermeabilização de estruturas*. 7ª edição. Disponível em: <https://www.vedanews.com.br/uploads/biblioteca/manual-tecnico-impermeabilizacao-de-estruturas-7.pdf> (acesso: 11 de julho de 2019).

## New model for complete design of rectangular isolated footings taking into account that the contact surface works partially in compression

A. Luévanos Rojas <sup>1\*</sup> 

\*Contact Author: [arnulfol\\_2007@hotmail.com](mailto:arnulfol_2007@hotmail.com)

DOI: <https://doi.org/10.21041/ra.v13i2.671>

Received: 21/02/2023 | Received in revised form: 13/04/2023 | Accepted: 20/04/2023 | Published: 01/05/2023

### ABSTRACT

This paper shows a new model for complete design of rectangular isolated footings under uniaxial and biaxial bending, considering that the footing area in contact with the soil partially works to compression. The methodology is presented by integration to obtain moments, flexural shearing and punching shearing. Numerical examples are presented for design of rectangular isolated footings under uniaxial and biaxial flexion and are compared with the current model (total area works in compression) in terms of concrete and steel volumes. The current model shows greater volumes of concrete and steel. Therefore, the new model is the most appropriate, since it presents better quality control in the resources used.

**Keywords:** rectangular isolated footings; new model for complete design; moments; flexural shearing; punching shearing.

**Cite as:** Luévanos Rojas, A. (2023), “*New model for complete design of rectangular isolated footings taking into account that the contact surface works partially in compression*”, Revista ALCONPAT, 13 (2), pp. 192 – 219, DOI: <https://doi.org/10.21041/ra.v13i2.671>

<sup>1</sup> Instituto de Investigaciones Multidisciplinarias, Universidad Autónoma de Coahuila, Torreón, Coahuila, México.

#### Contribution of each author

In this work there was only one author.

#### Creative Commons License

Copyright 2023 by the authors. This work is an Open-Access article published under the terms and conditions of an International Creative Commons Attribution 4.0 International License ([CC BY 4.0](https://creativecommons.org/licenses/by/4.0/)).

#### Discussions and subsequent corrections to the publication

Any dispute, including the replies of the authors, will be published in the first issue of 2024 provided that the information is received before the closing of the third issue of 2023.

## **Nuevo modelo para el diseño completo de zapatas aisladas rectangulares tomando en cuenta que la superficie de contacto funciona parcialmente en compresión**

### **RESUMEN**

Este documento muestra un nuevo modelo para diseño completo de zapatas aisladas rectangulares bajo flexión uniaxial y biaxial, tomando en cuenta que el área de la zapata en contacto con el suelo funciona parcialmente a compresión. La metodología se presenta por integración para obtener momentos, cortantes por flexión y penetración. Los ejemplos numéricos se presentan para el diseño de zapatas aisladas rectangulares bajo flexión uniaxial y biaxial, y se comparan con el modelo actual (área total funciona en compresión) en términos de volúmenes de concreto y acero. El modelo actual muestra mayores volúmenes de concreto y acero. Por lo tanto, el nuevo modelo es el más adecuado, ya que presenta mejor control de calidad en los recursos utilizados.

**Palabras clave:** zapatas aisladas rectangulares; nuevo modelo para diseño completo; momentos; cortante por flexión; cortante por penetración.

## **Um novo modelo para o dimensionamento completo de fundações isoladas retangulares levando em consideração que a superfície de contato funciona parcialmente em compressão**

### **RESUMO**

Este artigo mostra um novo modelo para o dimensionamento completo de fundações isoladas retangulares sob flexão uniaxial e biaxial, levando em consideração que a área da sapata em contato com o solo funciona parcialmente à compressão. A metodologia é apresentada por integração para obter momentos, cisalhamento por flexão e punção. Exemplos numéricos são apresentados para o projeto de fundações isoladas retangulares sob flexão uniaxial e biaxial e são comparados ao modelo atual (a área total funciona em compressão) em termos de volumes de concreto e aço. O modelo atual mostra maiores volumes de concreto e aço. Portanto, o novo modelo é o mais apropriado, pois apresenta melhor controle de qualidade nos recursos utilizados.

**Palavras-chave:** fundações isoladas retangulares; novo modelo para dimensionamento completo; momentos; cisalhamento de flexão; punção.

### **Legal Information**

Revista ALCONPAT is a quarterly publication by the Asociación Latinoamericana de Control de Calidad, Patología y Recuperación de la Construcción, Internacional, A.C., Km. 6 antigua carretera a Progreso, Mérida, Yucatán, 97310, Tel.5219997385893, [alconpat.int@gmail.com](mailto:alconpat.int@gmail.com), Website: [www.alconpat.org](http://www.alconpat.org)

Reservation of rights for exclusive use No.04-2013-011717330300-203, and ISSN 2007-6835, both granted by the Instituto Nacional de Derecho de Autor. Responsible editor: Pedro Castro Borges, Ph.D. Responsible for the last update of this issue, Informatics Unit ALCONPAT, Elizabeth Sabido Maldonado.

The views of the authors do not necessarily reflect the position of the editor.

The total or partial reproduction of the contents and images of the publication is carried out in accordance with the COPE code and the CC BY 4.0 license of the Revista ALCONPAT.

## 1. INTRODUCTION

The design of shallow footings supported on the ground depends of the loads and moments provided by the columns.

Figure 1 shows the distribution of soil pressure under the rigid footing that depends on the type of soil, and the position of the applied resultant force at the center of gravity of the base. Figure 1(a) presents a footing resting on sandy soil. Figure 1(b) shows a footing resting on clay soil. Figure 1(c) presents the uniform soil pressure distribution used in the current design.

The bearing capacity has been investigated for shallow footings subjected to biaxial bending, which takes into account a linear ground pressure distribution and this contact area works partly in compression (Irlés-Más and Irlés-Más, 1992; Özmen, 2011; Rodríguez-Gutierrez and Aristizabal-Ochoa, 2013a, b; Lee et al., 2015; Kaur and Kumar, 2016; Bezmalinovic Colleoni, 2016; Dagdeviren, 2016; Aydogdu, 2016; Girgin, 2017; Turedi et al., 2019; Al-Gahtani and Adekunle, 2019; Galvis and Smith-Pardo, 2020; Rawat et al., 2020; Lezgy-Nazargah et al., 2022; Gör, 2022).

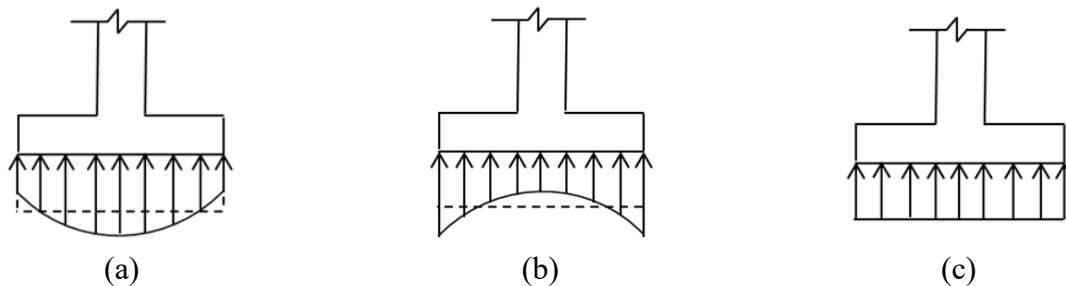


Figure 1. Pressure distribution under the footing

Source: Own elaboration

The mathematical models for the foundations design: for isolated footings have been developed for square, circular and rectangular shapes (Algin, 2000, 2007; Luévanos-Rojas, 2012a, b, 2013, 2014a, 2015a; Luévanos-Rojas et al., 2013, 2014b, 2016b, et al., 2017; Filho et al., 2017; López-Chavarría et al., 2017a, c, 2019; Khajehzadeh et al., 2014); For rectangular, trapezoidal, corner, T-shaped and strap combined footings (Jahanandish et al., 2012; Luévanos-Rojas, 2014c, 2015b, c, d, 2016<sup>a</sup>, b, et al., 2018a, b, 2020; López-Chavarría et al., 2017b; Velázquez-Santillán et al., 2019; Aguilera-Mancilla et al., 2019; Yáñez-Palafox et al., 2019). These papers take into account the entire contact area working under compression.

The models closest to this document are: Soto-García et al. (2022) proposed a mathematical model to obtain the minimum area for circular isolated footings, taking into account that footing area in contact with the soil works partially to compression, this model presents a case because the analysis is developed for the resultant moment. Vela-Moreno et al. (2022) developed a mathematical model to find the minimum surface for rectangular isolated footings, taking into account that footing area in contact with the soil works partially to compression, this model shows five cases for biaxial bending, two cases for uniaxial bending (Load is on the X axis) and another two cases for uniaxial bending (Load is on the Y axis). Kim-Sánchez et al. (2022) presented a mathematical model to obtain the thickness and the areas of transverse and longitudinal steel for circular isolated footings, taking into account that footing area in contact with the soil works partially to compression.

This investigation presents a new analytical model to obtain a complete design (thickness and areas of transverse and longitudinal steel) for rectangular isolated footings, taking into account that footing area in contact with the soil works partially to compression, this model is based on the area of contact with the soil (sides of footing) of the model proposed by Vela-Moreno *et al.* (2022). The formulation of the new model is developed by integration to find the moments, the flexural shearing

and the punching shearing under the code criteria (ACI 318S-19). Other authors present the equations to find the complete design of a rectangular isolated footing, but considering the total surface working under compression. Numerical examples are shown to find the complete design of rectangular isolated footings under axial load and moments in one and two directions and the results are compared with those of other authors to observe the differences. The ground contact areas presented in this document are based on the work proposed by Vela-Moreno et al. (2022). This model will have its impact on the construction industry with lower costs (materials and labor).

## 2. FORMULATION OF THE NEW MODEL

A rigid rectangular isolated footing is deformed in a planar shape, i.e., the distribution of soil pressure under the footing is considered linear.

The general equation for any footings subjected to biaxial bending under a factorized axial load and two factorized orthogonal moments is:

$$\sigma_u(x, y) = \frac{P_u}{h_x h_y} + \frac{12M_{ux}y}{h_x h_y^3} + \frac{12M_{uy}x}{h_x^3 h_y} \quad (1)$$

where:  $\sigma_u$  is the factorized pressure generated by the soil due to the factorized axial load and the factorized moments that are applied at the footing,  $P_u$  is the factorized axial load,  $M_{ux}$  is the factorized moment on the X axis,  $M_{uy}$  is the factorized moment on the Y axis,  $h_x$  and  $h_y$  are the sides of the footing,  $x$  and  $y$  are the coordinates where the pressure generated by the soil is located. The biaxial bending equation can be applied when the resultant force  $P_u$  is located inside the central nucleus (area working fully in compression), and when the resultant force  $P_u$  is outside of the central nucleus (area working partially in compression) is not valid.

When the resultant force  $P_u$  is outside of the central nucleus, the general equations of soil pressure under the footing subjected to uniaxial and biaxial bending are:

Uniaxial bending ( $P_u$  is located on the Y axis):

$$\sigma_z(x, y) = \frac{\sigma_{umax}(2h_{y1} - h_y + 2y)}{2h_{y1}} \quad (2)$$

Uniaxial bending ( $P_u$  is located on the X axis):

$$\sigma_z(x, y) = \frac{\sigma_{umax}(2h_{x1} - h_x + 2x)}{2h_{x1}} \quad (3)$$

Biaxial bending:

$$\sigma_z(x, y) = \frac{\sigma_{umax}[h_{y1}(2x - h_x) + h_{x1}(2y - h_y) + 2h_{x1}h_{y1}]}{2h_{x1}h_{y1}} \quad (4)$$

where:  $\sigma_{umax}$  is the factorized maximum pressure generated by the soil due to the factorized axial load and the factorized moments that are applied at the footing.

The critical sections for moments are located on the  $a-a$  and  $b-b$  axes, for the critical sections for the flexural shearing are located on the  $c-c$  and  $e-e$  axes, and the critical section for the punching shearing occurs in the perimeter formed by points 5, 6, 7 and 8 (ACI 318S-19).

**2.1. Rectangular isolated footing subjected to uniaxial bending**

Figure 2 shows the four possible cases to obtain the minimum area of a rectangular isolated footing subjected to uniaxial bending. Two cases when  $P$  is located on the  $Y$  axis: 1) when  $P$  is located inside the central nucleus; 2) when  $P$  is located outside the central nucleus. Two cases when  $P$  is located on the  $X$  axis: 1) when  $P$  is located inside the central nucleus; 2) when  $P$  is located outside the central nucleus.

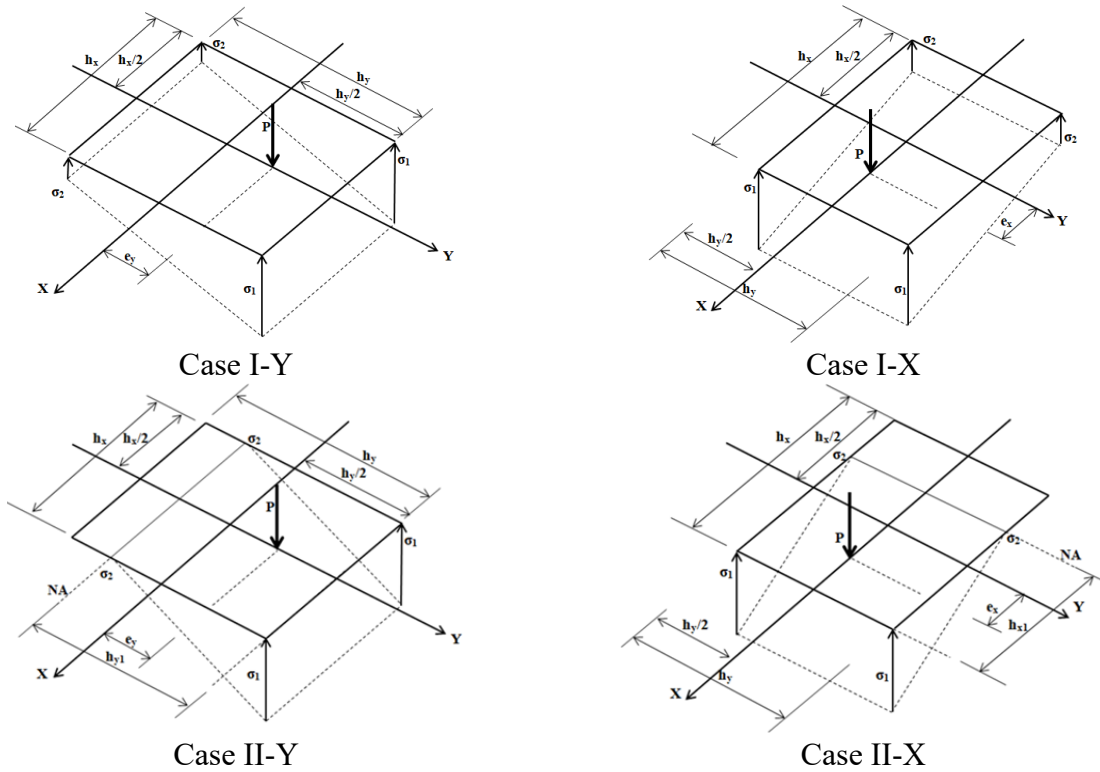


Figure 2. Four possible cases of minimum area for uniaxial bending  
Source: Own elaboration based on Vela-Moreno et al. (2022)

Figure 3 shows the critical sections for moments and flexural shearing of four possible cases: Case I-Y when  $P$  is located on the  $Y$  axis, and inside the central nucleus. Case II-Y when  $P$  is located on the  $Y$  axis, and outside the central nucleus: Case II-YA when the neutral axis is located  $h_y/2 - h_{y1} \geq c_1/2$  (moment) and  $h_y/2 - h_{y1} \geq c_1/2 + d$  (flexural shearing); Case II-YB when the neutral axis is located  $h_y/2 - h_{y1} \leq c_1/2$  (moment) and  $h_y/2 - h_{y1} \leq c_1/2 + d$  (flexural shearing). Case I-X when  $P$  is located on the  $X$  axis, and inside the central nucleus. Case II-X when  $P$  is located on the  $X$  axis, and outside the central nucleus: Case II-XA when the neutral axis is located  $h_x/2 - h_{x1} \geq c_2/2$  (moment) and  $h_x/2 - h_{x1} \geq c_2/2 + d$  (flexural shearing); Case II-XB when the neutral axis is located  $h_x/2 - h_{x1} \leq c_2/2$  (moment) and  $h_x/2 - h_{x1} \leq c_2/2 + d$  (flexural shearing).

**2.1.1. Flexural shearing and moments**

The general equations in the “c” and “e” axes for the factored flexural shearing “ $V_{uc}$ ” and “ $V_{ue}$ ”, and in the “a” and “b” axes for the factored moments “ $M_{ua}$ ” and “ $M_{ub}$ ” are:

**Case I-Y**

$$V_{uc} = \int_{\frac{c_1}{2}+d}^{\frac{h_y}{2}} \int_{-\frac{h_x}{2}}^{\frac{h_x}{2}} \sigma_u(x, y) dx dy \tag{5}$$

$$V_{ue} = \int_{\frac{c_2}{2}+d}^{\frac{h_x}{2}} \int_{-\frac{h_y}{2}}^{\frac{h_y}{2}} \sigma_u(x, y) dy dx \tag{6}$$

$$M_{ua} = \int_{\frac{c_1}{2}}^{\frac{h_y}{2}} \int_{-\frac{h_x}{2}}^{\frac{h_x}{2}} \sigma_u(x, y) \left( y - \frac{c_1}{2} \right) dx dy \tag{7}$$

$$M_{ub} = \int_{\frac{c_2}{2}}^{\frac{h_x}{2}} \int_{-\frac{h_y}{2}}^{\frac{h_y}{2}} \sigma_u(x, y) \left( x - \frac{c_2}{2} \right) dy dx \tag{8}$$

where:  $d$  is the effective depth of the footing,  $c_1$  and  $c_2$  are the sides of the column.

Note: Equation (1) is substituted into equations (5) to (8) and  $M_{uy} = 0$  and the integrals are developed to obtain the final equations.

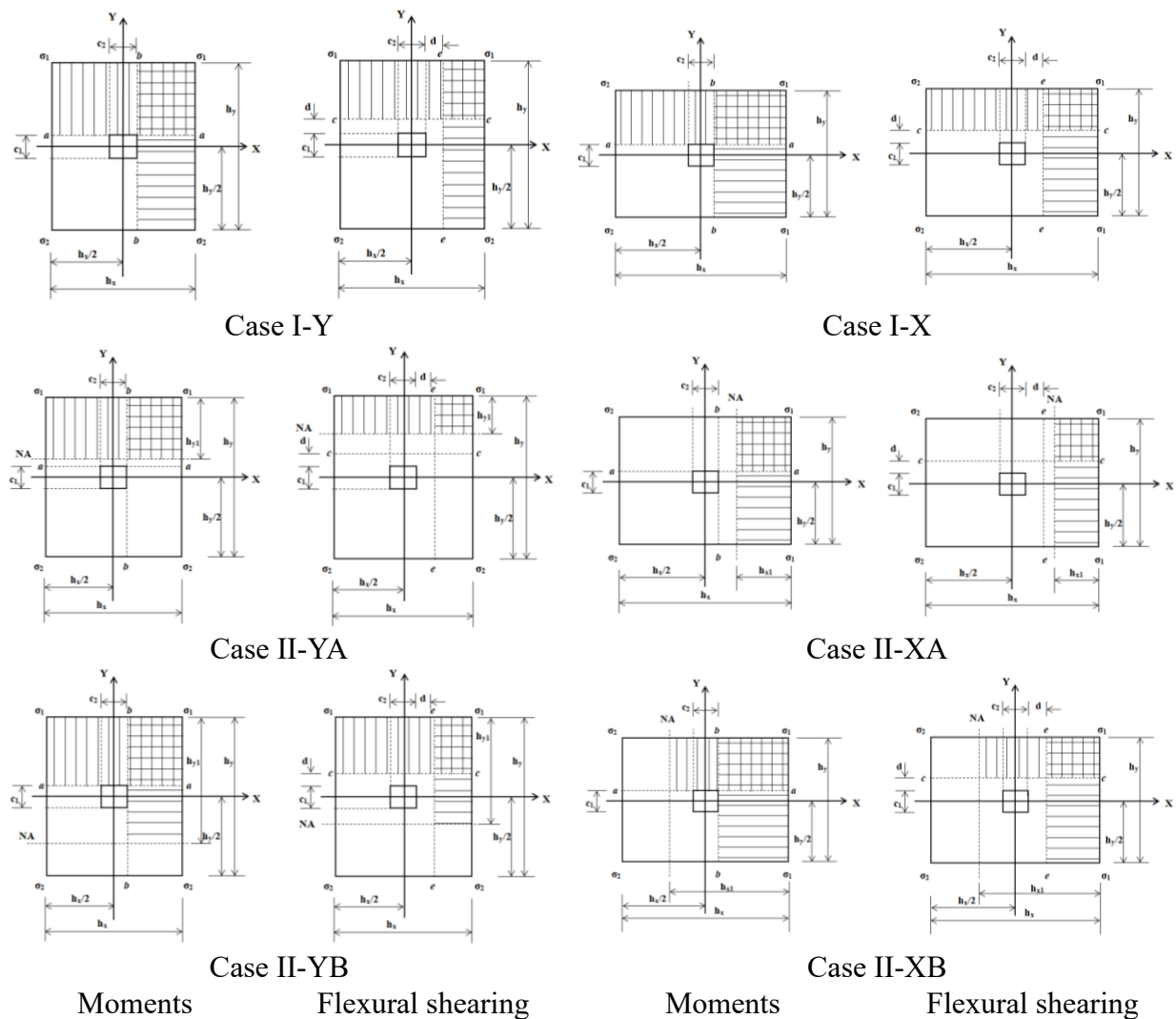


Figure 3. Moments and flexural shearing for uniaxial bending

Source: Own elaboration

**Case II-YA**

For  $h_y/2 - h_{y1} \geq c_1/2 + d$  (flexural shearing) and  $h_y/2 - h_{y1} \geq c_1/2$  (moment) are:

$$V_{uc} = \int_{\frac{h_y}{2}-h_{y1}}^{\frac{h_y}{2}} \int_{-\frac{h_x}{2}}^{\frac{h_x}{2}} \sigma_z(x, y) dx dy \tag{9}$$

$$V_{ue} = \int_{\frac{c_2}{2}+d}^{\frac{h_x}{2}} \int_{\frac{h_y}{2}-h_{y1}}^{\frac{h_y}{2}} \sigma_z(x, y) dy dx \tag{10}$$

$$M_{ua} = \int_{\frac{h_y}{2}-h_{y1}}^{\frac{h_y}{2}} \int_{-\frac{h_x}{2}}^{\frac{h_x}{2}} \sigma_z(x, y) \left(y - \frac{c_1}{2}\right) dx dy \tag{11}$$

$$M_{ub} = \int_{\frac{c_2}{2}}^{\frac{h_x}{2}} \int_{\frac{h_y}{2}-h_{y1}}^{\frac{h_y}{2}} \sigma_z(x, y) \left(x - \frac{c_2}{2}\right) dy dx \tag{12}$$

**Case II-YB**

For  $h_y/2 - h_{y1} \leq c_1/2 + d$  (flexural shearing) and  $h_y/2 - h_{y1} \leq c_1/2$  (moment) are:

$$V_{uc} = \int_{\frac{c_1}{2}+d}^{\frac{h_y}{2}} \int_{-\frac{h_x}{2}}^{\frac{h_x}{2}} \sigma_z(x, y) dx dy \tag{13}$$

$$V_{ue} = \int_{\frac{c_2}{2}+d}^{\frac{h_x}{2}} \int_{\frac{h_y}{2}-h_{y1}}^{\frac{h_y}{2}} \sigma_z(x, y) dy dx \tag{14}$$

$$M_{ua} = \int_{\frac{c_1}{2}}^{\frac{h_y}{2}} \int_{-\frac{h_x}{2}}^{\frac{h_x}{2}} \sigma_z(x, y) \left(y - \frac{c_1}{2}\right) dx dy \tag{15}$$

$$M_{ub} = \int_{\frac{c_2}{2}}^{\frac{h_x}{2}} \int_{\frac{h_y}{2}-h_{y1}}^{\frac{h_y}{2}} \sigma_z(x, y) \left(x - \frac{c_2}{2}\right) dy dx \tag{16}$$

Note: Equation (2) is substituted into equations (9) to (16) and the integrals are developed to obtain the final equations.

**Case I-X**

The general equations in the “c” and “e” axes for the factored flexural shearing “ $V_{uc}$ ” and “ $V_{ue}$ ”, and in the “a” and “b” axes for the factored moments “ $M_{ua}$ ” and “ $M_{ub}$ ” are equations (5) to (8). But in these equations  $M_{ux} = 0$  is substituted and the integrals are developed to obtain the final equations.

**Case II-XA**

For  $h_x/2 - h_{x1} \geq c_2/2 + d$  (flexural shearing) and  $h_x/2 - h_{x1} \geq c_2/2$  (moment) are:

$$V_{uc} = \int_{\frac{c_1}{2}+d}^{\frac{h_y}{2}} \int_{\frac{h_x}{2}-h_{x1}}^{\frac{h_x}{2}} \sigma_z(x, y) dx dy \tag{17}$$

$$V_{ue} = \int_{\frac{h_x}{2}-h_{x1}}^{\frac{h_x}{2}} \int_{-\frac{h_y}{2}}^{\frac{h_y}{2}} \sigma_z(x, y) dy dx \tag{18}$$

$$M_{ua} = \int_{\frac{c_1}{2}}^{\frac{h_y}{2}} \int_{\frac{h_x}{2}-h_{x1}}^{\frac{h_x}{2}} \sigma_z(x, y) \left( y - \frac{c_1}{2} \right) dx dy \tag{19}$$

$$M_{ub} = \int_{\frac{h_x}{2}-h_{x1}}^{\frac{h_x}{2}} \int_{-\frac{h_y}{2}}^{\frac{h_y}{2}} \sigma_z(x, y) \left( x - \frac{c_2}{2} \right) dy dx \tag{20}$$

**Case II-XB**

For  $h_x/2 - h_{x1} \leq c_2/2 + d$  (flexural shearing) and  $h_x/2 - h_{x1} \leq c_2/2$  (moment) are:

$$V_{uc} = \int_{\frac{c_1}{2}+d}^{\frac{h_y}{2}} \int_{\frac{h_x}{2}-h_{x1}}^{\frac{h_x}{2}} \sigma_z(x, y) dx dy \tag{21}$$

$$V_{ue} = \int_{\frac{c_2}{2}+d}^{\frac{h_x}{2}} \int_{-\frac{h_y}{2}}^{\frac{h_y}{2}} \sigma_z(x, y) dy dx \tag{22}$$

$$M_{ua} = \int_{\frac{c_1}{2}}^{\frac{h_y}{2}} \int_{\frac{h_x}{2}-h_{x1}}^{\frac{h_x}{2}} \sigma_z(x, y) \left( y - \frac{c_1}{2} \right) dx dy \tag{23}$$

$$M_{ub} = \int_{\frac{c_2}{2}}^{\frac{h_x}{2}} \int_{\frac{h_y}{2}-h_{y1}}^{\frac{h_y}{2}} \sigma_z(x, y) \left( x - \frac{c_2}{2} \right) dy dx \tag{24}$$

Note: Equation (3) is substituted into equations (17) to (24) and the integrals are developed to obtain the final equations.

**2.1.2. Punching shearing**

Figure 4 shows the critical sections for punching shearing of four possible cases: Case I-Y when  $P$  is located on the Y axis and inside the central nucleus. Case II-Y when  $P$  is located on the Y axis and outside the central nucleus: Case II-YA when the neutral axis is localized  $h_y/2 - h_{y1} \geq c_1/2 + d/2$ , Case II-YB when the neutral axis is localized  $h_y/2 - h_{y1} \leq c_1/2 + d/2$ . Case I-X when  $P$  is located on the X axis and inside the central nucleus. Case II-X when  $P$  is located on the X axis and outside the central nucleus: Case II-XA when the neutral axis is localized  $h_x/2 - h_{x1} \geq c_2/2 + d/2$ , Case II-XB when the neutral axis is localized  $h_x/2 - h_{x1} \leq c_2/2 + d/2$ .

The general equation for the factorized punching shearing “ $V_{up}$ ” is:

**Case I-Y**

$$V_{up} = P_u - \int_{-\frac{c_1}{2} - \frac{d}{2}}^{\frac{c_1}{2} + \frac{d}{2}} \int_{-\frac{c_2}{2} - \frac{d}{2}}^{\frac{c_2}{2} + \frac{d}{2}} \sigma_u(x, y) dx dy \tag{25}$$

Note: Equation (1) is substituted into equation (25) and  $M_{uy} = 0$  and the integral is developed to obtain the final equation.

**Case II-YA**

For  $h_y/2 - h_{yI} \geq c_1/2 + d/2$  is:

$$V_{up} = P_u \tag{26}$$

**Case II-YB**

For  $h_y/2 - h_{yI} \leq c_1/2 + d/2$  is:

$$V_{up} = P_u - \int_{y_s}^{\frac{c_1}{2} + \frac{d}{2}} \int_{-\frac{c_2}{2} - \frac{d}{2}}^{\frac{c_2}{2} + \frac{d}{2}} \sigma_z(x, y) dx dy \tag{27}$$

where:  $-c_1/2 - d/2 \leq y_s \leq c_1/2 + d/2$

Note: Equation (2) is substituted into equation (27) and the integral is developed to obtain the final equation.

**Case I-X**

Equation (1) is substituted into equation (25) and  $M_{ux} = 0$  and the integral is developed to obtain the final equation.

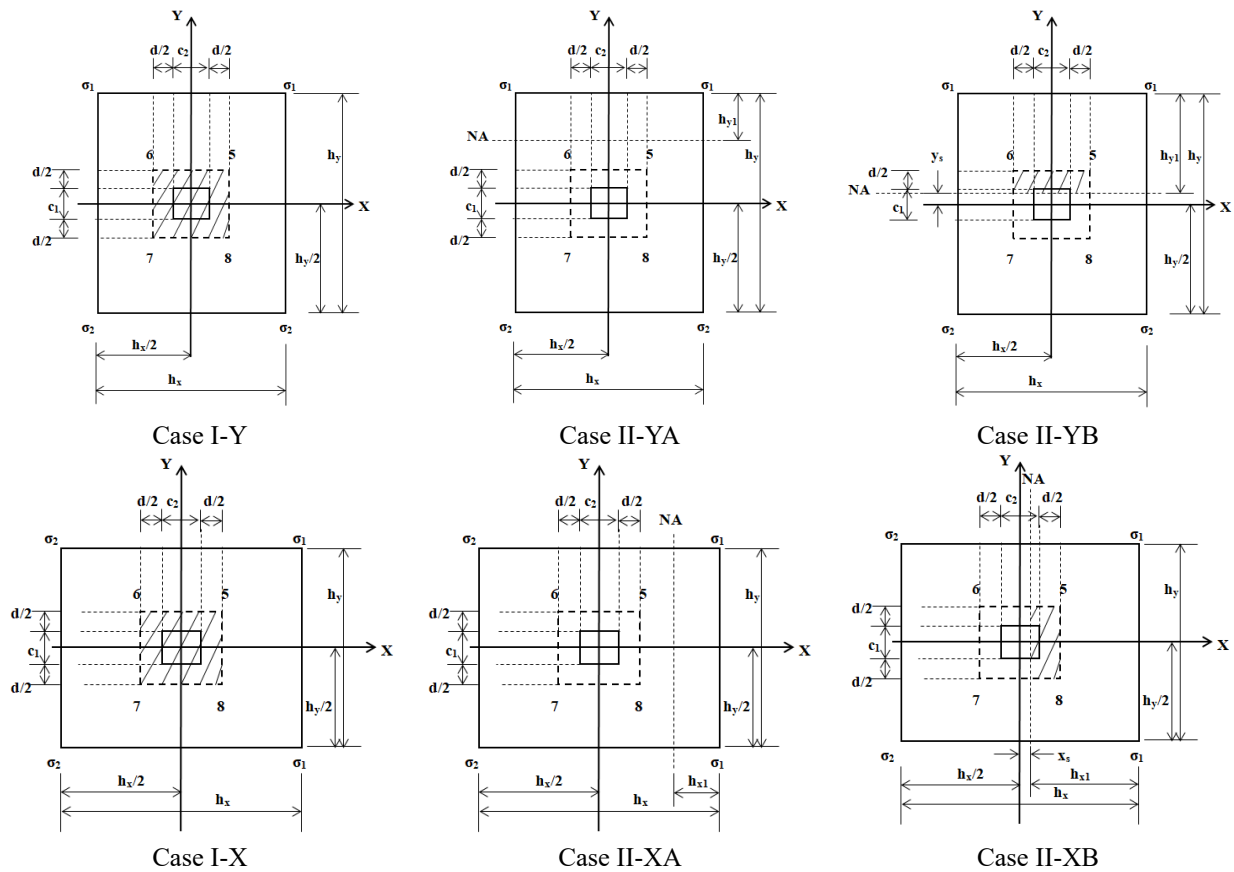


Figure 4. Punching shear for uniaxial bending  
Source: Own elaboration

**Case II-XA**

For  $h_x/2 - h_{x1} \geq c_2/2 + d/2$  is equation (26).

**Case II-XB**

For  $h_x/2 - h_{x1} \leq c_2/2 + d/2$  is:

$$V_{up} = P_u - \int_{x_s}^{\frac{c_2}{2} + \frac{d}{2}} \int_{-\frac{c_1}{2} - \frac{d}{2}}^{\frac{c_1}{2} + \frac{d}{2}} \sigma_z(x, y) dy dx \tag{28}$$

where:  $-c_2/2 - d/2 \leq x_s \leq c_2/2 + d/2$ .

Note: Equation (3) is substituted into equation (28) and the integral is developed to obtain the final equation.

**2.2. Rectangular isolated footing subjected to biaxial bending**

Figure 5 shows the five possible cases to obtain the minimum area of a rectangular isolated footing subjected to biaxial bending.

For case I, it is considered that the total surface of the footing works under compression. The pressure generated by the soil on the footing is obtained by equation (1) (biaxial bending).

For cases II, III, IV and V consider that the total surface of the footing works partially under compression, i.e., part of the surface has zero pressure. The pressure generated by the soil on the footing is obtained by equation (4).

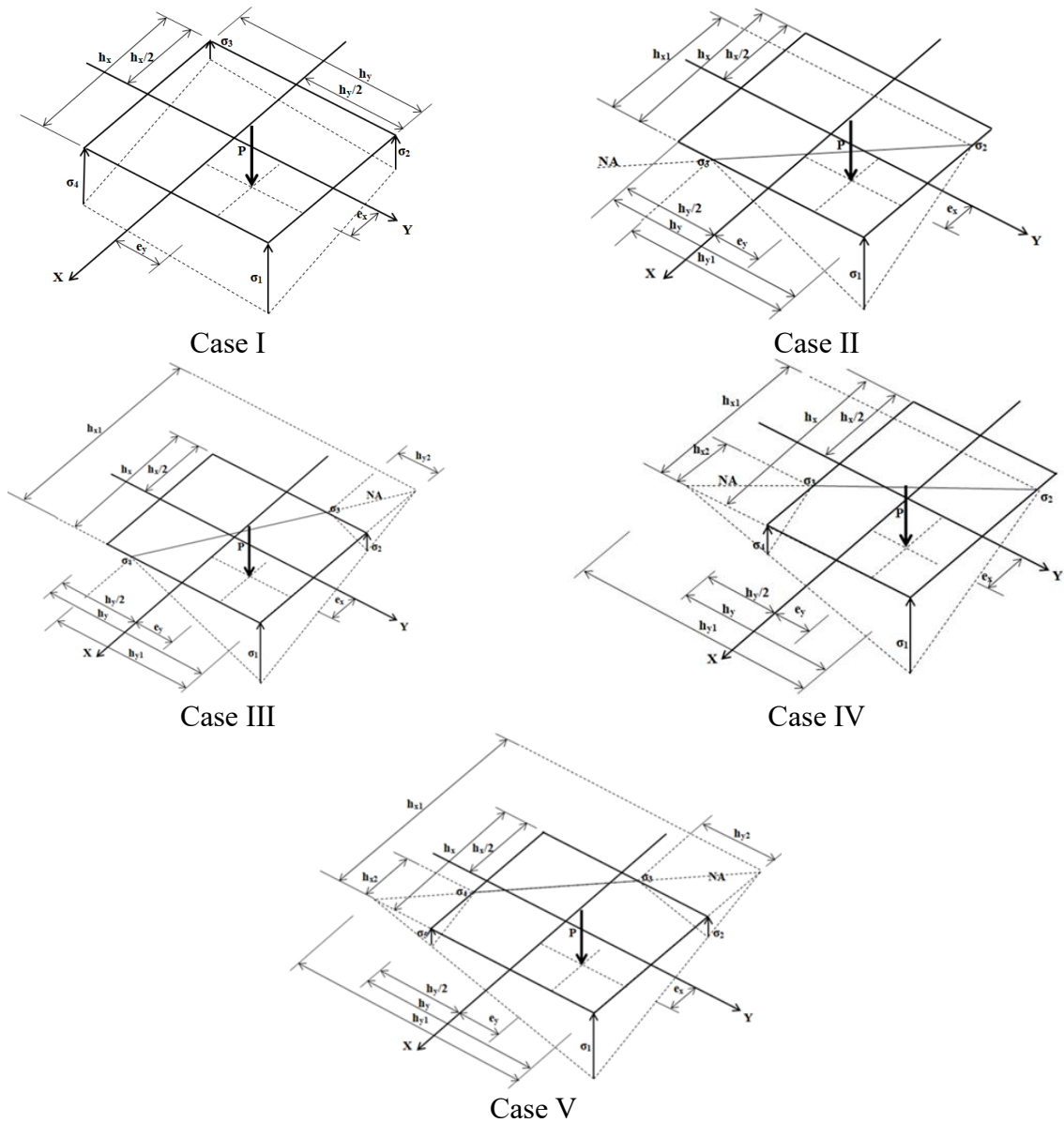


Figure 5. Five possible cases of minimum area for biaxial bending  
 Source: Own elaboration based on Vela-Moreno et al. (2022)

### 2.2.1. Flexural shearing and moments

Figure 6 shows the critical sections for flexural shearing and moments for all possible cases. The general equations on the “ $c$ ” and “ $e$ ” axes for the factorized flexural shearing “ $V_{uc}$ ” and “ $V_{ue}$ ”, on the “ $a$ ” and “ $b$ ” axes for the factorized moments “ $M_{ua}$ ” and “ $M_{ub}$ ” are:

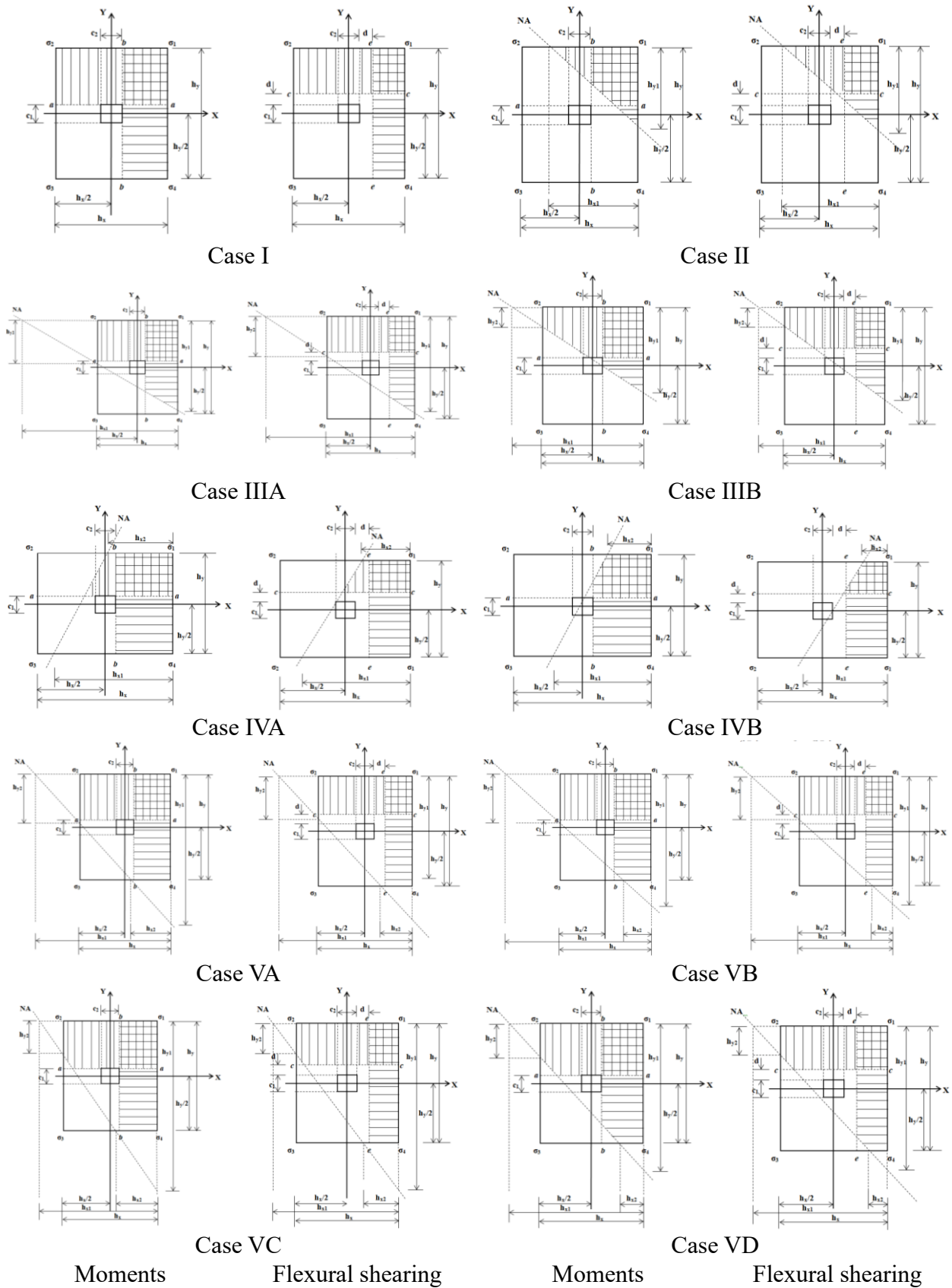


Figure 6. Moments and flexural shearing for biaxial bending

Source: Own elaboration

**Case I**

When  $P$  is located inside the central nucleus

Equation (1) is substituted into Equations (5) to (8) and the integrals are developed to obtain the final equations.

**Case II**

When  $P$  is located outside the central nucleus

$$V_{uc} = \int_{\frac{c_1}{2}+d}^{\frac{h_y}{2}} \int_{\frac{h_x}{2} + \frac{h_{x1}(h_y-2y)}{2h_{y1}} - h_{x1}}^{\frac{h_x}{2}} \sigma_z(x, y) dx dy \tag{29}$$

$$V_{ue} = \int_{\frac{c_2}{2}+d}^{\frac{h_x}{2}} \int_{\frac{h_y}{2} + \frac{h_{y1}(h_x-2x)}{2h_{x1}} - h_{y1}}^{\frac{h_y}{2}} \sigma_z(x, y) dy dx \tag{30}$$

$$M_{ua} = \int_{\frac{c_1}{2}}^{\frac{h_y}{2}} \int_{\frac{h_x}{2} + \frac{h_{x1}(h_y-2y)}{2h_{y1}} - h_{x1}}^{\frac{h_x}{2}} \sigma_z(x, y) \left( y - \frac{c_1}{2} \right) dx dy \tag{31}$$

$$M_{ub} = \int_{\frac{c_2}{2}}^{\frac{h_x}{2}} \int_{\frac{h_y}{2} + \frac{h_{y1}(h_x-2x)}{2h_{x1}} - h_{y1}}^{\frac{h_y}{2}} \sigma_z(x, y) \left( x - \frac{c_2}{2} \right) dy dx \tag{32}$$

**Case III**

When  $P$  is located outside the central nucleus of two possible cases: Case IIIA when the neutral axis is located  $h_y/2 - h_{y2} \leq c_1/2$  (moment) and  $h_y/2 - h_{y2} \leq c_1/2 + d$  (flexural shearing); Case IIIB when the neutral axis is located  $h_y/2 - h_{y2} \geq c_1/2$  (moment) and  $h_y/2 - h_{y2} \geq c_1/2 + d$  (flexural shearing).

**Case IIIA**

$$V_{uc} = \int_{\frac{c_1}{2}+d}^{\frac{h_y}{2}} \int_{-\frac{h_x}{2}}^{\frac{h_x}{2}} \sigma_z(x, y) dx dy \tag{33}$$

$$V_{ue} = \int_{\frac{c_2}{2}+d}^{\frac{h_x}{2}} \int_{\frac{h_y}{2} + \frac{h_{y1}(h_x-2x)}{2h_{x1}} - h_{y1}}^{\frac{h_y}{2}} \sigma_z(x, y) dy dx \tag{34}$$

$$M_{ua} = \int_{\frac{c_1}{2}}^{\frac{h_y}{2}} \int_{-\frac{h_x}{2}}^{\frac{h_x}{2}} \sigma_z(x, y) \left( y - \frac{c_1}{2} \right) dx dy \tag{35}$$

$$M_{ub} = \int_{\frac{c_2}{2}}^{\frac{h_x}{2}} \int_{\frac{h_y}{2} + \frac{h_{y1}(h_x-2x)}{2h_{x1}} - h_{y1}}^{\frac{h_y}{2}} \sigma_z(x, y) \left( x - \frac{c_2}{2} \right) dy dx \tag{36}$$

**Case IIIB**

$$V_{uc} = \int_{\frac{c_1}{2}+d}^{\frac{h_y}{2}-h_{y2}} \int_{\frac{h_x}{2}+\frac{h_{x1}(h_y-2y)}{2h_{y1}}-h_{x1}}^{\frac{h_x}{2}} \sigma_z(x, y) dx dy + \int_{\frac{h_y}{2}-h_{y2}}^{\frac{h_y}{2}} \int_{-\frac{h_x}{2}}^{\frac{h_x}{2}} \sigma_z(x, y) dx dy \quad (37)$$

$$V_{ue} = \int_{\frac{c_2}{2}+d}^{\frac{h_x}{2}} \int_{\frac{h_y}{2}+\frac{h_{y1}(h_x-2x)}{2h_{x1}}-h_{y1}}^{\frac{h_y}{2}} \sigma_z(x, y) dy dx \quad (38)$$

$$M_{ua} = \int_{\frac{c_1}{2}}^{\frac{h_y}{2}-h_{y2}} \int_{\frac{h_x}{2}+\frac{h_{x1}(h_y-2y)}{2h_{y1}}-h_{x1}}^{\frac{h_x}{2}} \sigma_z(x, y) \left(y - \frac{c_1}{2}\right) dx dy + \int_{\frac{h_y}{2}-h_{y2}}^{\frac{h_y}{2}} \int_{-\frac{h_x}{2}}^{\frac{h_x}{2}} \sigma_z(x, y) \left(y - \frac{c_1}{2}\right) dx dy \quad (39)$$

$$M_{ub} = \int_{\frac{c_2}{2}}^{\frac{h_x}{2}} \int_{\frac{h_y}{2}+\frac{h_{y1}(h_x-2x)}{2h_{x1}}-h_{y1}}^{\frac{h_y}{2}} \sigma_z(x, y) \left(x - \frac{c_2}{2}\right) dy dx \quad (40)$$

where:  $h_{y2} = h_{y1}(h_{x1} - h_x)/h_{x1}$ .

**Case IV**

When  $P$  is located outside the central nucleus of two possible cases: Case IVA when the neutral axis is located  $h_x/2 - h_{x2} \leq c_2/2$  (moment) and  $h_x/2 - h_{x2} \leq c_2/2 + d$  (flexural shearing); Case IIIB when the neutral axis is located  $h_x/2 - h_{x2} \geq c_2/2$  (moment) and  $h_x/2 - h_{x2} \geq c_2/2 + d$  (flexural shearing).

**Case IVA**

$$V_{uc} = \int_{\frac{c_1}{2}+d}^{\frac{h_y}{2}} \int_{\frac{h_x}{2}+\frac{h_{x1}(h_y-2y)}{2h_{y1}}-h_{x1}}^{\frac{h_x}{2}} \sigma_z(x, y) dx dy \quad (41)$$

$$V_{ue} = \int_{\frac{c_2}{2}+d}^{\frac{h_x}{2}} \int_{-\frac{h_y}{2}}^{\frac{h_y}{2}} \sigma_z(x, y) dy dx \quad (42)$$

$$M_{ua} = \int_{\frac{c_1}{2}}^{\frac{h_y}{2}} \int_{\frac{h_x}{2}+\frac{h_{x1}(h_y-2y)}{2h_{y1}}-h_{x1}}^{\frac{h_x}{2}} \sigma_z(x, y) \left(y - \frac{c_1}{2}\right) dx dy \quad (43)$$

$$M_{ub} = \int_{\frac{c_2}{2}}^{\frac{h_x}{2}} \int_{-\frac{h_y}{2}}^{\frac{h_y}{2}} \sigma_z(x, y) \left(x - \frac{c_2}{2}\right) dy dx \quad (44)$$

**Case IVB**

$$V_{uc} = \int_{\frac{c_1}{2}+d}^{\frac{h_y}{2}} \int_{\frac{h_x}{2} + \frac{h_{x1}(h_y-2y)}{2h_{y1}} - h_{x1}}^{\frac{h_x}{2}} \sigma_z(x, y) dx dy \tag{45}$$

$$V_{ue} = \int_{\frac{c_2}{2}+d}^{\frac{h_x}{2} - h_{x2}} \int_{\frac{h_y}{2} + \frac{h_{y1}(h_x-2x)}{2h_{x1}} - h_{y1}}^{\frac{h_y}{2}} \sigma_z(x, y) dy dx + \int_{\frac{h_x}{2} - h_{x2}}^{\frac{h_x}{2}} \int_{-\frac{h_y}{2}}^{\frac{h_y}{2}} \sigma_z(x, y) dy dx \tag{46}$$

$$M_{ua} = \int_{\frac{c_1}{2}}^{\frac{h_y}{2}} \int_{\frac{h_x}{2} + \frac{h_{x1}(h_y-2y)}{2h_{y1}} - h_{x1}}^{\frac{h_x}{2}} \sigma_z(x, y) \left( y - \frac{c_1}{2} \right) dx dy \tag{47}$$

$$M_{ub} = \int_{\frac{c_2}{2}}^{\frac{h_x}{2} - h_{x2}} \int_{\frac{h_y}{2} + \frac{h_{y1}(h_x-2x)}{2h_{x1}} - h_{y1}}^{\frac{h_y}{2}} \sigma_z(x, y) \left( x - \frac{c_2}{2} \right) dy dx + \int_{\frac{h_x}{2} - h_{x2}}^{\frac{h_x}{2}} \int_{-\frac{h_y}{2}}^{\frac{h_y}{2}} \sigma_z(x, y) \left( x - \frac{c_2}{2} \right) dy dx \tag{48}$$

where:  $h_{x2} = h_{x1}(h_{y1} - h_y)/h_{y1}$ .

**Case V**

When  $P$  is located outside the central nucleus of four possible cases: Case VA when the neutral axis is localized  $h_y/2 - h_{y2} \leq c_1/2 + d$  and  $h_x/2 - h_{x2} \leq c_2/2 + d$  (flexural shearing) and  $h_y/2 - h_{y2} \leq c_1/2$  and  $h_x/2 - h_{x2} \leq c_2/2$  (moment); Case VB when the neutral axis is localized  $h_y/2 - h_{y2} \leq c_1/2 + d$  and  $h_x/2 - h_{x2} \geq c_2/2 + d$  (flexural shearing) and  $h_y/2 - h_{y2} \leq c_1/2$  and  $h_x/2 - h_{x2} \geq c_2/2$  (moment); Case VC when the neutral axis is localized  $h_y/2 - h_{y2} \geq c_1/2 + d$  and  $h_x/2 - h_{x2} \leq c_2/2 + d$  (flexural shearing) and  $h_y/2 - h_{y2} \geq c_1/2$  and  $h_x/2 - h_{x2} \leq c_2/2$  (moment); Case VD when the neutral axis is localized  $h_y/2 - h_{y2} \geq c_1/2 + d$  and  $h_x/2 - h_{x2} \geq c_2/2 + d$  (flexural shearing) and  $h_y/2 - h_{y2} \geq c_1/2$  and  $h_x/2 - h_{x2} \geq c_2/2$  (moment).

**Case VA**

$$V_{uc} = \int_{\frac{c_1}{2}+d}^{\frac{h_y}{2}} \int_{-\frac{h_x}{2}}^{\frac{h_x}{2}} \sigma_z(x, y) dx dy \tag{49}$$

$$V_{ue} = \int_{\frac{c_2}{2}+d}^{\frac{h_x}{2}} \int_{-\frac{h_y}{2}}^{\frac{h_y}{2}} \sigma_z(x, y) dy dx \tag{50}$$

$$M_{ua} = \int_{\frac{c_1}{2}}^{\frac{h_y}{2}} \int_{-\frac{h_x}{2}}^{\frac{h_x}{2}} \sigma_z(x, y) \left( y - \frac{c_1}{2} \right) dx dy \tag{51}$$

$$M_{ub} = \int_{\frac{c_2}{2}}^{\frac{h_x}{2}} \int_{-\frac{h_y}{2}}^{\frac{h_y}{2}} \sigma_z(x, y) \left(x - \frac{c_2}{2}\right) dydx \quad (52)$$

**Case VB**

$$V_{uc} = \int_{\frac{c_1}{2}+d}^{\frac{h_y}{2}} \int_{-\frac{h_x}{2}}^{\frac{h_x}{2}} \sigma_z(x, y) dx dy \quad (53)$$

$$V_{ue} = \int_{\frac{c_2}{2}+d}^{\frac{h_x}{2}-h_{x2}} \int_{\frac{h_y}{2} + \frac{h_{y1}(h_x-2x)}{2h_{x1}} - h_{y1}}^{\frac{h_y}{2}} \sigma_z(x, y) dy dx + \int_{\frac{h_x}{2}-h_{x2}}^{\frac{h_x}{2}} \int_{-\frac{h_y}{2}}^{\frac{h_y}{2}} \sigma_z(x, y) dy dx \quad (54)$$

$$M_{ua} = \int_{\frac{c_1}{2}}^{\frac{h_y}{2}} \int_{-\frac{h_x}{2}}^{\frac{h_x}{2}} \sigma_z(x, y) \left(y - \frac{c_1}{2}\right) dx dy \quad (55)$$

$$M_{ub} = \int_{\frac{c_2}{2}}^{\frac{h_x}{2}-h_{x2}} \int_{\frac{h_y}{2} + \frac{h_{y1}(h_x-2x)}{2h_{x1}} - h_{y1}}^{\frac{h_y}{2}} \sigma_z(x, y) \left(x - \frac{c_2}{2}\right) dy dx + \int_{\frac{h_x}{2}-h_{x2}}^{\frac{h_x}{2}} \int_{-\frac{h_y}{2}}^{\frac{h_y}{2}} \sigma_z(x, y) \left(x - \frac{c_2}{2}\right) dy dx \quad (56)$$

**Case VC**

$$V_{uc} = \int_{\frac{c_1}{2}+d}^{\frac{h_y}{2}-h_{y2}} \int_{\frac{h_x}{2} + \frac{h_{x1}(h_y-2y)}{2h_{y1}} - h_{x1}}^{\frac{h_x}{2}} \sigma_z(x, y) dx dy + \int_{\frac{h_y}{2}-h_{y2}}^{\frac{h_y}{2}} \int_{-\frac{h_x}{2}}^{\frac{h_x}{2}} \sigma_z(x, y) dx dy \quad (57)$$

$$V_{ue} = \int_{\frac{c_2}{2}+d}^{\frac{h_x}{2}} \int_{-\frac{h_y}{2}}^{\frac{h_y}{2}} \sigma_z(x, y) dy dx \quad (58)$$

$$M_{ua} = \int_{\frac{c_1}{2}}^{\frac{h_y}{2}-h_{y2}} \int_{\frac{h_x}{2} + \frac{h_{x1}(h_y-2y)}{2h_{y1}} - h_{x1}}^{\frac{h_x}{2}} \sigma_z(x, y) \left(y - \frac{c_1}{2}\right) dx dy + \int_{\frac{h_y}{2}-h_{y2}}^{\frac{h_y}{2}} \int_{-\frac{h_x}{2}}^{\frac{h_x}{2}} \sigma_z(x, y) \left(y - \frac{c_1}{2}\right) dx dy \quad (59)$$

$$M_{ub} = \int_{\frac{c_2}{2}}^{\frac{h_x}{2}} \int_{-\frac{h_y}{2}}^{\frac{h_y}{2}} \sigma_z(x, y) \left(x - \frac{c_2}{2}\right) dy dx \quad (60)$$

**Case VD**

$$V_{uc} = \int_{\frac{c_1}{2}+d}^{\frac{h_y}{2}-h_{y2}} \int_{\frac{h_x}{2} + \frac{h_{x1}(h_y-2y)}{2h_{y1}} - h_{x1}}^{\frac{h_x}{2}} \sigma_z(x, y) dx dy + \int_{\frac{h_y}{2}-h_{y2}}^{\frac{h_y}{2}} \int_{-\frac{h_x}{2}}^{\frac{h_x}{2}} \sigma_z(x, y) dx dy \quad (61)$$

$$V_{ue} = \int_{\frac{c_2}{2}+d}^{\frac{h_x}{2}-h_{x2}} \int_{\frac{h_y}{2} + \frac{h_{y1}(h_x-2x)}{2h_{x1}} - h_{y1}}^{\frac{h_y}{2}} \sigma_z(x, y) dy dx + \int_{\frac{h_x}{2}-h_{x2}}^{\frac{h_x}{2}} \int_{-\frac{h_y}{2}}^{\frac{h_y}{2}} \sigma_z(x, y) dy dx \quad (62)$$

$$M_{ua} = \int_{\frac{c_1}{2}}^{\frac{h_y}{2}-h_{y2}} \int_{\frac{h_x}{2} + \frac{h_{x1}(h_y-2y)}{2h_{y1}} - h_{x1}}^{\frac{h_x}{2}} \sigma_z(x, y) \left(y - \frac{c_1}{2}\right) dx dy + \int_{\frac{h_y}{2}-h_{y2}}^{\frac{h_y}{2}} \int_{-\frac{h_x}{2}}^{\frac{h_x}{2}} \sigma_z(x, y) \left(y - \frac{c_1}{2}\right) dx dy \quad (63)$$

$$M_{ub} = \int_{\frac{c_2}{2}}^{\frac{h_x}{2}-h_{x2}} \int_{\frac{h_y}{2} + \frac{h_{y1}(h_x-2x)}{2h_{x1}} - h_{y1}}^{\frac{h_y}{2}} \sigma_z(x, y) \left(x - \frac{c_2}{2}\right) dy dx + \int_{\frac{h_x}{2}-h_{x2}}^{\frac{h_x}{2}} \int_{-\frac{h_y}{2}}^{\frac{h_y}{2}} \sigma_z(x, y) \left(x - \frac{c_2}{2}\right) dy dx \quad (64)$$

Note: Equation (4) is substituted into equations (29) to (64) and the integrals are developed to obtain the final equations.

**2.2.2. Punching shearing**

Figure 7 shows the critical sections for punching shearing of six possible cases (Critical perimeter formed by points 5, 6, 7 and 8).

For case I, it is considered that the total surface of the footing works under compression. The pressure generated by the soil on the footing is obtained by equation (1) (biaxial bending).

For cases II, III, IV, V and VI consider that the total surface of the footing works partially under compression, i.e., part of the surface has zero pressure. The pressure generated by the soil on the footing is obtained by equation (4).

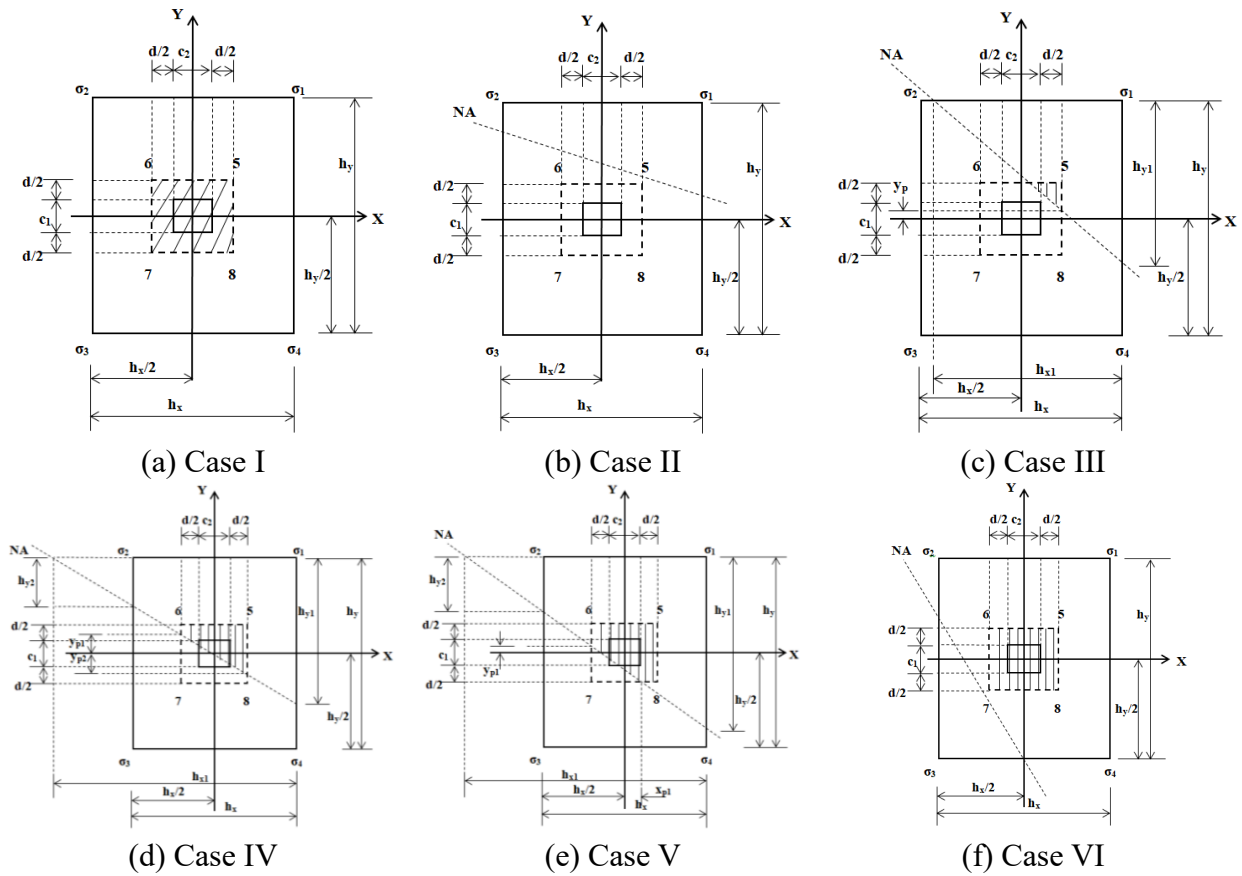


Figure 7. Punching shearing for biaxial bending  
Source: Own elaboration

The general equation for the factorized punching shearing “ $V_{up}$ ” is:

**Case I**

Equation (1) is substituted into equation (25) and the integral is developed to obtain the final equation.

**Case II**

The neutral axis does not reach the perimeter of the critical section; therefore, it is equation (26).

**Case III**

$$V_{up} = P_u - \int_{y_p}^{\frac{c_1+d}{2} + \frac{d}{2}} \int_{\frac{h_x}{2} - \frac{h_{x1}(2y-h_y)}{2h_{y1}} - h_{x1}}^{\frac{c_2+d}{2} + \frac{d}{2}} \sigma_z(x, y) dx dy \quad (65)$$

where:  $y_p = h_y/2 - h_{y1}(c_2 + d - h_x)/2h_{x1} - h_{y1}$  (If the neutral axis crosses the critical perimeter on the side formed by points 5 and 8) and  $y_p = -c_1/2 - d/2$  (If the neutral axis crosses the critical perimeter on the side formed by points 7 and 8).

**Case IV**

$$V_{up} = P_u - \int_{-\frac{c_2}{2}-\frac{d}{2}}^{\frac{c_2}{2}+\frac{d}{2}} \int_{\frac{h_y}{2}-\frac{h_{y1}(2x-h_x)}{2h_{x1}}-h_{y1}}^{y_{p1}} \sigma_z(x, y) dy dx - \int_{-\frac{c_2}{2}-\frac{d}{2}}^{\frac{c_2}{2}+\frac{d}{2}} \int_{y_{p1}}^{\frac{c_1}{2}+\frac{d}{2}} \sigma_z(x, y) dy dx \tag{66}$$

where:  $y_{p1} = h_y/2 + h_{y1}(c_2 + d + h_x)/2h_{x1} - h_{y1}$ .

**Case V**

$$V_{up} = P_u - \int_{-\frac{c_2}{2}-\frac{d}{2}}^{x_{p1}} \int_{\frac{h_y}{2}-\frac{h_{y1}(2x-h_x)}{2h_{x1}}-h_{y1}}^{y_{p1}} \sigma_z(x, y) dy dx - \int_{-\frac{c_2}{2}-\frac{d}{2}}^{\frac{c_2}{2}+\frac{d}{2}} \int_{y_{p1}}^{\frac{c_1}{2}+\frac{d}{2}} \sigma_z(x, y) dy dx - \int_{x_{p1}}^{\frac{c_2}{2}+\frac{d}{2}} \int_{-\frac{c_1}{2}-\frac{d}{2}}^{y_{p1}} \sigma_z(x, y) dy dx \tag{67}$$

where:  $x_{p1} = h_x/2 - h_{x1}(c_1 + d - h_y)/2h_{y1} - h_{x1}$  and  $y_{p1} = h_y/2 + h_{y1}(c_2 + d + h_x)/2h_{x1} - h_{y1}$ .

**Case VI**

$$V_{up} = P_u - \int_{-\frac{c_2}{2}-\frac{d}{2}}^{\frac{c_2}{2}+\frac{d}{2}} \int_{-\frac{c_1}{2}-\frac{d}{2}}^{\frac{c_1}{2}+\frac{d}{2}} \sigma_z(x, y) dy dx \tag{68}$$

where:  $x_{p1} = h_x/2 - h_{x1}(c_1 + d - h_y)/2h_{y1} - h_{x1}$  and  $y_{p1} = h_y/2 + h_{y1}(c_2 + d + h_x)/2h_{x1} - h_{y1}$ .

Note: Equation (4) is substituted into equations (65) to (68) and the integral are developed to obtain the final equations.

**3. RESULTS**

In this section the application of the new model is described, using the same examples to obtain the minimum area and the sides of a rectangular isolated footing proposed by Vela-Moreno et al. (2022).

Tables 1 and 2 present the four cases to obtain the complete design of the rectangular isolated footings subjected to uniaxial bending. Two cases when the axial load is located on the Y axis: Case I-Y, when the entire contact area works under compression; Case II-Y, when the contact area works partially in compression. Two cases when the axial load is located on the X axis: Case I-X, when the entire contact area works under compression; Case II-X, when the contact area works partially in compression.

Table 1 shows the results for  $c_1$  and  $c_2 = 0.40$  m,  $P_u = 720$  kN,  $M_{ux} = 360, 720, 1440, 2160$  kN-m,  $M_{uy} = 0$  kN-m and  $\sigma_{umax} = 250$  kN/m<sup>2</sup>.

The procedure used is the following:

For the case I-Y: Substituting  $P_u, M_{ux}, M_{uy} = 0, h_x, h_y$  into equation (1), and subsequently substituting equation (1),  $h_x, h_y, c_1, c_2$  and  $d$  into equations (5) to (8) and (25).

For the case II-Y: Substituting  $\sigma_{umax}, h_y, h_{y1}$  into equation (2), and subsequently substituting equation (2),  $h_x, h_y, c_1, c_2$  and  $d$  into equations (9) to (12) or (13) to (16), and (26) or (27) according to the case.

The value of  $d$  is fixed by the equations proposed by (ACI 318S-19).

Table 1. Complete design of the footing when the axial load is on the Y axis.  
(Source: Own elaboration)

Caso	M <sub>ux</sub> kN-m	h <sub>x</sub> m	h <sub>y</sub> m	d cm	M <sub>ua</sub> kN-m	M <sub>ub</sub> kN-m	V <sub>uc</sub> kN	V <sub>ue</sub> kN	V <sub>up</sub> kN	A <sub>smy</sub> cm <sup>2</sup>	A <sub>sminy</sub> cm <sup>2</sup>	A <sub>spy</sub> cm <sup>2</sup>	A <sub>smx</sub> cm <sup>2</sup>	A <sub>sminx</sub> cm <sup>2</sup>	A <sub>spx</sub> cm <sup>2</sup>
I-Y	360	1.00	3.65	52	410.97	32.40	342.89	*	553.04	22.00	17.32	22.80 (8Ø3/4")	1.65	63.20	65.55 (23Ø3/4")
II-Y		1.33	3.00	32	240.38	40.54	272.63	54.38	655.20	21.10	14.17	22.80 (8Ø3/4")	3.37	31.97	34.20 (12Ø3/4")
I-Y	720	1.00	6.00	67	794.45	32.40	420.46	*	582.61	33.32	22.31	34.20 (12Ø3/4")	1.28	133.87	136.89 (27Ø1")
II-Y		1.00	4.67	52	468.41	22.50	322.24	*	631.92	25.28	17.32	25.65 (9Ø3/4")	1.15	80.87	81.12 (16Ø1")
I-Y	1440	2.00	12.00	42	1693.21	115.20	500.88	136.80	699.83	130.51	27.97	131.82 (26Ø1")	7.27	167.83	172.38 (34Ø1")
II-Y		2.00	5.33	42	894.98	80.00	499.75	95.00	720.00	61.71	27.97	65.91 (13Ø1")	5.05	74.55	76.95 (27Ø3/4")
I-Y	2160	2.00	18.00	52	2592.81	115.20	510.05	100.80	703.07	161.36	34.63	162.24 (32Ø1")	5.87	311.69	314.34 (62Ø1")
II-Y		2.00	7.33	37	1268.16	80.00	350.12	107.50	720.00	109.86	24.64	111.54 (22Ø1")	5.73	90.31	91.20 (32Ø3/4")

where: A<sub>smy</sub> and A<sub>smx</sub> are the steel areas generated by the moments in the a (Y direction) and b (X direction) axes, A<sub>sminy</sub> and A<sub>sminx</sub> are the minimum steel areas in both directions, A<sub>spy</sub> and A<sub>spx</sub> are the proposed steel areas in the Y and X directions (ACI 318S-19). \* The axis is located outside the area of the footing.

Table 2 shows the results for c<sub>1</sub> and c<sub>2</sub> = 0.40 m, P<sub>u</sub> = 720 kN, M<sub>ux</sub> = 0 kN-m, M<sub>uy</sub> = 360, 720, 1440, 2160 kN-m and σ<sub>umax</sub> = 250 kN/m<sup>2</sup> (same procedure used in Table 1, but with the corresponding equations).

Table 2. Complete design of the footing when the axial load is on the X axis.  
(Source: Own elaboration)

Caso	M <sub>uy</sub> kN-m	h <sub>x</sub> m	h <sub>y</sub> m	d cm	M <sub>ua</sub> kN-m	M <sub>ub</sub> kN-m	V <sub>uc</sub> kN	V <sub>ue</sub> kN	V <sub>up</sub> kN	A <sub>smy</sub> cm <sup>2</sup>	A <sub>sminy</sub> cm <sup>2</sup>	A <sub>spy</sub> cm <sup>2</sup>	A <sub>smx</sub> cm <sup>2</sup>	A <sub>sminx</sub> cm <sup>2</sup>	A <sub>spx</sub> cm <sup>2</sup>
I-X	360	3.65	1.00	52	32.40	410.97	*	342.89	553.04	1.65	63.20	65.55 (23Ø3/4")	22.00	17.32	22.80 (8Ø3/4")
II-X		3.00	1.33	32	40.54	240.38	54.38	272.63	655.20	3.37	31.97	34.20 (12Ø3/4")	21.10	14.17	22.80 (8Ø3/4")
I-X	720	6.00	1.00	67	32.40	794.45	*	420.46	582.61	1.28	133.87	136.89 (27Ø1")	33.32	22.31	34.20 (12Ø3/4")
II-X		4.67	1.00	52	22.50	468.41	*	322.24	631.92	1.15	80.87	81.12 (16Ø1")	25.28	17.32	25.65 (9Ø3/4")
I-X	1440	12.00	2.00	42	115.20	1693.21	136.80	500.88	699.83	7.27	167.83	172.38 (34Ø1")	130.51	27.97	131.82 (26Ø1")
II-X		5.33	2.00	42	80.00	894.98	95.00	499.75	720.00	5.05	74.55	76.95 (27Ø3/4")	61.71	27.97	65.91 (13Ø1")
I-X	2160	18.00	2.00	52	115.20	2592.81	100.80	510.05	703.07	5.87	311.69	314.34 (62Ø1")	161.36	34.63	162.24 (32Ø1")
II-X		7.33	2.00	37	80.00	1268.16	107.50	350.12	720.00	5.73	90.31	91.20 (32Ø3/4")	109.86	24.64	111.54 (22Ø1")

Tables 1 and 2 present the complete design of the rectangular isolated footings subjected to uniaxial bending.

Table 1 shows the following: The effective depth is governed by the flexural shearing in the c axis for the two cases (M<sub>ux</sub> = 360, 720, 1440 kN-m), and by the moment in the a axis for the two cases (M<sub>ux</sub> = 2160 kN-m). The smallest effective depth is presented in case II-Y for M<sub>ux</sub> = 360, 720, 2160 kN-m, and for M<sub>ux</sub> = 1440 kN-m the effective depth is the same in case I-Y and II-Y. The smallest proposed steel area appears in case II-Y for the two cases in both directions except at M<sub>ux</sub> = 360

kN-m which are the same in case I-Y and II-Y in Y direction.

Table 2 presents the following: The effective depth is governed by the flexural shearing in the *e* axis for the two cases ( $M_{uy} = 360, 720, 1440$  kN-m), and by the moment in the *b* axis for the two cases ( $M_{uy} = 2160$  kN-m). The smallest effective depth is presented in case II-X for  $M_{uy} = 360, 720, 2160$  kN-m, and for  $M_{uy} = 1440$  kN-m the effective depth is the same in case I-X and II-X. The smallest proposed steel area appears in case II-X for the two cases in both directions except at  $M_{uy} = 360$  kN-m which are the same in case I-X and II-X in X direction.

Tables 3 to 6 present the complete design of the rectangular isolated footings subjected to biaxial bending.

Tables 3 to 6 present the two cases to obtain the complete design of the isolated rectangular footings subjected to biaxial bending, a case when the entire contact area works under compression (Case I), and another case when the contact area works partially under compression (the smaller area of cases II, III, IV and V).

The procedure used for Tables 3 to 6 is as follows:

For case I: Substituting  $P_u, M_{ux}, M_{uy}, h_x, h_y$  into equation (1), and later equation (1),  $h_x, h_y, c_1, c_2$  and *d* is substituted into equations (5) to (8) and (25).

For cases II, III, IV and V: Substituting  $\sigma_{umax}, h_x, h_{x1}, h_y, h_{y1}$  into equation (4), and subsequently substituting equation (4),  $h_x, h_{x1}, h_y, h_{y1}, c_1, c_2$  and *d* into equations (29) to (32) (case II), into equations (33) to (36) (case IIIA), into equations (37) to (40) (case IIIB), into equations (41) to (44) (case IVA), into equations (45) to (48) (case IVB), into equations (49) to (52) (case VA), into equations (53) to (56) (case VB), into equations (57) to (60) (case VC), into equations (61) to (64) (case VD), and (26), (65) to (68) as the case may be.

Table 3 shows the results for  $c_1$  and  $c_2 = 0.40$  m,  $P_u = 720$  kN,  $M_{ux} = 360, 720, 1440, 2160$  kN-m,  $M_{uy} = 360$  kN-m and  $\sigma_{umax} = 250$  kN/m<sup>2</sup>. The smallest area appears in the case V for  $M_{ux} = 360$  and 720 kN-m, and in the case II for  $M_{ux} = 1440$  and 2160 kN-m.

Table 3. Complete design of the footing for  $M_{uy} = 360$  kN-m.  
(Source: Own elaboration)

Caso	$M_{ux}$ kN-m	$h_x$ m	$h_y$ m	<i>d</i> cm	$M_{ua}$ kN-m	$M_{ub}$ kN-m	$V_{uc}$ kN	$V_{ue}$ kN	$V_{up}$ kN	$A_{smy}$ cm <sup>2</sup>	$A_{smiy}$ cm <sup>2</sup>	$A_{spx}$ cm <sup>2</sup>	$A_{smx}$ cm <sup>2</sup>	$A_{sminx}$ cm <sup>2</sup>	$A_{spx}$ cm <sup>2</sup>
I	360	6.00	6.00	27	632.43	632.43	391.39	391.39	711.02	65.04	53.95	65.55 (23Ø3/4")	65.04	53.95	65.55 (23Ø3/4")
V		2.72	2.72	22	229.25	229.25	305.04	305.04	698.58	29.25	19.93	31.35 (11Ø3/4")	29.25	19.93	31.35 (11Ø3/4")
I	720	6.00	12.00	27	1351.21	632.43	421.25	391.39	715.51	148.38	53.95	152.10 (30Ø1")	63.43	107.89	111.54 (22Ø1")
V		2.22	4.45	27	472.00	196.31	367.54	298.13	709.58	51.44	19.93	55.77 (11Ø1")	19.61	40.01	42.75 (15Ø3/4")
I	1440	6.00	24.00	32	2790.60	632.43	434.23	384.90	717.41	278.09	63.94	278.85 (55Ø1")	52.71	255.74	258.57 (51Ø1")
II		1.87	7.46	37	948.06	174.75	419.11	254.16	720.00	78.18	23.04	79.80 (16Ø1")	12.56	91.91	94.05 (33Ø3/4")
I	2160	6.00	36.00	42	4230.40	632.43	437.49	371.76	717.76	311.87	83.92	314.34 (62Ø1")	39.96	503.50	507.00 (100Ø1")
II		1.71	10.24	42	1428.46	165.34	447.01	210.14	720.00	109.68	23.02	111.54 (22Ø1")	10.44	143.22	145.35 (51Ø3/4")

Table 3 shows the following: The effective depth is governed by the punching shearing for the two cases ( $M_{ux} = 360, 720$  kN-m), and by the moment in the *a* axis for the two cases ( $M_{ux} = 1440, 2160$  kN-m). The smallest effective depth occurs in case V for  $M_{ux} = 360$  kN-m, smallest effective depth occurs in case I for  $M_{ux} = 1440$  kN-m, and for  $M_{ux} = 720, 2160$  kN-m the effective depth is the same in both cases. The larger proposed steel area appears in case I for the two cases in both directions.

Table 4 shows the results for  $c_1$  and  $c_2 = 0.40$  m,  $P_u = 720$  kN,  $M_{ux} = 360, 720, 1440, 2160$  kN-m,  $M_{uy} = 720$  kN-m and  $\sigma_{umax} = 250$  kN/m<sup>2</sup>. The smallest area appears in the case V for  $M_{ux} = 360$  kN-m, and in the case II for  $M_{ux} = 720, 1440$  and  $2160$  kN-m.

Table 4. Complete design of the footing for  $M_{uy} = 720$  kN-m.  
(Source: Own elaboration)

Caso	$M_{ux}$ kN-m	$h_x$ m	$h_y$ m	d cm	$M_{ua}$ kN-m	$M_{ub}$ kN-m	$V_{uc}$ kN	$V_{ue}$ kN	$V_{up}$ kN	$A_{smy}$ cm <sup>2</sup>	$A_{smiy}$ cm <sup>2</sup>	$A_{spsy}$ cm <sup>2</sup>	$A_{smx}$ cm <sup>2</sup>	$A_{smix}$ cm <sup>2</sup>	$A_{spx}$ cm <sup>2</sup>
I	360	12.00	6.00	27	632.43	1351.21	391.39	421.25	715.51	63.43	107.89	111.54 (22Ø1")	148.38	53.95	152.10 (30Ø1")
V		4.45	2.22	27	196.31	472.00	298.13	367.54	709.58	19.61	40.10	42.75 (15Ø3/4")	51.44	19.96	54.15 (19Ø3/4")
I	720	12.00	12.00	27	1351.21	1351.21	421.25	421.25	717.76	139.46	107.89	141.96 (28Ø1")	139.46	107.89	141.96 (28Ø1")
II		3.73	3.73	27	430.31	430.31	392.78	392.78	720.00	44.47	33.54	45.63 (9Ø1")	44.47	33.54	45.63 (9Ø1")
I	1440	12.00	24.00	27	2790.60	1351.21	435.76	421.25	718.88	307.84	107.89	309.27 (61Ø1")	135.74	215.78	218.01 (51Ø1")
II		3.22	6.45	27	913.51	408.86	458.25	423.74	720.00	104.20	28.95	106.47 (21Ø3/4")	41.21	57.99	59.85 (21Ø3/4")
I	2160	12.00	36.00	27	4230.40	1351.21	440.54	421.25	719.25	508.33	107.89	512.07 (101Ø1")	134.59	323.68	324.48 (64Ø1")
II		3.00	9.00	32	1404.83	403.75	480.92	433.67	720.00	140.24	31.97	141.96 (28Ø1")	33.85	95.90	96.90 (34Ø3/4")

Table 5 shows the results for  $c_1$  and  $c_2 = 0.40$  m,  $P_u = 720$  kN,  $M_{ux} = 360, 720, 1440, 2160$  kN-m,  $M_{uy} = 1440$  kN-m and  $\sigma_{umax} = 250$  kN/m<sup>2</sup>. The smallest area appears in the case II for  $M_{ux} = 360, 720, 1440$  and  $2160$  kN-m.

Table 5. Complete design of the footing for  $M_{uy} = 1440$  kN-m.  
(Source: Own elaboration)

Caso	$M_{ux}$ kN-m	$h_x$ m	$h_y$ m	d cm	$M_{ua}$ kN-m	$M_{ub}$ kN-m	$V_{uc}$ kN	$V_{ue}$ kN	$V_{up}$ kN	$A_{smy}$ cm <sup>2</sup>	$A_{smiy}$ cm <sup>2</sup>	$A_{spsy}$ cm <sup>2</sup>	$A_{smx}$ cm <sup>2</sup>	$A_{smix}$ cm <sup>2</sup>	$A_{spx}$ cm <sup>2</sup>
I	360	24.00	6.00	32	632.43	2790.60	384.90	434.23	717.41	52.71	255.74	258.57 (51Ø1")	278.09	63.94	278.85 (55Ø1")
II		7.46	1.87	37	174.75	948.06	254.16	419.11	720.00	12.56	91.91	94.05 (33Ø3/4")	78.18	23.04	79.80 (16Ø1")
I	720	24.00	12.00	27	1351.21	2790.60	421.25	435.76	718.88	135.74	215.78	218.01 (51Ø1")	307.84	107.89	309.27 (61Ø1")
II		6.45	3.22	27	408.86	913.51	423.74	458.25	720.00	41.21	57.99	59.85 (21Ø3/4")	104.20	28.95	106.47 (21Ø1")
I	1440	24.00	24.00	27	2790.60	2790.60	435.76	435.76	719.44	288.54	215.78	288.99 (57Ø1")	288.54	215.78	288.99 (57Ø1")
II		5.73	5.73	27	899.07	899.07	484.27	484.27	720.00	94.95	51.52	96.33 (19Ø1")	94.95	51.52	96.33 (19Ø1")
I	2160	24.00	36.00	27	4230.40	2790.60	440.54	435.76	719.63	451.51	215.78	456.30 (90Ø1")	283.13	323.68	324.48 (64Ø1")
II		5.41	8.12	32	1399.94	898.75	498.17	495.32	720.00	157.03	48.64	157.17 (31Ø1")	92.67	73.01	94.05 (33Ø3/4")

Table 4 shows the following: The effective depth is governed by the punching shearing for the two cases ( $M_{ux} = 360, 720, 1440$  kN-m), and by the moment in the  $a$  axis for the two cases ( $M_{ux} = 2160$  kN-m). The smallest effective depth occurs in case I for  $M_{ux} = 2160$  kN-m, and for  $M_{ux} = 360, 720, 1440$  kN-m the effective depth is the same in both cases. The larger proposed steel area appears in case I for the two cases in both directions.

Table 5 shows the following: The effective depth is governed by the punching shearing for the two cases ( $M_{ux} = 720, 1440, 2160$  kN-m), and by the moment in the  $a$  axis for the two cases ( $M_{ux} = 360$  kN-m). The smallest effective depth occurs in case I for  $M_{ux} = 360$  kN-m, and for  $M_{ux} = 720, 1440,$

2160 kN-m the effective depth is the same in both cases. The larger proposed steel area appears in case I for the two cases in both directions.

Table 6 shows the results for  $c_1$  and  $c_2 = 0.40$  m,  $P_u = 720$  kN,  $M_{ux} = 360, 720, 1440, 2160$  kN-m,  $M_{uy} = 2160$  kN-m and  $\sigma_{umax} = 250$  kN/m<sup>2</sup>. The smallest area appears in the case II for  $M_{ux} = 360, 720, 1440$  and  $2160$  kN-m.

Table 6. Complete design of the footing for  $M_{uy} = 2160$  kN-m.

(Source: Own elaboration)

Caso	$M_{ux}$ kN-m	$h_x$ m	$h_y$ m	d cm	$M_{ua}$ kN-m	$M_{ub}$ kN-m	$V_{uc}$ kN	$V_{ue}$ kN	$V_{up}$ kN	$A_{smy}$ cm <sup>2</sup>	$A_{sminy}$ cm <sup>2</sup>	$A_{spy}$ cm <sup>2</sup>	$A_{smx}$ cm <sup>2</sup>	$A_{sminx}$ cm <sup>2</sup>	$A_{spx}$ cm <sup>2</sup>
I	360	36.00	6.00	42	632.43	4230.40	371.76	437.49	717.76	39.96	503.50	507.00 (100Ø1")	311.87	83.92	314.34 (62Ø1")
II		10.24	1.71	42	165.34	1428.46	210.14	447.01	720.00	10.44	143.22	145.35 (51Ø3/4")	109.68	23.92	111.54 (22Ø1")
I	720	36.00	12.00	27	1351.21	4230.40	421.25	440.54	719.63	134.59	323.68	324.48 (64Ø1")	307.84	107.89	309.27 (61Ø1")
II		9.00	3.00	32	403.75	1404.83	433.67	480.92	720.00	33.85	95.90	96.90 (34Ø3/4")	140.24	31.97	141.96 (28Ø1")
I	1440	36.00	24.00	27	2790.60	4230.40	435.76	440.54	719.44	283.13	323.68	324.48 (64Ø1")	451.51	215.78	456.30 (90Ø1")
II		8.12	5.41	27	898.75	1399.94	495.32	498.17	720.00	92.67	73.01	94.05 (33Ø3/4")	157.03	48.64	157.17 (31Ø1")
I	2160	36.00	36.00	27	4230.40	4230.40	440.54	440.54	719.75	437.69	323.68	441.09 (87Ø1")	437.69	323.68	441.09 (87Ø1")
II		7.73	7.73	32	1396.69	1396.69	498.81	498.81	720.00	149.44	69.50	152.10 (30Ø1")	149.44	69.50	152.10 (30Ø1")

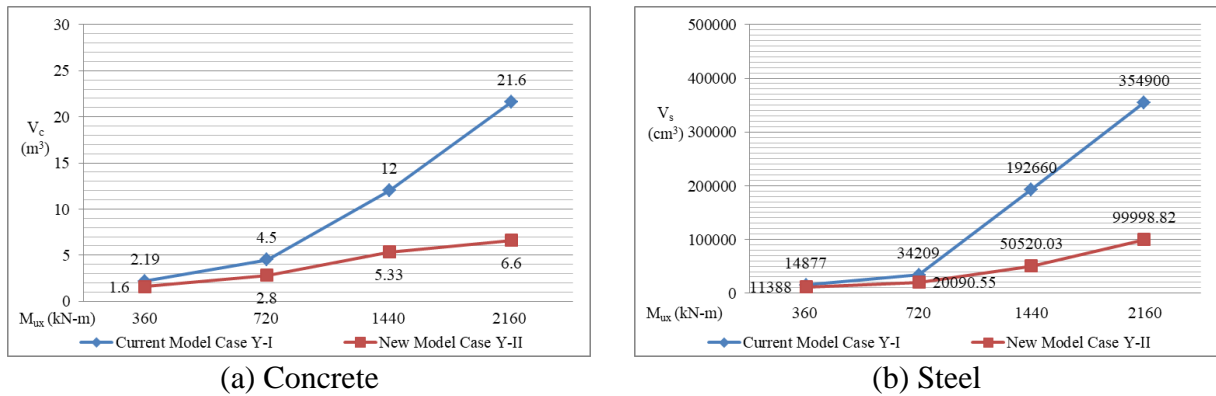
Table 6 shows the following: The effective depth is governed by the punching shearing for the two cases ( $M_{ux} = 1440, 2160$  kN-m), and by the moment in the  $a$  axis for the two cases ( $M_{ux} = 360, 720$  kN-m). The smallest effective depth occurs in case I for  $M_{ux} = 720$  kN-m, and for  $M_{ux} = 360, 1440, 2160$  kN-m the effective depth is the same in both cases. The larger proposed steel area appears in case I for the two cases in both directions.

Figure 8 shows the comparison for uniaxial bending (Axial load on the Y axis) of the current model (Case I-Y) and new model (Case II-Y) in terms of volume of concrete and steel of the considered examples.

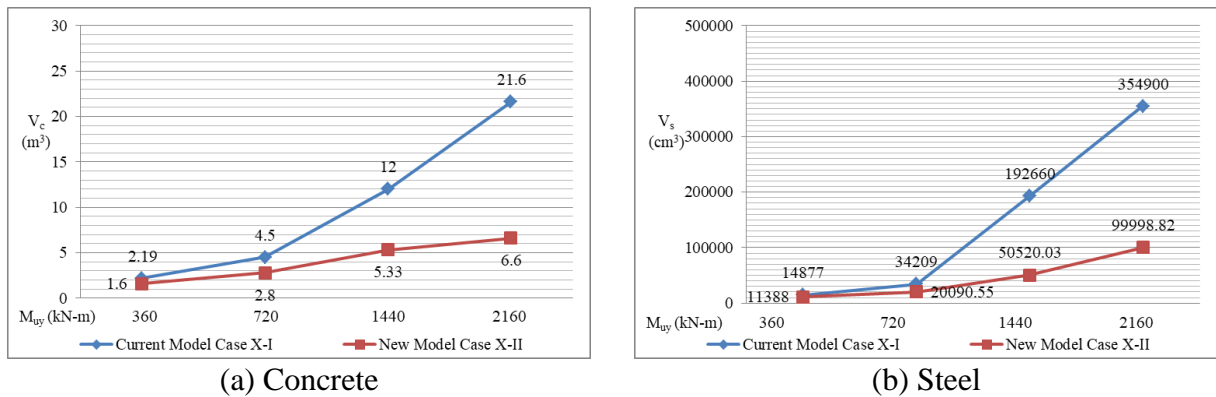
Figure 8 shows the following: The new model presents smaller volumes of concrete and steel in all cases than the current model. The smallest difference in volumes of concrete and steel occurs at  $M_{ux} = 360$  kN-m of 1.37 times for concrete and 1.31 times for steel. The biggest difference in volumes of concrete and steel occurs at  $M_{ux} = 2160$  kN-m of 3.27 times for concrete and 3.55 times for steel.

Figure 9 shows the comparison for uniaxial bending (Axial load on the X axis) of the current model (Case I-X) and new model (Case II-X) in terms of volume of concrete and steel of the considered examples.

Figure 9 presents the following: The new model presents smaller volumes of concrete and steel in all cases than the current model. The smallest difference in volumes of concrete and steel occurs at  $M_{uy} = 360$  kN-m of 1.37 times for concrete and 1.31 times for steel. The biggest difference in volumes of concrete and steel occurs at  $M_{uy} = 2160$  kN-m of 3.27 times for concrete and 3.55 times for steel.



(a) Concrete  
(b) Steel  
Figure 8. Comparison for uniaxial bending ( $M_{uy} = 0$ )  
Source: Own elaboration



(a) Concrete  
(b) Steel  
Figure 9. Comparison for uniaxial bending ( $M_{ux} = 0$ )  
Source: Own elaboration

Figure 10 shows the comparison for biaxial bending of the current model (Case I) and new model (Case II or V) in terms of volume of concrete and steel of the considered examples.

Figure 10 shows the following:

The new model presents smaller volumes of concrete and steel in all cases than the current model. The smallest differences occur at  $M_{ux} = 360$  kN-m for all cases in the volumes of concrete and steel of 5.68 times for concrete and 4.61 times for steel ( $M_{uy} = 360$  kN-m), 7.28 times for concrete and 7.43 times for steel ( $M_{uy} = 720$  kN-m), 9.17 times for concrete and 10.69 times for steel ( $M_{uy} = 1440$  kN-m), 12.33 times for concrete and 10.32 times for steel ( $M_{uy} = 2160$  kN-m).

The largest differences occur at  $M_{ux} = 2160$  kN-m for all cases in the volumes of concrete and steel of 12.33 times for concrete and 10.32 times for steel ( $M_{uy} = 360$  kN-m), 14.00 times for concrete and 14.24 times for steel ( $M_{uy} = 720$  kN-m), 19.66 times for concrete and 13.57 times for steel ( $M_{uy} = 1440$  kN-m), 21.69 times for concrete and 13.51 times for steel ( $M_{uy} = 2160$  kN-m).

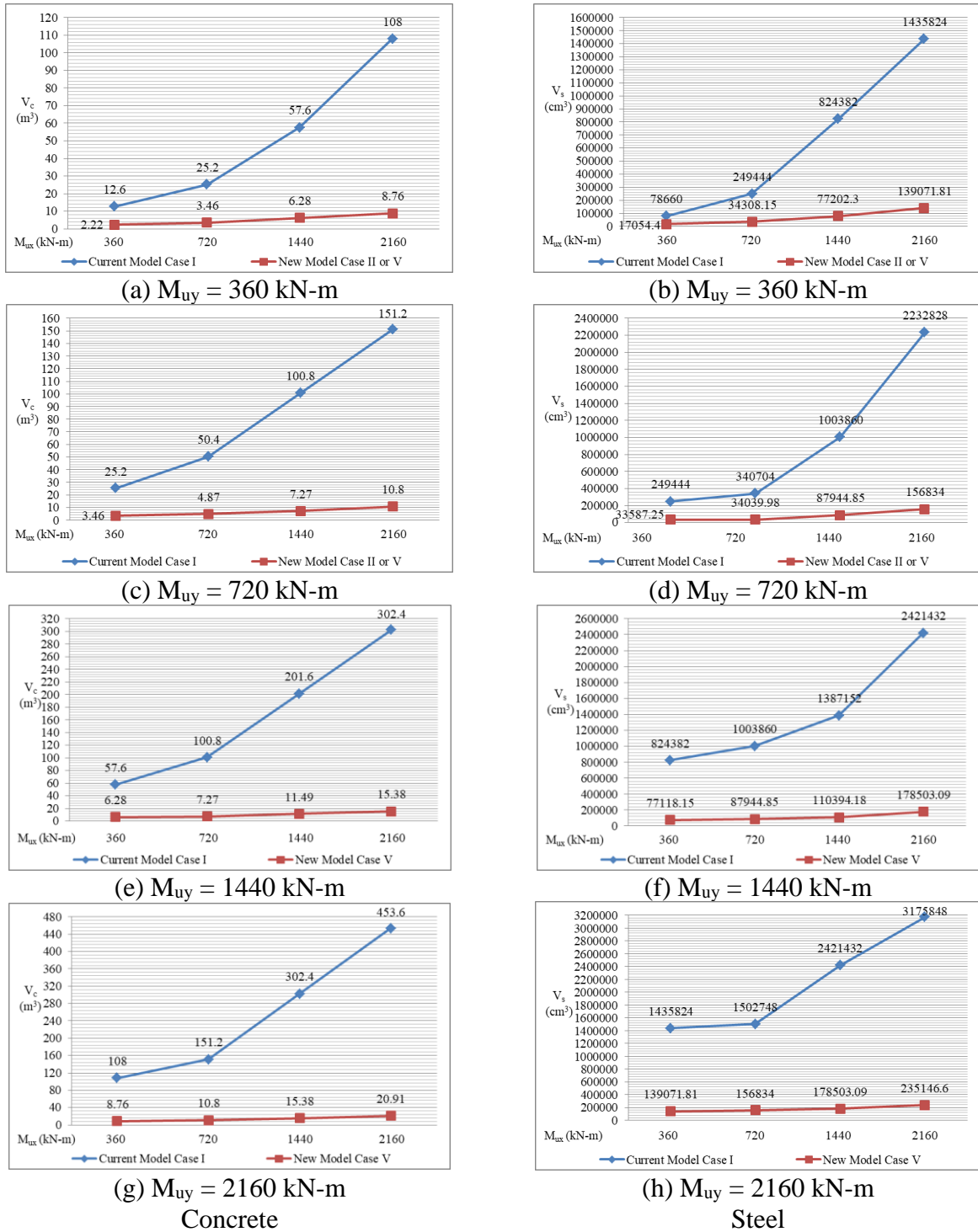


Figure 10. Comparison for biaxial bending  
Source: Own elaboration

#### 4. CONCLUSIONS

This work presents a new complete design mathematical model to obtain the thicknesses and areas of transverse and longitudinal steel for rectangular isolated footings subjected to uniaxial and biaxial bending supported on elastic soils, which considers the total surface working partially under compression and it is assumed that the distribution of pressures on the ground is linear.

The main contributions in this work are:

The main contributions of this work for these examples are:

- 1.- This work shows a significant reduction in the volumes of concrete and steel than the current model, if the contact surface with the ground working partially under compression.
- 2.- This work shows a significant reduction in the volume of excavation than the current model, because the new model occupies less volume.
- 3.- The thickness for both models are governed by moments and flexural shearing for uniaxial bending, and by moments and punching shearing for biaxial bending.
- 4.- The new model can be used for any building code, simply taking into account the moments, the flexural shearing and the punching shearing that resist to define the effective depth, and the equations to determine the reinforcing steel areas proposed by each building code.
- 5.- The new model can be used when the load  $P_u$  is located outside the central nucleus ( $e_x/h_x + e_y/h_y > 1/6$ ), and the current model is used when load  $P_u$  is located inside the central nucleus ( $e_x/h_x + e_y/h_y \leq 1/6$ ), where  $e_x = M_y/P$  and  $e_y = M_x/P$ .

This work shows an effective and robust solution applied to obtain the complete design for rectangular isolated footings subjected to uniaxial and biaxial bending supported on elastic soils working partially under compression, and the variation of the pressure diagram is linear.

The suggestions for the next research:

- 1.- Complete design for combined footing (rectangular, trapezoidal, strap, corner and shaped-T) subjected to uniaxial and biaxial bending supported on elastic soils working partially under compression.
- 2.- Footings supported on totally cohesive soils (clay soils) and/or totally granular soils (sandy soils), the pressure diagram is different, because the pressure diagram is not linear as it is presented in this work.

## 5. REFERENCES

- ACI 318S-19 (2019), “*Building Code Requirements for Structural Concrete and Commentary*, Committee 318”, New York, USA.
- Aguilera-Mancilla, G., Luévanos-Rojas, A., López-Chavarría, S. and Medina-Elizondo, M. (2019), *Modeling for the strap combined footings Part I: Optimal dimensioning*. Steel and Composite Structures. 30(2):97-108. <https://doi.org/10.12989/scs.2019.30.2.097>
- Al-Gahtani, H.J. and Adekunle, S.K. (2019), *A boundary-type approach for the computation of vertical stresses in soil due to arbitrarily shaped foundations*. World Journal of Engineering. 16(3): 419-426. <https://doi.org/10.1108/WJE-02-2018-0051>
- Algin, H.M. (2000), *Stresses from linearly distributed pressures over rectangular areas*. International Journal for Numerical and Analytical Methods in Geomechanics. 24(8):681-692. [https://doi.org/10.1002/1096-9853\(200007\)24:8<681::AID-NAG89>3.0.CO;2-X](https://doi.org/10.1002/1096-9853(200007)24:8<681::AID-NAG89>3.0.CO;2-X)
- Algin, H.M. (2007), *Practical formula for dimensioning a rectangular footing*. Engineering Structures. 29(6):1128-1134. <https://doi.org/10.1016/j.engstruct.2006.08.009>
- Aydogdu, I. (2016), *New Iterative method to Calculate Base Stress of Footings under Biaxial Bending*. Journal of Engineering and Applied Sciences. 8(4):40-48. <https://doi.org/10.24107/ijeas.281460>
- Bezmalinovic Colleoni, A.S. (2016), *Fórmulas analíticas para la presión de contacto lineal en fundaciones rectangulares altamente excéntricas*. IX Chilean Congress on Geotechnical Engineering, Chilean Geotechnical Society, Universidad Austral de Chile.
- Dagdeviren, U. (2016), *Shear stresses below the rectangular foundations subjected to biaxial bending*, Geomechanics Engineering. 10(2):189-205. <https://doi.org/10.12989/gae.2016.10.2.189>

- Filho, W.L., Carvalho, R.CH., Christoforo, A.L. and Lahr, F.A.R. (2017), *Dimensioning of Isolated Footing Submitted to the under Biaxial Bending Considering the Low Concrete Consumption*. International Journal of Materials Engineering. 7(1):1-11. <http://article.sapub.org/10.5923.j.ijme.20170701.01.html>
- Galvis, F.A. and Smith-Pardo, J.P. (2020), *Axial load biaxial moment interaction (PMM) diagrams for shallow foundations: Design aids, experimental verification, and examples*. Engineering Structures. 213:110582. <https://doi.org/10.1016/j.engstruct.2020.110582>
- Girgin, K. (2017), *Simplified formulations for the determination of rotational spring constants in rigid spread footings resting on tensionless soil*. Journal Civil Engineering and Management. 23(4):464-474. <https://doi.org/10.3846/13923730.2016.1210218>
- Gör, M. (2022), *Analyzing the bearing capacity of shallow foundations on two-layered soil using two novel cosmology-based optimization techniques*. Smart Structures and Systems. 29(3):513-522. <https://doi.org/10.12989/sss.2022.29.3.513>
- Irles-Más, R. and Irles-Más, F. (1992), *Alternativa analítica a la determinación de tensiones bajo zapatas rectangulares con flexión biaxial y despegue parcial*. Informes de la Construcción. 44(419):77-89. <https://dialnet.unirioja.es/servlet/articulo?codigo=2768804>
- Jahanandish, M., Veiskarami, M. and Ghahramani, A. (2012), *Effect of Foundation Size and Roughness on the Bearing Capacity Factor,  $N_\gamma$ , by Stress Level-Based ZEL Method*. Arabian Journal for Science and Engineering. 37(7):1817-1831. <https://doi.org/10.1007/s13369-012-0293-3>
- Kaur, A. and Kumar, A. (2016), *Behavior of eccentrically inclined loaded footing resting on fiber reinforced soil*. Geomechanics Engineering. 10(2):155-174. <https://doi.org/10.12989/gae.2016.10.2.155>
- Khajehzadeh, M., Taha M.R. and Eslami, M. (2014), *Multi-objective Optimization of foundation using global-local gravitational search algorithm*. Structural Engineering and Mechanics. 50(3): 257-273. <https://doi.org/10.12989/sem.2014.50.3.257>
- Kim-Sánchez, D.S., Luévanos-Rojas, A., Barquero-Cabrero, J.D., López-Chavarría, S., Medina-Elizondo, M. and Luévanos-Soto, I. (2022). *A New Model for the Complete Design of Circular Isolated Footings Considering that the Contact Surface Works Partially under Compression*. International Journal of Innovative Computing, Information and Control. 18(6):1769-1784. <http://www.ijcic.org/ijcic-180607.pdf>
- Lee, J., Jeong, S. and Lee, J.K. (2015), *3D analytical method for mat foundations considering coupled soil springs*. Geomechanics Engineering. 8(6):845-850. <https://doi.org/10.12989/gae.2015.8.6.845>
- Lezgy-Nazargah, M., Mamazizi, A. and Khosravi, H. (2022), *Analysis of shallow footings rested on tensionless foundations using a mixed finite element model*. Structural Engineering and Mechanics. 81(3):379-394. <https://doi.org/10.12989/sem.2022.81.3.379>
- López-Chavarría, S., Luévanos-Rojas, A. and Medina-Elizondo, M. (2017a), *A mathematical model for dimensioning of square isolated footings using optimization techniques: general case*. International Journal of Innovative Computing, Information and Control. 13(1):67-74. <http://www.ijcic.org/ijcic-130105.pdf>
- López-Chavarría, S., Luévanos-Rojas, A. and Medina-Elizondo, M. (2017b), *Optimal dimensioning for the corner combined footings*. Advances in Computational Design. 2(2):169-183. <https://doi.org/10.12989/acd.2017.2.2.169>
- López-Chavarría, S., Luévanos-Rojas, A. and Medina-Elizondo, M. (2017c), *A new mathematical model for design of square isolated footings for general case*. International Journal of Innovative Computing, Information and Control. 13(4):1149-1168. <http://www.ijcic.org/ijcic-130406.pdf>

- López-Chavarría, S., Luévanos-Rojas, A., Medina-Elizondo, M., Sandoval-Rivas, R. and Velázquez-Santillán, F. (2019), *Optimal design for the reinforced concrete circular isolated footings*. *Advances in Computational Design*. 4(3):273-294. <https://doi.org/10.12989/acd.2019.4.3.273>
- Luévanos-Rojas, A. (2012a), *A Mathematical Model for Dimensioning of Footings Square*. *International Review of Civil Engineering*. 3(4):346-350.
- Luévanos-Rojas, A. (2012b), *A Mathematical Model for the Dimensioning of Circular Footings*. *Far East Journal of Mathematical Sciences*. 71(2): 357-367.
- Luévanos-Rojas, A. (2013), *A Mathematical Model for Dimensioning of Footings Rectangular*. *ICIC Express Letters Part B: Applications*. 4(2):269-274.
- Luévanos-Rojas, A., Faudoa-Herrera, J.G., Andrade-Vallejo, R.A. and Cano-Alvarez, M.A. (2013), *Design of Isolated Footings of Rectangular Form Using a New Model*. *International Journal of Innovative Computing, Information and Control*. 9(10):4001-4022. <http://www.ijicic.org/ijicic-12-10031.pdf>
- Luévanos-Rojas, A. (2014a), *A Comparative Study for Dimensioning of Footings with Respect to the Contact Surface on Soil*. *International Journal of Innovative Computing, Information and Control*. 10(4):1313-1326. <http://www.ijicic.org/ijicic-13-08003.pdf>
- Luévanos-Rojas, A. (2014b), *Design of isolated footings of circular form using a new model*. *Structural Engineering and Mechanics*. 52(4):767-786. <http://dx.doi.org/10.12989/sem.2014.52.4.767>
- Luévanos-Rojas, A. (2014c), *Design of boundary combined footings of rectangular shape using a new model*. *DYNA Colombia*. 81(188):199-208. <https://doi.org/10.15446/dyna.v81n188.41800>
- Luévanos-Rojas, A. (2015a), *A New Approach for Dimensioning of Rectangular Footings Using Optimization Techniques*. *ICIC Express Letters Part B: Applications*. 6(11):3141-3146.
- Luévanos-Rojas, A. (2015b), *A New Mathematical Model for Dimensioning of the Boundary Trapezoidal Combined Footings*. *International Journal of Innovative Computing, Information and Control*. 11(4):1269-1279. <http://www.ijicic.org/ijicic-110411.pdf>
- Luévanos-Rojas, A. (2015c), *A new model for the design of rectangular combined boundary footings with two restricted opposite sides*. *Revista ALCONPAT*. 6(2):172-187. <http://dx.doi.org/10.21041/ra.v6i2.137>
- Luévanos-Rojas, A. (2015d), *Design of boundary combined footings of trapezoidal form using a new model*. *Structural Engineering and Mechanics*. 56(5):745-765. <https://doi.org/10.12989/sem.2015.56.5.745>
- Luévanos-Rojas, A. (2016a), *A Mathematical Model for the Dimensioning of Combined Footings of Rectangular Shape*. *Revista Técnica de la Facultad de Ingeniería Universidad del Zulia*. 39(1):3-9. <https://produccioncientificaluz.org/index.php/tecnica/article/view/21090/20946>
- Luévanos-Rojas, A. (2016b), *Un nuevo modelo para diseño de zapatas combinadas rectangulares de lindero con dos lados opuestos restringidos*. *Revista ACONPAT*. 6(2):173-189. <http://dx.doi.org/10.21041/ra.v6i2.137>
- Luévanos-Rojas, A., López-Chavarría, S. and Medina-Elizondo, M. (2017), *Optimal design for rectangular isolated footings using the real soil pressure*. *Ingeniería e Investigación*. 37(2):25-33. <http://dx.doi.org/10.15446/ing.investig.v37n2.61447>
- Luévanos-Rojas, A., López-Chavarría, S. and Medina-Elizondo, M. (2018a), *A new model for T-shaped combined footings Part I: Optimal dimensioning*. *Geomechanics Engineering*. 14(1):51-60. <https://doi.org/10.12989/gae.2018.14.1.051>
- Luévanos-Rojas, A., López-Chavarría, S. and Medina-Elizondo, M. (2018b), *A new model for T-shaped combined footings Part II: Mathematical model for design*. *Geomechanics Engineering*. 14(1):61-69. <https://doi.org/10.12989/gae.2018.14.1.061>

- Luévanos Rojas, A., López Chavarría, S., Medina Elizondo, M., Sandoval Rivas, R., Farías Montemayor, O. M. (2020), *Un modelo analítico para el diseño de zapatas combinadas de esquina*. Revista ALCONPAT. 10(3):317-335. <https://doi.org/10.21041/ra.v10i3.432>
- Özmen, G. (2011), *Determination of Base Stresses in Rectangular Footings under Biaxial Bending*. Teknik Dergi Digest. 22(4):1519-1535. [http://www.imo.org.tr/resimler/dosya\\_ekler/7b559795bd3f63b\\_ek.pdf?dergi=472](http://www.imo.org.tr/resimler/dosya_ekler/7b559795bd3f63b_ek.pdf?dergi=472)
- Rawat, S., Mittal, R.K. and Muthukumar, G. (2020), *Isolated Rectangular Footings under Biaxial Bending: A Critical Appraisal and Simplified Analysis Methodology*. Practice Periodical on Structural Design and Construction. 25(3):04020011. [https://doi.org/10.1061/\(ASCE\)SC.1943-5576.0000471](https://doi.org/10.1061/(ASCE)SC.1943-5576.0000471)
- Rodriguez-Gutierrez, J.A. and Aristizabal-Ochoa, J.D. (2013a), *Rigid Spread Footings Resting on Soil Subjected to Axial Load and Biaxial Bending. I: Simplified Analytical Method*. International Journal of Geomechanics. 13(2):109-119. [https://doi.org/10.1061/\(ASCE\)GM.1943-5622.0000218](https://doi.org/10.1061/(ASCE)GM.1943-5622.0000218)
- Rodriguez-Gutierrez, J.A. and Aristizabal-Ochoa, J.D. (2013b), *Rigid Spread Footings Resting on Soil Subjected to Axial Load and Biaxial Bending. II: Design Aids*. International Journal of Geomechanics. 13(2):120-131. [https://doi.org/10.1061/\(ASCE\)GM.1943-5622.0000210](https://doi.org/10.1061/(ASCE)GM.1943-5622.0000210)
- Soto-Garcia, S., Luévanos-Rojas, A., Barquero-Cabrero, J.D., López-Chavarría, S., Medina-Elizondo, M., Farías-Montemayor, O.M. and Martínez-Aguilar, C. (2022). *A New Model for the Contact Surface With Soil of Circular Isolated Footings Considering that the Contact Surface Works Partially Under Compression*. International Journal of Innovative Computing, Information and Control. 18(4):1103-1116. <http://www.ijicic.org/ijicic-180406.pdf>
- Vela-Moreno, V.B., Luévanos-Rojas, A., López-Chavarría, S., Medina-Elizondo, M., Sandoval-Rivas, R. and Martínez-Aguilar, C. (2022), *Optimal area for rectangular isolated footings considering that contact surface works partially to compression*. Structural Engineering and Mechanics. 84(4):561-573. <https://doi.org/10.12989/sem.2022.84.4.561>
- Velázquez-Santillán, F., Luévanos-Rojas, A., López-Chavarría, S., Medina-Elizondo, M. and Sandoval-Rivas, R. (2018), *Numerical experimentation for the optimal design for reinforced concrete rectangular combined footings*. Advances in Computational Design. 3(1):49-69. <https://doi.org/10.12989/acd.2018.3.1.049>
- Yáñez-Palafox, J.A., Luévanos-Rojas, A., López-Chavarría, S. and Medina-Elizondo, M. (2019), *Modeling for the strap combined footings Part II: Mathematical model for design*. Steel and Composite Structures. 30(2):109-121. <https://doi.org/10.12989/scs.2019.30.2.109>

## Analysis of the correlation between the condition of urban pavements and elements of the drainage system

M. Diniz<sup>1\*</sup>  R. Melo<sup>1</sup> 

\*Contact author: [mariaingridydiniz@gmail.com](mailto:mariaingridydiniz@gmail.com)

DOI: <https://doi.org/10.21041/ra.v13i2.604>

Received: 08/05/2022 | Received in revised form: 23/03/2023 | Accepted: 29/03/2023 | Published: 01/05/2023

### ABSTRACT

The research in question aimed to analyze the correlation between the pavement condition index and the condition of two surface drainage elements: culverts and gutters. The study was carried out from the analysis of 19 stretches, distributed by the neighborhood of Tambaú, in João Pessoa-PB. The calculation for the condition of the pavements was carried out using the PCI method and the condition of the drainage elements was verified through subjective analysis. The research results showed when the elements fit or not in the ideal conditions, and although the drainage elements are considered in the performance of the pavements, the statistical evaluation showed a weak correlation between the condition of the pavements and the evaluated drainage elements.

**Keywords:** infrastructure systems; statistic; urban roads.

**Cite as:** Diniz, M., Melo, R. (2023), "*Análise da correlação entre a condição de pavimentos urbanos e elementos do sistema de drenagem*", Revista ALCONPAT, 13 (1), pp. 220 – 234, DOI: <https://doi.org/10.21041/ra.v13i2.604>

<sup>1</sup> Centro de Tecnologia, Universidade Federal da Paraíba, João Pessoa, Brasil.

#### Contribution of each author

In this work, author 1 contributed with the activity of literature review, data collection, writing of the work, discussion of results and conclusions, corresponding to 60% of the work, author 2 contributed with the activity of the original idea, review of the work final, opinions in the discussions, corresponding to 40%.

#### Creative Commons License

Copyright 2023 by the authors. This work is an Open-Access article published under the terms and conditions of an International Creative Commons Attribution 4.0 International License ([CC BY 4.0](https://creativecommons.org/licenses/by/4.0/)).

#### Discussions and subsequent corrections to the publication

Any dispute, including the replies of the authors, will be published in the first issue of 2024 provided that the information is received before the closing of the third issue of 2023.

## **Análise da correlação entre a condição de pavimentos urbanos e elementos do sistema de drenagem**

### **RESUMO**

A pesquisa em questão objetivou analisar a correlação entre o índice de condição dos pavimentos e a condição de dois elementos de drenagem superficial: bocas de lobo e sarjetas. O estudo foi realizado a partir da análise de 19 trechos, distribuídos pelo bairro de Tambaú, em João Pessoa-PB. O cálculo para a condição dos pavimentos foi realizado pelo método do PCI e a condição dos elementos de drenagem foi verificada por meio de análise subjetiva. Os resultados da pesquisa mostraram quando os elementos se enquadravam ou não nas condições ideais, e embora os elementos de drenagem sejam considerados no desempenho dos pavimentos, a avaliação estatística apresentou uma correlação fraca entre a condição dos pavimentos e os elementos de drenagem avaliados.

**Palavras-chave:** sistemas de infraestrutura; estatística; vias urbanas.

## **Análisis de la correlación entre el estado de los pavimentos urbanos y los elementos del sistema de drenaje**

### **RESUMEN**

La investigación en cuestión tuvo como objetivo analizar la correlación entre el índice de condición del pavimento y la condición de dos elementos de drenaje superficial: desagües pluviales y cunetas. El estudio fue realizado a partir del análisis de 19 tramos, distribuidos por el barrio de Tambaú, en João Pessoa-PB. El cálculo del estado de los pavimentos se realizó por el método PCI y el estado de los elementos de drenaje se verificó mediante análisis subjetivo. Los resultados de la investigación mostraron cuando los elementos encajan o no en las condiciones ideales, y aunque los elementos de drenaje son considerados en el desempeño del pavimento, la evaluación estadística mostró una débil correlación entre la condición del pavimento y los elementos de drenaje evaluados.

**Palabras clave:** sistemas de infraestructura; estadística; caminos urbanos.

### **Legal Information**

Revista ALCONPAT is a quarterly publication by the Asociación Latinoamericana de Control de Calidad, Patología y Recuperación de la Construcción, Internacional, A.C., Km. 6 antigua carretera a Progreso, Mérida, Yucatán, 97310, Tel.5219997385893, [alconpat.int@gmail.com](mailto:alconpat.int@gmail.com), Website: [www.alconpat.org](http://www.alconpat.org)

Reservation of rights for exclusive use No.04-2013-011717330300-203, and ISSN 2007-6835, both granted by the Instituto Nacional de Derecho de Autor. Responsible editor: Pedro Castro Borges, Ph.D. Responsible for the last update of this issue, Informatics Unit ALCONPAT, Elizabeth Sabido Maldonado.

The views of the authors do not necessarily reflect the position of the editor.

The total or partial reproduction of the contents and images of the publication is carried out in accordance with the COPE code and the CC BY 4.0 license of the Revista ALCONPAT.

## 1. INTRODUCTION

Considered as the main mode of transport, highways are of great importance in the development of the country (PIRES E MENDES, 2021), and for roads to fulfill their function properly, they must have an appropriate state of conservation.

A pavement with a structure that does not perform adequately can lead to undesired consequences. In this perspective, the drainage of a road helps in its conservation, in addition to preventing accidents on the roads. Therefore, one of the main objectives of draining highways is to protect the infrastructure from the negative action of water, such as reducing the floor structure and breaking up embankments (LIMA et al., 2022).

According to Pinheiro, Coutinho and Ferreira (2021), the drainage system is an essential element with regard to the performance of most of the elements that make up an urban road. Still according to the author, the correct conduction of water is the main function of the drainage system, being able to preserve the characteristics of the pavement design layers, such as the base, sub-base and subgrade, in addition to ensuring greater durability of the pavement, in addition to preventing the accumulation of water on the surface.

One way to make sure that the drainage system works correctly is by checking the good condition of the elements that compose it. In addition to the structure, cleaning and maintenance of the elements are also essential for the system to fulfill its design functions.

Therefore, the work in question proposed to evaluate the correlation between the condition of the selected pavements and the condition of two surface drainage elements of the stretches: culverts and gutters. From the correlation, it is intended to ascertain to what extent there is influence of the state of conservation of the drainage elements on the condition of the pavements. Finally, those responsible for managing the infrastructure systems can use the metrics presented as an aid for the maintenance and recovery of the evaluated structures.

## 2. LITERATURE REVISION

### 2.1 Pavementss

Road pavements are of great importance with regard to the development of a country in helping to carry out basic services, such as the transport of goods and the movement of the population. In view of their importance, it is necessary that the roads are in a good state of conservation so that they can offer their services in an adequate and safe way for users (LIMA et al., 2022).

One way to check whether pavements are in an acceptable state of repair is to calculate their condition index. One of these evaluations can be done from Pavement Condition Index (PCI), developed by the United States Army Corps of Engineers (USACE) in 1976. Initially developed only for the evaluation of airport pavements, and later in 1979 adapted to a specific version for the evaluation of road and urban pavements.

According to ASTM D6433-2018 - Standard Practice for Roads and Parking Lots pavement Condition Index Surveys, it is necessary to select a sample of size  $225 \text{ m}^2 \pm 90\text{m}^2$ . The evaluation consists of carrying out the survey of defects, in addition to the quantity and severity of each one of them. Table 1 presents types of defects that must be identified during the application of the method.

Table 1. Asphalt pavement defects and measurement unit for the PCI Method

Defect	Measuring Form	Defect	Measuring Form
Fatigue Cracking	Area	Patches	Area
Bleeding	Area	Polished Aggregate	Area
Block Cracking	Area	Potholes	Unit
Elevations/settlements	Meter	Rail crossing	Area
Corrugation	Area	Rutting	Area
Localized sinking	Area	Shoving	Area
Edge crack	Meter	Cracks due to sliding masses	Area
Reflection Cracking at Joints	Meter	Swelling	Area
Gap between Pavement and shoulder	Meter	Raveling	Area
Longitudinal and transverse cracking	Meter	-	-

Source: ASTM (2018) – Adapted

To calculate the pavement condition index, it is necessary to obtain the Deduction Values (DV) according to the type, severity and extent of the defect, which represents the influence it has on the pavement condition, ranging from 0 and 100, where 0 means the defect does not impact the condition of the pavement and 100 means the defect has the maximum harmful interference. DV values are obtained with the aid of abacuses available in ASTM D6433-2018. By adding up the DVs, it is possible to obtain the Total Deduction Value (VTD) for the pavements analyzed with the help of equation 1.

$$VTD = \sum_{i=1}^p \sum_{j=1}^{mi} a(T_j, S_i, D_{ij}) \times F(t, q) \tag{1}$$

Where:

$a(T_j, S_i, D_{ij})$ : capacity loss function to serve traffic, whose independent variables are the type of:

$T_j$ : types of defects;

$S_i$ : severity levels;

$D_{ij}$ : defect densities;

$i$ : counter of types of defects;

$j$ : severity levels counter;

$p$ : total number of defect types;

$mi$ : severity level number for the  $n$ th defect type;

$F(t, q)$ : adjustment factor to reduce the effect of excess types of defects. ( $t$ ) depends on the number of functions ( $a$ ), and ( $q$ ) is the number of numerical values of functions ( $a$ ) greater than 5.

In possession of the VTD, it is necessary to correct it depending on the number of defects present

in each section, according to abacus 20 of the same standard. Therefore, it is possible to find the Corrected Deduction Amount (VDC) and, therefore, the PCI value resulting from Equation 2.

$$PCI = 100 - VDC \quad (2)$$

From the value obtained for the PCI in the section analyzed, the pavement is classified according to Table 2, varying its value from 0 (poor condition) to 100 (excellent condition).

Table 2. PCI Classification

Classification	PCI value
Great	86 – 100
Very Good	71 -85
Good	56 – 70
Average	41 – 55
Bad	26 – 40
Very Bad	11 - 25
Terrible	0 - 10

Source: Shahin (2005)

## 2.2 Drainage of Urban Pavements

According to Corrêa and Dutra (2018), the drainage system can be understood as the set of elements that aim to guarantee the integrity of the roads and their surroundings, in addition to promoting safety for users. Such devices direct the water to a suitable location, being properly planned during the construction or restoration of a road (REIS, 2016).

When referring to the urban drainage system, it is necessary to understand its subdivision into macro drainage and micro drainage (RESPLANDES et al., 2021). According to the Department of Sanitary Engineering at the University of São Paulo (2015), macro drainage can be defined as a cursor that directs a high volume of water, such as rivers and streams. In the case of micro drainage, it can be considered as the part of the system responsible for directing rainwater to the macro system. This is composed of elements such as gutters, manholes, manholes, manholes and galleries. In the case of urban pavements on a road, the existence of a micro-drainage system for directing rainwater is essential, since it is necessary to maintain such essential infrastructure in ideal operating conditions (SOUZA, 2012).

With regard to the accumulation of water, whether surface or groundwater, it can be a harmful factor for highways. According to Lima et al. (2022), the accumulation of water on the roadway can severely impair the conditions of adhesion of the roadway, and may cause accidents.

In the case of floods, it is also possible to observe significant damage to the pavements and, consequently, to the population. In addition to the change in traffic with the visible reduction in safety, water is capable of infiltrating the layers of the pavement, reducing its useful life. The water that remains contained in the layers, in addition to that coming from the water table, can cause damage such as a reduction in the support capacity of the subgrade layer, in addition to sinking and even rupture (REIS, 2016).

### 3. METHODOLOGY

To fulfill the objective proposed by the research, the following sequence of activities was developed:

- i) delimitation of the study area;
- ii) preparation of forms for data collection;
- iii) survey of data on the condition of the pavements;
- iv) survey of data on the condition of drainage elements;
- v) analysis of the correlation between the results found.

The evaluated excerpts are the subject of study by undergraduate and graduate students at the Federal University of Paraíba – UFPB. Due to the availability of a database on the stretches in question (item 3.1) and because it is considered a tourist district in the city where the quality of the roads needs to be presented in ideal conditions, it was decided to evaluate the correlation between the information.

Regarding the pavements, the survey of defects was carried out by analyzing images available in the database used, using the form available in NBR 006/2003 – PRO. To help the defects quantification step, concomitantly with the measurement, a photographic record was made for each defect so that their severity could be assessed, helping in the subsequent use of the abacuses of appendix X3 of Standard ASTM D6433 – 18, during the step of qualification.

To obtain data regarding the surface urban drainage system, a survey was carried out of the elements that made up the network, adapted from the study by Novaes et. al. (2019), based on filling in the forms prepared to quantify the existence of storm drains and gutters, as well as the qualification of their respective conservation conditions, which can be good, regular or terrible.

#### 3.1 Characterization of the Excerpts

The evaluated stretches were distributed throughout the neighborhood of Tambaú, in the city of João Pessoa - PB. Roads that simultaneously had flexible paving and a surface drainage system were chosen. The location of the sections is shown in Figure 1.

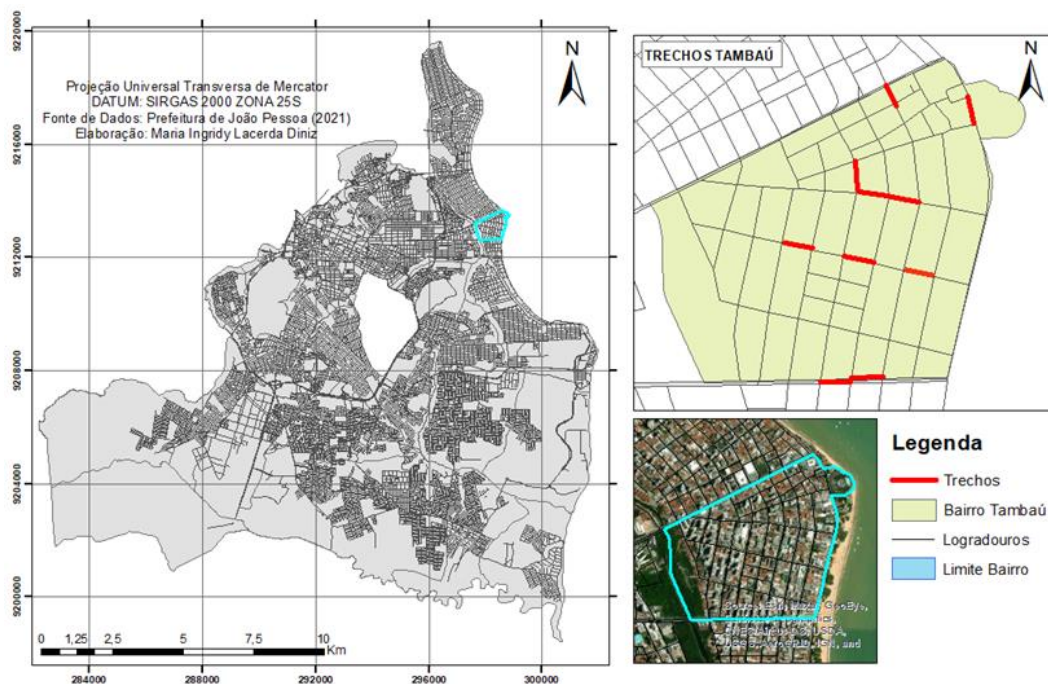


Figure 1. Location of the Study Area and Excerpts

The information detailed information about the locations of each section can be found at Table 3. To maintain the proportionality of the samples, all had the same length of 80 meters.

Table 3. Information about the Sections

Section	Range	Streat	Sense	Limits		Length (m)
				Start	Final	
1	Left	Road Our Mrs dos Navegantes	Tambaú - Manaíra	Space of being	Handicraft Market – Av. Ruy Carneiro	80
2	Right	Senhora dos Navegantes Road	Tambaú - Manaíra	Space of being	Handicraft Market - Ruy Carneiro Ave.	
3	Left	Nego Ave.	Beach	Infante Dom Henrique St.	Prof. Maria Sales Ave.	
4	Right	Nego Ave.	Beach	Infante Dom Henrique St.	Prof. Maria Sales Ave.	
5	Left	Nego Ave.	Beach	Av. Prof. Maria Sales	N. Sra dos Navegantes St.	
6	Right	Nego Ave.	Beach	Ave. Prof. Maria Sales	N. Sra dos Navegantes St.	
7	Left	Infante Dom Henrique St.	Tambaú - Manaíra	Nego Ave.	Av. Olinda	
8	Right	Infante Dom Henrique St.	Tambaú - Manaíra	Nego Ave.	Av. Olinda	
9	Left	Helena Meira Lima Street	Center	Prof. Maria Sales Ave.	Infante Dom Henrique St.	
10	Right	Helena Meira Lima Street	Center	Av. Prof. Maria Sales	Infante Dom Henrique St.	
11	Left	Helena Meira Lima Street	Center	Streat Monteiro Lobato	Streat Silvino Lopes	
12	Right	Helena Meira Lima Street	Center	Monteiro Lobato St.	Before the crosswalk with Silvino Lopes St.	
13	Left	Helena Meira Lima Street	Center	Antonio Lira Ave	Senhora dos Navegantes Road	
14	Right	Helena Meira Lima Street	Center	Antonio Lira Ave.	Senhora dos Navegantes Road	
15	Left	Pres. Epitácio Pessoa St.	Bessa	Road Senhora dos Navegantes	Prof. Maria Sales Ave.	
16	Right	Pres. Epitácio Pessoa St.	Bessa	Road Senhora dos Navegantes	Prof. Maria Sales Ave.	
17	Left	Pres. Epitácio Pessoa St.	Bessa	Manoel Cavalcante de Sousa Ave.	Prof. Maria Sales Ave.	
18	Right	Pres. Epitácio Pessoa St.	Bessa	Manoel Cavalcante de Sousa Ave.	Prof. Maria Sales Ave.	
19	Right	Adm. Tamandare Ave.	Bessa	Olinda Ave.	Sto. Antonio Square	

### 3.2 Statistic Analysis

It is possible to verify the existence of the relationship, as well as the intensity, existing between

two variables from the analysis of your correlation. For this, the Pearson Correlation coefficient (r) presented by equation 3 (MERGH, 2019; OLIVEIRA *et al.*, 2022) was used.

$$r = \frac{\sum_{i=1}^n (X_i - \bar{X})(Y_i - \bar{Y})}{\sqrt{[\sum_{i=1}^n (X_i - \bar{X})^2][\sum_{i=1}^n (Y_i - \bar{Y})^2]}} \quad (3)$$

Where:

n: number of pairs of observations;

X<sub>i</sub>: observation i of variable X;

Y<sub>i</sub>: observation i of variable Y;

$\bar{X}$ : average of X values;

$\bar{Y}$ : average of Y values.

In agreement with Francisco & Dantas Neto (2021), it is possible take intervals to help with interpretation of the results of r, as presented at table 4.

Table 4. Interpretation of Correlation Coefficient Values (r)

Correlation Coefficients (r)	Types of Correlations
r=1	Perfect Positive
0.8 ≤ r < 1	Strong Positive
0.5 ≤ r < 0.8	Moderate Positive
0.1 ≤ r < 0.5	Weak Positive
0 < r < 0.1	Intimate Positive
0	Null
0.1 < r < 0	Intimate Negative
-0.5 < r ≤ -0.1	Weak Negative
-0.8 < r ≤ -0.5	Moderate Negative
-1 < r ≤ -0.8	Strong Negative
r = -1	Perfect Negative

Source: Francisco & Dantas Neto (2021) Adapted

For the analysis in question, the PCI value, due to its calculation methodology present bigger accuracy of the real quantification of the state of condition of the evaluated element (pavements), will be considered with independent variable (X). The dependent variables will therefore be the manholes (Y<sub>1</sub>) and the gutters (Y<sub>2</sub>).

To assist in analysis statistics, the hypothesis statistical test was performed to ascertain the difference between the averages obtained. In this case, the following will be determined hypotheses:

$$H_0: \mu_1 - \mu_2 = 0 \quad (4)$$

$$H_A: \mu_1 - \mu_2 \neq 0 \quad (5)$$

Where:

H<sub>0</sub>: Null hypothesis;

H<sub>A</sub>: Alternative hypothesis;

μ<sub>1</sub> and μ<sub>2</sub>: Averages of populations 1 and 2, respectively (Being the population related to the pavements and the population 2 each of the drainage elements at a time).

In that study, the case considered was that of data not paired, with population standard deviations \_ known, resulting in two mean comparisons. The procedure consists of testing the mean differences between the populations, adopting the order of 0.5 based on the study by Medeiros et al. (2017). Then, the analysis verifies the following hypothesis:

$$H_0: \mu_d = 0,5 \quad (6)$$

$$H_A: \mu_d > 0,5 \quad (7)$$

Where:

$\mu_d$ : Difference of means between populations.

## 4. RESULTS AND DISCUSSION

### 4.1 Pavements Condition

The survey of the defects found in the pavements is shown in Table 5. The defects of block cracking, elevation and settlement, corrugation, joint reflection cracking, pavement/side slope unevenness, railway crossing, mass slippage, cracking due to slipping and swelling were not found during the survey, and due to this, there is no quantification of the aforementioned defects in Table 5.

Table 5. Quantification of Pavement Defects

Sec.	TF	E	AL	TB	TLV	R	AP	P	TR	D
	Area [m <sup>2</sup> ]	Area [m <sup>2</sup> ]	Area [m <sup>2</sup> ]	Meter	Meter	Area [m <sup>2</sup> ]	Area [m <sup>2</sup> ]	Items.	Area [m <sup>2</sup> ]	Area [m <sup>2</sup> ]
1	-	-	-	12	143	5	-	-	-	50
2	88	-	-	-	90	2	-	-	15	200
3	59	-	0.5	42	46		-	1	-	210
4	79	-		38.7	42	11.25	-	-	-	220
5	-	-	-	-	43	4.25	-	-	-	38
6	-	-	-	-	21		-	1	-	26
7	-	-	-	-	-	-	-	-	-	5
8	-	-	-	-	35	-	-	-	-	13
9	-	0.1	-	-	-	-	-	-	-	46
10	-	-	-	-	-	4.5	-	-	-	61
11	-	-	-	-	-	2	-	-	-	9
12	-	0.5	-	-	-	-	-	-	-	19
13	-	-	-	-	-	1	6	-	-	-
14	-	-	-	-	-	-	-	-	-	36
15	-	-	-	-	49	-	-	-	-	73
16	32	-	-	-	-	-	2	-	-	54
17	-	-	-	-	6	-	-	-	-	80
18	-	-	-	-	-	-	-	-	-	32
19	-	-	-	-	-	-	-	-	-	15

Caption: TLV: Longitudinal and Transverse Crack, TF: Settlements, E: Bleeding, AL: Localized Sinking, TB: Block Crack, R: Patch, AP: Polished Aggregate, P: Potholes, TR: Rutting, D: Raveling.

From the evaluation of the survey of defects of the sections, it was it is possible to point out that the defect with wear and tear was the greatest record, appearing in almost all evaluated locations, with exception of Section 13.

A large number of the cracks presented may have been caused by reflection of the cracks at the base of parallelepipeds. It is important to highlight that no he was possible to acquire the information with City Hall about which flexible pavements evaluated had or no this type of base in parallel. the observation this factor was only possible when the base was exposed due to some pavements defect.

in agreement with Bernucci *et al.* (2008), these cracks also can be caused by too much, such as the action of repetitive traffic loads, climate action (thermal gradients), the possible binder aging and loss of flexibility, inefficient compaction of the coating, deficiency in asphalt binder content, undersizing, differential settlements, among others.

After weighting the affected area as determined by ASTM D6433/2018, it was possible to calculate the condition of the pavements from the PCI. The index values for each stretch, as well as the respective classification, are found in Table 6.

Table 6. Pavement Condition Classification by the PCI method

Section	PCI	Classification
1	56	Good
2	20	Too bad
3	37	Bad
4	50	Average
5	81	Very Bad
6	74	Very Good
7	98	Great
8	88	Great
9	92	Great
10	89	Great
11	94	Great
12	95	Great
13	99	Great
14	94	Great
15	62	Good
16	64	Good
17	83	Very Good
18	80	Very Good
19	85	Very Good

#### 4.2 Condition of Drainage Elements

Existence and conditions of the drainage elements (mouths and gutters) were observed in the evaluated stretches. Information about the elements can be found at Table 7. The absence of both elements was found in excerpts 15 and 17. concomitant presence of the elements in the most of the sections evaluated, with exception of section 4, which does not featured wolf's mouths on the your extension, however counted with the presence of gutter.

Table 7. Quantification and Qualification of Drainage Elements

Section	Quantification of Elements		Qualification of Elements					
			Wolf mouth			Gutter		
	Wolf mouth	Gutter	Good	Regular	Terrible	Good	Regular	Terrible
1	3	Yes	x	-	-	-	-	x
2	two	Yes	-	x	-	-	x	-
3	1	Yes	x	-	-	-	x	-
4	0	Yes	-	-	-	-	x	-
5	1	Yes	x	-	-	-	x	-
6	1	Yes	x	-	-	-	x	-
7	2	Yes	-	-	x	-	x	-
8	2	Yes	--	x	-	-	x	-
9	1	Yes	x	-	-	x	-	-
10	1	Yes	x	-	-	x	-	-
11	1	Yes	x	-	-	x	-	-
12	1	Yes	x	-	-	x	-	-
13	1	Yes	-	x	-	x	-	-
14	1	Yes	x	-	-	x	-	-
15	0	No	-	-	-	-	-	-
16	1	Yes	x	-	-	-	x	-
17	0	No	-	-	-	-	-	-
18	1	Yes	-	-	x	-	x	-
19	1	Yes	x	-	-	-	x	-

in agreement with table 7, sections 1, 2, 7 and 8 presented more than one manhole to be evaluated. In this case, only one marking he was done in the element qualification column, since all the culverts of the same stretch had the same condition, such as stretches 2 and 8, which had two manholes each, and both pieces were in fair condition.

He was possible to verify that most of the culverts of the stretches, adding a total of 57.9%, fit at good condition category.

Regarding the condition of the gutters, only stretch 1 presented the Bad conditions. Then, even if the section has presented 3 culverts, the condition of the gutter possibly prevents the directing of water to them, which interferes with the functioning of the system. The other stretches had the gutters in regular (52.6%) or good (31.6%) conditions.

#### 4.3 Correlation between Pavement Condition and Drainage Elements

Table 8 presents the comparison between the indices found for the condition of each evaluated element. To allow comparison between the data, adapted from Silva, Diniz and Melo (2020), the PCI values were divided by 25 (twenty-five) and converted to the same scale as the condition of the gutters and culverts, or that is, values between 0 and 4.

Table 8. Comparison between condition indices of evaluated elements

Section	Values			Condition Classification		
	PCI (Pavements)	Wolf's mouths	Gutter	PCI (Pavements)	Wolf's mouths	Gutter
1	2.24	3	1	Good	Good	Terrible
2	0.8	2	2	Very Bad	Regular	Regular
3	1.48	3	2	Bad	Good	Regular
4	2	0	2	Average	Does not exist	Regular
5	3.24	3	2	Very Bad	Good	Regular
6	2.96	3	2	Very Good	Good	Regular
7	3.92	1	2	Great	Terrible	Regular
8	3.52	2	2	Great	Regular	Regular
9	3.68	3	3	Great	Good	Good
10	3.56	3	3	Great	Good	Good
11	3.76	3	3	Great	Good	Good
12	3.8	3	3	Great	Good	Good
13	3.96	2	3	Great	Regular	Good
14	3.76	3	3	Great	Good	Good
15	2.48	0	0	Good	Does not exist	Does not exist
16	2.56	3	2	Good	Good	Regular
17	3.32	0	0	Very Good	Does not exist	Does not exist
18	3.2	1	2	Very Good	Terrible	Regular
19	3.4	3	2	Very Good	Good	Regular

From table 5, it is observed that in 5 sections (9, 10, 11, 12 and 14) the condition of all the evaluated elements was maximum, being “excellent” for the pavements and “good” for the storm drains and gutters. However, even if the best pavements evaluation as well has been achieved in sections 7, 8 and 13, the condition of the drainage elements no reached the same classification, varying between “regular” and “terrible”.

It is necessary to highlight the situation presented by excerpts 15 and 17, which, even with none of the drainage elements evaluated in the research present in the roads, the pavement presented itself in conditions acceptable to users, with second- best classification on the previously presented scale at Table 2. This result conflicts in the sense in which it is suggested that for a good functioning of the roads is necessary the direction adequate amount of water present in the pavement surface.

Table 9 presents the average values, deviation pattern and variance of the results found for each evaluated element. the deviation standard it was considered of the sampling type (n-1).

Table 9. Mean and Deviation Standard Element Condition Indices

Element	Average ( $\mu$ )	Detour Standard sample ( $\sigma$ )	variance ( $\sigma^2$ )
Pavements (PCI)	3.03	0.89	0.79
Mouths of Wolf	2.16	1.17	1.37
gutters	2.05	0.91	0.82

It is possible to observe that for the three evaluated elements (Table 9), the deviation standard was high, indicating high dispersion between the values collected in the field. Also he was A comparison is made between the elements based on the difference between the averages of the results of each evaluation to verify the previously determined null hypothesis presented at Table 10.

Table 10. Difference of Means and Null Hypothesis Analysis \_

<b>Analysis</b>	<b>Difference of Means (<math>\mu d</math>) _</b>	<b>null hypothesis (H<sub>0</sub>)</b>
Pavements x Bocas de Lobo	0.88	reject
Pavements x Gutters	0.98	reject

It is possible to check in Table 10 rejection of the null hypothesis in both analyzes carried out, since the difference between the evaluated elements was presented above 0.5. Therefore, the values found do not can be considered acceptable for the correlation between the elements. To assess the level of correlation, the analysis was carried out separately for each drainage element combined with the pavement condition index, or i.e., the correlation between the condition of the pavements and the storm drains was verified, and then the correlation between the pavements and the gutters. The results found are presented at Table 11.

Table 11. Pearson's Correlation and Determination Coefficients

<b>Combination</b>	<b>Correlation Coefficient (r)</b>	<b>Coefficient of Determination (r<sup>2</sup>)</b>
Pavements x Bocas de Lobo	0.14	0.02
Pavementss x Gutters	0.39	0.15

From Table 11, it is possible to verify that both correlations were within the interval of  $0.1 \leq r \leq 0.5$ , being thus considered as weak and positive. However, it is necessary to point out that the comparison with the interpretation of Francisco and Dantas Neto (2021) is considered arbitrary, since the values do not take into account the context of the study.

Although the results do not show clear behavior of a 3rd degree equation, in an attempt to improve the value of  $r^2$ , a degree 3 polynomial regression for both analyses. From Figure 2, it is possible to observe the dispersion between the condition of the pavements related to the condition of the culverts (Figure 2-A) and gutters (Figure 2-B), respectively.

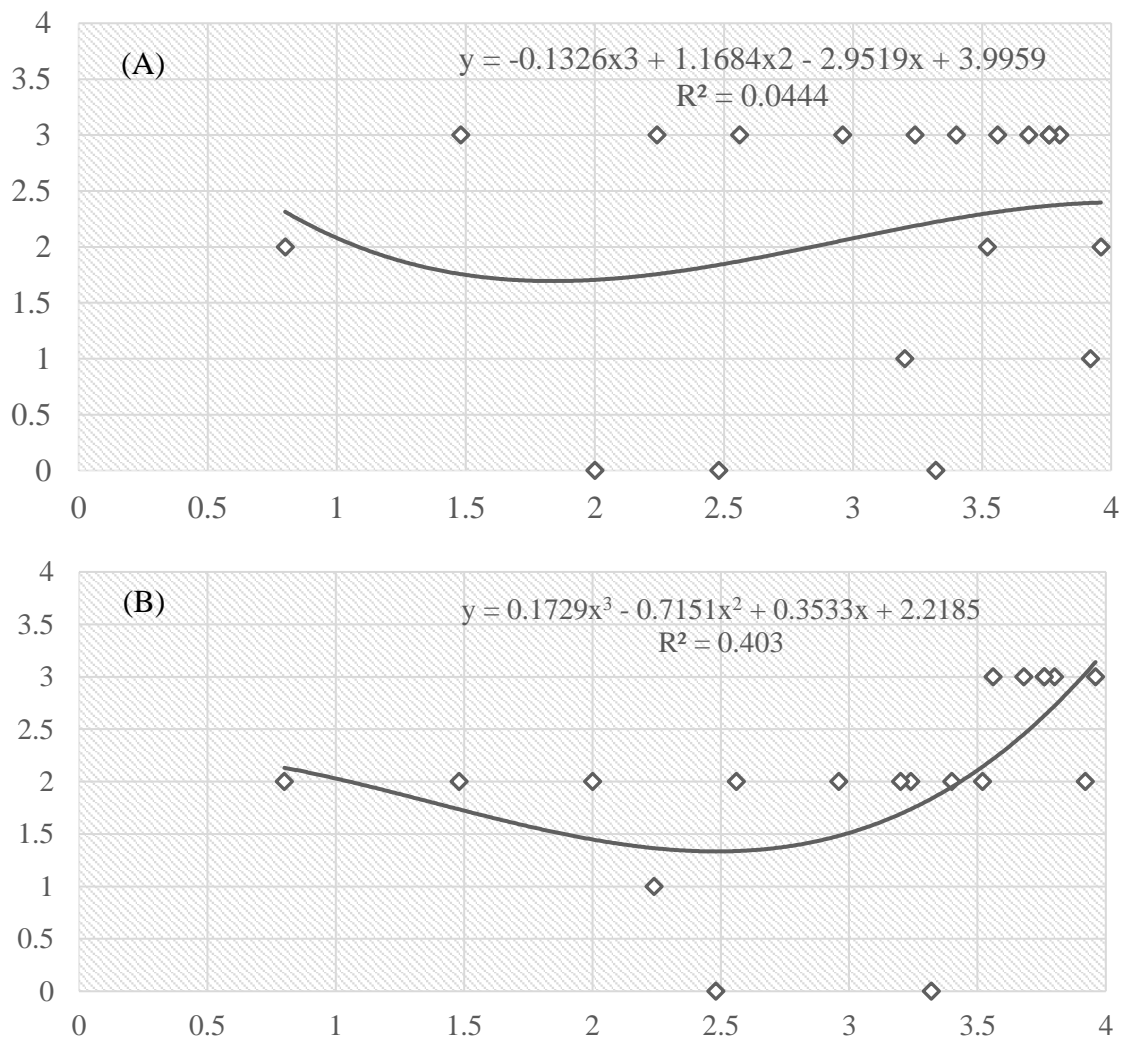


Figure 2. Polynomial Regression: A) Pavements x Gutters, B) Pavements x Gutters

From the analysis of the results it is possible to verify that for the first verification (Figure 2-A) data dispersion is presented with accuracy low, in which the attempt of polynomial adjustment of the curve did not prove to be adequate, with a value of  $r^2 < 0.1$ , considered low. In the second case (Figure 2-B), the results showed better accuracy when compared to the first analysis. In the case of curve fitting, the result showed moderately satisfactory behavior, achieving an  $r^2 = 0.4$ .

## 5. FINAL CONSIDERATIONS

From the bibliographic survey, the drainage elements were presented as primordial criteria for the good performance of the pavements, and, although the statistical evaluation has shown a weak correlation between the condition of the pavements and the evaluated drainage elements, it is necessary to highlight the level of complexity of urban road elements, such as the presence of other infrastructure systems (water distribution, sewage collection, energy, gas, etc.) use, frequency of corrective maintenance, existence of preventive maintenance, among others.

With regard to the condition of the analyzed infrastructure, the data collected and evaluated present a comprehensive overview of the assessment of the situation, since for each element all types of conditions existing in the assessment forms were found, from systems considered in good condition to those classified as the worst condition. Therefore, this holistic representation of infrastructure

systems could provide combinations of situations to exemplify the need and importance of monitoring the condition of the elements.

The indication of the severity, scope and extent proved to be adequate for the context of the work, however, to make it even more coherent with the recorded reality, it is recommended to calculate the condition of the pavements by other methods, such as Distress Manifestation Index Network Level (DMINL, 2010) and Urban Pavement Condition Index (UPCI, 2015), in addition to surveying the condition of other elements present on the road that may influence the condition of the pavements.

Although it was not the objective of the research to suggest maintenance proposals for the evaluated elements, the classification of severity levels together with the integration of the data of the elements, presented itself as a viable instrument for planning and pointing out priorities for intervention in the roads, as well as acceptability assessments of the state of functionality and usefulness of the elements, thus being able to establish goals for possible maintenance interventions by the responsible bodies.

## 6. REFERENCES

- ASTM International. (2018), *ASTM D6433-18, Standard Practice for Roads and Parking Lots Pavement Condition Index Surve*. DOI: <https://doi.org/10.1520/D6433-18>
- Bernucci, L. B., et al. (2008), “*Pavimentação asfáltica: Formação básica para engenheiros.*” 1<sup>o</sup>ed. Programa Asfalto nas Universidades, Petrobras Distribuidora S.A.
- DEPARTAMENTO NACIONAL DE INFRAESTRUTURA DE TRANSPORTES. (2003). *NORMA 006/2003 – PRO: Avaliação objetiva da superfície de pavimentos flexíveis e semi-rígidos – Procedimento*. Rio de Janeiro: DNIT.
- Francisco, M. R. P., Dantas Neto, J. (2021), *A282 Água: uso racional e sustentável*. 113 f.: il. color. Campina Grande: EPTEC.
- Lima, W. A. S., Sousa, J. P., Matos, O. S., Silva, F. G. S., Oliveira, M. M., Pacheco, G. V. (2022), *Sistemas de drenagem: a importância para a infraestrutura do transporte rodoviário brasileiro*. Brazilian Road Transport Infrastructure, v.8, n.3, p. 17813-17831. <https://doi.org/10.34117/bjdv8n3-153>
- Medeiros, R. S., Albuquerque, T. P., Morais, L. M. B., Araújo, L, G, C., Melo, R. A. (2018), “*Avaliação Das Condições De Conservação De Pavimentos, Drenagem E Calçadas Em Vias Da Cidade De João Pessoa.*” 32<sup>o</sup> Congresso de Pesquisa e Ensino em Transporte da ANPET, p. 1297–1308.
- Mergh, L. S. (2019), “*Análise de Indicadores da Gestão de Produção em Obras Corporativas*”, Dissertação de Mestrado em Construção Civil. Universidade Federal de Minas Gerais, Belo Horizonte.
- Novaes, M. P., Carvalho, M. B., Silva, D. C., Rodrigues, H. S., Amorim, M. C. C. (2019), *Avaliação das condições de infraestrutura em drenagem pluvial urbana no município de Curaçá-BA*. Brazilian Journal of Development, Curitiba, v. 5, n. 11, p. 25043-25048. <https://doi.org/10.34117/bjdv5n11-178>
- Oliveira, T. S., Anjos, J. S., Ribeiro, S. E., Oliveira, D. M. (2022), *Análise Descritiva e de Correlação dos Indicadores de Desempenho: Custo, Prazo E Ritmo*. Revista de Engenharia e Tecnologia. V. 14, Nº. 1, 2022. ISSN 2176-7270
- Pires, J. C. M., Mendes, A. T. (2021), *Manifestações patológicas em pavimentação asfáltica: estudo de caso na TO-050, no trecho do anel viário em Porto Nacional/TO*. Engineering Sciences, v.9, n.1, p.28-39. <http://doi.org/10.6008/CBPC2318-3055.2021.001.0004>

Resplandes, I. S., Toledo, F. R. S., Resplandes, H. D. de A., Santos, W. S., Borges, K., Carvalho, C. M. (2021). *Ausência de sistemas de drenagem urbana nos pavimentos de Santana do Araguaia-PA e seus impactos*. The Journal of Engineering and Exact Sciences, 7(1), 12111–01. <https://doi.org/10.18540/jcecvl7iss1pp12111-01-09e>

Silva, A. N. A., Diniz, M. I L., Melo., R. A. (2020). “*Avaliação das condições do pavimento em vias urbanas na cidade de João pessoa/PB: uma comparação entre índices*” in: 34° Congresso de Pesquisa e Ensino em Transportes da ANPET. Anais do 34° ANPET - Infraestruturas.

## Total Corrosion Management. Documentary analysis

M. Donadio<sup>1\*</sup> , J. Capacho<sup>2</sup> , L. Santander<sup>3</sup> 

\*Contact author: [donadio.michel@fr.sika.com](mailto:donadio.michel@fr.sika.com)

DOI: <https://doi.org/10.21041/ra.v13i2.690>

Received: 27/02/2023 | Received in revised form: 17/04/2023 | Accepted: 23/04/2023 | Published: 01/05/2023

### ABSTRACT

The aim of this report is to provide a documentary analysis of the different corrosion mitigation techniques currently available, such as repair mortars, active and passive corrosion inhibitors, protective coatings and galvanic or induced current cathodic protection. These structures, built to last for a long time, are subject to ageing due to environmental influences such as water, atmospheric carbon dioxide and other harmful elements such as chlorides and pollution. The most common deterioration process in reinforced concrete structures is corrosion and subsequent expansion of the steel reinforcement, leading to cracking and spalling of the concrete.

**Keywords:** corrosion; corrosion inhibitor; cathodic protection; galvanic anodes.

**Cite as:** Donadio, M., Capacho, J., Santander, L. (2023), “Total Corrosion Management. Documentary analysis”, Revista ALCONPAT, 13 (2), pp. 235 – 253, DOI: <https://doi.org/10.21041/ra.v13i2.690>

<sup>1</sup> Technical Manager, Sika Services AG, Suiza.

<sup>2</sup> Business Development Manager LATAM, Sika Mexicana SA de CV, México

<sup>3</sup> Product Engineer, Sika Mexicana SA de CV, México

#### Contribution of each author

In this work the author Michel Donadio wrote the article. The authors Luis Santander and Juan Capacho made contributions and adaptations of form and content.

#### Creative Commons License

Copyright 2022 by the authors. This work is an Open-Access article published under the terms and conditions of an International Creative Commons Attribution 4.0 International License ([CC BY 4.0](https://creativecommons.org/licenses/by/4.0/)).

#### Discussions and subsequent corrections to the publication

Any dispute, including the replies of the authors, will be published in the first issue of 2024 provided that the information is received before the closing of the third issue of 2023.

## Gestión integral de la corrosión. Análisis documental

### RESUMEN

El objetivo de este informe es hacer un análisis documental sobre las diferentes técnicas de mitigación de la corrosión disponibles en la actualidad, como los morteros de reparación, los inhibidores activos y pasivos de la corrosión, los revestimientos protectores y la protección catódica con corriente inducida o galvánica. Estas estructuras, construidas para durar mucho tiempo, están sometidas al envejecimiento por influencias de su entorno, como el agua, el dióxido de carbono atmosférico y otros elementos nocivos como los cloruros y la contaminación. El proceso de deterioro más común en las estructuras de concreto armado es la corrosión y la consiguiente dilatación de la armadura de acero, lo que provoca la fisuración y el desconchado del concreto.

**Palabras clave:** corrosión; inhibidor de corrosión; protección catódica, ánodo galvánico.

## Gestão Total da Corrosão. Análise documental

### RESUMO

O objetivo deste relatório é apresentar as diferentes técnicas de mitigação da corrosão atualmente disponíveis, tais como argamassas de reparo, inibidores de corrosão (ativos ou passivos), revestimentos de proteção e proteção catódica por corrente induzida ou galvânica. As estruturas, construídas para durar muito tempo, estão sujeitas ao envelhecimento precoce devido a influências ambientais como água, dióxido de carbono atmosférico e outros elementos nocivos, como cloretos e poluição. O processo de deterioração mais comum em estruturas de concreto armado é a corrosão e posterior expansão devida aos produtos de corrosão do aço, levando à fissuração e ao destacamento superficial do concreto.

**Palavras-chave:** corrosão; inibidor de corrosão; proteção catódica; ânodos galvânicos.

### Legal Information

Revista ALCONPAT is a quarterly publication by the Asociación Latinoamericana de Control de Calidad, Patología y Recuperación de la Construcción, Internacional, A.C., Km. 6 antigua carretera a Progreso, Mérida, Yucatán, 97310, Tel.5219997385893, [alconpat.int@gmail.com](mailto:alconpat.int@gmail.com), Website: [www.alconpat.org](http://www.alconpat.org)

Reservation of rights for exclusive use No.04-2013-011717330300-203, and ISSN 2007-6835, both granted by the Instituto Nacional de Derecho de Autor. Responsible editor: Pedro Castro Borges, Ph.D. Responsible for the last update of this issue, Informatics Unit ALCONPAT, Elizabeth Sabido Maldonado.

The views of the authors do not necessarily reflect the position of the editor.

The total or partial reproduction of the contents and images of the publication is carried out in accordance with the COPE code and the CC BY 4.0 license of the Revista ALCONPAT.

## 1. INTRODUCTION

Reinforced concrete structures such as buildings, bridges, etc. are designed to last a long time – it is not uncommon for bridge structures to have a design life of 100 years or more.

By having the correct concrete cover with an appropriate mix design, the concrete itself generally provides the necessary corrosion protection for the embedded steel reinforcement bars.

During hydration, cement generates hydrated lime that produces a highly alkaline environment in the pore liquid of the cement matrix. In this way, the steel reinforcing bars are held in a passivated condition, as stable iron oxides are formed on the steel surface.

However, due to the natural process of carbonation, the concrete can progressively lose its high alkalinity, or due to the localized action of chlorides the stable iron oxides can be broken down, meaning that the steel reinforcing bars are no longer in a passive environment, and they can start to corrode.

These issues happen when for example, the concrete cover is less than specified, or during construction there has been a lack of compaction, or inadequate concrete curing.

The corrosion of steel reinforcing bars embedded in concrete behaves in the same way as the corrosion of a metal in electrolyte solutions, corrosion always occurs at the anodes as described in the figure 1.

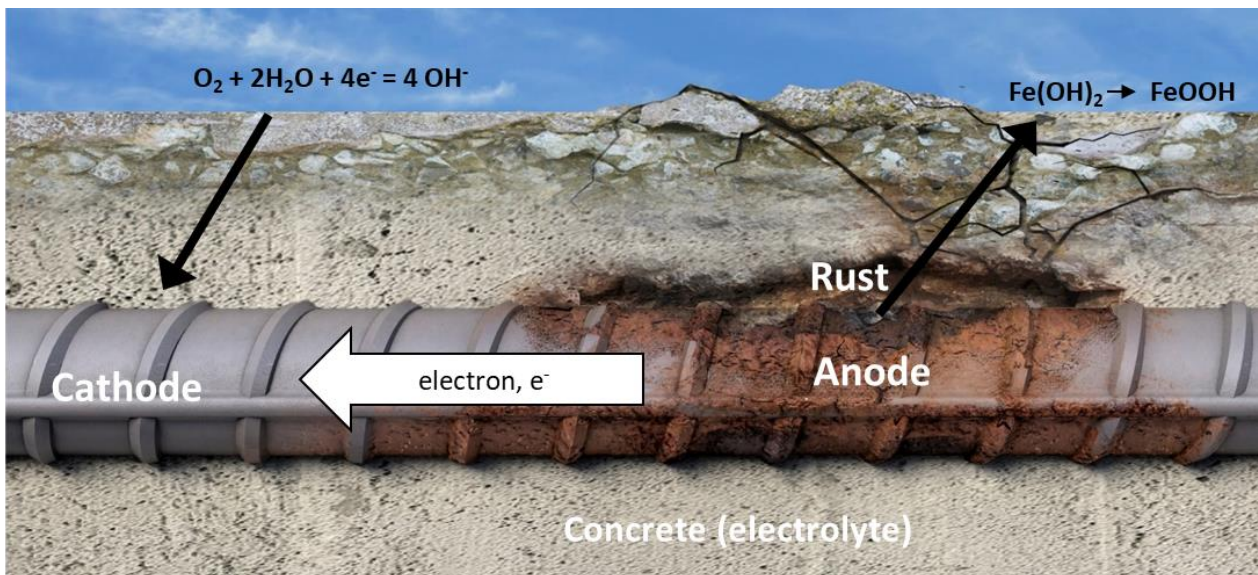


Figure 1. schematic model of corrosion of reinforcing steel in concrete.

Conditions required for steel corrosion:

- Loss of alkaline passivity (due to carbonation, or the presence of chloride).
- Moisture in the concrete pores (electrolyte).
- The presence of Oxygen near the reinforcing bars.

All three criteria must be present for the steel to corrode.

### 1.1 Carbonation induced corrosion

When atmospheric carbon dioxide meets hydrated lime in the pore liquid of non-carbonated concrete, a carbonation reaction occurs, and the highly alkaline calcium hydroxide ( $\text{Ca}(\text{OH})_2$  with a pH ~13), from the hydrated lime, is converted into low alkaline (pH ~9), relatively insoluble calcium carbonate as shown in the equation 1:

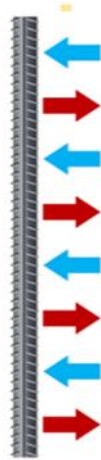


Figure 2. Adapted from Angst. The anode and cathode are of similar size in carbonation-induced corrosion.



Figure 3. Carbonation-induced corrosion in areas of poor or inadequate concrete cover.

Corrosion initiating from carbonation generates a series of microcell anodic / cathodic areas (figure 2), which lead to what can be seen as widespread corrosion, but which progresses rather slowly, typically a 1/100 to 1/10 mm reduction of the rebar per year (Angst et al, 2020). This type of corrosion frequently affects large areas of reinforcement near exposed concrete surfaces in zones of low or inadequate concrete cover, such the building façade wall shown in the figure 3.

### 1.2 Chloride induced corrosion

Even in highly alkaline conditions of non-carbonated concrete, when there is the ingress of chloride ions, e.g., in marine atmospheres or when de-icing salts etc. are applied, these reach the surface of the embedded reinforcement, there is a localised generation of acid, which attacks the steel causing pitting corrosion (Silva, 2013), with the formation of local anodic areas, as shown in figures 4 and 5 below:

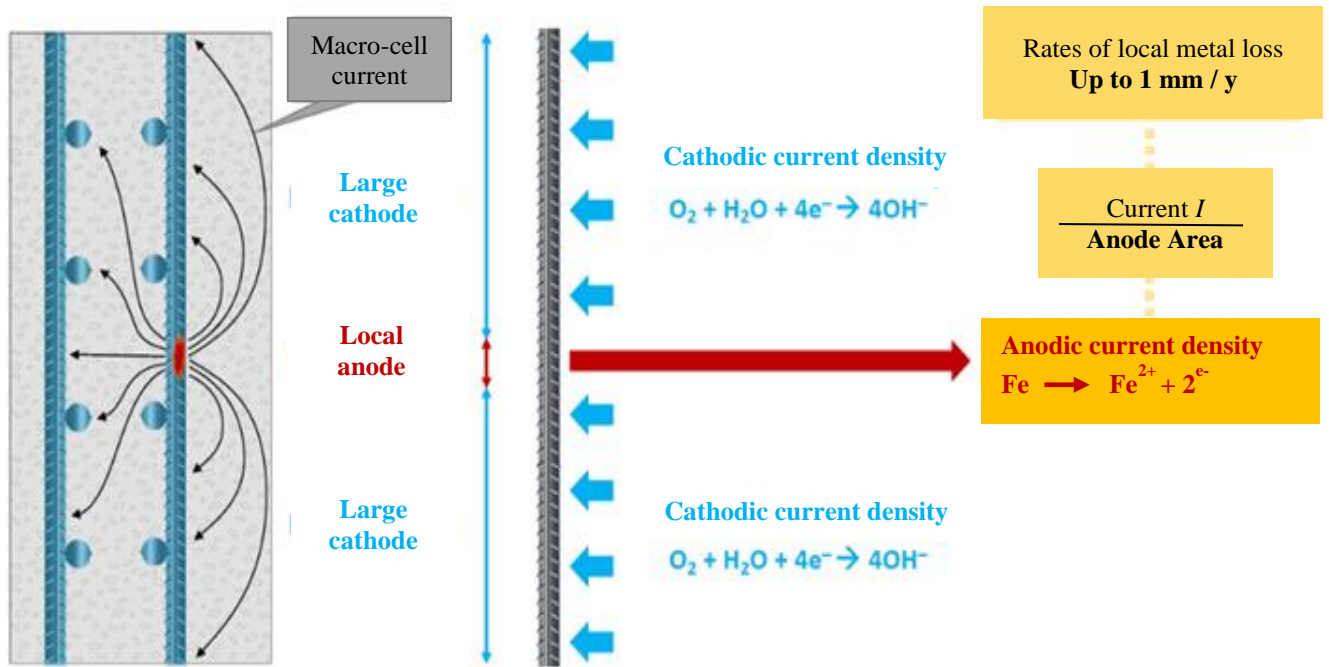


Figure 4. Adapted from Angst. Formation of a localized anode in chloride contaminated concrete.



Figure 5. Typical pitting chloride induced corrosion.

The rate of chloride induced corrosion can be fast, very local and may produce no externally visible signs, until the concrete cracks and cover delaminates as shown in figure 6. The sudden devastating collapse of structures due to this local loss of reinforcement cross section can happen, without prior warning signs.

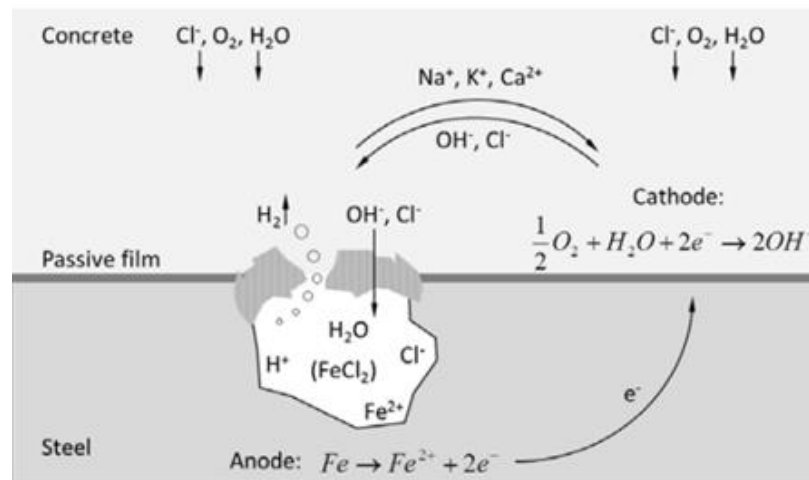


Figure 6. Adapted from Silva (Silva, 2013). Schematic representation of chloride-induced pitting corrosion.

### 1.3 Corrosion management systems

Different types of corrosion management systems are available to address the problem of corrosion in reinforcing steels:

- Concrete repair mortars
- active and passive corrosion inhibitors
- Anti-carbonation coatings
- Induced current cathodic protection
- Galvanic anodes (embedded, discrete and surface-applied)

Other available systems are mentioned in the European standard EN 1504, however, they are not described in this article.

The aim of this paper is to carry out a documentary analysis of some of the most widely used corrosion management systems mentioned above.

## 2. CORROSION MANAGEMENT SYSTEMS

### 2.1 Concrete repair mortar

Repair mortars are used to provide concrete cover when this is below the designed thickness, and / or to replace concrete spalling due to steel reinforcement corrosion.

Corrosion of steel reinforcement adversely affects many concrete structures. Patch repair is a common technique that involves the removal of physically deteriorated concrete (e.g., mechanically with chisels, or by hydro demolition), cleaning the exposed steel surfaces, and then restoring the original profile with a suitable repair mortar(s).

This process renders the steel within the repair area to a passive condition (Page & Sergi, 2000).

In a significant number of cases, subsequent corrosion-induced damage has been observed in what had seemed to be sound concrete in the immediate area around the patch repairs as seen in the figures 7 & 8. This has sometimes been within a few months following completion of the patch repair process (Qian, et al 2006). This phenomenon is known as incipient or ring anode formation, or the halo effect (Bertolini, et al 2004).



Figure 7. Spalling due to chloride corrosion.

The concept that macrocell activity (the formation of spatially separated anodes and cathodes) causes the incipient anode effect was first introduced by Page and Treadaway (Page & Treadaway, 1982). They suggested that the redistribution of anodic and cathodic sites following concrete repair affects future corrosion risk. Christodoulou (Christodoulou, 2012) shows a widely held view that the cause of incipient anodes is the loss of natural cathodic protection provided by the corroding steel to the steel in the parent concrete adjacent to the patch repair.

The Conrep Project (Tilly et al., 2007) indicates that 20% of repair works fail within 5 years & 55% within 10 years. The paper also indicates that only 30% of patch repairs were successful when used as stand-alone, while this percentage rose to 50% when combined with a protective surface coating.

We can therefore summarize the incipient anode process as follows:

- Spalling due to reinforcing steel chloride induced corrosion occurs in the anodic zones.
- Removal of the concrete is done in these affected areas.
- Repair is carried out with proprietary cement-based repair material that is highly alkaline.
- The freshly repaired zone is now changed to a cathodic zone (due to the high alkalinity of the repair mortar).
- The cathodic zones that were surrounding the anodic zones (spalled areas) are now turned to anodic zones as they are less alkaline than the freshly applied repair mortar and most likely they already contain some chlorides.
- The reinforcing steel that was previously in the protected cathodic zones is now no longer in a passivating environment as this zone has become an anode.
- Acceleration of the corrosion occurs then in these newly formed anodic zones (surrounding the patch repair areas) – refer to figures 7 & 8.

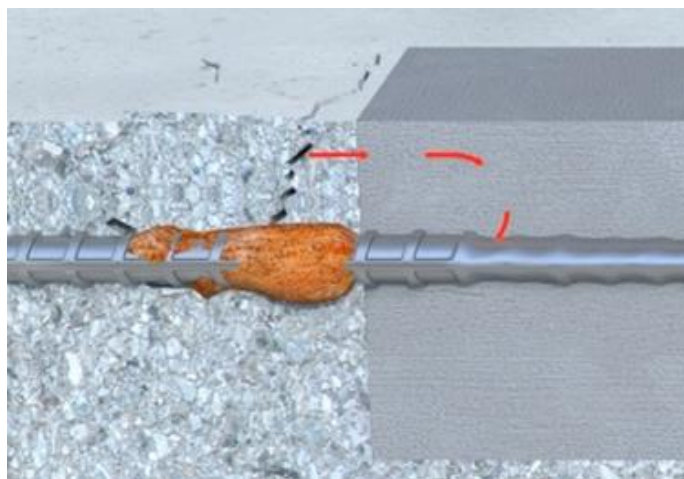


Figure 8. Spalling in the adjacent areas due to the formation of the incipient anode corrosion.

Therefore, particularly in case of chloride induced reinforcement corrosion, concrete repair with patch repair mortars alone, might not provide the desired long-term efficacy of the repair. As a result, patch repair work needs to be combined with suitable systems to avoid formation of incipient anodes.

## 2.2 Corrosion Inhibitors

An inhibitor is a substance that either delays or retards the rate of a chemical reaction. A corrosion inhibitor is defined as a substance that delays the onset of corrosion or reduces the rate of existing steel corrosion.

Corrosion inhibitors for reinforced concrete, are available as admixtures that can be mixed with concrete, repair mortar or replacement concrete, or as surface applied impregnating products; the latter being the type most commonly used for concrete repair works.

There are 2 main types of corrosion inhibitor available in the market:

- Active corrosion inhibitors that require the active component to penetrate and reach the reinforcing bars to be able to provide a continuous film on the surface, which protects the steel bars from corrosion.
- Passive corrosion inhibitors, which act in different way, which is by preventing liquid water to penetrate and migrate through the concrete, whilst allowing the evaporation of entrapped moisture by vapor diffusion. This increases the resistivity of the concrete surrounding the reinforcing steel. An advantage of this technique is that it also prevents future chloride ingress to the structure.

### 2.2.1 Active corrosion inhibitor

There are also different active corrosion inhibitor technologies available in the market

- Anodic corrosion inhibitors that suppress the anodic reaction – typical product is nitrite-based inhibitor. Their use can be critical if their concentration is not high enough, accelerated corrosion may occur.
- Cathodic corrosion inhibitors that either slow the cathodic reaction itself or selectively precipitate on cathodic areas to increase the surface impedance and limit the diffusion of reducible species to these areas – Typical products are zinc compound (precipitation of oxide forming a protective film on the rebar) or sodium sulphite acting as an oxygen scavenger. These are considered as safe, but they are less efficient than anodic inhibitors
- Ambiodic (mixed) corrosion inhibitors that act simultaneously on both the anodic and cathodic zones. This class of inhibitor has a synergistic effect, combining the benefits of both anodic and cathodic types, even at low dosage. They are safe at a low dosage, no corrosion acceleration has been found, only a lowering effect.
- Ambiodic inhibitors are typically based on a mixture of an amino alcohol and its amino acid salt. These molecules are very small and very volatile. They do not react with cement, and so they are able to migrate freely within the cement matrix (Tritthart, 2002).

In summary, ambiodic corrosion inhibitors:

- Penetrate the concrete in both liquid & vapor phases
- Displace hydroxides on the steel surface in carbonated concrete
- Displace chlorides on the steel surface (in certain conditions)
- Form an adsorbed chemical layer 100-1000 angstrom thick on the surfaces of the steel reinforcement
- Reduce iron dissolution at the anode
- Reduce oxygen access at the cathode

However, in many countries surface applied corrosion inhibitor technology has only found limited acceptance, and indeed there can be significant limitations with regards to their use and efficacy:

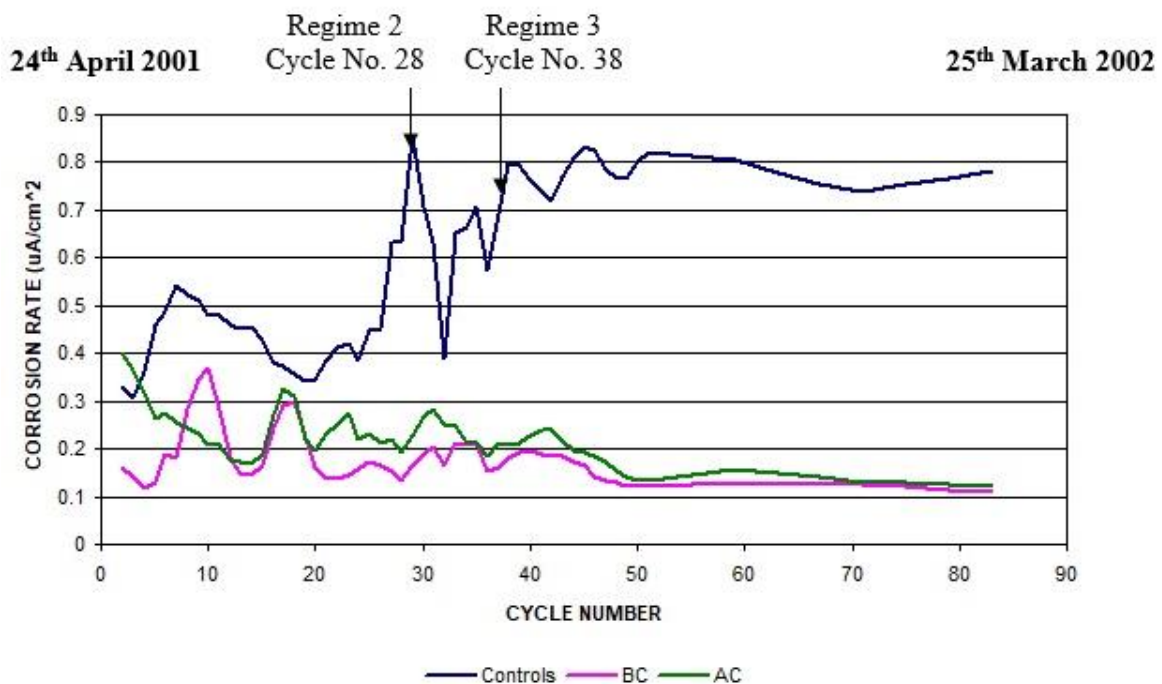
- The first limitation is their ability to migrate in sufficient quantity to be effective. If the concrete is of high quality and/or the cover is relatively thick, then the inhibitor molecule's ability to migrate deep enough in sufficient quantity at the level of the reinforcing bars, is limited. This situation is most likely to arise in civil engineering structures.
- The second major limitation is when there are already chlorides present in the concrete. Based on experience and following intensive research such as in the SAMARIS project (SAMARIS, 2003-2005), , these inhibitors are not effective if certain level of chlorides is already present near the reinforcing bars.

In summary, for marine, or civil engineering structures exposed to de-icing salts, active corrosion inhibitors are not the optimum solution to mitigate existing corrosion.

However, there are some positive results for the use of these inhibitors in chloride induced corrosion – the SAMARIS project also presents one of them – Fleet Flood Bridge, where the inhibitor was successfully used to address the issue of incipient anode corrosion.

As shown by Heiyandtuduwa (Heiyantuduwa, 2006) and Taché (Taché, 2000) (refer to the figure 9 where a strong reduction of corrosion is noted with the effect of inhibitors that are applied before or after accelerated carbonation), this technology works best in reinforced concrete with carbonation-induced steel corrosion for three main reasons:

- Carbonation induced corrosion is often associated with low concrete cover. Hence it is easier for the inhibitor to reach the reinforcement steel
- Carbonation occurs mainly in concrete of lower quality – hence it is of lower density, and respectively there is better penetration (depth and quantity) of the inhibitor.
- Corrosion rates associated with carbonation are relatively slow, so it is easier for the inhibitor to be effective.



**Three-point moving averages of corrosion rates for 10 mm cover samples**

Figure 9. Carbonated concrete - effect of active inhibitor (applied before and after carbonation). (Heiyantuduwa, 2006)

When suitable, active corrosion inhibitor technology is a very cost-effective technique. Typically, active corrosion inhibitors will be more efficient at reducing carbonation induced corrosion in buildings, rather than to mitigate chloride induced corrosion in civil engineering or marine structures.

### 2.2.2 Passive Corrosion Inhibitors

As indicated above, passive corrosion inhibitors work by significantly increasing the resistivity of the concrete at the level of the reinforcing bars.

Concentrated silane passive corrosion inhibitors with an active content around 80% for cream types, or more than 90% for liquid types, are effective solutions to reduce water penetration into dense concrete structures. Numerous field reports also attest their long performance. Christodoulou (Christodoulou, et al 2012) has shown that “Treatments carried out 20 years ago can still provide a residual protective effect”.

These passive corrosion inhibitors are very efficient at preventing chloride migration in concrete. Eva Rodum (Rodum, 2012) has carried out tests on existing structures and shown that the hydrophobic impregnations used are very effective in preventing chloride migration, even 10 years after their application (refer to the figure 10) where the reference concrete has a very high chloride content while the concretes treated with the different hydrophobic treatments have chloride levels close to zero. Studies over a 11-year period carried out by M. Brem (Brem, et al 2022) show that corrosion rate and the concrete electrical resistivity correlate very well, confirming that the corrosion reaction is mainly controlled by the moisture content of concrete at the level of the steel reinforcement. In this study, a cream silane was applied to the concrete leaving an unapplied part as a reference. Monitoring systems have been installed to measure the resistivity at different depths in the concrete and the corrosion activity of the reinforcement. After 11 years, there is no moisture penetration in the treated area (in blue in figure 11) with almost no corrosion activity. On the other hand, there are high corrosion activity and high moisture in the untreated area (black in figure 11). This study also shows the positive advantage of this silane treatment in terms of longevity and corrosion protection.

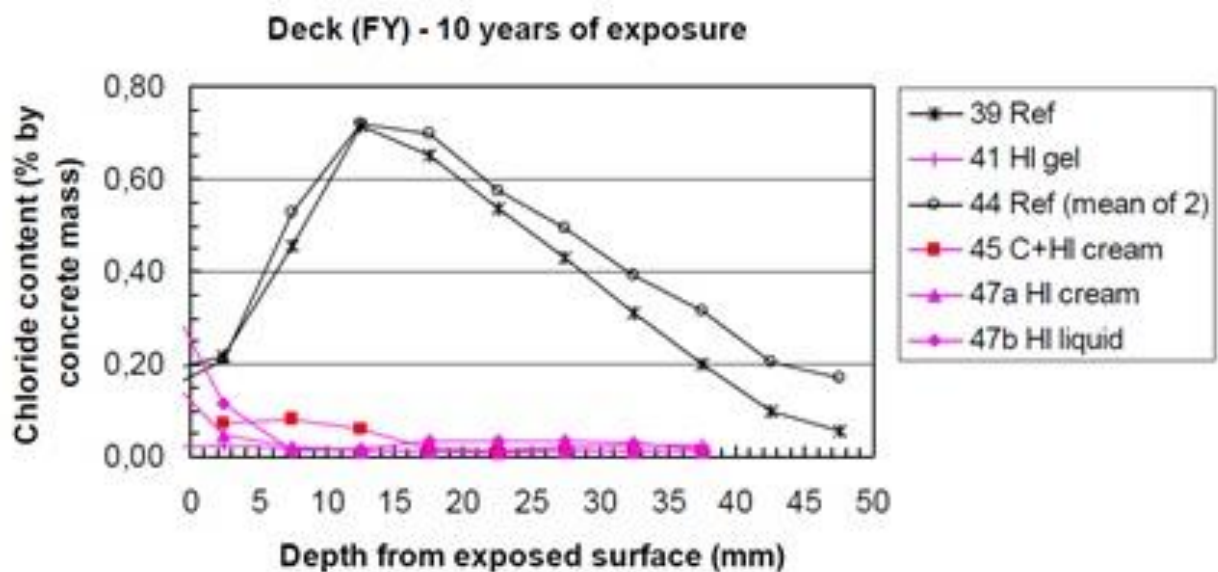


Figure 10. Chloride concrete profiles of the substructure of a pier in Norway. (Rodum, 2012)

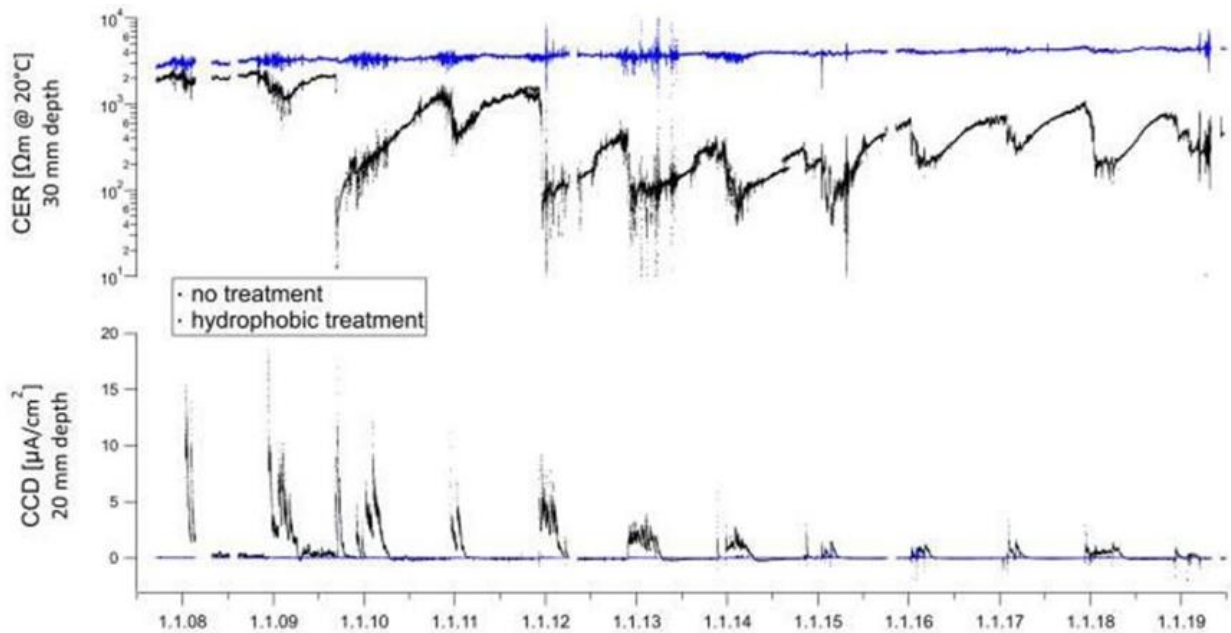


Figure 11. CER Concrete Electrical Resistivity (top) and CCD Corrosion Current Density (bottom) of untreated (black) and treated (blue) surfaces with a cream hydrophobic impregnation from a tunnel ceiling over a period of 11-years (Brem, et al 2022).

In summary, passive corrosion inhibitors are very effective for long-term prevention of chloride induced corrosion.

Their ability to mitigate existing corrosion is more debatable and the efficiency may depend on the level of corrosion, and their ability to penetrate sufficiently enough the concrete surface (not requiring reaching the reinforcing bars). Additionally, the concrete must still allow each-way vapor diffusion for moisture to evaporate and the concrete to dry out at the level of the reinforcement.

### 2.3 Protective coating

The primary function of protective coating on concrete surfaces is generally to halt the progress of the carbonation front in the cement matrix.

These coatings can be also formulated to be elastic and effectively bridge cracks, even at very low temperatures (down to -20°C).

Depending on the product, surface preparation and application, a typical durability of 10-15 years can be observed for a flexible acrylic-based water dispersion coating, or 15-20 years for a rigid methacrylate resin-based solvent dispersion coating. (Mozaryn, et al 2009). After which a refresher coat may be needed to maintain the protective performance. However, there are examples where premature failure was observed, due primarily to corrosion being too far advanced, excess moisture content, or inadequate surface preparation and application.

After concrete repairs are carried out, protective coatings can be used to stop the future ingress of deleterious elements (e.g., chlorides and CO<sub>2</sub>), and to provide a homogeneous visual appearance of the substrate by hiding differences in color due to the patch repair works.

Breathable protective coatings will provide corrosion mitigation in the same way as hydrophobic impregnations, by preventing further ingress of deleterious agents (e.g., Chlorides, and CO<sub>2</sub>) and by allowing the concrete to dry out.

But if the corrosion is too advanced and/or if non-breathable coatings are used, there is a risk of entrapped moisture with all the ingredients present in the concrete for corrosion to proceed.

## 2.4 Cathodic protection

There is a recently produced updated European Standard which applies: Cathodic protection of steel in concrete (ISO 12696:2016). This is valid for both induced current cathodic protection and galvanic protection.

### 2.4.1 Induced current cathodic protection

The corrosion protection is providing by placing an anode, made from Titanium mesh for example, at the surface of the concrete and connected directly to the reinforcement network (refer to the figure 12).

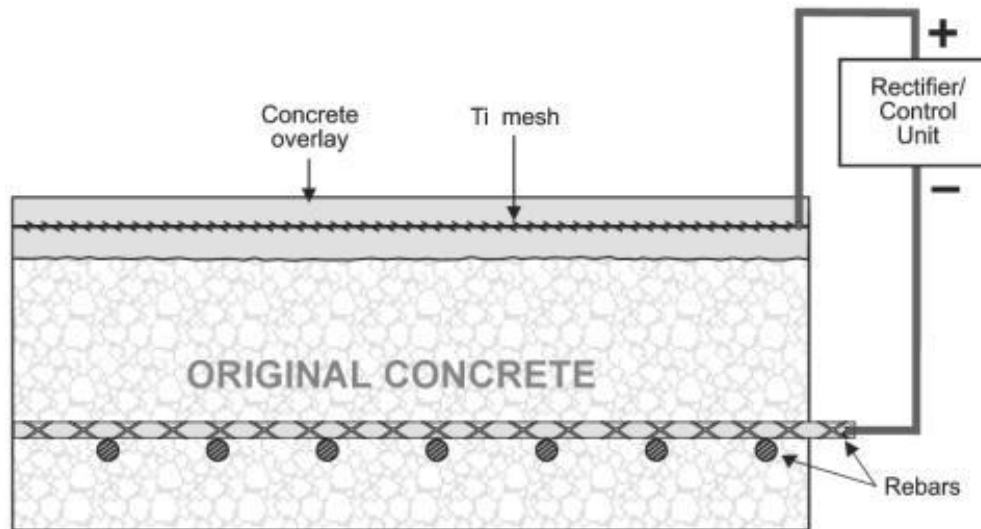


Figure 12. Induced current cathodic protection.

A current is then drawn through this system that maintains the rebars in the cathodic zone, meaning no corrosion can occur in this area, even in the presence of high chloride contents.

When installed properly, this is the only system available that completely arrests corrosion activities. However, it requires high skill levels to design and install such systems. It also requires continuous provision of the electrical current, and continuous monitoring through the entire service life, to ensure that the system is running properly. Any lack of such service might eventually result in destructive effects from induced current in the structure

The National Cooperative Highway Research Program of USA in their synthesis 398 (National Cooperative Highway Research Program, 2009), suggests that insufficient or no monitoring and maintenance is being performed by many agencies and this is the most important reason for the disappointing performance of many such systems.

In summary, induced current cathodic protection is a very effective system to stop corrosion activities, but it is very complex to design and install, as well as being very costly to install, continuously supply and monitor throughout its service life.

Additionally, this technique can only be used on prestressed concrete structures with additional measures as a precaution due to the risk of hydrogen embrittlement.

### 2.4.2 Galvanic protection

Galvanic corrosion protection of steel in concrete is based on the formation of a galvanic element if a metal less noble than steel (refer to the figure 13), in direct contact with the concrete overlay, is electrically connected to the steel reinforcement bars. The reinforcing steel is protected from corrosion as long as sufficient galvanic current flows between the galvanic element (acting as anode) and the steel reinforcement (acting as cathode). Most commonly, zinc is used as the sacrificial element / anode material. The galvanic cell that is formed corresponds to a conventional zinc/air battery. The first known application of a galvanic corrosion protection system for reinforced concrete, was on a bridge deck in Illinois in 1977.

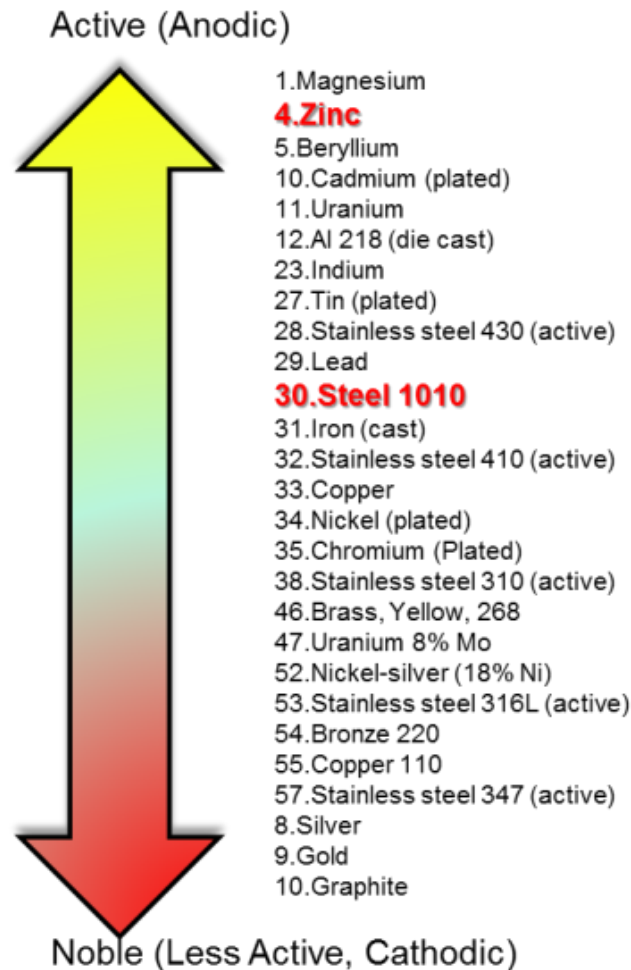


Figure 13. Potential difference of various metals.

The efficiency of galvanic corrosion protection depends on the lasting activity and durability of the zinc anode. However, passivation of the zinc anode by formation of a passive layer that reduces current flow on the zinc surface can be caused by:

- Deposition of anodic (zinc corrosion) products on the zinc element surface
- Contact with alkaline calcium hydroxide in concrete pore solution.

The first galvanic systems applied on reinforced concrete structures suffered from rapid passivation of the zinc anodes and therefore lost their protective effect after a short time. This passivation had to be addressed by the introduction of suitable activation agents – which could also result in excessive self-corrosion, consuming up to 70% of the zinc without producing the necessary protective current.

Critical reports about mixed results from early applications created resistance to the use of galvanic systems, which has continued up to now in some countries. Huge research and development effort was put into development of better galvanic anodes with balanced activation for long lasting effectiveness. All the known successful approaches developed to date, are extensively protected by patents. However, there is also now evidence of a useful proprietary system service life of more than 20 years.

Various systems of galvanic protection are available:

- Incipient anodes mitigation:
  - Embedded anodes in the patch repaired area
  - Discrete anodes installed at the periphery of the patch repaired area
- Control of corrosion in sound but contaminated concrete:
  - Hybrid discrete anodes
  - Galvanic discrete anodes
  - Surface installed anodes

Typical advantages of galvanic systems over impressed current cathodic protection are:

- No need for external hard wiring the anodes (no risk of copper wire thefts)
- Simple installation, relatively low cost
- No risk of hydrogen embrittlement in prestressed or post-tensioned tendons
- Self-adjusting current density
- No continual service or monitoring required (although monitoring is always recommended when a design life of more than 15 years is required)

#### 2.4.2.1. Incipient anodes mitigation

These anodes are placed and embedded in the patch repair zone (Figure 14) and need to use a mortar with a specific resistivity to fill the patch (Loziquez, et al 2018; Christodoulou, et al 2014), or within the concrete surrounding the patch repair zone (Figure 15). The efficiency of these latest anodes does not depend on the resistivity of the mortar used to fill the patch (Loziquez, et al 2018; Christodoulou, et al 2014) to solve the problem of incipient corrosion of the anodes.

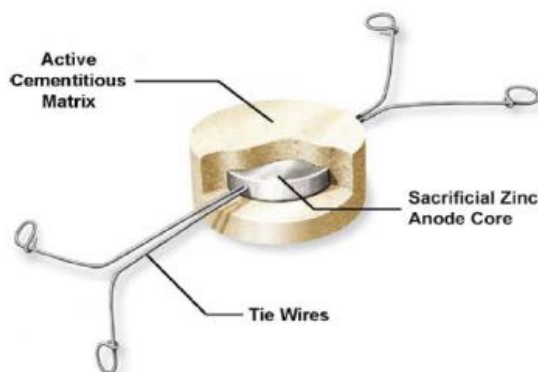


Figure 14. Cut-away of a proprietary anode  
To be placed in the repair mortar patch.



Figure 15. Anodes to be placed in the vicinity  
of the repair patch area.

Galvanic anode technology for corrosion protection of reinforced concrete has been available for more than 20 years.

Sergi George (George et al, 2010) has shown, from several field experiments, the long-term durability of these anodes, and a good correlation between their estimated life span (from the anode consumption) and the actual measurement of residual zinc remaining in the puck after 10 years.

The anodes placed in the repair patch areas, require a repair mortar to be used with a low resistance, which unfortunately also limits the quality level of the mortar

When anodes are placed in the original concrete outside the repair patches, e.g., outside but in their vicinity, the repair work can be carried out using high quality mortar, as there is no limitation in the resistivity of the mortar. In Cancun, Mexico, a field test was carried out, installing anodes inside the host concrete to protect the reinforcing steel against the incipient effect of anode corrosion. In situ measurements showed the level of protection of the installed anodes (figure 16).



Figure 16. Installation of anodes inside host concrete with installation verification in Cancun, Mexico.

Independent papers (Loziquez, et al 2018; Christodoulou, et al 2014) have shown the importance of placing the anodes in the surrounding parent concrete and not in the patch areas.

This is a relatively simple but effective system to prevent the development of incipient anodes, even in the presence of high chloride contents in good quality sound concrete. If the anodes are installed inside the patch, the repair mortar to fill the patch must have a specified resistivity. On the contrary, if anodes are placed around the patch, a high-quality mortar can be used.

#### **2.4.2.2. Corrosion prevention with discrete anodes**

These anodes are placed in healthy but contaminated concrete and then linked together to produce the galvanic current as can be seen in the photo in figure 17, which shows the preparation for installing these anodes and linking them together.

Some issues (Holmes et al, 2011) have been raised regarding the efficiency of this system especially in concrete structures with heavy existing corrosion. When running purely in galvanic mode, in the presence of high chlorides, it has been found that the anode current output is the same as the current output of anodes placed in concrete with no chlorides present. This means that the effectiveness of discrete anodes might be limited if used to stop on-going corrosion in area of high chloride induced corrosion.



Figure 17. Discrete anodes on a bridge parapet.

The use of galvanic anode is a simple system, but with some limitations in areas of high chloride-induced corrosion as the level of galvanic current released by the anodes may not be sufficient to remove the chlorides and consequently repassivate the steel.

#### ***2.4.2.3. Corrosion prevention with hybrid systems***

More than 15 years ago, a UK based company patented and launched a hybrid system that combines both induced current and galvanic protection.

During the induced current phase (typically used initially for 1 to 2 weeks depending on the voltage used), the steel reinforcement is re-passivated by the formation of hydroxide ions due to the induced current output, whilst chlorides are removed from the surrounding pore liquid. Once the steel is back in passivated form, the current is switched off, and the anodes are then connected so the system can run in pure galvanic mode.

In the previously mentioned study, Holmes (Holmes et al, 2011), figure 18 compared the activity of a zinc anode in concrete containing 2.5% chloride, operating at 100% in galvanic mode, with the same anode that had previously been activated for one week by an external current. These two systems were compared with the activity of the same galvanic anode placed in concrete without chlorides. The study shows that the anode operating in pure galvanic mode generates as much current as the anode placed in concrete without chlorides, demonstrating its ineffectiveness in protecting the steel. Whereas the anode that has been previously activated, is very active due to the presence of these chlorides. It sacrificed itself instead of the surrounding steel (see figure 19).

If required by the consultant, monitoring systems similar to those installed in the eddy current cathodic protection system can be installed using a reference electrode and monitored according to the recommendations of EN ISO 12696.

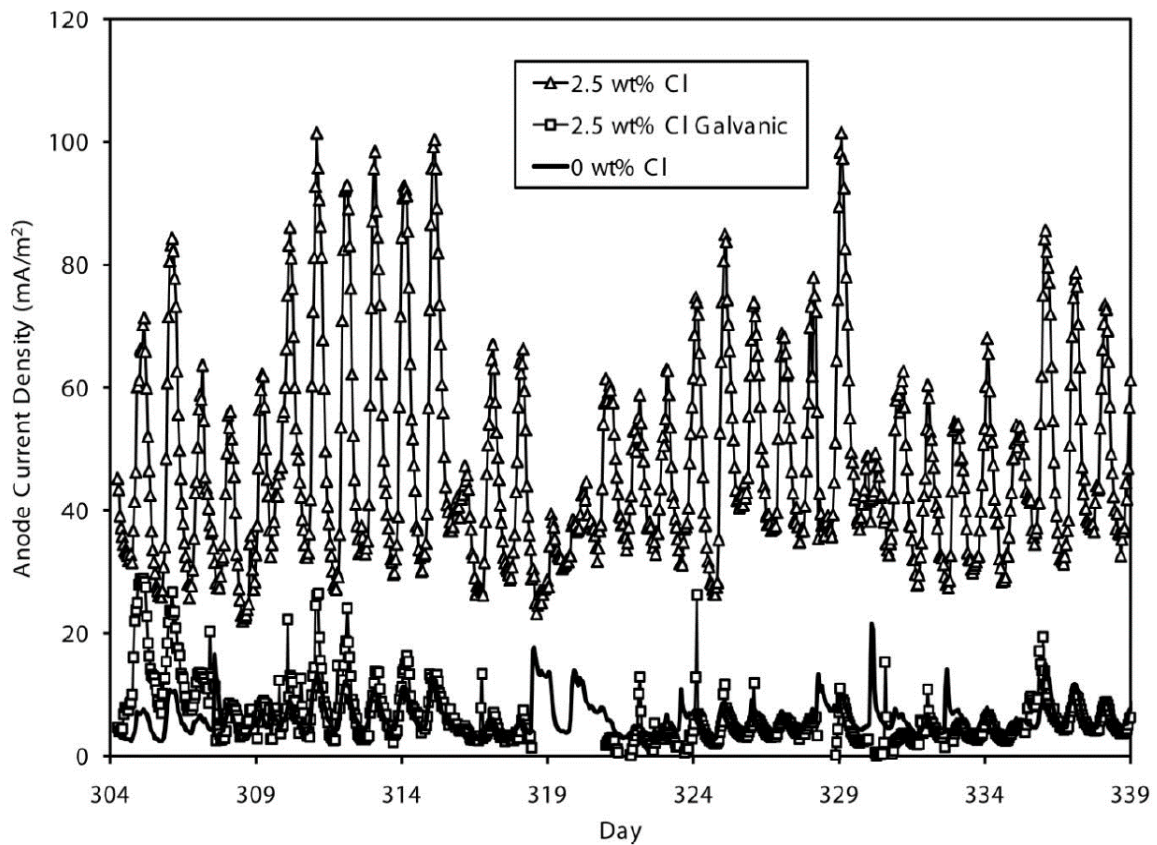


Figure 18. Comparison between the anode (2.5% Cl. galvanic) operating in pure galvanic mode and the anode (2.5% Cl.) being activated by the induced current for a short period of time before operating in galvanic mode. (Holmes et al, 2011).

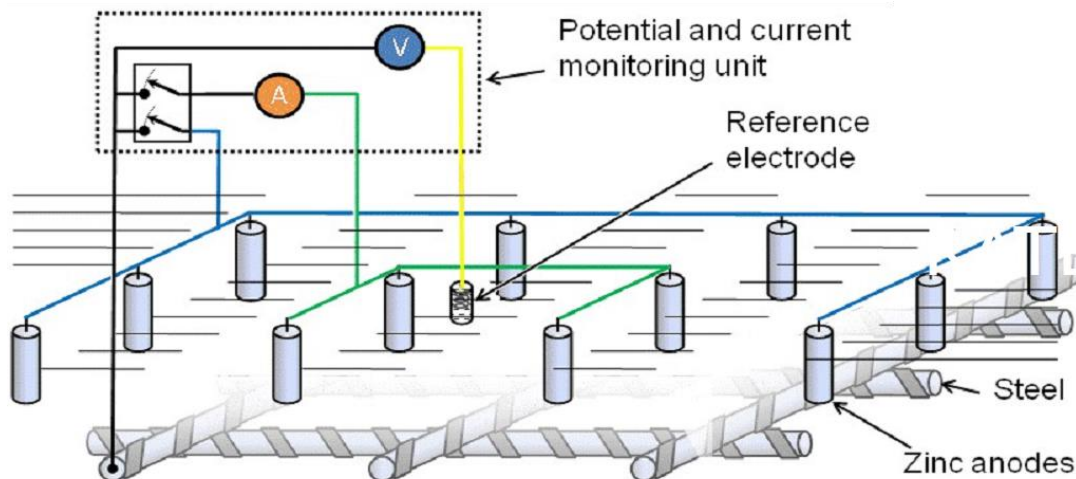


Figure 19. Schematic description of reference electrode monitoring system

Installed at the Whiteadder Bridge, Scotland in UK, this hybrid system still responds to the environment long after the installation (Dodds, 2018).

The hybrid system is very attractive, as illustrated in Figure 20, as it provides a certain level of performance warranty, such as those offered by the induced current cathodic protection system, by being less complex and not requiring the same levels of long-term maintenance with constant adjustment of the current input as required in the ICCP.



#### 4. REFERENCES

- Angst, U.; Moro, F.; Geiker, M.; Kessler, S.; Beushausen, H.; Andrade, C.; Lahdensivu, J.; Köliö, A.; Imamoto, K.-ichi; von Greve-Dierfeld, S.; Serdar, M. (2020), *Corrosion of steel in carbonated concrete: mechanisms, practical experience, and research priorities – a practical review by RILEM TC 281-CC*. RILEM Technical Letters, Vol. 5, 85-100, DOI: <https://doi.org/10.21809/rilemtechlett.2020.127>
- Bertolini, L., Elsener, B., Pedferri, P., Redaelli, Elena., Polder, R. B. (2004), *Corrosion of steel in concrete, prevention, diagnosis, repair*. Wiley-VCH Verlag GmbH & Co. KGaA, Weinheim, DOI: <https://doi.org/10.1002/3527603379>
- Brem, M., Lohner, J., Büchler, M. (2022), A long-term study on the effect of a hydrophobic treatment on the moisture balance and durability of a reinforced concrete structure in a road tunnel. MATEC Web of Conferences 364, 04005, ICCRRR, DOI: <https://doi.org/10.1051/mateconf/202236404005>
- Christodoulou, C., Goodier, C., Austin, S., Glass, G. K., Webb, J. (2012). *Assessing the long-term durability of silanes on reinforced concrete structures* (Version 1). Loughborough University. <https://hdl.handle.net/2134/10925>
- Christodoulou, C., Goodier, C., Austin, S., Webb, J., Glass, G. K. (2013), *Diagnosing the cause of incipient anodes in repaired reinforced concrete structures*. Corrosion Science, Volume 69, Pages 123-129, DOI: <https://doi.org/10.1016/j.corsci.2012.11.032>
- Christodoulou, C., Goodier, C. I., Austin, S. A. (2014): *Site performance of galvanic anodes in concrete repairs*. IN: Grantham, M, etal (eds). Concrete Solutions 2014. Proceedings of Concrete Solutions, the 5th International Conference on Concrete Repair, 1st-3rd September 2014, Belfast. Boca Raton, FL: CRC Press, pp. 167-172, <https://dspace.lboro.ac.uk/2134/16552>
- Dodds, W., Christodoulou, C. (2018), *Hybrid anode concrete corrosion protection – independent study*. Proceedings of the Institution of Civil Engineers - Construction Materials, 171(4), pp: 149-160, DOI: <https://doi.org/10.1680/jcoma.16.00024>
- Guy, T. (2000), *CEBTP, France, report No 2393.6.100*.
- Heiyantuduwa, R., Alexander, M. G., Mackechnie, J. R. (2006), *Performance of a Penetrating Corrosion Inhibitor in Concrete Affected by Carbonation-Induced Corrosion*. Journal of Materials in Civil Engineering, Vol. 18, Issue 6, DOI: [https://doi.org/10.1061/\(ASCE\)0899-1561\(2006\)18:6\(842\)](https://doi.org/10.1061/(ASCE)0899-1561(2006)18:6(842))
- Holmes, S., Glass, G. K., Wilcox, G. D., Robins, P. J., Roberts, A. C. (2011), *The Response of Protective Current to Environmental Conditions During Hybrid Anode Concrete Repair Treatments*. NACE Conference Papers, 11005.
- Loziquez, E., Barthélémy, J. -F., Bouteiller, V., Desbois, T. (2018), *Contribution of Sacrificial Anode in reinforced concrete patch repair: Results of numerical simulations*. Construction and Building Materials, Volume 178, 30, Pages 405-417, DOI: <https://doi.org/10.1016/j.conbuildmat.2018.05.063>
- Mozaryn, T., Kokowska, J. (2009), *Service life of coating systems applied on cooling towers - A laboratory study and in-situ investigations*. Book title: NUCPERF 2009 - Long Term Performance of Cementitious Barriers and Reinforced Concrete in Nuclear Power Plants and Waste Management. Editor(s): V. L'Hostis, R. Gens, C. Gallé. Publisher: RILEM Publications SARL.
- Page, C. L., Treadaway, K. W. J. (1982), *Aspects of the electrochemistry of steel in concrete*, Nature, 297, 109-115, DOI: <https://doi.org/10.1038/297109a0>
- Page, C. L., Sergi, G. (2000), *Developments in cathodic protection applied to reinforced concrete*, Journal of Materials in Civil Engineering, Vol. 12, Issue 1, 8-15. DOI: [https://doi.org/10.1061/\(ASCE\)0899-1561\(2000\)12:1\(8\)](https://doi.org/10.1061/(ASCE)0899-1561(2000)12:1(8))
- Qian, S., Zhang, J., Qu, D. (2006), *Theoretical and experimental study of microcell and macrocell*

- corrosion in patch repairs of concrete structures*, Cement and Concrete Composites, Volume 28, Issue 8, Pages 685-695, DOI: <https://doi.org/10.1016/j.cemconcomp.2006.05.010>
- Rodum, E., et al, (2012), The Norwegian Public Roads Administration, Trondheim, Norway, effect of different surface treatment products after 10 years of field exposure, presented at ICDC conference in June, Norway
- SAMARIS (2003-2005), *Sustainable and Advanced Materials for Road Infrastructure*, European, URL: <https://trimis.ec.europa.eu/project/sustainable-and-advanced-materials-road-infrastructure>
- Sergi, G., Whitmore, D. (2010), *Performance of Zinc Sacrificial Anodes For Long-term Control of Reinforcement Corrosion*. NACE - International Corrosion Conference Series.
- Silva, N. (2013), *Chloride Induced Corrosion of Reinforcement Steel in Concrete*. Department of Civil and Environmental Engineering, Chalmers University of Technology, Sweden. Thesis for the degree of Doctor of Philosophy.
- Tilly, G. P., Jacobs, J. (2007) *Concrete repairs – Performance in service and current practice*. CONREPNET, ISBN 978-1-86.81-974-2.
- Tritthart, J. (2003), *Transport of a surface applied corrosion inhibitor in cement paste and in concrete*. Cement and Concrete Research, 33(6):829-834, DOI: [https://doi.org/10.1016/S0008-8846\(02\)01067-0](https://doi.org/10.1016/S0008-8846(02)01067-0)
- Transportation Research Board of the National Academies (2009), *NCHRP SYNTHESIS 398, Cathodic Protection for Life Extension of Existing Reinforced Concrete Bridge Elements A Synthesis of Highway Practice*, CONCORR Inc, NATIONAL COOPERATIVE HIGHWAY RESEARCH PROGRAM.

## Sustainability strategies for increased competitiveness in the Mexican cement industry

P. Angulo<sup>1\*</sup>, C. Ochoa<sup>1</sup>

\*Contact author: [tapy\\_angulo@hotmail.com](mailto:tapy_angulo@hotmail.com)

DOI: <https://doi.org/10.21041/ra.v13i2.637>

Received: 06/09/2022 | Received in revised form: 11/04/2023 | Accepted: 14/04/2023 | Published: 01/05/2023

### ABSTRACT

The objective of this research is to identify and discuss the most eco-efficient sustainable strategies for utilizing or reducing emissions of NO<sub>x</sub>, SO<sub>x</sub>, and SiO<sub>2</sub> dust in cement manufacturing, in order to improve competitiveness in the Mexican cement industry. The research design was qualitative, observational, and deductive. Results showed that SO<sub>x</sub> waste bioreactors have greater eco-efficiency, followed by domes for capturing and utilizing SiO<sub>2</sub> and bag filters. These strategies are effective for specific contaminants derived from cement production. This study delves into a scarcely addressed topic in Mexico: cement sustainability. By applying these strategies, the Mexican cement sector would boost its business competitiveness.

**Keywords:** business competitiveness; competitiveness indicators; sustainability; cement industry.

**Cite as:** Angulo, P., Ochoa, C. (2023), “Sustainability strategies for increased competitiveness in the Mexican cement industry”, Revista ALCONPAT, 13 (2), pp. x-x, DOI: <https://doi.org/10.21041/ra.v13i2.637>

<sup>1</sup> Fundación Universitaria Iberoamericana, Ciudad de México, México.

#### Contribution of each author

In this paper, the author Patricia Angulo contributed with the original idea, the collection of data and the writing of the paper. The author Carlos Ochoa contributed with the methodological approach, the discussion of results and the revision of the article.

#### Creative Commons License

Copyright 2023 by the authors. This work is an Open-Access article published under the terms and conditions of an International Creative Commons Attribution 4.0 International License ([CC BY 4.0](https://creativecommons.org/licenses/by/4.0/)).

#### Discussions and subsequent corrections to the publication

Any dispute, including the replies of the authors, will be published in the first issue of 2024 provided that the information is received before the closing of the third issue of 2023.

## **Estrategias de sostenibilidad para la mayor competitividad en la industria cementera de México**

### **RESUMEN**

El objetivo de esta investigación es identificar y discutir las estrategias sostenibles más ecoeficientes para aprovechar o reducir emisiones de NO<sub>x</sub>, SO<sub>x</sub> y polvos de SiO<sub>2</sub> en la fabricación de cemento, con el objetivo de mejorar la competitividad en la industria cementera de México. El diseño de investigación fue cualitativo, observacional y deductivo. Los resultados mostraron que los biorreactores de residuos de SO<sub>x</sub> tienen mayor ecoeficiencia; seguido de los domos para capturar y aprovechar el SiO<sub>2</sub> y los filtros de mangas. Estas estrategias son efectivas para contaminantes específicos derivados de la producción de cemento. Este estudio indaga en un tema escasamente abordado en México, la sostenibilidad del cemento. Al aplicar estas estrategias, el sector cementero mexicano impulsaría su competitividad empresarial.

**Palabras clave:** competitividad empresarial; indicadores de competitividad; sostenibilidad; industria cementera.

## **Estratégias de sustentabilidade para maior competitividade na indústria cimenteira do México**

### **RESUMO**

O objetivo desta pesquisa é identificar e discutir as estratégias sustentáveis mais ecoeficientes para aproveitar ou reduzir as emissões de poeiras de NO<sub>x</sub>, SO<sub>x</sub> e SiO<sub>2</sub> na fabricação de cimento, com o objetivo de melhorar a competitividade da indústria cimenteira no México. Seguiu-se um desenho de pesquisa qualitativa, observacional e dedutiva. Os resultados mostraram que os biorreatores de resíduos de SO<sub>x</sub> têm maior ecoeficiência; seguido por cúpulas para capturar e aproveitar SiO<sub>2</sub> e filtros de mangas. Estas estratégias são eficazes para contaminantes específicos derivados da produção de cimento. Este estudo investiga um tema raramente abordado no México, a sustentabilidade do cimento. Ao aplicar estas estratégias, o sector do cimento mexicano aumentaria a sua competitividade empresarial.

**Palavras-chave:** competitividade empresarial; indicadores de competitividade; sustentabilidade; indústria de cimento.

### **Legal Information**

Revista ALCONPAT is a quarterly publication by the Asociación Latinoamericana de Control de Calidad, Patología y Recuperación de la Construcción, Internacional, A.C., Km. 6 antigua carretera a Progreso, Mérida, Yucatán, 97310, Tel.5219997385893, [alconpat.int@gmail.com](mailto:alconpat.int@gmail.com), Website: [www.alconpat.org](http://www.alconpat.org)

Reservation of rights for exclusive use No.04-2013-011717330300-203, and ISSN 2007-6835, both granted by the Instituto Nacional de Derecho de Autor. Responsible editor: Pedro Castro Borges, Ph.D. Responsible for the last update of this issue, Informatics Unit ALCONPAT, Elizabeth Sabido Maldonado.

The views of the authors do not necessarily reflect the position of the editor.

The total or partial reproduction of the contents and images of the publication is carried out in accordance with the COPE code and the CC BY 4.0 license of the Revista ALCONPAT.

## 1. INTRODUCTION

Competitiveness aligned with environmental sustainability regimes guarantees any business organization productive success, a stable economy, and business survival. It also enables the adoption of transformations required by the changes in the globalized world. Scientific innovation and technological development provide the necessary tools and means for designing better and eco-efficient production strategies, thus helping in making more objective decisions (Jaramillo, 2017). This study focuses on the cement industry, a sector that releases a large amount of greenhouse gases and other polluting compounds into the environment. This situation represents a significant challenge that must be addressed to ensure the health of future generations (León-Velez & Guillén-Mena, 2020; Rodgers, 2018; Kumar, 2018). In this context, developing competitiveness implies an analysis of the viability and applicability of sustainable and eco-efficient strategies in the cement production process. The study of these strategies strengthens quality control in the manufacturing of this material. It also provides a better understanding and mastery of topics such as the environment, legal aspects, ethics, costs, and safety management in the construction sector. The results of international and local cement companies contribute to improving the use and preservation of resources in the Mexican cement industry.

### 1.1 Business competitiveness from a sustainable perspective

Business competitiveness from a sustainable approach aims to achieve greater stability, market competition, and productivity based on sustainable processes. In this way, the life of a company is guaranteed in the long term. The adoption of more eco-efficient production strategies is in line with the prerogatives outlined in the 2030 Agenda to meet the Sustainable Development Goals (SDGs). These goals were proposed by the United Nations (UN) in 2016 (Rivera-Hernández et al., 2018; UN, 2018).

Sustainability refers to the appropriate use, development, and recovery of all tangible, intangible, material, and natural resources available to a business or industrial organization. Consequently, it enables long-term stability and productivity (Roy, 2021). At this point, it is important not to confuse the concepts of sustainability and sustainability. The former deals with the care and use of natural resources, while the latter refers to development related to environmental care (Rivera-Hernández et al., Ruggiero, 2021).

The SDGs that are directly related to a sustainable industrial sector are responsible production and consumption, climate action, preservation of underwater life and terrestrial ecosystems, clean water and sanitation, as well as access to non-polluting energy. These SDGs are linked to community human development at local, regional, and global levels. In addition, they converge with environmental sustainability and promote optimal community development and health (UN, 2018; Balanzátegui et al., 2019; The Cement Sustainability Initiative or CSI, 2019).

An industrial corporation that operates under the terms of Sustainability, Corporate Social Responsibility (CSR), and Corporate Environmental Responsibility (CER) can obtain certain benefits. It improves its development, social reputation, business image, and generates long-term economic returns. This effect is enhanced if their actions go beyond legal interests and obligations (González & Cuesta, 2018). The general process to develop greater business competitiveness in sustainable terms involves:

- Identifying suitable objectives and goals for each organization's characteristics.
- Defining strategic action plans.
- Generating a system of indicators that show the information derived from business activity.
- Applying evaluations of their behavior.

It is important to note that the design of strategies and actions is different in each company because it depends on the results of a previous diagnosis that shows its deficiencies, potentialities, resources, etc. (Vega, 2017). Some actions that strengthen the CER of any industry are reusing industrial waste as raw material in production processes or implementing innovative production based on other eco-efficient strategies. Experience shows that their implementation reduces production costs, gas emissions, and the generation of polluting compounds (Bravo & Arroyo, 2018; Pérez et al., 2016; Lin et al., 2017).

### **1.2 Competitiveness indicators applicable in the cement industry**

Productivity and economic performance are basic indicators of competitiveness in the cement industry. Pérez et al. (2013) proposed other potential indicators that can be addressed at the organizational level. These indicators promote business competitiveness in this sector and include:

- Participation in the global market and a strong international position. Generates greater growth and integration of the domestic market.
- Development of CSR and CER. Maximizes functions and improves corporate image.
- Price competitiveness. Drives attractive prices for the market.
- Technological competitiveness. Increases productivity by offering differentiated products.
- Authentic or genuine competitiveness. Increases quality and productive efficiency by taking advantage of economies of scale and product differentiation.
- Spurious competitiveness. Generates a system of protected industrialization, reduces excessive local competition, and leads to financial stability. Additionally, it allows companies to receive government subsidies arising from currency devaluation and wage depression.

Authors such as López (2018) and the Future Cities group of Siemens (2018) point out that technological innovation also contributes to improving productive efficiency and massive data processing. These innovations include the use of drones, automated computer systems with real-time functions, adoption of the internet of things, maintenance 4.0, and the use of advanced materials. Likewise, eco-industrial technologies minimize the emission of residual gases and lead to lower consumption of renewable energies. The CSI also establishes practices and performance indicators for sustainable development, focusing on safety, climate protection, air emissions, use of fuels and raw materials, communications, and local impacts on land and communities. It should be noted that the CSI brings together companies from around the world (CSI, 2012).

In summary, the implementation of sustainable and eco-efficient strategies in cement production is a necessity for the industry worldwide because it contributes to reducing its harmful effect on the environment and promotes the competitiveness of companies. For these reasons, this research aims to identify the most sustainable and eco-efficient strategies to exploit or reduce the emission of NO<sub>x</sub>, SO<sub>x</sub>, and SiO<sub>2</sub> dust in the manufacture of cement, in order to improve the competitiveness of the Mexican cement industry.

## **2. PROBLEM STATEMENT**

Currently, the application of technological strategies focused on the care and preservation of the environment is an almost obligatory prerogative in the entire business productive sector because it benefits their technological and innovative competitiveness. Likewise, its application is aligned with the UN SDGs (2018).

Business competitiveness in the cement industry is reflected in its economic performance and level of competition in the market, as well as in its results on the emission of polluting waste. In this sense, technologies adopted to reduce the emission of sulfur oxides ( $\text{SO}_x$ ), nitrogen oxides ( $\text{NO}_x$ ), and  $\text{SiO}_2$  dust can improve their business competitiveness because it is the industrial sector that pollutes the most and damages the environment.

Portland cement (“gray cement”) mainly consists of a fine powder or clinker containing compounds such as calcium silicates and calcium aluminates. These compounds set and harden at room temperature or underwater when mixed with water. Cement types vary in formulation depending on their use and the desired strength (Sanjuán & Chinchón, 2014).

Industrial cement production includes the phases of cooking and cooling that stand out for their adverse ecological implications. Most of it is produced during the burning of fuels such as coal, petroleum coke, heavy fuel oil, among others. The chemical transformation that produces the clinker is called “decarbonation” and consists of the decomposition of calcium carbonate ( $\text{CaCO}_3$ ) at  $900\text{ }^\circ\text{C}$ . This reaction produces calcium oxide (CO) and releases significant amounts of carbon dioxide ( $\text{CO}_2$ ). In addition, CO reacts at high temperatures with  $\text{SiO}_2$  dust, alumina or aluminum oxide ( $\text{Al}_2\text{O}_3$ ), and iron oxide ( $\text{Fe}_2\text{O}_3$ ). The result of this process is the formation of compounds that harm the environment such as calcium silicates, aluminates, and ferrites. All of these are clinker-forming elements (Sanjuán & Chinchón, 2014; Ashby, 2024).

The cooling of the clinker also has adverse environmental consequences (León-Velez & Guillén-Mena, 2020; Sanjuán & Chinchón, 2014). During this phase, electric fans are used that generate a secondary waste of air-energy that is released at a temperature of  $800\text{ }^\circ\text{C}$ . During cooling, polluting gases are also emitted into the atmosphere. Mainly CO, nitrogen monoxide (NO), and sulfur dioxide ( $\text{SO}_2$ ). These gases are released especially when an adequate mechanism for their treatment is not available.

According to recent data, the cement industry consumes approximately 40% of the planet's primary energy. This percentage is due to the high use of petroleum, natural gas, coal, biomass, wind, and solar radiation. This industry also consumes 60% of the raw materials extracted from the earth's lithosphere (silicates, crust, and mantle) and produces 5% to 8% of global  $\text{CO}_2$  emissions (León-Velez & Guillén-Mena, 2020; Rodgers, 2018).

A study conducted by the Dutch Environmental Assessment Agency during the years 2010 to 2017 addressed the relationship between the amount of cement produced and the total  $\text{CO}_2$  emissions. Its results showed that China is the largest cement producer and  $\text{CO}_2$  emitter globally. Behind it are India, the European Union, the United States, Vietnam, Turkey, Egypt, and other producing countries (Rodgers, 2018).

According to several 2020 studies conducted by the Global Cement and Concrete Association (GCCA), cement is the most consumed material in the world. Its production process generates the highest  $\text{CO}_2$  emissions (around 150 tons per second) and a total of 14 billion cubic meters of concrete is used each year (France 24, 2021). As can be seen, the environmental damage caused by the massive production of cement represents an obstacle to strengthening business competitiveness, as its environmental effects violate the SDGs (UN, 2018). Therefore, it is not possible to consider it as a sustainable sector in real terms.

More actions are needed in addition to the commitment to reduce the ravages of climate change adopted by cement industry leaders. For example, each company needs to apply eco-efficient strategies that lead to the transformation of their production processes and demonstrate a reduction in their polluting emissions. This can be accredited through evaluations backed by scientific evidence (Rodgers, 2018).

The application of systematic models to evaluate polluting emissions before, during, and after the implementation of sustainable strategies represents an objective reference framework that goes beyond a simple commitment speech. According to some experts, this approach stands out as the

main tool for a real estimation of possible scenarios. In this way, it is possible to make decisions based on the results provided by scientific evidence. All of this leads to designing viable alternative solutions oriented towards better future actions (Gessa, 2016).

## 2.1 Context of the problem in Mexico

In Mexico, the cement industry is strong, highly productive, and profitable. Cement production contributes 1% of the national Gross Domestic Product (GDP). According to data from the International Trade Center, this industry was in first place as a cement marketer in Latin America, ranked 19<sup>th</sup> as a cement exporter worldwide, and ranked 22<sup>nd</sup> as a cement importer in 2018. However, more recent data from 2020 revealed that the Mexican cement industry currently ranks second in Latin America. The reason for this decline is due to competition from the Chinese cement industry (Clavijo & Guevara, 2020; Aguilar, 2019; Martínez & Alexandre, 2020).

According to the National Chamber of Cement (2020), the Mexican cement industry is made up of the following companies: Grupo Cemex, Cementos de Chihuahua (GCC) Group, CYCNA, Cement and Concrete Moctezuma, Holcim Cement, Cementos Fortaleza, and Cementos Cruz Azul. These companies make up the National Chamber of Cement (CANACEM). According to this organization, the Mexican cement sector produces a total of 40 million tons of cement per year and generates more than 170,000 direct and indirect jobs in the country. Some of these companies have adopted the following strategies to reduce their pollutant emissions:

- Grupo Cemex. Implementación de un modelo de sustentabilidad en sus operaciones que incluye infraestructura energéticamente sustentable (Grupo Cemex, 2021).
- GCC. Promotion of environmental responsibility and protection of the climate for economic sustainability (GCC, 2023).
- Cemento y Concreto Moctezuma. Development of technology and modernization of cement plants to reduce environmental impacts (Cemento y Concreto Moctezuma, n.d.).
- Cementos Cruz Azul. Some of its plants have water treatment and rainwater harvesting systems for use. They also use alternative sources of energy such as biomass obtained through the nopal plant (Cooperativa La Cruz Azul, 2016).

In 2020, the CANACEM reported the main strategy to improve CSR in this sector: to seek better management of the co-processing or incineration of urban solid waste. These waste come from different states of the Republic, such as Colima, Baja California Sur, Mexico City, Michoacán, Nayarit, Quintana Roo, and Sinaloa. To comply with the strategy, this organization intervenes through the installation of transfer, reception, separation, crushing, compaction, composting, and biodigestion centers for waste. Additionally, it subjects them to adequate treatment for their inclusion in the industrial production of cement (National Chamber of Cement, 2020).

Even with the implementation of these measures, it cannot be affirmed that the Mexican cement sector is a sustainable industry. This sector shows clear deficiencies in scientifically demonstrating the eco-efficiency of its production processes. For example, among Mexican companies, only CEMEX has reported a 30% reduction in its carbon footprint in its production processes. Similarly, it claims to have reduced its water consumption by 10.2% in the last 10 years (García-Muñoz & Pérez-Sánchez, 2020). Regarding this, it is necessary to emphasize that such data lacks clear information on the evaluation model that supports them.

Companies such as CEMEX and Cementos Cruz Azul have implemented strategic actions that demonstrate their intention to align with the UN's 2030 Agenda goals (García-Muñoz & Pérez-Sánchez, 2020). But there is no data that fully supports their results. That is why the Mexican cement industry needs to more systematically demonstrate the eco-efficiency in the implementation of its sustainable strategies (León-Velez & Guillén-Mena, 2020).

In the context of the above, international and national scientific evidence shows that the application of eco-efficient analysis allows quantifying the environmental impact of cement production, mainly

when seeking to take advantage of the substitution of raw materials for savings in non-renewable natural resources such as fuel and water. It is also useful when it comes to using waste from the production process itself to reduce the emission of polluting gases (Pérez et al., 2013; Sanjuán & Chinchón, 2014; Ruiz et al., 2017).

During the cement production process, CO<sub>2</sub>, NO<sub>x</sub>, SO<sub>x</sub> gases, and SiO<sub>2</sub> dust are released into the atmosphere (Kumar, 2018; Semarnat, n.d. ; Cooperativa La Cruz Azul, n.d.). The NO<sub>x</sub> and SO<sub>x</sub> gases diminish the air quality and contribute to the greenhouse effect. On the other hand, SiO<sub>2</sub> dust represents a significant risk to the lung health of workers inside a cement production plant. In Mexico, there are no studies that scientifically demonstrate the eco-efficiency of sustainable strategies applied to residual emissions of SO<sub>x</sub> and NO<sub>x</sub> gases and SiO<sub>2</sub> dust. Although some companies such as CEMEX and Cementos Cruz Azul claim to apply strategies that seem to align with the SDGs of the UN's 2030 Agenda. This research aims to know these strategies, which also allow improving the business competitiveness of the cement sector.

### 3. RESEARCH METHOD

A qualitative-observational-deductive research design was used (Hernández et al., 2014). Research strategies such as information search and selection, document analysis, and data interpretation were also applied.

Literature search was conducted through online scientific research platforms such as Redalyc, Dialnet, Google Scholar, and Scielo. Keywords such as “cement production and gases”, “greenhouse gases”, “sustainable cement production”, and “industrial waste utilization” were used in the search engines. An approximate body of 35 documents was selected, consisting mainly of indexed and academic journal articles written in Spanish and English.

Document analysis consisted of identifying key concepts and innovative ideas about the methods and analysis of the processes of interest. The visualization of viable solutions to the problem was based on finding new data for the Mexican context. The main document analysis tools used were:

- Classification of the literature that makes up the state of the art of the addressed problem.
- Elaboration of informative tables.
- Construction of schemes, diagrams, or conceptual maps.
- Elaboration of study cards (Hernández et al., 2014).

Interpretation of qualitative design study data consisted of “isolating portions of discourse” (Schettini & Cortazzo, 2015). This process involved a particular selection of information that the researchers made by inferring some aspects of their research. During this procedure, not only the hypothesis and objectives influence but also the sociocultural world, intuition, and life experience of the interpreter.

### 4. RESULTS, DISCUSSION AND PROPOSAL

#### 4.1 Results

The literature review yielded the following results it was identified that during the base processing of cement, a myriad of chemical reactions occur, such as exothermic reactions. They are called exothermic because they release energy in the form of heat, light, or sound during the formation of clinker. These reactions are a source of residual compounds such as molecular nitrogen (N<sub>2</sub>), amino radical (NH<sub>2</sub>), and water (H<sub>2</sub>O). The greatest amount of polluting emissions of SO<sub>2</sub> is generated during this phase of the process, as well as in grinding, cooling, and packaging of the finished product. The maximum allowable level of emissions for this type of waste is around 400 mg/m<sup>3</sup>. This indicator is measured annually using the “non-dispersive infrared NMX-AA-55-1979”

method, as stipulated by the Mexican Ministry of Environment and Natural Resources (Semarnat, n.d.).

SiO<sub>2</sub> is part of the raw material used in cement production, although it can also be released as waste from the process, even in the storage phase. The dust generated from the production of clinker is a mixture of silica + oxygen + carbon + aluminum + calcium microparticles. It has been observed that this mixture affects the health of workers inside a cement production plant. Inhalation of the mixture can cause irritation in the respiratory tract and skin and can cause severe eye damage. These effects are related to the development of chronic diseases such as silicosis, tuberculosis, lung cancer, or chronic obstructive pulmonary disease (COPD) (Kumar, 2018; Cobo & Estébanez, 2021).

To minimize NO<sub>x</sub>, SO<sub>x</sub>, and SiO<sub>2</sub> waste during industrial cement processing, the chemical properties of the raw material used must be considered. The application of eco-efficient strategies is also required, such as the substitution of fossil fuels, the design of systems for waste capture, the use of nanotechnology (Poudyal & Kushal, 2021), and other strategies that lead to this objective in the short, medium, and long term. Table 1 analyzes strategies that have been applied in Mexico and other countries to reduce the emission of these wastes.

Table 1. International and national strategies to reduce NO<sub>x</sub>, SO<sub>x</sub>, and SiO<sub>2</sub> dusts derived from the cement production process

Author, country, and year	Objective	Strategy to take advantage of or reduce the emission of NO <sub>x</sub> , SO <sub>x</sub> , and SiO <sub>2</sub>	Demonstrated ecoefficiency	Conclusions
European Commission, Europe, 2010	Keep low emissions of SO <sub>x</sub> residues during the clinker manufacturing phase.	Best Available Techniques (BAT): 1.- Allows reducing combustion gases in two phases: preheating and precalcination of the kiln. Achieved through the addition of absorbent material or a wet scrubber. 2.- Optimizes raw material grinding processes for dry processes.	Daily average emission value obtained from SO <sub>2</sub> : <50 mg/Nm <sup>3</sup> when the sulfur content in the material is <0.10% 250-400 mg/Nm <sup>3</sup> , if the sulfur content is >0.25% mg/Nm <sup>3</sup> .	Emission margins depend on the sulfur content in the raw material used. Therefore, the strategy is to select raw materials with the lowest concentrations of this chemical.
CEMEX, Mexico, 2012 and 2016.  CSI, 2014.	Replace fossil fuels and gas with urban or organic solid waste during clinker formation.	Use of urban solid waste: used tires, waste solvent residue, used oils, among others. Use of organic waste: rice husk, coffee, sediment from wastewater, among others.	CEMEX reduced its carbon footprint by 22.7% in 2012. In 2016, it reported obtaining 26.6% of the energy for its kilns from biomass and waste. No data	Publishing data on the eco-efficiency of these strategies can help support the reduction of the carbon footprint.

Author, country, and year	Objective	Strategy to take advantage of or reduce the emission of NO <sub>x</sub> , SO <sub>x</sub> , and SiO <sub>2</sub>	Demonstrated ecoefficiency	Conclusions
			was found on the eco-efficiency of these strategies. They also did not present results for NO <sub>x</sub> , SO <sub>x</sub> , and SiO <sub>2</sub> residues.	
Rocha et al., Bolivia and Brazil, 2022.		Use of energy and raw materials with lower ecological	85% of Clinker was produced with conventional fuels in 1990. In 2014, that percentage was reduced to 23%.	
Sagástegui, Peru, 2012.	Captar la mezcla de polvos fugitivos en una planta productora de cemento.	Capture the fugitive powder mixture in a cement production plant. Installation of domes for capturing fugitive dust. These domes have an air filtration system from the outside that helps minimize fugitive dust emissions. They are installed on temporary storage or in the clinker yard.	<ul style="list-style-type: none"> <li>• Directly benefits the health of workers.</li> <li>• Maintenance does not have excessive costs.</li> </ul>	Micro-particles of SiO <sub>2</sub> do not have a significant environmental impact. But they can harm the health of those who inhale their dust. For this reason, it is also recommended that workers use special protective equipment with a mask.
Sanjuán and Chinchón, Spain, 2014	Reduce the particles of dust and polluting gases emitted by localized sources.	Use of electrostatic precipitator or bag filters  SO <sub>2</sub> absorbents. They are applied in dry kilns.	Generally, emissions are <50 mg/Nm <sup>3</sup> .	Both the precipitator and the bag filters work at loading, unloading, and transportation points. They have shown to reduce NO <sub>x</sub> and SO <sub>x</sub> gases.

Author, country, and year	Objective	Strategy to take advantage of or reduce the emission of NO <sub>x</sub> , SO <sub>x</sub> , and SiO <sub>2</sub>	Demonstrated ecoefficiency	Conclusions
Feijoó et al., Cuba, 2016.  CSI, 2012.	Perform a balance of the main chemical reactions that sulfur undergoes during cement processing.	Stoichiometric chemical monitoring system. Based on the calculation of the molar mass of sulfur and its chemical reactions.	Detects standard reference values of SO <sub>3</sub> and Na <sub>2</sub> O, necessary for cement processing to occur optimally.	This system allows knowing when strategies should be applied to avoid sulfur rings in the furnace.
Veana et al., Mexico, 2019.	Producing bioenergy in the form of pure methane biogas.	using a bioreactor that processes agro-industrial waste. The process involves a biochemical interaction of organic compounds with biogas, carbon dioxide, water vapor, hydrogen, and hydrogen sulfide.	It is based on biochemical reactions of chemolithotrophic bacteria. The processing guarantees lower emission of gases and contaminating waste.	This bioreactor stands out for its dual functionality in the cement production process. On the one hand, it allows for the processing of waste generated by SO <sub>x</sub> . On the other hand, it produces methane biogas that can be used instead of fossil fuels.
Badillo et al., Mexico, 2020.	Thermal valorization in the separation of waste to produce alternative sources of fuel for the cement sector.	Thermal valorization and its utilization. Textile waste, among others, is processed as fuel in the production of clinker.	There is no specificity for waste types such as NO <sub>x</sub> , SO <sub>x</sub> , and SiO <sub>2</sub> dust.	This method could promote a change in behavior among the population by encouraging waste separation. It requires joint collaboration between the population and the cement sector.

Author, country, and year	Objective	Strategy to take advantage of or reduce the emission of NO <sub>x</sub> , SO <sub>x</sub> , and SiO <sub>2</sub>	Demonstrated ecoefficiency	Conclusions
Poudyal and Kushal, United States, 2021.	Integrated approach for sustainable cement production.	Capturing CO <sub>2</sub> to produce CaCO <sub>3</sub> that can be used as input.	Integration of three strategies: emissions capture, substitution of materials and fuel, and the use of nanotechnology.	Adopting these strategies can have benefits for the environment and society.

Source: own elaboration based on data collected from the European Commission (2010), CEMEX (2012), CEMEX (2016), CSI (2014), Rocha et al. (2022), Sagástegui (2012), Sanjuán & Chinchón (2014), Feijoó et al. (2016), CSI (2012), Veana et al. (2019), Badillo et al. (2020), and Poudyal & Kushal (2021).

#### 4.2 Discussion

When comparing these strategies with other studies or documentary reviews, some similarities were found. Regarding the substitution of fossil fuels, CEMEX stated that 26% of its kilns operated with biomass or waste in 2016 (CEMEX, 2016). This figure is consistent with that reported by Teja et al. (2022), which ranged from 20% to 30%. It should be noted that it is possible to substitute 3% to 80% of clinker with biomass ashes. In contrast, Huh et al. (2018) reported that the major problem for substituting fossil fuels with biomass is that the latter is still more expensive. In their study, they compared the marginal utilities of Korean companies using different types of fuels in their processes. They found that coal is still cheaper than other alternative energy sources, which makes it difficult to use in many companies.

Guo et al. (2023) also conducted a documentary review to identify strategies to reduce the ecological impact of cement production. Their results showed that some focus on improving process efficiency and reducing energy consumption, mainly in Asian countries such as China and India. These strategies coincide with the substitution of fossil fuels with alternative fuels identified in this review (Badillo et al., 2020; CEMEX, 2016). Similarly, they agree with some strategies that contribute to maintaining adequate levels of pollutant emissions. An example is the stoichiometric chemical monitoring system or the bag filters (Figure 1 and Figure 2).

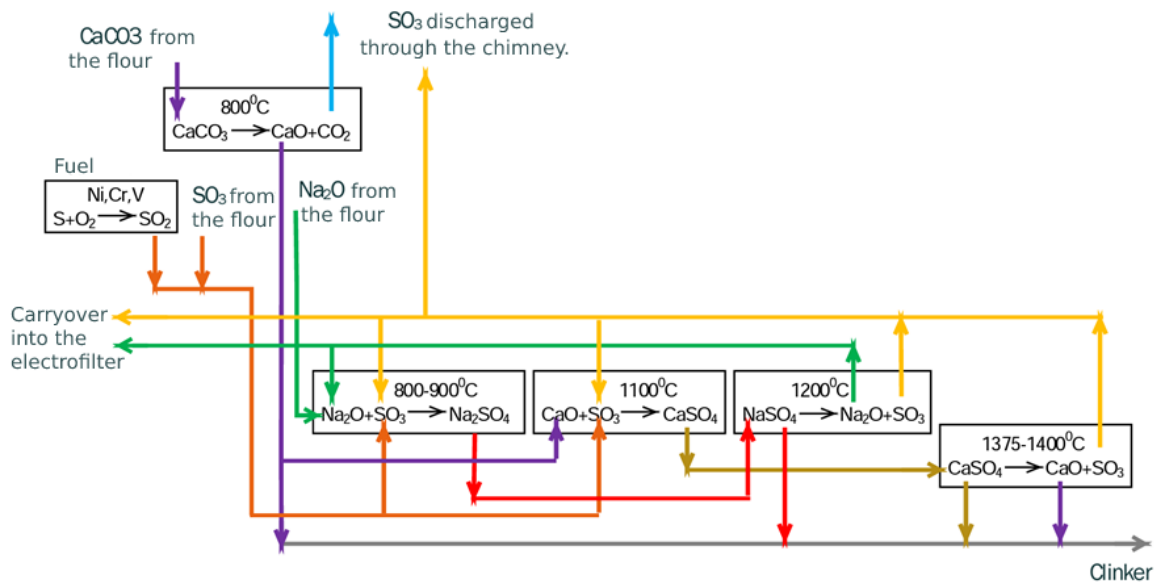


Figure 1. Stoichiometric chemical monitoring system. Source: Feijóo et al. (2016).

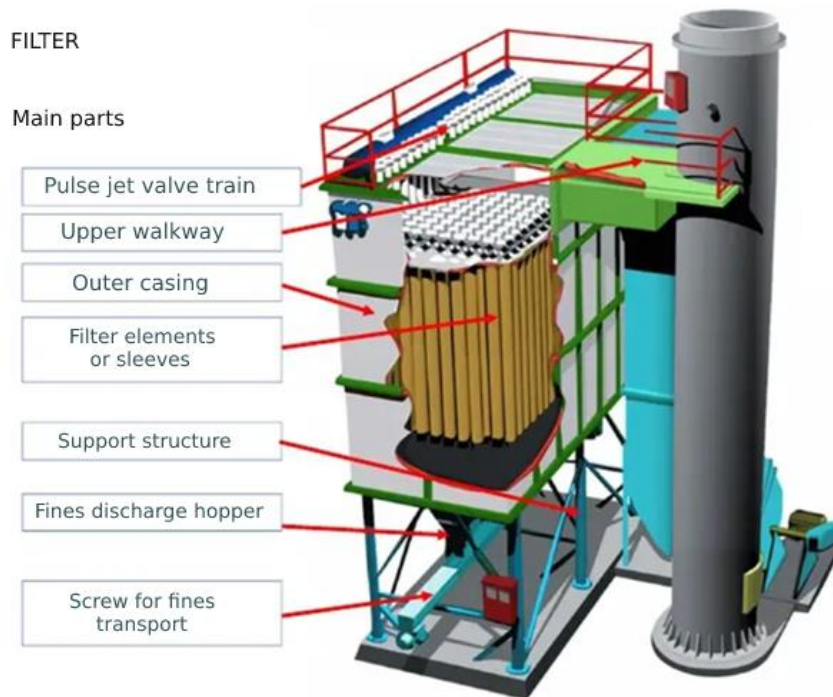


Figure 2. Bag filter used in the cement industry. Source: Camargo (n.d.).

Another type of strategy reported by Guo et al. (2023) is related to the development of technologies to capture, utilize, and store carbon emissions. In this case, their implementation occurs mainly in European countries. In this study, strategies of this type adopted in Mexico and other Spanish-speaking countries were found. Some examples are domes to capture  $\text{SiO}_2$  (Sagástegui, 2012) or the transformation of SOX waste into bioreactors through sulfur oxidation processes (Figure 3).

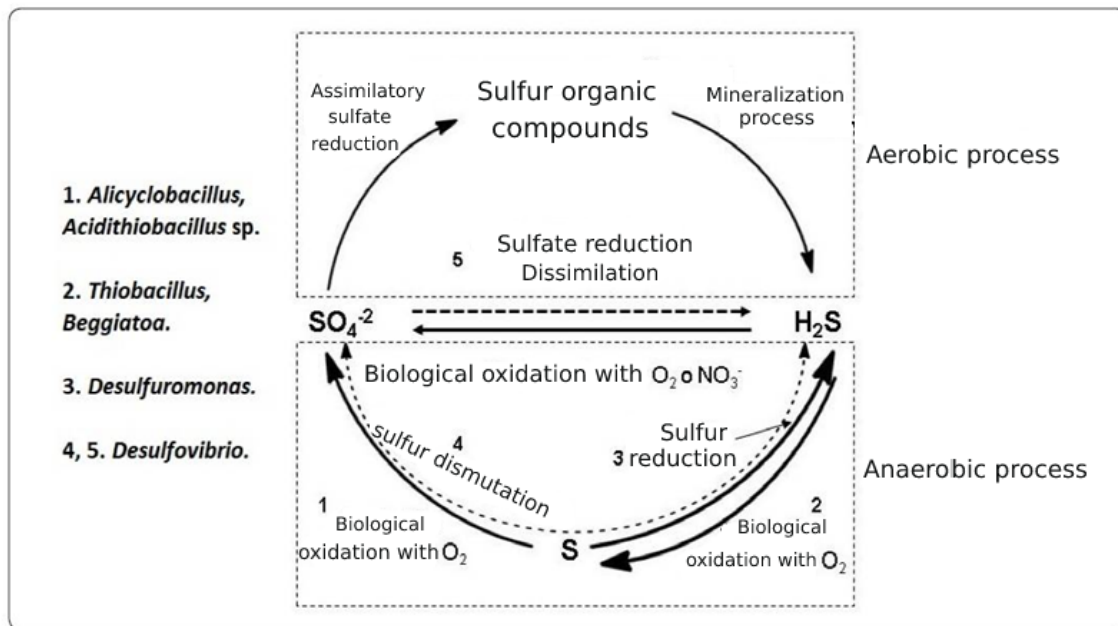


Figure 3. Example of the cycle generated in a bioreactor. Source: Veana et al. (2020).

### 4.3 Proposal

Figure 4 presents the sustainable strategies analyzed in this study arranged according to their feasibility of implementation in the cement industry sector in Mexico. This allows visualizing their priority and importance. The options located at the top of the pyramid showed greater eco-efficiency and benefits, according to the scientific evidence that supports them.

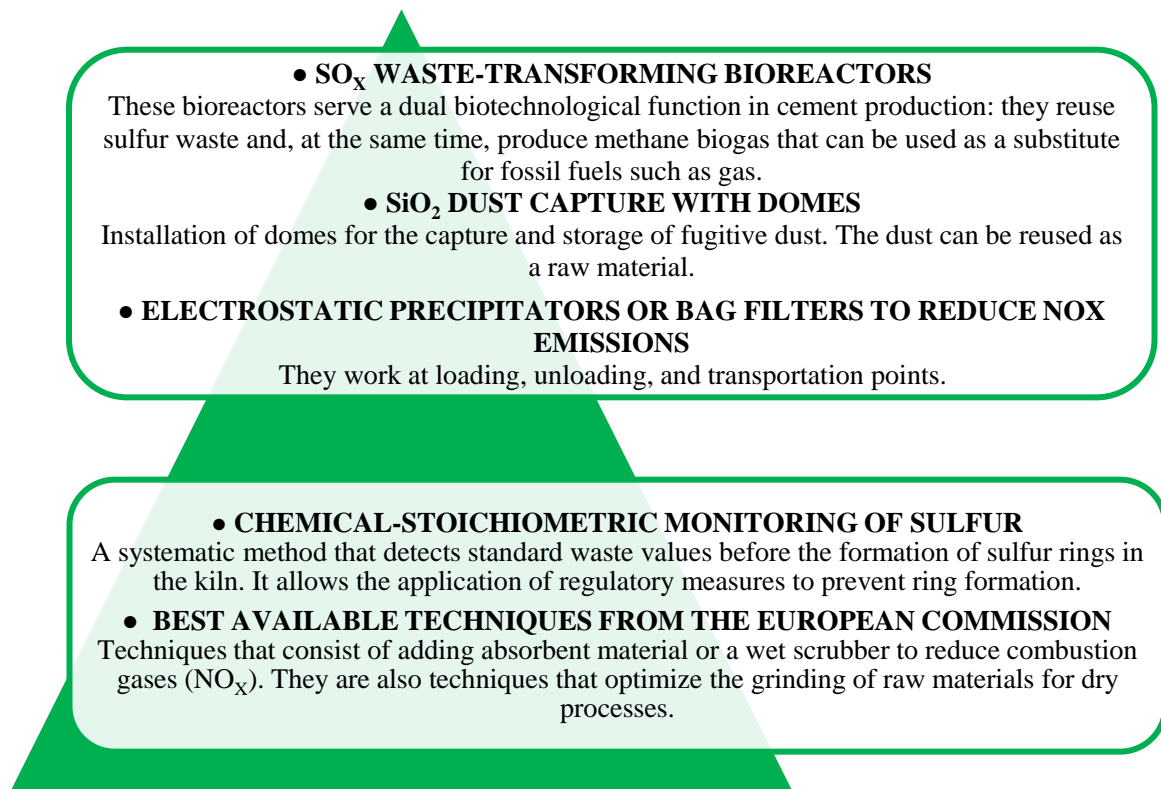


Figure 4. Hierarchical diagram of eco-efficient strategies that have proven to reduce the emission of NO<sub>x</sub>, SO<sub>x</sub>, and SiO<sub>2</sub> dust residues to the maximum during cement production.

## 5. CONCLUSIONS

The SO<sub>x</sub> bioreactors exhibit higher eco-efficiency since they reuse sulfur waste and produce methane biogas which can be used as fuel. The domes capture SiO<sub>2</sub> dust that can be reused as raw material. Finally, the bag filters were able to reduce the emission of NO<sub>x</sub> residual gases. The adoption of these strategies would allow the Mexican cement sector to demonstrate the eco-efficiency of their production processes with scientific evidence.

As of the writing of this article, only CEMEX and Cementos Cruz Azul have adopted strategies such as replacing fossil energy sources with biomass or waste. However, they do not refer to the application of other strategies considered in this proposal to mitigate emissions.

Likewise, Mexican cement companies would obtain added value in their production processes and finished cement by applying eco-efficient processes. This would contribute to strengthening their business competitiveness. Furthermore, the benefits of this strengthening go beyond simply obtaining the environmental certifications required by law.

It will be necessary to double efforts to review more thoroughly whether the strategies adopted by cement companies in Mexico are truly sustainable and aligned with the UN SDGs. Again, CEMEX and Cementos Cruz Azul are the only cement companies that appear to align with these objectives through their fossil fuel substitution strategies. The rest of the Mexican cement companies express a commitment to sustainable development, but do not present strategies or indicators to reduce their environmental impact.

Finally, it is suggested to implement better methods to evaluate the results before, during, and after the application of sustainable strategies in this sector. This would provide greater certainty about their eco-efficiency. It is reiterated that the great challenge facing this sector is to demonstrate the eco-efficiency of the sustainable methods they apply with scientific evidence.

## 6. REFERENCES

- Aguilar, J. D. (2019), *Cemento, el oro gris mexicano*. Consultado el 23 de marzo de 2023. <https://www.milenio.com/especiales/cemento-el-oro-gris-mexicano>
- Ashby, M. F. (2024), “*Materials and Sustainable Development*”. Elsevier, España, pp. 377–390. <https://doi.org/10.1016/B978-0-323-98361-7.00016-6>
- Badillo, M. M., Martínez, L. A., Flores, J. R., y Flores, J. I. (2020), “*La termovaloración de combustibles alternativos y materias primas (AFR) en hornos para la producción de cemento Portland: una opción sostenible*”. *Academia Journals*, Hidalgo, México.
- Balanzátegui, R. I., Coba, L. M. y Vega, J. G. (2019), *Desarrollo sostenible de proyectos productivos sobre la base de la ley de Economía Popular Solidaria*. *Revista Espacios*. 40(22): 4–21.
- Bravo, D. N. y Arroyo, F. R. (2018), *Innovación sustentable: un camino al desarrollo productivo del Ecuador*. *Innova Research Journal*. 3(5): 29–44. <https://doi.org/10.33890/innova.v3.n5.2018.512>
- Cámara Nacional del Cemento (2020), *Co-procesamiento en la industria del cemento: Alternativa de manejo de residuos ambientalmente segura*. Consultado el 24 de marzo de 2023. [https://comisiones.senado.gob.mx/ambiente/reu/docs/presentacion4\\_e121020.pdf](https://comisiones.senado.gob.mx/ambiente/reu/docs/presentacion4_e121020.pdf)
- Camargo, G. (s. f.), *Filtro de Mangas Partes y Funcionamiento*. Consultado el 05 de abril de 2023. <https://es.scribd.com/document/439978098/Filtro-de-Mangas-Partes-y-Funcionamiento#>
- Cemento y Concreto Moctezuma (s. f.), *Compromiso por contribuir al desarrollo social*. Consultado el 05 de abril de 2023. <https://www.cmoctezuma.com.mx/desarrollo-sostenible>
- CEMEX (2016), “*La contribución de CEMEX hacia un futuro bajo en carbono. Postura de CEMEX respecto al cambio climático*”. CEMEX, México.

- CEMEX. (2012), “*Construyendo las ciudades del futuro. Informe de desarrollo sustentable*”. CEMEX, México.
- Ciudades del Futuro (2018), *Cemento 4.0: la disrupción tecnológica llega a la industria cementera*. Siemens. Consultado el 20 de marzo de 2023. <https://ciudadesdelfuturo.es/cemento-4-0-la-disrupcion-tecnologica-llega-la-industria-cementera.php>
- Clavijo, P. A. y Guevara, M. M. (2019), “*Análisis Sostenible de la Cementera Holcim con Repercusiones de Mercadeo y Finanzas*”, Trabajo de Grado, Universidad del Rosario, Bogotá.
- Cobo, M. E. y Estébanez, S. (2021), “*Guía para el control de la exposición a polvo de sílice*”. Asepeyo prevención, Madrid, España.
- Comisión Europea (2017), “*Prevención y control integrados de la contaminación. Documento de referencia sobre las mejores técnicas disponibles en la industria de fabricación de cemento, cal y óxido de magnesio*”. Observatorio de la economía circular en la industria cementera, Sevilla, España.
- Cooperativa la Cruz Azul (2016), *La Cruz Azul y los Objetivos de Desarrollo Sostenible*. Consultado el 05 de abril de 2023. <https://www.aciamericas.coop/IMG/pdf/apolinarortiz.pdf>
- Cooperativa La Cruz Azul (s. f.), *Medición isocinética a fuentes fijas y perimetral de partículas*. Consultado el 18 de marzo de 2023. <https://acortar.link/MpNMyg>
- Feijoó, J. A., Fabelo, J. A. y Rodríguez, I. L. (2017), *Evaluación del ciclo del azufre en el horno de la fábrica de cemento de Cienfuegos*. Revista Centro Azúcar. 44(2): 1-9.
- France 24 (2021), *El hormigón, tercer emisor mundial de gases de efecto invernadero*. Consultado el 21 de marzo de 2023. <https://www.france24.com/es/minuto-a-minuto/20211019-el-hormig%C3%B3n-tercer-emisor-mundial-de-gases-de-efecto-invernadero>
- García-Muñoz, A. C. y Pérez-Sánchez, B. (2020), *La responsabilidad social en CEMEX*. Investigación Valdizana. 14(4): 175–87. <https://doi.org/10.33554/riv.14.4.728>
- Gessa, P. A. y Sancha, D. M. P. (2016), *Alternativas de reducción de las emisiones de dióxido de carbono (CO2) en la producción de cemento. Propuesta de un modelo de evaluación*. Innovar. 26(60): 51–66. <https://doi.org/10.15446/innovar.v26n60.55532>
- González, M. J. y Cuesta, V. P. (2018), *De responsabilidad social a sostenibilidad corporativa: una revisión actualizada*. Revista Internacional de Investigación en Comunicación. 17(7): 46-71. <https://doi.org/10.7263/adresic-017-04>
- Grupo Cemex (2021), *Sostenibilidad*. Consultado el 05 de abril de 2023. <https://www.cemexmexico.com/sostenibilidad>
- Grupos de Cemento Chihuahua (2023), *Sustentabilidad*. Consultado el 05 de abril de 2023. <https://www.gcc.com/es/sustentabilidad/#:~:text=La%20estrategia%20de%20sustentabilidad%20de,para%20esta%20y%20pr%C3%B3ximas%20generaciones.>
- Guo, Y., Luo, L., Liu, T., Hao, L., Li, Y., Liu, P. y Zhu, T. (2024), *A review of low-carbon technologies and projects for the global cement industry*. Journal of Environmental Sciences. 136: 682–697. <https://doi.org/10.1016/j.jes.2023.01.021>
- Hernández, R., Fernández, C. y Baptista, M. P. (2014), “*Metodología de la investigación*”. Mc Graw Hill Education, Distrito Federal, México.
- Huh, S.Y., Lee, H., Shin, J., Lee, D. y Jang, J. (2018), *Inter-fuel substitution path analysis of the korea cement industry*. Renewable and Sustainable Energy Reviews. 82: 4091–4099. <https://doi.org/10.1016/j.rser.2017.10.065>
- Jaramillo, R. A. (2017), *Una Mirada a la competitividad*. Dictamen libre. 20:87-98.
- Kumar, C. A. (2018), “*Cement production technology. Principles and Practice*”. CRC Press, Florida, Estados Unidos.
- León-Velez, A. y Guillén-Mena, V. (2020), *Energía contenida y emisiones de CO2 en el proceso de fabricación del cemento en Ecuador*. Ambiente Construido. 20(3): 611-25. <https://doi.org/10.1590/s1678-86212020000300448>

- Lin, K.-L., Lo, K.-W., Hung, M.-J., Cheng, T.-W., y Chang, Y.-M. (2017), *Recycling of spent catalyst and waste sludge from industry to substitute raw materials in the preparation of Portland cement clinker*. *Sustainable Environment Research*, 27(5). <https://doi.org/10.1016/j.serj.2017.05.001>
- López, N. V. (2018), *El papel de la innovación tecnológica industrial y la sustentabilidad. Un acercamiento a la industria cementera*. *Tekhné Revista de la Facultad de Ingeniería*. 21(2): 83-95.
- Martínez, L. M. y Alexandre, P. M. (2020), *Industria cementera en México: Sin señales de recuperación a pesar de tocar fondo el año pasado*. Consultado el 24 de febrero de 2022. <https://www.spglobal.com/assets/documents/ratings/es/2020-01-22-industria-cementera-mexico.pdf>
- Organización de las Naciones Unidas y Comisión Económica para América Latina y el Caribe. (2018), *“La Agenda 2030 y los objetivos de desarrollo sostenible: Una oportunidad para América Latina y el Caribe”*. ONU-CEPAL, Santiago de Chile, Chile.
- Pérez, E. M. J., Espinoza, C. C. y Peralta, M. B. (2016), *La responsabilidad social empresarial y su enfoque ambiental: una visión sostenible a futuro*. *Revista Universidad y Sociedad*. 8(3): 169-78.
- Pérez, S. B., Guzmán, S. A., Mayo, C. A. y Heredia, R. H. (2013), *Evolución histórica de cementos mexicanos: un grupo económico de capital nacional*. *Hitos de Ciencias Económico Administrativas*. 19(55): 115-30. <https://doi.org/10.19136/hitos.a0n55.113>
- Poudyal, L. y Adhikari, K. (2021), *Environmental sustainability in cement industry: An integrated approach for green and economical cement production*. *Resources, Environment and Sustainability*. 4, 100024. <https://doi.org/10.1016/j.resenv.2021.100024>
- Rivera-Hernández, J. E., Alcántara-Salinas, G., Blanco-Orozco, N., et.al. (2017), *¿Desarrollo sostenible o sustentable? La controversia de un concepto*. *Revista Posgrado y Sociedad*. 15(1): 57-67. <https://doi.org/10.22458/rpys.v15i1.1825>
- Rocha, J. H. A., Toledo Filho, R. D. y Cayo-Chileno, N. G. (2022), *Sustainable alternatives to CO2 reduction in the cement industry: A short review*. *Materials Today: Proceedings*. 57, 436–439. <https://doi.org/10.1016/j.matpr.2021.12.565>
- Rodgers, L. (2018), *La enorme Fuente de emisiones de CO2 que está por todas partes y que quizás no conocías*. Consultado el 17 de marzo de 2023. <https://www.bbc.com/mundo/noticias-46594783>
- Roy, M. (2021), *“Sustainable Development Strategies”*. Elsevier, España, pp. 1–25. <https://doi.org/10.1016/B978-0-12-818920-7.00005-0>
- Ruiz, Y., Domínguez, E. R., Sánchez, S., Castillo, L., Martirena, J. F. y Suppen, N. (2017), *Análisis de ecoeficiencia de la producción de cementos de bajo carbono mediante la sustitución de clínker*. *Revista Centro Azúcar*. 44: 77–88.
- Ruggerio, C. A. (2021), *Sustainability and sustainable development: A review of principles and definitions*. *Science of The Total Environment*, 786. <https://doi.org/10.1016/j.scitotenv.2021.147481>
- Sagástegui, D. A. (2012), *“Propuesta para reducir las emisiones de polvo fugitivo en el proceso productivo de una empresa cementera”*, Tesis de ingeniería, Universidad Peruana de Ciencias Aplicadas, Santiago de Surco, Perú.
- Sanjuán, M. A. y Chinchón, S. (2014), *“Introducción a la fabricación y normalización del cemento Portland”*. Universidad de Alicante, España.
- Schenttini, P. y Cortazzo, I. (2015), *“Análisis de datos cualitativos en la investigación social. Procedimientos y herramientas para la interpretación de información cualitativa”*. Editorial de la Universidad Nacional de la Plata, La Plata, Argentina.
- Secretaría del Medio Ambiente y Recursos Naturales. (s. f.), *“Guía para la elaboración de la cédula de operación anual. Industria del cemento, cal y yeso”*. SEMARNAT, México.

- Teja, R., Hiremath, R.B, Rajesh, P., Kumar, B., y Renukappa, S. (2022), *Sustainable transition towards biomass-based cement industry: A review*. Renewable and Sustainable Energy Reviews, 163. <https://doi.org/10.1016/j.rser.2022.112503>
- The Cement Sustainability Initiative (2012), “*The Cement Sustainability Initiative*”. World Business Council for Sustainable Development, Washington, DC, Estados Unidos.
- The Cement Sustainability Initiative (2014), “*Cement Industry Energy and CO2 Performance Getting the Numbers Right (GNR)*”. World Business Council for Sustainable Development.
- The Cement Sustainability Initiative (2019), “*Indian Cement Sector SDG Roadmap*”. World Business Council for Sustainable Development, Ginebra, Suiza.
- Veana, F., González-Purata, P. Y., Wong-Paz, J. E., Aguilar-Zárate, P., Muñoz-Márquez, D. B. (2019), *Tendencias de la bioenergía: del metagenoma de hábitats ricos en azufre a la purificación del biogás*. Revista Especializada en Ciencias Químico-Biológicas. 22: 1-11. <https://doi.org/10.22201/fesz.23958723e.2019.0.190>
- Vega, L. A. (2017), *Sustentabilidad y competitividad en empresas hortícolas de México*. Sapientiae. 2(2): 110-26.